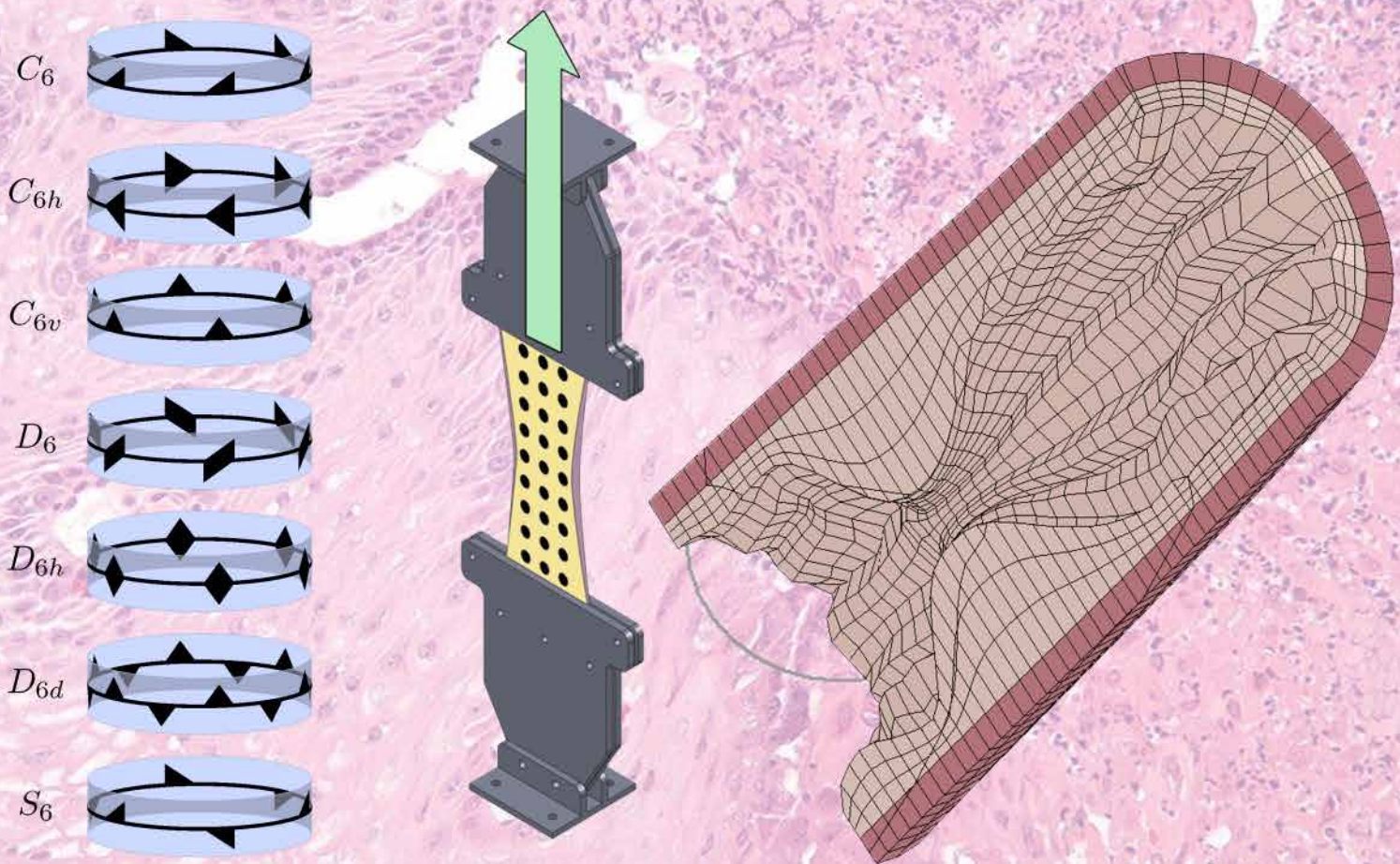# A Constitutive Model of Human Esophagus Tissue with Application for the Treatment of Stenosis

Experimental Characterization and Numerical Simulation

C_6

C_{6h}

C_{6v}

D_6

D_{6h}

D_{6d}

S_6

David Sánchez Molina

UPC

DOCTORAL STUDIES

DOCTORAL THESIS
– SEPTEMBER 3, 2013 –

A CONSTITUTIVE MODEL OF HUMAN ESOPHAGUS TISSUE WITH APPLICATION FOR THE TREATMENT OF STENOSIS: EXPERIMENTAL CHARACTERIZATION AND NUMERICAL SIMULATION

Student: David Sánchez-Molina

Advisors: Carlos Arregui-Dalmases
             Gabriel Bugeda Castelltort

UNIVERSITAT POLITÈCNICA
DE CATALUNYA
BARCELONATECH

Title:	A Constitutive Model of Human Esophagus Tissue with Application for the Treatment of Stenosis: Experimental Characterization and Numerical Simulation
Author:	David Sánchez-Molina
Advisors:	Carlos Arregui-Dalmases
	Gabriel Bugeda Castelltort
Date:	September 3, 2013

Abstract: This dissertation is a research about the mechanical behavior of the human esophagus. This work is intended to construct a computational model to simulate forced dilatations, required by esophageal diseases.

The study summarizes the previous works on esophageal tissues by other authors. A short explanation about the microcontinuum theory is given, as well as a summary of the non-linear hyperelastic constitutive models (with large deformation). This study required extensive testing of esophageal tissue in order to characterize the in vitro mechanical behavior. Optical motion track analysis was used for accurate computation of the strains in the tissue. The testing included tensile tests and inflation tests. The results of the tests were used for adjusting the mechanical properties that characterize the mechanical behavior of esophagus; their values were used for conduct some numerical simulations based on the models.

The main result is a constitutive non-linear microstretch anisotropic hyperelastic constitutive model with large deformations (and with residual stresses) to characterize the multi-layered tissue of human esophagus. This model is suitable for numerical simulation. In addition, a number of theoretical results were obtained. Some significant correlations between anthropometric factors, such as the body mass index, and some mechanical properties were found in the analysis of the data.

Dissertation presented by David Sánchez-Molina in partial fulfillment of the
requirements for the degree of
Doctor per la Universitat Politècnica de Catalunya

In memoriam cāræ mātris
meæ, quæ perīit dum
dissertātiōnem hanc
scrībebam ... etiam uxōrī,
frātrī, sorōrī, patrīque

[Dedicated to my beloved mother
who passed away when this
dissertation was being written...
also to my wife, my brother, my
sister, and my father]

Acknowledgements

Summary

This dissertation is a research about the mechanical behavior of the human esophagus. This work is intended to be applied in the treatment of stenosis and other esophageal diseases that frequently require a procedure of forced dilation, that involves high pressures on the esophagus wall. This study proposes a constitutive model to simulate forced dilatations. This study includes the experimental characterization of the mechanical behavior of human esophagus. In addition, some theoretical questions and experimental issues were addressed and solved.

This dissertation summarizes the previous work on esophageal tissues by other authors. Additionally, a short explanation about the microcontinuum theory developed in the last decades is given, as well as a summary of the general theory of non-linear hyperelastic constitutive models (with large deformation). This study required extensive testing of esophageal tissue in order to characterize the in vitro mechanical behavior. The testing included mainly tensile tests and complementary inflation tests. Optical motion track analysis was used for accurate computation of the strains in the tissue. The results of the tests were used for adjusting the mechanical properties that characterize the mechanical behavior of esophagus in the proposed models of the literature. The statistical analysis of the data revealed, some significant correlations between anthropometric factors, such as the body mass index, and some mechanical properties were found in the analysis of the data. The typical values of the mechanical properties were used to perform some numerical finite element simulations based on the proposed models. In addition, a number of theoretical results were obtained concerning the residual stress and the predictions of statistical mechanics for a system of collagenous fibers inside a soft tissue.

The main result is a constitutive non-linear microstretch anisotropic hyperelastic constitutive model with large deformations (and with residual stresses) to characterize the multi-layered tissue of human esophagus. This model is suitable for numerical simulation.

Contents

CONTENTS

CONTENTS

List of Figures

LIST OF FIGURES

List of Tables

LIST OF TABLES

List of Symbols

1

Introduction

1.1 Motivation and antecedents

A frequent pathological condition of the esophagus is the occurrence of benign stenoses in the esophageal tract. Those stenoses make eating and swallowing difficult. Independently of the cause of the disease, the initial recommended treatment is an endoscopic one, often involving forced dilatation. The worst complication of this treatment is the eventual puncture of damaged tissues, which leads to high morbidity [21, 58]. As forced dilations are performed empirically, it is not always possible to foresee eventual punctures.
Some of the objectives of this study are:

- To find approximate values (involving the thickness of the wall and the resistance of the tissue) that make possible to predict an eventual puncture.

- To describe the biomechanics of the esophageal tissues –both normal and damaged– by means of stress-strain relations, which allow us to simulate the effect of the treatment.

- To predict the most likely effect caused by medical instruments used to dilate the esophageal tract and to make it possible to determine in advance if a failure of the esophageal wall it is likely to happen.

- To establish procedures regarding the loading of the esophageal wall in order to improve the forced dilation treatments. This project has required several tests for the *in vitro* characterization of the esophagus. The obtained results can be used to assess the existent treatments.

The observation of the current treatments of forced dilation conducted by most endoscopists, in a completely empirical way, is the origin of this study. We have observed that occasionally, current treatments lead to some secondary problems due to the impossibility to predict the biomechanical resistance of the esophagus wall. Recently, some multidisciplinary studies have analyzed medical problems with the help of numerical simulations [23,39]. In the present study, the conducted empirical work and the theoretical analysis are intended to provide a reliable description of the esophagus tissue, which are useful for numerical simulation. Two main diseases can require forced dilation: stenosis and achalasia; since in both cases there is a narrowing of the esophageal tract [9]. These two diseases may disturb the ingestion of food and the usual emergency treatment is forced dilation. The aim of a computational model is to predict by means of simulation the likely effect of the medical instruments used in forced dilation. Notice that the esophagus deformation may reach critical values at endoscopies, more rarely by mandatory lung ventilation, closed chest traumata, etc. [27,57,73,85].

The development of an adequate constitutive model is an important issue for performing realistic numerical simulations. These simulations can be used to assess the consequences of the different conventional treatments of forced dilation (gastric balloons, progressive dilators, stents, ...). Thus, one of the general objectives of this dissertation is to characterize –experimentally– and to simulate –numerically– some aspects of the mechanical behavior of human esophagus. The mechanical properties in this study were obtained from *in vitro* tests. Two different tests have been performed: uniaxial tensile tests and some additional inflation tests. The data obtained, mainly from uniaxial tests, can be used to check the adequacy of some proposed models of soft tissue. In addition, a new model that includes an account of the micro-structures inside the tissues is being proposed. The experimental data have allowed us to obtain the values of the mechanical constants which are needed for numerical parameters in simulations.

1.2 Physiological bases

The primary function of the esophagus is to impulse the *bolus*, i.e. the mass of food that has been chewed at the point of swallowing, from the pharynx to the stomach. This transportation of the bolus is carried through an alternating succession of muscular contractions and temporal relaxations of the lower esophageal sphincter or *cardia*. This transportation process is called *peristaltic transportation*. Peristaltic transportation consists of a sequence of contractions or peristaltic waves that hauls the bolus by an alternation of compression and relaxation of the esophageal wall. It is important to highlight that peristaltic
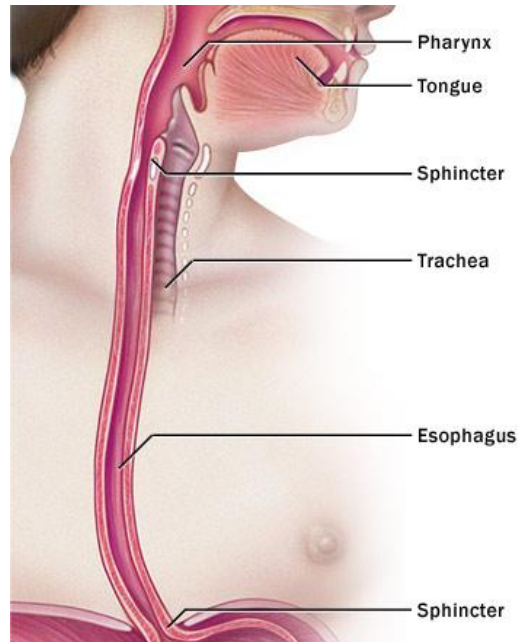
Figure 1.1. Depiction of a human esophagus (from Mayo Foundation for Medical Education and Research.)

transportation of the swallowed material is an involuntary neuromuscular function that allows us to swallow, even in the absence of gravity. Unfortunately, the peristaltic mechanism can be affected by some diseases (dysphagia, esophageal stenosis, achalasia) [2, 15, 75, 76]. All the transportation from upper esophagus to the stomach can be done in a few seconds, without any abrupt change of pressure or interruption of respiration in any moment. Structurally, the human esophagus is a two-layered tubular structure of 20 to 25 cm long. The two main layers are:

- **The inner layer or *mucosa-submocosa*.** The submucosa is a layer of dense irregular connective tissue or loose connective tissue that supports the mucosa. It joins the mucosa to the bulk of overlying the smooth muscle (fibers running circularly within layers of longitudinal muscle), thus the submucosa layer is placed between the mucosa and the outer layer. On the other hand, the mucosa layer is a stratified epithelial lining covering the submucosa. It covers completely the inner part of the esophageal cavity and has an exterior surface adequate for the sliding of the bolus with no difficulty.
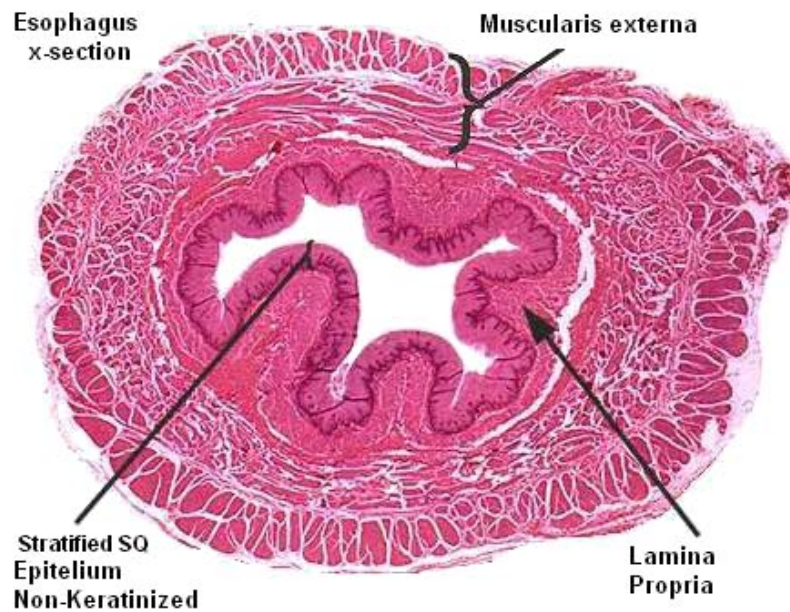
Figure 1.2. A cross section in upper esophagus, showing the *muscularis externa* (outer part) and the *mucosa-submucosa* (inner part).

- **The outer layer or *muscularis externa*** is a muscle layer. It is involved in gut movements and in peristalsis (peristaltic transportation). The muscularis externa is adjacent to the submucosa membrane.

The two described layers are not completely homogeneous; a certain sub-layers and tissue arrangements can be distinguished in histological inspection.

1.3 Research approach

One of the concerns of the methods and models used in this dissertation is the generality of the mathematical formulation. A mathematically rigorous approach is used for gaining in generality and clarification of the relations of the cornerstones of the theory. A special effort has been made in order to use a convenient notation (although some expressions are repeated in the more frequent notations used in engineering, when there are clear equivalences). Obviously, there is some discussion about the most convenient approach, as stated by Marsden and Hughes (1983) [72]:

> [...] *researchers in elasticity are very opinionated, even when they are wrong. During our own work in this field we have refused to fight, and in keeping with this pacifist approach, we now issue these disclaimers: This book is neither complete nor unbiased. [...] To a mathematician, a tensor $\boldsymbol{t}$ is a section of a certain bundle over a manifold. To an engineer or physicist, a tensor t^{ijk} is an object dressed in indexes. This is one of the many unfortunate paper barriers that have retarded the growth of, and interest in, mathematical elasticity. The beginner should learn to speak both languages and to ignore notational disputes. For example, beginners who are already trained in some geometry an who realize that ∇f is a vector, while df is a one-form, will recognize at once that the deformation gradient $\mathbf{F}$ is not a gradient at all, but is simply the derivative of the deformation (a map of original configuration into the environment space). They may also recognize that the rate of deformation tensor is just the derivative of the Riemannian metric on space, and that the Cauchy–Green tensor is the pull-back of the Riemanninan metric on space by the deformation.*

Usual expositions of the Theory of Elasticity (even those dealing with non-linear solid mechanics) restrict the generality of the theory by using expressions that are valid only in Cartesian coordinate systems or inertial frames of reference, and thus, considering only rigid changes of coordinates (translations and rotations). A full covariant approach allows us to use general curvilinear coordinates and arbitrary frames of reference (not only inertial frames). A review on manifolds, maps between manifolds, tensorial analysis, covariant derivative and other related topics is given in Appendix B. For many practical purposes, the non-covariant approach keeps many things simple, but possibly some important connections and generalizations are lost. There are clear advantages in the covariant approach and in the use of manifolds and the full tensorial formulation. To support this approach, three good physical reasons can be adduced:

- **Compatibility equations**. Many books about elasticity present compatibility equations as an abstract requirement for integrability of the deformation tensor $\boldsymbol{\varepsilon}$ ensuring the existence of a displacement vector field $\mathbf{u}$ for the deformed body. But in terms of Riemann manifolds there is a much more clear interpretation, being the deformation tensor related to the metric tensor of the space (see section B.7).The compatibility equations are equivalent

to state that the environment space is Euclidean (that is, a manifold of zero curvature) [16] (in fact, there is exactly one compatibility equation for each component of the Riemann curvature tensor!). When considering, for example, generalizations of elasticity in the context of Astrophysics or Einstein's theory of General Relativity, the compatibility equations represent the curvature of the space-time. Observe that in a curved space-time, the space does not have the structure of vectorial space as $\mathbb{R}^n$ and the concept of *displacement vector* does not make sense; but the compatibility equations still retain their geometrical interpretation. Thus, the lack of generality deprives the compatibility equations of their geometric sense, disguising them as a technical integrability condition.

- **Arbitrary frames**. Most books about elasticity fail to formulate the equations in an arbitrary system of reference, since it could be enough to use inertial frames for many practical purposes. However, the formulation of the Elasticity theory in arbitrary frames of reference and in arbitrary coordinates can be useful in some specific contexts and brings a better understanding of the general theory of continuous media. In addition, assuming that the environment space is Euclidean –although reasonable in most practical situations– is not a correct assumption (at lest at cosmological scale). A physical elegant theory needs to be valid for general frames of reference, as Einstein understood in seeking its theory of General Relativity. Indeed, Einstein found that both issues (to have a theory completely general for any observer or reference frame and the geometry of space) are connected. Thus, a completely satisfactory theory of elasticity should not assume that the space is Euclidean or that we are using an inertial frame of reference. For this purpose, we will seek a full covariant formulation without assuming any system or reference (we will assume in some cases that the space is Euclidean, then we will proceed to a full covariant formulation removing this particular assumption).

- **Residual stress**. Biological tissues are influenced by stresses since growth depends on stress [10, 93], this leads to an interesting issue. If a part of the tissue is surgically removed, some parts shrink but the final state is not stress free because the newly generated cells have distorted the original geometry and the tissue has no possibility to return to an "original" shape. The difficulties in dealing mathematically with this problem is interestingly related to the problem of relativistic elasticity. In relativistic elasticity

there is no way to separate the "deformation" of the background space from the deformation of the body. Thus, there is no natural way to define the undeformed shape of the body. Mathematically the residual stress can be treated by defining a non-Euclidean metric tensor (as it is required for working in curved space-time).

This dissertation takes advantage of a full covariant formulation, Riemann geometry, covariant derivative, and a manifold approach. This will allow us to attach the right geometrical meaning to some concepts, to have a satisfactorily general theory and, in addition, to deal with residual stresses (so common in biological tissues in an elegant and general way). A final comment about the chosen mathematical approach: nowadays mathematicians, physicists and engineers agree that the distinction between a linear transformation and a matrix is worth fussing over. In the same spirit, manifolds should be used:

> *They are unquestionably the appropriate setting for tensor analysis and continuum mechanics. Resistance to the use of abstract manifolds is frequently encountered, simply because most work in elasticity in* $\mathbb{R}^3$. *In the literature,* $\mathbb{R}^3$ *is often replaced by abstract vector spaces. This arena is* not *suitable for general tensor analysis. Indeed, as Einstein has so profoundly taught us, deep insights can be gained by removing one's blinders to see the theory in the grander time-proven context of covariant formulations. This is why we encourage the use of manifolds.* [72, p. xiii]

1.4 Research contributions

Every well-formulated research attempts to answer some set of well-settled and properly formulated questions. This dissertation seeks to answer the following questions:

1. What type of stress-strain response can be expected for a soft tissue like the esophageal wall?

2. Being the response non-linear and anisotropic, how can we deal with these features from a mathematical point of view?

3. Being soft tissues complex biological structures with a lot of micro-structure, is it possible to characterize these micro-structures by incorporating them in a constitutive model?

4. How can we use a mathematical model for improving the medical treatments that involve forced dilation?

A partial short response for the previous questions is the following:

The main objective of this dissertation is to formulate rigorously a complete **nonlinear microstretch anisotropic hyperelastic constitutive model with large deformations** (and with residual stresses) to characterize the multi-layered tissue of human esophagus, the model is intended to be compared with *in vivo* measurement in order to predict possible failure of tissues during procedures of **forced dilation** in patients with some common diseases that may require them.

As we mentioned in the previous sections, this research encloses the following sub-goals:

- **Analysis of micro-structure.** The microcontinuum theory is used for modeling small scale structure present in biological tissues (microstructure). The micro-structure of collagenous tissues and the arrangement of fibers are examined in order to produce a physically motivated constitutive model.

- **Analysis of anisotropy.** A general analysis of different types of anisotropy based on exact mathematical results is reviewed for both classical continuum models and microcontinuum models.

- **Describing a complete procedure** for experimentation with soft tissue, sample preparation, marking and use of motion tracking for obtaining accurate displacements and strains, reducing the dispersion of the data.

- **Assessing maximal deformations and expected efforts** on the esophagus wall during treatments.

All details and justifications of the partial answer just quoted is the object of the following chapters.

2

Antecedents

2.1   Motivation and Antecedents

This chapter explains some details of the relevant anatomy for the mechanical behavior of esophagus. The basics of the classical theory continuous media and constitutive theory are summarized here. In addition, an introduction to the theory of microcontinuoum media is given. The chapter closes with a discussion about the possible types of anisotropy in elasticity and the general theory for dealing with them.

2.2   Anatomy and diseases of esophagus

To understand the mechanical behavior of the esophagus for improving medical treatments, it is necessary to know the anatomy of esophagus and its multi-layered structure. From the anatomical point of view, the esophagus is a two-layered tubular structure: the inner layer is the *mucosa-submucosa* and the outer

layer is the *muscularis externa*, a muscular layer. The mucosa-submucosa layer is constituted by two parts that are not easy to separate; for this reason we are considering it as one single layer. In figure 2.1 the basic anatomy of esophagus is presented. Mechanically, the mucosa-submucosa layer is rich in collagen and is more rigid than the outer layer [33].
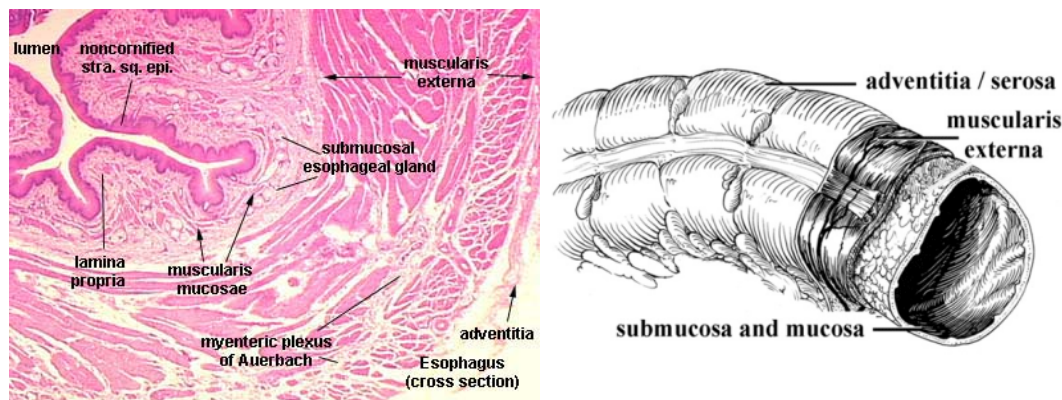
Figure 2.1. *Left*: Histological view of a typical cross section of human esophagus (Histology page of G. M. Caplan, Owensboro Community & Technical College), *Right* Multi-layered structure of the esophageal tube (after Natali, 2009, [80])

Both layers exhibit a nonlinear anisotropic viscoelastic behavior. This complex mechanical behavior requires to measure many different material constants. The value of the material constants can be obtained using *in vitro* testing of tissues from animals or cadavers [99, 115]. Due to the low velocities involved in the forced dilatation treatments $\dot{\varepsilon} \leq 10^{-2}$, the viscoelastic effects may be ignored for practical purposes. The anisotropy of the tissue is due to an asymmetric disposition of the collagenous fibers within both layers (see figure 2.2)

In its intact state, the esophagus is slightly stretched along its longitudinal direction. Moreover, this intact state is not a natural state (free-stress state) because there are residual stresses along circumferential direction of the tube. The presence of residual circumferential stress for arteries is well established since 1983 when Vaishnav and coworkers measured it [107, 108]. For esophagus, the works of Gregersen and coworkers established similar distributions of residual stress [45, 69]. Currently, we know that these residual stresses are typical of many biological tissues, in fact, it is a consequence of the growth and the remodeling of the tissue and it is modulated by mechanical factors (such as the average stress, see Rodriguez *et al.* (1994) [93]). For example, in cardiac hypertrophy, alter-
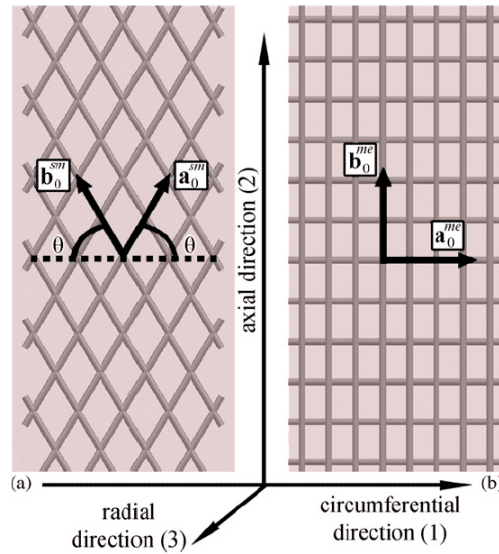
Figure 2.2. Planar representation of fiber disposition in submucosa (a) and muscularis externa (b) (after Natali, 2009, [80]).

ations in wall stress arising from changes in mechanical loading lead to cardiac growth and remodeling. Rodriguez proposed a general continuum formulation for finite volumetric growth in soft tissues adequate for modeling this type of growth. In the formulation of Rodriguez, the change in shape of a tissue during the growing process is described by a mapping analogous to the deformation gradient tensor. This mapping is decomposed into a transformation of the local zero-stress reference state and a supplementary elastic deformation; this ensures the compatibility of the total growth deformation. In these growth models, the residual stresses arise from the uneven growth deformation.

2.2.1 Esophageal diseases

Many people experience a burning sensation in their chest occasionally, caused by stomach acids refluxing into the esophagus, normally called *heartburn*. Extended exposure to heartburn may erode the lining of the esophagus, potentially leading to a *Barrett's esophagus* which is associated with an increased risk of adenocarcinoma most commonly found in the distal one-third of the esophagus. Some people also experience a sensation known as *globus esophagus*, where it feels as if a ball is lodged in the lower part of the esophagus. These two are the two

most common esophageal diseases but properly none of these common conditions constitute a dysphagia (the medical term for the symptom of difficulty in swallowing), although the heartburn can lead to some other problems implying some degree of dysphagia (see figure 2.3). In this section, we summarize two types of diseases that frequently involve more severe dysphagia: the stenosis and the achalasia.

Stenosis. The term stenosis (classical Greek *stenōsis* 'narrowing') refers to an abnormal or pathological reduction of the lumen of a tubular organ or an anatomic structure. This abnormal narrowing can occur in different tubular structures in the body, for example, we have the following types of stenoses:

- **Arterial stenoses** that include various subtypes: Angina pectoris (coronary artery stenosis), carotid artery stenosis, and renal artery stenosis.
- **Stenoses of the valves of the heart** (stenosis of pulmonary, mitral, tricuspid or aortic valves).
- **Stenoses in digestive system**, pyloric stenosis (gastric outflow obstruction), esophageal stenosis (it can be produced by different factors: accidental ingestion of caustic substances, chronic reflux and reflux esophagitis, etc.), biliary tract stenosis (obstructive jaundice).
- **subglottic stenosis** (narrowing of the subglottic airway).
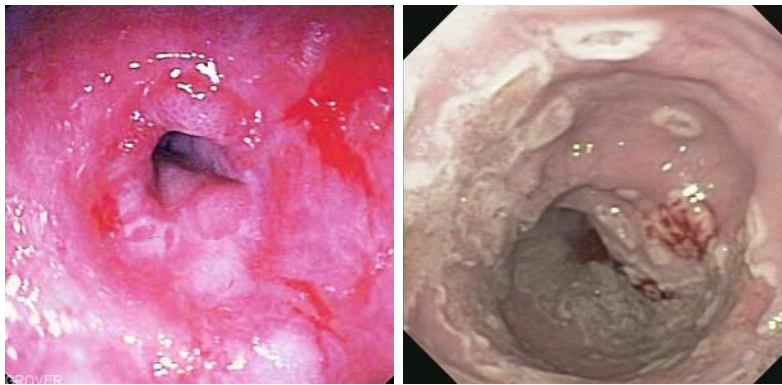
Figure 2.3. *Right*: Peptic stricture showing narrowing of the esophagus near the junction with the stomach due to chronic gastroesophageal reflux (Wikimedia commons, 2006), *Left* acute herpetic esophagitis (Hudesman *et al.*, 2009, [54])

In particular, esophageal stenosis consists in an internal regrowing of the the esophageal wall reducing the lumen of esophageal tract. This can obstruct severely the transit of the bolus, in some cases, it may provoke the complete

inability for swallowing and for eating normally. The most severe cases require emergency surgery to open the lumen. The causes of this disease are diverse. The most common one is the chronic gastro-esophageal reflux that can lead to a stenosis requiring forced dilatation combined with a treatment for acid reflux suppression. But about 25% of the cases seem to be due to other causes (esophagitis or inflammation of esophagus (see figure 2.4), diseases in some sphincter (cardia or pylorus), disorders in muscular motility, hiatus hernia, ingestion of caustic substances, regrowth of an internal scar due to a previous surgery (anastomatosis), secondary stenosis by irradiation in cancer treatments or rare dermatological diseases (*e. g.* dystrophic epidermolysis bullosa).
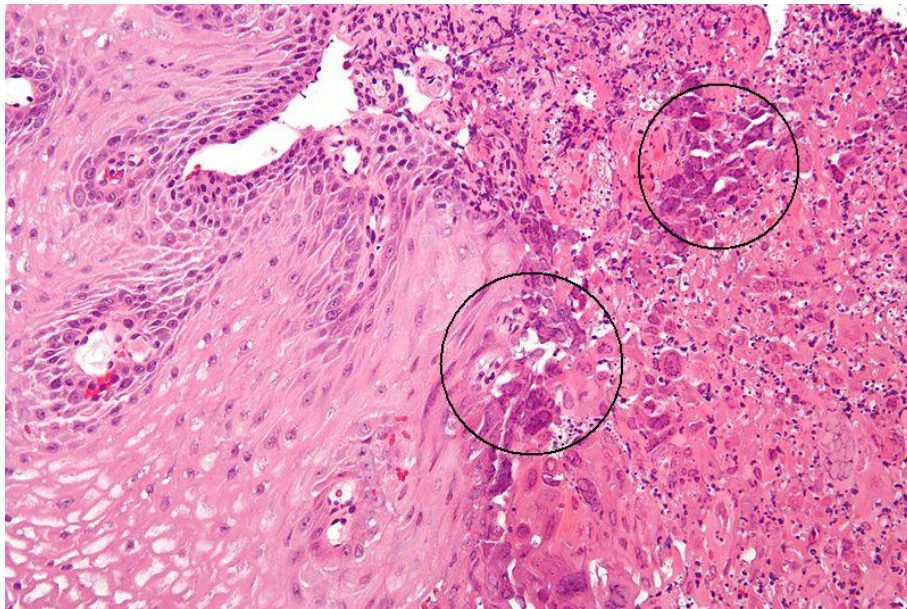
Figure 2.4. Detail of esophageal tissue affected by herpetic virus, some alterations in the cellular nucleus can be seen [marginalization (of chromatin), multi-nucleation, molding of nuclei]

Achalasia. The achalasia is another disease that may require a treatment of forced dilatation. The achalasia involves the loss of peristalsis in distal esophagus (lower part) and impedes its normal emptying. Only when the hydrostatic pressure of the accumulation of food exceeds a certain threshold the cardia opens (see figure 2.5). Its annual incidence in Europe and the US is inferior to 1 case per 100,000 people. The incidence seems to be the same for men and women, and although it may appear at any age it is very rare during adolescence; most of the patients are 19 to 60 years old. Since the 1930s, it is known that the

disease is due to failure of the superior esophageal sphincter (cardia), which fails to relax completely, hence, the denomination (classical Greek *achalasis* 'lack of relaxation').
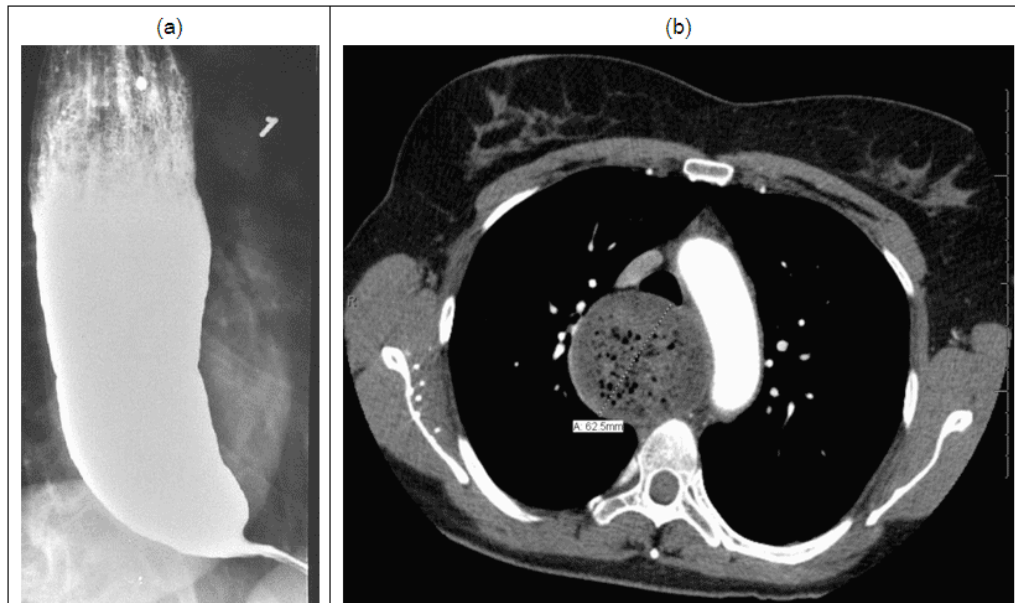
Figure 2.5. (a) Barium swallow. Dilated esophagus with retained column of barium and "bird's beaking" suggestive of achalasia (Wikimedia commons, 2007) (b) A transverse CT image showing marked dilatation of the esophagus due to accumulation of bolus (Wikimedia commons, 2010).

2.3 Continuum mechanics and Microcontinuum mechanics

The French mathematician Augustin-Louis Cauchy was the pioneer in formulating, in a rigorous, systematic way, a theory of continuum mechanics in the 19th century, but research in the area continues today. The modern formulation of continuum mechanics models define a deformable body as a continuous collection of material particles, *i. e.* an assignment $X : \mathcal{B} \to \mathbb{R}^3$, where $\mathcal{B}$ is a subset of a topological space (usually, a subset of 3-dimensional Euclidean space; in general, a subset of a n-dimensional manifold in the case of microcontinuum mechanics). The study of continuum/microcontinuum mechanics involves:

(a) the definition of kinematics and the study of deformation and strains,

(b) the study of stress and balance principles (conservation of mass, energy, momentum, etc.),

(c) the study of constitutive theory and the relation between stress and strain (the constitutive equations are what differentiate fluent media from solid media, for example).

(d) the existence, the uniqueness and the properties of the solutions of different continuum problems.

The next two sections present a brief overview for the case of classical continuum mechanics, and then in the following sections present the case in microcontinuum in more detail.

2.3.1 Motion, strain and compatibility equations in continuum mechanics

A solid continuum body is modeled as an open set occupying a 3-dimensional region (for each point in this set, a collection of physical magnitudes such as density, temperature, velocity, exterior force, strain, stress [state], etc. is defined). Each magnitude has its own tensorial type. Thus, density and temperature are scalars (0-tensors), velocity and exterior force are vectors (1-tensors), and strain and stress state are 2-tensors. "Exotic" materials such as liquid crystals, or materials with micro-structure require an n-dimensional region (with $n > 3$ and extra degrees of freedom for describing the orientation and the internal states of the micro-structure). In sake of conceptual clarity and to use a unified approach, all the formulation is presented in terms of manifolds and tensorial equations (a review of the key concepts and definitions about manifolds is given in Appendix B).

Definition 2.3.1. *A **simple body** is an open set $\mathcal{B} \subset \mathbb{R}^3$. A **configuration** of $\mathcal{B}$ is a mapping $\phi : \mathcal{B} \to \mathbb{R}^3$. The set of all configurations of $\mathcal{B}$ is denoted by $\mathscr{C}_{\mathcal{B}}$ (or simply by $\mathscr{C}$). Points in $\mathcal{B}$ are denoted by capital letters.*

A configuration represents a deformed state of the body. As the body moves, a collection of configurations are obtained, depending on time t. The set of
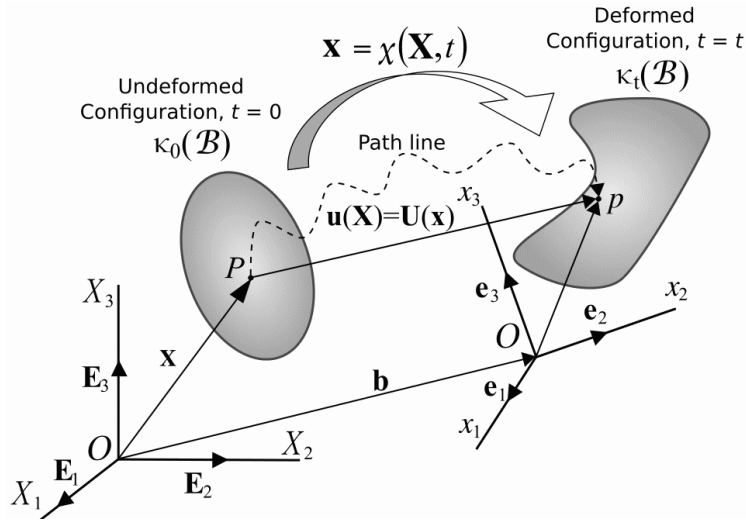
Figure 2.6. A representation of a deformation process in Cartesian coordinates: initial configuration (or undeformed configuration) [*right*], deformed configuration at time t [*left*] . P is the initial position of a material point or particle, and p represents the same particle at the time t. The set of coordinates $\boldsymbol{x}$ is a function of the time t and the initial coordinates $\boldsymbol{X}$. The rôle of the two bases $\{\boldsymbol{E}_1, \boldsymbol{E}_2, \boldsymbol{E}_3\}$ and $\{\boldsymbol{e}_1, \boldsymbol{e}_2, \boldsymbol{e}_3\}$ is explained in appendices (see B.2)

all configurations can be represented by an infinite-dimensional manifold, for example a typical election could be $\mathscr{C}_{\mathcal{B}} \subset \mathrm{Diff}(\mathcal{B})$ (the set of diffeomorphisms, see B.3.5, of $\mathcal{B} \to \mathcal{S}$, where $\mathcal{S}$ is a three-dimensional manifold or simply $\mathbb{R}^3$). A *motion* or continuous deformation in time is defined as a collection of configurations:

Definition 2.3.2. *A* motion *of a simple body* $\mathcal{B}$ *is a curve in* $\mathscr{C}$*; that is, a mapping* $t \mapsto \phi_t \in \mathscr{C}$ *(or some open interval of* $\mathbb{R}$ *to* $\mathscr{C}$*). For* $t \in \mathbb{R}$ *fixed, we write* $\phi_t(X) = \phi(X,t)$*. The map* $\boldsymbol{V}_t : \mathcal{B} \to \mathbb{R}^3$ *defined by:*

$$\boldsymbol{V}_t = \boldsymbol{V}(X,t) = \frac{\partial \phi(X,t)}{\partial t}$$

*(assuming the derivative exists) is called **material velocity** of the motion, and is a vector field over the initial configuration of the body.*

In the same vein, the acceleration can be defined:

Definition 2.3.3. *The **material acceleration** of a motion is defined by:*

$$\boldsymbol{A}_t = \boldsymbol{A}(X,t) = \frac{\partial \boldsymbol{V}(X,t)}{\partial t}$$

(assuming the derivative exists)

Remark For performing the above computation in arbitrary coordinates, we need to use covariant derivatives (see section B.6.2) ■.

Intuitively, a regular motion is one for which nothing "mathematically irregular" like ripping, pinching, or interpretation of matter takes place. We will assume for convenience in all cases that the motions are regular, because some of the commonly encountered physical magnitudes of continuum mechanics are not well defined if ϕ is not regular. We need to highlight that some important physical cases that are not regular (such as contact problems in which $\mathcal{B}$ may consist of two disconnected pieces that ϕ brings together). The velocity and the accelerations can be represented in a different picture by using spatial coordinates (instead of the material coordinates or labels), for this reason, we define spatial velocities and accelerations:

Definition 2.3.4. *Let ϕ_t be a $\mathcal{C}^1$ regular motion of $\mathcal{B}$. The **spatial velocity** of the motion is defined by:*

$$\boldsymbol{V}_t : \phi_t(\mathcal{B}) \to \mathbb{R}^3, \qquad \boldsymbol{v}_t = \boldsymbol{V}_t \circ \phi_t^{-1}$$

*If ϕ_t is a $\mathcal{C}^2$ regular motion, we define the **spatial acceleration** by*

$$\boldsymbol{a}_t : \phi_t(\mathcal{B}) \to \mathbb{R}^3, \qquad \boldsymbol{a}_t = \boldsymbol{A}_t \circ \phi_t^{-1}$$

The velocities and accelerations just defined are true vectors (1-tensor magnitudes) that transform according to the usual rules (see propositions B.2.1 and B.2.2 in appendix B)

Now, our objective is to compare lengths, angles and volumes in the deformed configuration $\phi_t(\mathcal{B}) \subset \mathcal{S}$ of a simple body $\mathcal{B}$ with the initial ones, in the undeformed configuration. We know that lengths, angles, areas and volumes are "metric concepts" that require the use of a *metric tensor* on a Riemann manifold[1]. The Euclidean space with the usual inner product $\mathbb{E}^n = (\mathbb{R}^n, \cdot)$ is the prototypical example of Riemann manifold [with zero curvature]. In the following, we just assume that the space in which a motion takes place is an n-dimensional Riemann

---

[1] A Riemann manifold is a manifod with a metric tensor defined on its tangent bundle, see section B.5

manifold $(\mathcal{S}, \mathbf{g})$ (not necessarily the Euclidean space). Under this assumption, the length of a curve $\mathcal{C} : [a, b] \subset \mathbb{R} \to \mathcal{S}$ is given by the following expression:

$$\text{length}(\mathcal{C}) = \int_a^b \left[g_{ab} \frac{dx^a}{dt} \frac{dx^b}{dt} \right]^{1/2} dt \tag{2.1}$$

where the metric tensor is $\mathbf{g} = g_{ab} \boldsymbol{e}^a \otimes \boldsymbol{e}^b = g_{ab} dx^a \otimes dx^b$ of $\mathcal{S}$ and $\{x^a\}$ is a set of coordinates in $\mathcal{S}$. The angle α between two vectors $\boldsymbol{V} = V^a \boldsymbol{e}_a$ and $\boldsymbol{W} = W^a \boldsymbol{e}_a$ is given by:

$$\cos \alpha = \frac{g_{ab} V^a W^b}{(g_{cd} V^c V^d)^{1/2} (g_{ef} W^e W^f)^{1/2}} = \frac{\langle \boldsymbol{V}, \boldsymbol{W} \rangle}{\|\boldsymbol{V}\| \|\boldsymbol{W}\|} \tag{2.2}$$

The n-volume is defined by the n-form $\mathbf{dv} = \sqrt{g} \, \boldsymbol{e}^1 \wedge \boldsymbol{e}^2 \wedge \cdots \wedge \boldsymbol{e}^n = \sqrt{g} \, dx^1 \wedge dx^2 \wedge \cdots \wedge dx^n$, where $g = \det(g_{ab})$ is the [non-vanishing] determinant of the metric tensor, and $\wedge$ denotes the exterior [antisymmetric] product[2]. Thus, the n-volume of a domain $\mathcal{D} \subset \mathcal{S}$ is given by:

$$\text{volume}(\mathcal{D}) = \int_{\mathcal{D}} \mathbf{dv} = \int_{\mathcal{D}} \sqrt{\det(g_{ab})} \, dx^1 \wedge dx^2 \wedge \cdots \wedge dx^n \tag{2.3}$$

In addition, the area of a curved surface or the m-volumes of an m-submanifold $(m < n)$ in $\mathcal{S}$ can be defined in terms of of the *metric tensor* $\mathbf{g}$. Given the previous definitions, now we can compare deformed lengths with non-deformed lengths; this comparison leads to the strain measures. If we select a coordinate system $\{x^a\}$ in $\mathcal{S}$ and a regular motion ϕ_t, then we can compute the *pull-back* $\phi_t^* \mathbf{g}$ of the metric tensor[3] $\mathbf{g} = g_{ab} dx^a \otimes dx^b$, by means of the *deformation gradient*[4] $\mathbf{F} = T\phi_t$:

$$\begin{aligned} \phi_t^* \mathbf{g} \quad &= \phi_t^* \left(g_{ab} dx^a \otimes dx^b \right) \\ &= g_{ab} \left(F^a{}_A dX^A \right) \otimes \left(F^b{}_B dX^B \right) \\ &= \left(g_{ab} F^a{}_A F^b{}_B \right) dX^A \otimes dX^B \\ &= C_{AB} dX^A \otimes dX^B = \mathbf{C}^\flat \end{aligned} \tag{2.4}$$

---

[2]For the notion of *exterior product*, see definition B.4.3
[3]For the notion of *pull-back*, see section B.3 for the technical details.
[4]For the notion of *deformation gradient*, see definition B.7.1

The (0,2)-tensor $\mathbf{C}^\flat \in T_2^0 \mathcal{B}$ is the *full covariant associated tensor* of the **right Cauchy-Green tensor**[5] (in the above computation, the $F^a{}_A$ are the components of the deformation gradient $\mathbf{F}$). By computing the difference between this tensor and the metric tensor of $\mathcal{B}$, *i.e.* $\mathbf{G} = G_{AB} dX^A \otimes dX^B$, we can define the **material [or Lagrangian] strain tensor**:

$$\mathbf{E}^\flat = E_{AB} dX^A \otimes dX^B = \frac{1}{2}(C_{AB} - G_{AB}) dX^A \otimes dX^B = \frac{1}{2}(\mathbf{C}^\flat - \mathbf{G}) \qquad (2.5)$$

Obviously, $\mathbf{E}^\flat = 0$ implies that $\mathbf{G} = \mathbf{C}^\flat$ and thus, we have no change in shape. The material strain tensor is the most commonly used type of strain tensor, but other alternative tensors are used to characterize the deformed configuration of a body: the deformation gradient $\mathbf{F} = T\phi_t$, the right Cauchy-Green tensor $\mathbf{C}$, the Piola deformation tensor $\mathbf{B}$, the left Cauchy-Green tensor $\mathbf{b}$ (also called the Finger deformation tensor), the [forward] Cauchy tensor $\mathbf{c}$ (also called the Finger tensor or the Piola tensor) and the spatial or Euler-Almansi strain tensor $\mathbf{e}$ (see section for the definition of all these alternative tensors B.7). Notice that not all these tensors are defined on the same tangent bundle[6]: $\mathbf{C}, \mathbf{B}, \mathbf{E} \in T_1^1 \mathcal{B}$ but $\mathbf{c}, \mathbf{b}, \mathbf{e} \in T_1^1 \mathcal{S}$. Notice, in addition, the effect of the $\flat$ isomorphism (see section B.5, for mathematical details). The pull-back and the push-forward can be used to represent the current relations among all these deformation measures (we repeat here the equation B.13):

$$\begin{array}{ll} \mathbf{C}^\flat = \phi^\star(\mathbf{g}), & \mathbf{c}^\flat = \phi_\star(\mathbf{G}), \\ \mathbf{B}^\sharp = \phi^\star(\mathbf{g}^\sharp), & \mathbf{b}^\sharp = \phi_\star(\mathbf{G}^\sharp), \\ \mathbf{E}^\flat = \phi^\star(\mathbf{e}^\flat), & \mathbf{e}^\flat = \phi_\star(\mathbf{E}^\flat). \end{array} \qquad (2.6)$$

Examining the Euclidean case in Cartesian coordinates, it is easy to see why there are four types of possible deformation tensors $(\mathbf{C}, \mathbf{c}, \mathbf{B}, \mathbf{b})$. In this particular case the above equations imply:

$$\begin{array}{ll} \mathbf{C} = \mathbf{F}^T \mathbf{F}, & \mathbf{c} = \mathbf{F}^{-T} \mathbf{F} \\ \mathbf{B} = \mathbf{F}^{-1} \mathbf{F}^{-T}, & \mathbf{b} = \mathbf{F} \mathbf{F}^T. \end{array} \qquad (2.7)$$

We conclude this section with an interesting mathematical question: *Given*

---

[5] For the notion of *full covariant associated tensor*, see definition B.5.2

[6] For the notion of *tangent bundle*, see details in definition B.3.2.

a twice differentiable symmetric positive-definite tensor field $\mathbf{C}^{\flat} \in T_2^0 \mathcal{M}$, *when* $\mathbf{C}^{\flat}$ *is the deformation tensor of a configuration?.* We can answer "locally" the previous question: if certain *compatibility equations* are satisfied, then there is a configuration ϕ such that $\mathbf{C} = \mathbf{F}^T \mathbf{F}$ with $\mathbf{F} = T\phi$. The compatibility equations are:

$$\frac{\partial \Gamma_{IK}^J}{\partial X^L} + \frac{\partial \Gamma_{IL}^J}{\partial X^K} + \Gamma_{IK}^M \Gamma_{ML}^J + \Gamma_{IL}^M \Gamma_{MK}^J = 0, \qquad 1 \le I, J, K, L \le n \qquad (2.8)$$

where

$$\Gamma_{IJ}^K := (C^{-1})^{KL} \Gamma_{ILJ}, \qquad \Gamma_{IKJ} := \frac{1}{2} \left(\frac{\partial C_{IK}}{\partial X^J} + \frac{\partial C_{JK}}{\partial X^I} - \frac{\partial C_{IJ}}{\partial X^K} \right) \qquad (2.9)$$

Interestingly, the compatibility equations are precisely the components of a *Riemann curvature tensor*[7] for the tensor $\mathbf{C}^{\flat}$. This allows to give a quite simple geometrical interpretation to the *compatibility equations*, many textbooks only present the compatibility equation as a technical necessary condition for the integrability of the strain tensor, but such practice disguises the well founded geometrical and natural interpretation of these equations. This geometrical interpretation is formally stated in the following proposition:

Proposition 2.3.1. *Let $\phi : \mathcal{B} \to \mathcal{S}$ be a regular configuration, then:*
(i) *Let $\mathcal{B}$ be an open set in $\mathbb{R}^n$ and $\mathcal{S} = \mathbb{R}^n$. Let $\hat{\mathsf{R}}_{BCD}^A$ be the "curvature tensor" obtained by using the deformation tensor C_{AB} in place of G_{AB}. Then $\hat{\mathsf{R}}_{BCD}^A = 0$.*
(ii) *Let $\mathcal{B}$ be an open set in $\mathbb{R}^n$ and $\mathcal{S} = \mathbb{R}^n$. Let C_{AB} be a given positive-definite symmetric two-tensor whose curvature tensor vanishes: $\hat{\mathsf{R}}_{BCD}^A = 0$. Then given any point $x_0 \in \mathcal{B}$, there is a neighborhood $\mathcal{U}$ of x_0 and a regular map $\phi : \mathcal{U} \to \mathbb{R}^n$ whose deformation tensor is C_{AB}*

▶*Proof*
(i) Comparing the definition of curvature, we can see that $\hat{\mathsf{R}}_{BCD}^A$ is the pull-back of $\mathsf{R}^a{}_{bcd}$, the curvature tensor of $\mathbb{R}^3$. But $\mathsf{R}^a{}_{bcd} = 0$, so $\hat{\mathsf{R}}_{BCD}^A = 0$ as well.
(ii) The hypothesis states that the Riemann manifold $(\mathcal{B}, C_{AB})$ is flat. Thus, in

---

[7]For the notion of *Riemann curvature tensor*, see section B.5

a neighborhood $\mathcal{U}$ of x_0, there is a coordinate system $\chi : \mathcal{U} \to \mathbb{R}^n$ in which the C_{AB}'s are constants. By following χ with a linear transformation $\mathbf{L}$, we can bring C_{AB} into diagonal for δ_{AB}. Let $\phi = \mathbf{L} \circ \chi$. Then $(\phi_* C)_{ab}$ is the Euclidean metric; that is, C_{AB} is the deformation tensor of ϕ. ∎

This latter result show that the manifold approach serves to clarify the true geometrical significance of the compatibility equations.

2.3.2 Stress and balance principles in continuum mechanics

This section presents the dynamical equations of continuum mechanics. To define the concept of stress, we will review the *Stress Principle of Cauchy*. This principle involves the notion of *stress*, a notion originally introduced by Cauchy himself (1823,1827) [12] a century and a half after Newton. According to Cauchy, the stress represents the interaction of a material point with surrounding material in terms of surface contact forces. Following the modern formulations of the Stress Principle of Cauchy, we postulate the existence of a vector field $\boldsymbol{t}(x, t, \boldsymbol{n})$ depending on time t, the spatial point x, a unit vector $\boldsymbol{n}$, and, implicitly, the motion $\phi_t(X)$ itself. Physically, $\boldsymbol{t}(x, t, \boldsymbol{n})$ *represents the force per unit area exerted on a surface element oriented with normal* $\boldsymbol{n}$. We shall call $\boldsymbol{t}$ the *Cauchy stress vector*.

Initially, we shall assume $\mathcal{B}$ is a simple body moving in a space $\mathcal{S} = \mathbb{R}^n$. We shall let ϕ_t be a regular $\mathscr{C}^1$ motion of $\mathcal{B}$ in $\mathcal{S}$, and, as usual, let $\boldsymbol{v}(x, t)$ and $\boldsymbol{V}(X, t)$ be its spatial and material velocities (introduced in the previous section). Let $\rho(x, t)$ be a positive-definite function called *mass density* function (at some points we shall use the "principle of conservation of mass" in the deductions). Finally, we assume that forces other than surface contact forces (tractions) arise form an external force field $\boldsymbol{b}$, an example of which is the gravitational force of the electrical force in a charged continuum. For classical continuum mechanics, we will assume the following Stress Principle of Cauchy:

> **Definition 2.3.5.** *Consider a body $\mathcal{B}$ occupying a region $\phi(\mathcal{B}) \subset \mathcal{S}$ and subject to applied forces represented by the force density $\boldsymbol{b} : \phi(\mathcal{B}) \to T\mathcal{S}$. Assume the existence of continuous and differentiable fields: on scalar field representing mass density $\rho(x, t)$ and one vector field representing the vector stresses $\boldsymbol{t} : \phi(\mathcal{B}) \times S^1 \to T\mathcal{S}$, where $S^1 = \{\boldsymbol{u} \in T\phi(\mathcal{B})|\ \mathbf{g}(\boldsymbol{u}, \boldsymbol{u}) = \|\boldsymbol{u}\|^2 = 1\}$:*

(i) *We say that the **balance of linear momentum** is satisfied provided that for every nice open set $\mathcal{U} \subset \mathcal{B}$*

$$\boxed{\frac{d}{dt} \int_{\phi_t(\mathcal{U})} \rho \boldsymbol{v} \; \mathbf{dv} = \int_{\phi_t(\mathcal{U})} \rho \boldsymbol{b} \; \mathbf{dv} + \int_{\partial \phi_t(\mathcal{U})} \boldsymbol{t} \; \mathbf{da}}$$

where $\boldsymbol{v}$ denotes the spatial velocity field.

(ii) *We say that the **balance of angular momentum** is satisfied provided that for every nice open set $\mathcal{U} \subset \mathcal{B}$:*

$$\boxed{\frac{d}{dt} \int_{\phi_t(\mathcal{U})} \boldsymbol{x} \times \rho \boldsymbol{v} \; \mathbf{dv} = \int_{\phi_t(\mathcal{U})} \boldsymbol{x} \times \rho \boldsymbol{b} \; \mathbf{dv} + \int_{\partial \phi_t(\mathcal{U})} \boldsymbol{x} \times \boldsymbol{t} \; \mathbf{da}}$$

The integral form of momentum balance is subject to an important criticism: it is not form-invariant under *general* coordinate transformations, although the dynamical equations themselves are. Because of these the approach which departs from energy balance as an axiom could be preferable. More specifically, the above balances of momentum explicitly uses the linear structure of $\mathbb{R}^n$ since vector functions are integrated. It is correct to interpret this equation component-wise in Cartesian coordinates z^i but *not* in a general coordinate system. In this sense, the *balances of momentum are not a tensorial postulates*. It can be proven that the balances of momentum follow from an energy principle that does not require $\mathcal{S}$ to be a linear.[8] The following proposition shows that from the above principle we can derive the existence of a stress tensor:

Proposition 2.3.2. *Assume that balance of linear momentum holds, that $\phi_t(X)$ is $\mathscr{C}^1$, and $\boldsymbol{t}(x, t, \boldsymbol{n})$ is a continuous function of all its arguments. Then there is a unique $\binom{2}{0}$ tensor field, denoted by $\boldsymbol{\sigma}$, depending only on x and t such that*

$$\boxed{\boldsymbol{t}(x, t, \boldsymbol{n}) = \langle \boldsymbol{\sigma}(x, t), \boldsymbol{n} \rangle_x}$$

In coordinates $\{x^a\}$ on $\mathcal{S}$, the preceding equation reads

$$t^a(x, t, \boldsymbol{n}) = \sigma^{ac}(x, t) g_{bc} n^b = \sigma^a{}_b n^b$$

---

[8]For relativistic elasticity it is essential to have a basic postulate that is covariant –such as balance of four momentum– and for classical elasticity it is desiderable.

▶*Proof* Let $\boldsymbol{u}_0$ be a vector in $\mathbb{R}^n$. Then

$$\frac{d}{dt} \int_{\phi_t(\mathcal{U})} \rho \langle \boldsymbol{v}, \boldsymbol{u}_0 \rangle \, \mathbf{dv} = \int_{\phi_t(\mathcal{U})} \rho \langle \boldsymbol{b}, \boldsymbol{u}_0 \rangle \, \mathbf{dv} + \int_{\partial \phi_t(\mathcal{U})} \langle \boldsymbol{t}, \boldsymbol{u}_0 \rangle \, \mathbf{da}$$

By *Cauchy's theorem*, there is a vector field $\boldsymbol{c}$ such that $\langle \boldsymbol{t}, \boldsymbol{u}_0 \rangle = \langle \boldsymbol{c}, \boldsymbol{n} \rangle$ [16, 72]. Since $\langle \boldsymbol{t}, \boldsymbol{u}_0 \rangle$ depends linearly on $\boldsymbol{u}_0$, $\boldsymbol{c}$ must also be a linear function of $\boldsymbol{u}_0$, and so defines the required tensor $\boldsymbol{\sigma}$. In Cartesian coordinates, picking $\boldsymbol{u}_0 = \hat{\boldsymbol{i}}_i$ gives a vector field $\boldsymbol{c}^i$ such that $\boldsymbol{t}^i = \langle \boldsymbol{c}^i, \boldsymbol{n} \rangle = n^j \sigma^{ik} \delta_{jk}$, where σ^{ik} are the components of $\boldsymbol{c}^i$. Obviously, $\boldsymbol{\sigma}$ is uniquely determined. ∎

The tensor whose existence is asserted in the above theorem is called the **Cauchy stress tensor** $\boldsymbol{\sigma} = \sigma^{ab} \, \boldsymbol{e}_a \otimes \boldsymbol{e}_b = \sigma^{ab} \, (\partial/\partial x^a) \otimes (\partial/\partial x^b)$ (where $\{x^a\}$ is a coordinate system over $\mathcal{S}$). And the tensor with components $\sigma^a{}_b$ is the associated tensor to $\boldsymbol{\sigma}$ of type $(1,1)$. In addition we define the **first Piola-Kirchhoff stress tensor P** is the two-point tensor obtained by performing a Piola transformation of the tensor $\boldsymbol{\sigma}$. In coordinates:

$$\boxed{P^{aA} = J(\mathbf{F}^{-1})^A{}_b \sigma^{ab}} \tag{2.10}$$

Here $\mathbf{P} = P^{aA} \, \boldsymbol{e}_a \otimes \boldsymbol{E}_A$ is a function of (X, t) and σ^{ab} is evaluated at (X, t), where $x = \phi(X, t)$.

It can be proven that the balance of linear moment in 2.3.9 can be written in terms of the first Piola-Kirchhoff stress tensor:

$$\frac{d}{dt} \int_{\mathcal{U}} \rho_0 \boldsymbol{V} \, \mathbf{dV} = \int_{\mathcal{U}} \rho_0 \boldsymbol{B} \, \mathbf{dv} + \int_{\partial \mathcal{U}} \langle \mathbf{P}, \boldsymbol{N} \rangle \, \mathbf{dA} \tag{2.11}$$

where $\boldsymbol{B}(X, t) = \boldsymbol{b}(x, t)$, ρ_0 is the mass density in the material configuration, $\langle \mathbf{P}, \boldsymbol{N} \rangle = P^{aA} N_A$, $\boldsymbol{V}$ is the material velocity and $\mathbf{dV} = \det(G_{AB})^{1/2} \, dX^1 \wedge \cdots \wedge dX^n$ is the n-volume form in the material configuration. The last expression is called *balance of linear momentum in material configuration*. Both forms of balance of linear momentum (material and spatial) can be written locally in differential form, as the following proposition shows:

Proposition 2.3.3. *Assuming: (a) that the balance of linear momentum in integral form holds, (b) the conservation of mass holds, (c) the functions involved are differentiable then the following differential equations hold:*

$$\boxed{\rho \dot{\boldsymbol{v}} = \rho \boldsymbol{b} + \mathrm{div} \boldsymbol{\sigma}}$$

where $(\mathrm{div}\boldsymbol{\sigma})^a = \sigma^{ab}{}_{|b}$. *In general coordinates* $\{x^a\}$, *the above equation can be written as follows:*

$$\rho\left(\frac{\partial v^a}{\partial t} + v^b\frac{\partial v^a}{\partial x^b} + \gamma^a_{bc}v^bv^c\right) = \rho b^a + \frac{\partial\sigma^{ab}}{\partial x^b} + \sigma^{ac}\gamma^b_{cb} + \sigma^{cd}\gamma^a_{cb}$$

In terms of the first Piola-Kirchhoff tensor the local differential equation representing the balance of linear momentum is:

$$\boxed{\rho_0\boldsymbol{A} = \rho_0\boldsymbol{B} + \mathrm{DIV}\mathbf{P}}$$

where $\boldsymbol{A}$ *is the material acceleration and* DIV *is the divergence operator in the material coordinates* $\{X^A\}$.

This proposition is a direct consequence of the *Reynolds' transport theorem* [72]. In this section we have found that the general notion of stress can be represented by two types of tensors the Cauchy stress tensor, and the first Piola-Kirchhoff stress tensor, but as in the case of strain there are other possibilities such defined in the next proposition:

Definition 2.3.6. *The* **Second Piola–Kirchhoff stress tensor** $\mathbf{S}$ *is obtained by pull-back by* ϕ_t *of the mixed tensor* $\mathbf{P} = P^{aB}\,(\partial/\partial x^a)\otimes(\partial/\partial X^B)$. *In coordinates:*

$$S^{AB} = (F^{-1})^A{}_a P^{aB} = J(F^{-1})^A{}_a(F^{-1})^B{}_b\sigma^{ab}, \qquad \mathbf{S} = J\mathbf{F}^{-1}\boldsymbol{\sigma}\mathbf{F}^{-T}$$

The **special convected stress tensor** $\tilde{\mathbf{T}}$ *is the pull-back of the associate tensor* $\boldsymbol{\sigma}^\flat$. *In components:*

$$\tilde{T}_{AB} = JF^a{}_A\sigma_{ab}F^b{}_B, \qquad \tilde{\mathbf{T}} = J\mathbf{F}^T\boldsymbol{\sigma}\mathbf{F}$$

Finally the **Kirchhoff stress tensor** *is defined by* $\boldsymbol{\tau} = J\boldsymbol{\sigma}^\flat$. *In coordinates:*

$$\tau_{ab} = Jg_{ac}g_{bd}\sigma^{cd}$$

The relation among deformation tensors and stress tensors is summarized in the table 2.1.

Table 2.1. Deformation tensors and Stress tensors.

Stress tensors		Energy conjugate deformation tensors	
Material	Spatial	Material	Spatial
$\mathbf{S}$ $= J\phi^\star\boldsymbol{\sigma}$	$\boldsymbol{\sigma}$	$\mathbf{C}^\flat$ $= \phi^*\mathbf{g}$	$\mathbf{g}$
$\tilde{\mathbf{T}}$ $= \phi^*\boldsymbol{\tau}^\flat$	$\boldsymbol{\sigma}^\flat$ $= J^{-1}\boldsymbol{\tau}$	$\mathbf{B}^\sharp$ $= \phi^*\mathbf{g}^\sharp$	$\mathbf{g}^\sharp$
$\mathbf{S}$	$\boldsymbol{\sigma}$ $= J^{-1}\phi_*\mathbf{S}$	$\mathbf{G}$	$\mathbf{c}^\flat$ $= \phi_*\mathbf{G}$
$\tilde{\mathbf{T}}$	$\boldsymbol{\sigma}^\flat$	$\mathbf{G}^\sharp$	$\mathbf{b}^\sharp$ $= \phi_*\mathbf{G}^\sharp$
Mixed		Mixed	
$\mathbf{P}$		$\mathbf{F}$	

2.3.3 Introduction to microcontinuum mechanics

Microcontinuum mechanics is a generalization of the ordinary continuum mechanics (classical continuum mechanics) [72]. Microcontinuum mechanics is a type of *generalized continuum* mechanics that allows to incorporate some effects of characteristic lengths of the materials micro-structure into constitutive modeling [24, 37]. In the last decades, the use of the microcontinuum approach has become more popular and currently suitable variational formulations for Finite Element Method (FEM) have been developed [34]. This dissertation describes some notable findings in the field of biomechanics using FEM and microcontinuum approach. For instance, it seems that a micropolar material has better resistance to the propagation of a crack in a fragile material. In particular, bones seem to take advantage of these properties [3, 42, 95]. This section reviews the main characteristics of microcontinuum mechanics.

Most principles of classical continuum mechanics remain valid in microcontinuum mechanics. For example, the assumption of local action (meaning that stress at a point depends only on quantities defined at that point) remains valid in both classical continuum mechanics and microcontinuum mechanics. For defining a microcontinuum medium, the *classical Cauchy* continuum can be enhanced by introducing 3 rotational degrees of freedom, which leads to the *Cosserat mechanics*, very earlier introduced by the Cosserat brothers in 1909 [19]. By adding even

more degrees of freedom, more general microcontinuum media can be defined (see table 2.2). A comprehensive account of the mechanics of higher order continua can be found in the references [31]. Thus, we can construct a hierarchy:

- **Cauchy continuum**, the type of continuum used in classical continuum mechanics without extra degrees of freedom. There are only three degrees of freedom: the three usual translation degrees of freedom (see for example [105]).

- **Microdilatation continuum**, the type of continuum in which micro-structure can only undergo micro-volume changes. It is the cheapest model in terms of degrees of freedom, with only one additional degree of freedom with respect to classical continuum mechanics (see [101]).

- **Micropolar continuum**, the type of continuum that appears in the Cosserat theory (see for example [31]). It is the most extensively used model of microcontinuum type.

- **Microstretch continuum**, an intermediate type, combining Cosserat effects and micro-volume changes, i. e. rotation and stretch of the micro-structure, which was proposed by Eringen (1990) in order to limit the number of additional degrees of freedom (see [30]). This is the main type of continuum use in this dissertation.

- **Microstrain continuum**, the type in which the micro-structure is representable by a parallelogram formed by the triad of (micro-)vectors that change in form, but can not rotate. The full micromorphic theory can be seen as the combination of the micropolar and microstrain theories.

- **Micromorphic continuum**, the type of continuum where the underlying micro-structure at a material point can rotate and be deformed. Therefore, it has 9 additional degrees of freedom. The micro-structure evolution is represented by the deformation of a triad of vectors. (see [32, 74])

The description of all these higher order continua is usually based on the first gradient theory (as it happens with classical continuum mechanics), meaning that the first gradient of all degrees of freedom is supposed to play a rôle in the material response.

Table 2.2. The hierarchy of higher order continua.

Continuum type	Number of DoF	DoF	Magnitude type	Reference
Cauchy	3	$\boldsymbol{u}$	$\mathbb{R}^3$	Truesdell & Toupin (1960)
Microdilatation	4	$\boldsymbol{u}, j$	$\mathbb{R}^3, \mathbb{R}$	Forest & Sievert (2006)
—	5			—
Micropolar	6	$\boldsymbol{u}, \mathbf{R}$	$\mathbb{R}^3, \mathbf{SO}(3)$	Cosserat & Cosserat (1909)
Microstretch	7	$\boldsymbol{u}, \mathbf{R}, j$	$\mathbb{R}^3, \mathbf{SO}(3), \mathbb{R}$	Eringen (1990)
Incompressible Microstrain	8	$\boldsymbol{u}, \mathbf{K}$	$\mathbb{R}^3, \mathbf{SL}(3)$ $\mathbf{K}$ symmetric	Forest & Sievert (2006)
Microstrain	9	$\boldsymbol{u}, \mathbf{K}$	$\mathbb{R}^3, \mathbf{GL}(3)$ $\mathbf{K}$ symmetric	Forest & Sievert (2006)
—	10			—
Incompressible Micromorphic	11	$\boldsymbol{u}, \mathbf{K}$	$\mathbb{R}^3, \mathbf{SL}(3)$	
Micromorphic	12	$\boldsymbol{u}, \mathbf{K}$	$\mathbb{R}^3, \mathbf{GL}(3)$	Mindlin (1964), Eringen (1999)

The choice of the proper higher order model for a given material depends on the relevant microscopic deformation mechanism. The Cosserat is well-suited for granular media made of constituents that can rotate independently from the macromotion [79]. This continuum model is also appropriate for the description of materials with a bending-stiff substructure, like reinforcements of composites. However, in porous media like soils, polymers and metal foams, the rotation of cells is not the unique deformation mode so the full micromorphic theory is required. The micromorphic approach was also used recently in the case of the deformation of crystals [47]. A good trade-off in terms of numerical efficiency and precision of microstructure description is to use the microstretch approach, as done in soft biomaterials [95]. The mechanics of higher order continua is especially relevant to address nonlinear phenomena like large deformations and nonlinear behavior. Geometrically nonlinear formulations of the micropolar, micromorphic and microstretch theories are available since the early 1970s.
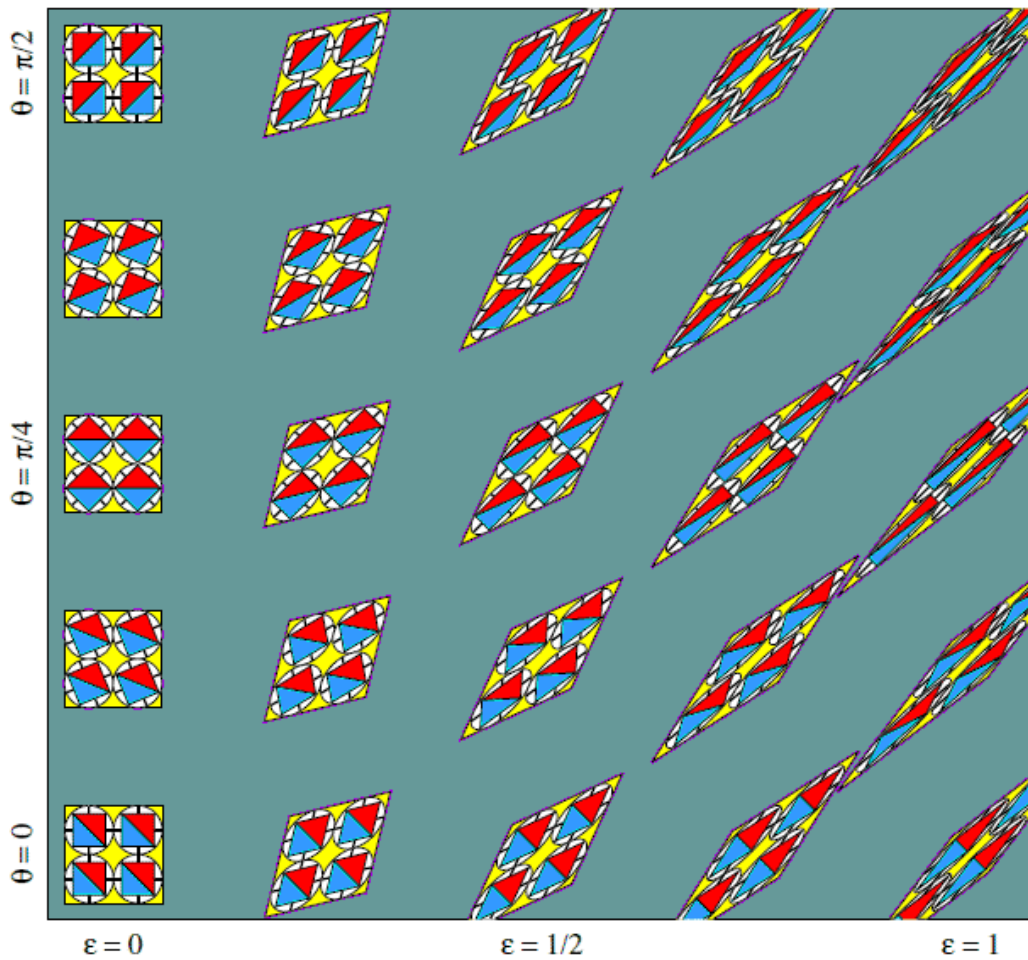
Figure 2.7. Representation of different planar deformations in a micropolar continuum. In the horizontal axis the parameter ε is the shear and in the vertical axis the parameter θ is the micropolar angle rotated by the micro-structure, here the micro-structure are the red/blue squares (after Tarantola, 2006) [102].

2.3.4 Experimental results supporting microcontinuum theories

The main goals of any physical theory (or scientific model) is to explain adequately the experimental data, offer a good representation of empirical phenomena, and make correct predictions. Although in many practical situations the predictions of classical continuum mechanics seem to be in good accordance with data, the microcontinuum mechanics predicts new phenomena that have been verified experimentally.

This section summarizes some relatively new experimental results that confirm the utility and suitability of microcontinuum mechanics in materials where microstructure is present. The current evidences justify the increasing use of this microcontinuum approach in biomechanics (and other areas).

One impressive success of micropolar theory is the prediction of two "optical branches" (TO and LO) or modes of elastic waves present in certain crystalline materials, such as ferroelectric crystals. Micropolar effects become important in high-frequency and short wavelength regions of waves. In order to display these effects and the new physical phenomena predicted, some researchers studied the dispersion of plane harmonic elastic waves in isotropic solids.

Figure 2.8. Dispersion relations for different types of planar waves. The acoustic modes (LA, TA) are predicted by classical elasticity, but the observed optical modes (LO, TO) are not predicted by means of classical elasticity (after Chen, 2004) [14].

This also provided a base for experimental observations of the relevancy and necessity of micropolar theory in such contexts. According to the experimental findings and the micropolar elasticity, four different wave propagating modes exist with four different phase velocities for plane harmonic waves. The dispersion

curves show that two modes are scalar waves and the other two are coupled vector waves. Longitudinal and transversal acoustic branches are also predicted by classical elasticity, but the other two (a longitudinal optic branch LO and a transversal optic branch TO are the two new branches that fall outside the domain of classical elasticity). The fact that these new optical branches are also observed in phonon dispersion experiments has been crucial for the acceptance of micropolar elasticity. Obviously the new optical branches are due to additional degrees of freedoms not present in all crystalline solids.
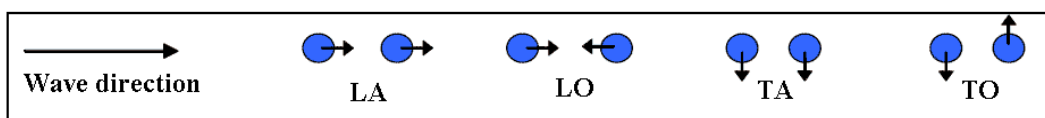
Figure 2.9. Schematic representation of longitudinal and transversal, optical and acoustic modes of propagation (after Chen, 2004) [14].

Other interesting case in biomechanics is the stress concentration around cracks or holes. It is long suspected that the osteons are involved in the stress concentration reduction in order to avoid the propagation of cracks. A primary mechanism for the stress concentration reduction appears to be the softening by embedding it in a compliant region; and a reinforcing ring that increases the stiffness, and the presence of a ring of lamellar bone along the foramen inside edge, which might serve to reduce the chance of cracks forming there [44]. An early work that studied the possibility of using the micropolar theory for describing the microstructure around osteons is Yang (1982) [113], this study found size effects in quasi-static bending of compact bone. The effects seem consistent with micropolar theory. A similar study is that of Rosenberg (2003) who studied the stress concentration around circular holes (mechanically an osteon present a hole in its center) by means of micropolar theory [95]. A well know result of classical elasticity is that the stress concentration factor around a circular hole is $K_\sigma = 3$, but micropolar elasticity predicts lower stress concentration around a circular hole (see figure 2.10), being K_σ a function of R/c, being R the radius of the hole and $c = \sqrt{\gamma(\mu + \kappa)/\kappa(2\mu + \kappa)}$ a characteristic length associated to the microstructure (μ is the second Lamé coefficient and the remaining κ, γ are additional moduli occurring in the constitutive linear equations used).

As a last example we will cite the work of Goda *et. al* (2012) which explains how to model a biological tissue with a regular random microstructure by means of an homogeneous microcontinuum model [42]. The use of homogeneous materials
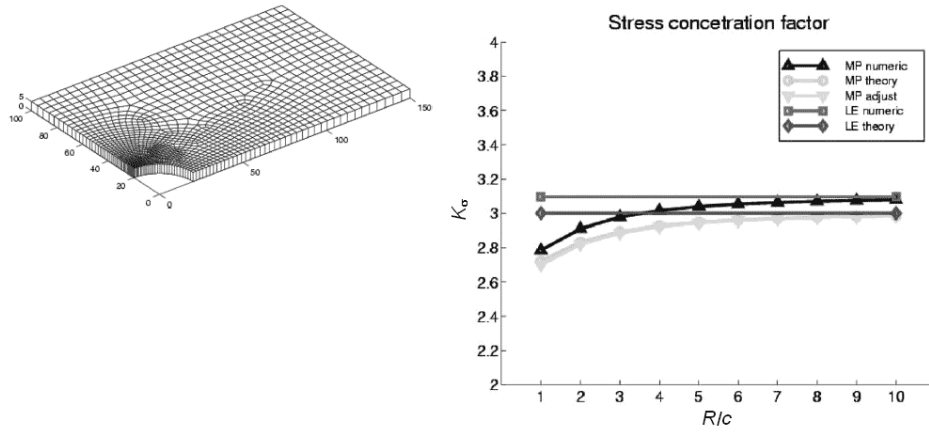
Figure 2.10. Stress concentration factor around a circular hole, according to linear elasticity theory and micropolar elasticity theory (after Rosenberg, 2003) [95].

that take into account the microstructure allows to treat these materials from a macroscopic point of view.
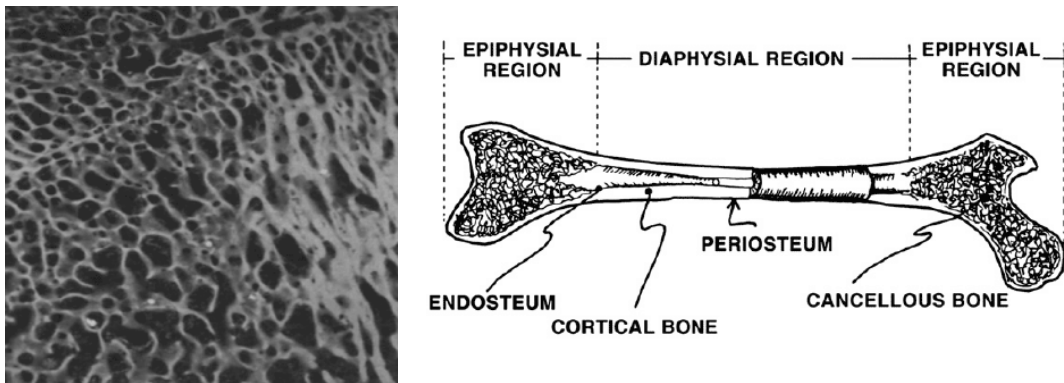
Figure 2.11. (after Cowin and Doty, 2007) [20].

If we take a look at the trabecular structure or the cancellous bone tissue, as in figure 2.11, it is clear that in addition to the Euclidean displacement the reorientation of the porous microstructure needs to be represented.

Goda and co-researchers tried to use a micropolar model. They studied linear plane strain problems and considered the bone as the microcontinuum limit of a set of unit cells (a typical cell is shown in figure 2.12). They modeled each solid part as a Timoshenko beam and related the displacements and gyrations with the forces and torques existing at the nodes of the unit cell. Then, using the classical matrix method of rigidity and the homogenization procedure of Dos Reis for periodical media [25, 26], the authors obtained the following constitutive equation:
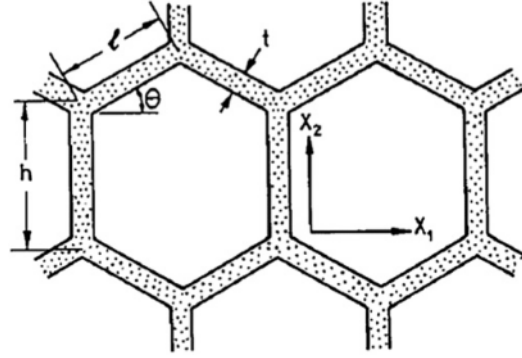
Figure 2.12. Periodical unit cell arrangement used for representing the random structure of cancellous bone, the geometric parameters h, ℓ, t, θ are related to the elastic constants of the micropolar model (after Goda *et al.*, 2012) [42].

$$
\begin{bmatrix} \sigma_{xx} \\ \sigma_{yy} \\ \sigma_{xy} \\ \sigma_{yx} \\ \mu_{xz} \\ \mu_{yz} \end{bmatrix} = \begin{bmatrix} K_{11} & K_{12} & 0 & 0 & 0 & 0 \\ K_{21} & K_{22} & 0 & 0 & 0 & 0 \\ 0 & 0 & K_{33} & K_{34} & 0 & 0 \\ 0 & 0 & K_{43} & K_{44} & 0 & 0 \\ 0 & 0 & 0 & 0 & K_{55} & 0 \\ 0 & 0 & 0 & 0 & 0 & K_{66} \end{bmatrix} \begin{bmatrix} \varepsilon_{xx} \\ \varepsilon_{yy} \\ \varepsilon_{xy} \\ \varepsilon_{yx} \\ \kappa_{xz} \\ \kappa_{yz} \end{bmatrix} \tag{2.12}
$$

where the σ_{ij} are components of the stress tensor (not symmetric in the micropolar case $\sigma_{xy} \neq \sigma_{yx}$), the μ_{ij} are components of the couple stress tensor, the ε_{ij} components of the macrostrain tensor, and the κ_{ij} are components of the microstrain tensor. The constants K_{ij} are functions of the microscopic elastic moduli E_m, G_m (used for modeling the Timoshenko beams) and the geometric parameters h, ℓ, t, θ. Goda *et al.* compared the results of stress distribution for this mircropolar continuum across the cracks with the corresponding distribution obtained for a Cauchy continuum. A significant stress concentration reduction was observed for the micropolar medium (a reduction of 50.7% for the normal stress $\sigma = S_{11}$, and a 39.2% for the tangent stress $\tau = S_{12}$, the distribution for S_{11} is shown in figure 2.13). This suggest that bones reduce fragility by the presence of micro-structure.
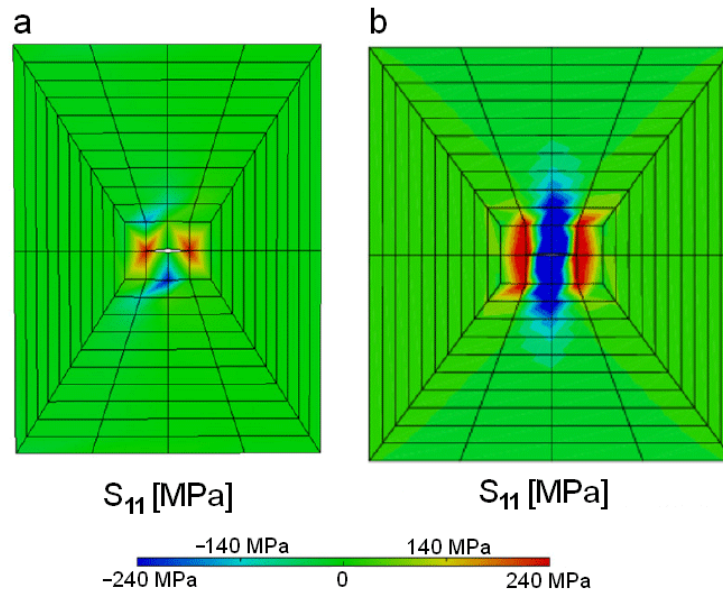
Figure 2.13. Simulation of a planar stress problem: a square with a small crack in the center. Uniform traction forces perpendicular to direction are applied on the upper and lower sides of the square. The figure shows the stress distribution of S_{11} of (a) a micropolar medium and (b) a classical Cauchy medium (based on Goda *et al.*, 2012) [42].

2.3.5 Motion, strain and compatibility equations in microcontinuum mechanics

We start this section explaining the *physical picture* associated to microcontinuum theory. In the atomic scale, crystalline solids possess primitive cells in the form of geometrical structures (lattice structures) like cubes, hexagons, etc. For example, cesium chloride (CsCl) has a cubic structure with Cs^+ located at the center of the cube and Cl^- at the eight corners of the cube (see figure 2.14). This spatial distribution of atoms of different masses allows new modes of propagation of elastic mechanic waves. The additional degrees of freedom need to be incorporated for the elastic problem where the

Figure 2.14. Cubic strcutre of a cell of Cesium Chloride

typical length scale is comparable with the microstrucutre. In biological tissues,

33

$$\mathbf{x} = \phi(\mathbf{X}, \Xi, t)$$

Undeformed
configuration
$\kappa_0(\mathcal{B})$

Q

Ξ

P

$\mathbf{X}'$

X_3

$\mathbf{X}$

$\mathbf{x}'$

$\mathbf{x}$

O

X_2

X_1

q

ξ

p

Deformed
configuration
$\kappa_t(\mathcal{B})$
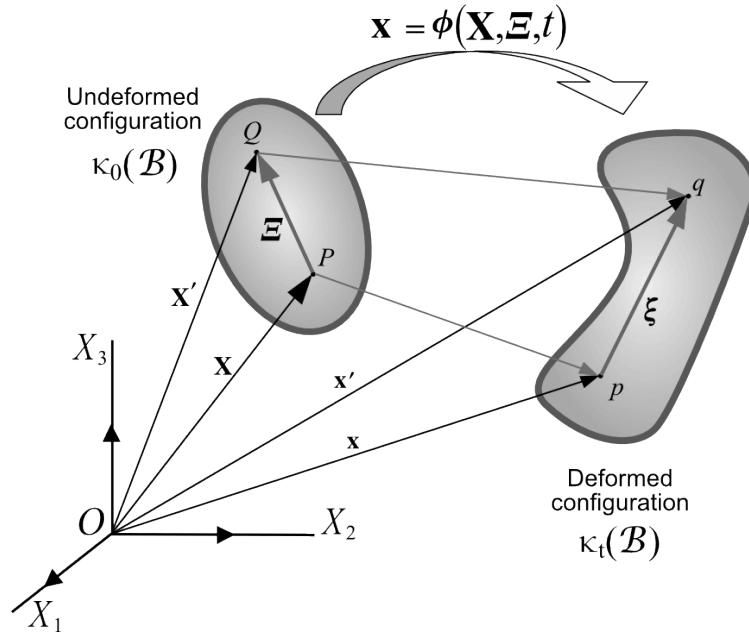
Figure 2.15. A representation of a deformation of a microparticle of a microcontinuum medium: initial configuration (or undeformed configuration) [*right*], deformed configuration at time t [*left*] . P is the initial position of the centroid of a microparticle (a material point with microstructure), and p represents the same point after at the time t (macrodeformation). Q is another point insider the microparticle (Ξ is a tangent vector of $T_X\hat{\mathcal{B}}$, after the microdeformation the of the microparticle the same point will be q (the vector Ξ changes to ξ). The coordinates $(\boldsymbol{x}, \xi)$ are a function of time t and the initial coordinates $(\boldsymbol{X}, \Xi)$.

micro-mechanically we observe fibers and discrete microstructures inside the tissues, if these microstructures show an organized arrangement new additional degrees of freedom for describing the relative motion of these microstructures are needed. In addition, there are fluids with oriented molecules, for example, the liquid crystals used in many technological applications (most contemporary electronic displays use liquid crystals.). The liquid crystals possess dipolar elements in the form of short bars and platelets. The classical example, p-azoxyanisole (PAA) is composed of rigid bars of length approximately Å.

The following formulation was partially based on Eringen [31], although this author presented the theory for $\mathbb{R}^3$. Here a first attempt to present the theory in the manifold approach. This allows to identify and properly formulate the objects of the theory as mappings over the tangent bundle of a manifold (being the dots the position of particles and the additional degrees of freedom elements

of a vector bundle). In this sense, this exposition goes a little beyond the cited source.

A solid microcontinuum body can be modeled as an open set of a the tangent bundle (see for a definition), this implies that locally the a solid can be seen as a set $\mathcal{U} \times \mathbb{R}^3$, where $\mathcal{U}$ is an open set of a 3-dimensional manifold (all tensorial physical magnitudes are defined over this tangent bundle):

Definition 2.3.7. *A **microcontinuum body** is an open set $\hat{\mathcal{B}} = T\mathcal{B} \approx \mathcal{B} \times \mathbb{R}^3$, where $\mathcal{B}$ is a simply body. A **configuration** of $\hat{\mathcal{B}}$ is a mapping $\phi : \hat{\mathcal{B}} \to \mathrm{Lin}(\mathcal{S})$ (where $\mathrm{Lin}(\mathcal{S})$ is the linear bundle of $\mathcal{S}$, a 3-dimensional manifold, see B.8.1, usually one has $\mathcal{S} = \mathbb{R}^3$). The set of all configurations of $\hat{\mathcal{B}}$ is denoted by $\hat{\mathscr{C}}_{\hat{\mathcal{B}}} = \mathscr{C}_{\mathcal{B}} \times \mathbf{GL}^+(n)$ (or simply by $\hat{\mathscr{C}}$), i.e. the product of the set of simply body configurations $\mathscr{C}_{\mathcal{B}}$ with the set of linear invertible mappings for describing the microstrucre. Points in $\hat{\mathcal{B}}$ are denoted by pairs, formed by a capital Latin letter and a capital Greek letter, e.g. (X, Ξ).*

Given the fact that the microstructure is microscopic in relation to the dimensions of the body, the microstructure is represented only by vectors in a neighborhood of the origin of coordinates of the tangent space at the point. For these reasons, the deformation of the microstructure has ben represented by an invertible linear transformation, *i.e.* a member of the General Linear group $\mathbf{GL}(3)$. More specifically, the deformation of the microstructure is a member of a connected Lie subgroup $\mathbf{GL}^+(3)$ with positive determinant . The following definition, analogous to definition 2.3.2, takes into account this latter restriction:

Definition 2.3.8. *A **motion** of a microcontinuum body $\hat{\mathcal{B}}$ is a curve in $\hat{\mathscr{C}}$; that is, a mapping $t \mapsto \hat{\phi}_t \in \hat{\mathscr{C}}$ (or some open interval of $\mathbb{R}$ to $\hat{\mathscr{C}}$). For $t \in \mathbb{R}$ fixed, we write $\hat{\phi}_t(X) = (\phi(X, t), \chi(X, \Xi, t))$, where $\chi(X, \cdot, t)$ is an invertible linear map in $\mathscr{L}(T_{(X, \Xi)}\hat{\mathcal{B}})$, the only restriction on $\phi(X, t)$ is to be regular. The map $(\boldsymbol{V}_t, \boldsymbol{\beta}_t) : \hat{\mathcal{B}} \to \mathbb{R}^3 \times \mathbb{R}^3$ defined by:*

$$\boldsymbol{V}_t = \boldsymbol{V}(X, t) = \frac{\partial \phi(X, t)}{\partial t}, \qquad \boldsymbol{\beta}_t = \nu_b^a \chi_c^b \Xi^c \frac{\partial}{\partial x^a}$$

(the velocity is well defined if ϕ_t regular and if $\chi \in \mathbf{GL}(3)$, the vector $\boldsymbol{V}_t$ is called [translational] material velocity *of the motion, and is a vector field over the initial configuration of the body. The 2-tensor $\boldsymbol{\nu} = \nu_b^a dx^b \otimes \frac{\partial}{\partial x^a}$ is called microgyration tensor:*

$$\nu_b^a = \dot{\chi}_A^a (\chi^{-1})_b^A$$

If we consider "partial" coordinates (x, ξ) over the deformed configuration, the motion can be represented as:

$$\begin{cases} x^a = \phi^a(\boldsymbol{X}, t) \\ \xi^a = \chi^a(\boldsymbol{X}, \boldsymbol{\Xi}, t) = \chi_b^a(\boldsymbol{X}, t)\Xi^b \end{cases} \tag{2.13}$$

Then the x^a and ξ^a can be considered as real functions over the manifold $\hat{\mathcal{B}}$. These coordinates allow to rewrite the velocity field simply as $V^a = \dot{x}^a$ and the mycrogiration tensor is characterized by $\dot{\xi}^a = \nu_b^a \xi^b$ [9]. In addition, it is easy to see that the exterior derivatives dx^a and $d\xi^a$ represent the (co)vectors of three-dimensional spaces then one can consider the function:

$$\pi^{(0)} : T_P^* \hat{\mathcal{B}} \to \mathbb{R}^3$$

$$(dx^a, d\xi^a) \mapsto \left(\frac{dx^a}{dZ^j} + \frac{d\xi^a}{dZ^j} \right) \hat{\boldsymbol{i}}_j$$

This means that the increments in the position x of a point, and the other degrees ξ can be added, *i.e* this is the recognition that the total velocity of the microstructure is the translational velocity (macrovelocity) and the local rate of change (microvelocity). This latter composition is possible because the cotangent bundle $T^* \hat{\mathcal{B}}$ is a *trivial bundle* isomorphic to the product manifold $\hat{\mathcal{B}} \times \mathbb{R}^6$ (that is the cotangent space $T_{(X,\Xi)}^* \hat{\mathcal{B}} = \mathbb{R}^3 \oplus \mathbb{R}^3$ in a point (X, Ξ), *i. e.* the direct sum of two copies of the three dimensional space, that allows to define the function $\pi^{(0)}$).

$$d\boldsymbol{Z} = d\boldsymbol{x} + d\boldsymbol{\xi} = d\boldsymbol{x} + d(\boldsymbol{\chi}_K \Xi^K) \in \pi_{(X,\Xi)}^{(0)}(T_{(X,\Xi)}^* \hat{\mathcal{B}}),$$

$$dZ^a = \frac{\partial x^a}{\partial X^K} dX^K + \chi_K^a d\Xi^K + \frac{\partial \chi_J^a}{\partial X^K} \Xi^J dX^K$$

Using the abbreviated notation $\{\cdot\}_{|A} = \partial(\cdot)/\partial X^A$ we have:

---

[9]The linear aplication with matrix components ν_a^b can be interepted as an element of Lie algebra of $\mathbf{GL}(3)$, that is, $\boldsymbol{\nu} \in \mathfrak{gl}^+(3)$

$$dZ^a = x^a_{|K}dX^K + \chi^a_K d\Xi^K + \chi^a_{J|K}\Xi^J dX^K \tag{2.14}$$

Note that the above expression can be rewrite as $dZ^a = \hat{F}^a_B dX^B + \chi^a_C d\Xi^C$. For a particular point the components $\hat{F}^a_B$ and χ^a_C can be put together for assembling a 3×6 matrix $\tilde{\mathbf{F}} = [\hat{F}^a_B|\chi^a_C]$. Taking the Z^a as Cartesian coordinates we can assemble the metric tensor:

$$
\begin{aligned}
g = \delta_{ab}dZ^a \otimes dZ^b = \quad & [x^a_{|A}x_{a|B} + 2(x^a_{|A}\chi_{aC|B} + x^a_{|B}\chi_{aC|A})\Xi^C + \ldots \\
& \cdots + \chi^a_{C|A}\chi_{aD|A}\Xi^C\Xi^D]dX^A \otimes dX^B + \ldots \\
& \cdots + (x^a_{|A} + \chi_{aL} + \chi^a_B\chi_{aC|A})(dX^A \otimes d\Xi^B + \ldots \\
& \cdots + d\Xi^A \otimes dX^B) + \chi^a_A\chi_{aB}d\Xi^A \otimes dX^B)
\end{aligned}
\tag{2.15}
$$

The notation $_{|A}$ is used for the components of derivatives (see the end of section B.6.2). Although we have mentioned the Cartesian coordinates the final expression remains valid in any coordinate system. The components of this metric tensor provide the strain measures needed for a microcontinuum theory. If the same computation is done for a continuum theory only $\chi^a_B = 0$ and the only surviving term is the right Cauchy-Green $C_{AB} = x^a_{|A}x_{a|B} = g_{ab}x^a_{|A}x^b_{|B}$ (see [16, 105]). But microcontinuum is a more general theory and two other strain measures are needed, according to the last expression:

$$\hat{K}_{AB} := g_{ab}\frac{\partial x^a}{\partial X^A}\chi^b_B = x^a_{|A}\chi_{aB}, \qquad \hat{\Gamma}_{ABC} := g_{ab}\frac{\partial x^a}{\partial X^A}\frac{\partial \chi^b_B}{\partial X^C} = x^a_{|A}\chi_{aB|C} \tag{2.16}$$

(where we have used g_{ab} for the components of the metric tensor, if we use Euclidean coordinates $g_{ab} = \delta_{ab}$). Using these measures of strain the equation 2.15 can be rewritten as:

$$
\begin{aligned}
g = \quad & [C_{AB} + 2\Xi^C\hat{\Gamma}_{ABC} + \Xi^C\Xi^D\hat{\Gamma}_{ECB}\hat{\Gamma}_{FDA}(C^{-1})^{EF}]dX^A \otimes dX^B + \ldots \\
& \cdots + [\hat{K}_{AB} + \Xi^C\hat{K}_{DB}\hat{\Gamma}_{FCA}(C^{-1})^{DF}](d\Xi^A \otimes dX^B + dX^A \otimes d\Xi^B) + \ldots \\
& \cdots + \hat{K}_{CA}\hat{K}_{DB}(C^{-1})^{CD}d\Xi^A \otimes d\Xi^B
\end{aligned}
\tag{2.17}
$$

Thus, the change of length can be accounted for in terms of the three strain measures $\mathbf{C}, \hat{\mathbf{K}}, \hat{\mathbf{\Gamma}}$. For the undeformed configuration one has:

$$C_{AB} = \hat{K}_{AB} = \delta_{AB}, \qquad \hat{\Gamma}_{ABC} = 0$$

The set of strain measures $\mathbf{C}, \hat{\mathbf{K}}, \hat{\mathbf{\Gamma}}$ form a complete set, but there are some other possibilities. Eringen [31, p. 15] recommends this other set of measures:

$$D_{AB} := x_{|A}^a (\chi^{-1})_{Ba}, \quad K_{AB} := \chi_A^a \chi_{aB}, \quad \Gamma_{ABC} := (\chi^{-1})_A^a \chi_{aB|C} \tag{2.18}$$

The set $\mathbf{D}, \mathbf{K}, \mathbf{\Gamma}$ is also a complete set that leads to somewhat simpler results, particularly in the constitutive equations. We will call these tensors: the *macrodeformation tensor* (or Cosserat deformation tensor), the *microdeformation tensor*, and the *wryness tensor*.

Particularization The above equations are valid for the most general type of microcontinuum theory. For micropolar, microdilatation, microstretch and microstrain theories (being particular cases of micromorphic continuum) some simplifications can be made. Here we center our attention in micropolar and microstretch cases. A **microstretch continuum** is a microcontinuum continuum, if the angles between two pair of directors remain unchanged, mathematically this implies:

$$(\chi^{-1})_a^A = \frac{1}{j^2} \chi_A^a \tag{2.19}$$

Where $j = \det \chi_A^a = 1/\det(\chi^{-1})_a^A$ and consequently we have:

$$\chi_A^a \chi_b^A = j^2 \delta_b^a, \qquad \chi_A^a \chi_a^B = j^2 \delta_A^B$$

A **micropolar continuum** continuum is a microstretch $j = 1$. For a microstretch continuum the deformation tensors satisfy:

$$D_{AB} := j^{-2} x^a_{|A} (\chi)_{Ba}, \quad K_{AB} := j^{-2} \delta_{AB}, \quad \Gamma_{ABC} := j^{-2} \chi^a_A \chi_{aB|C} \tag{2.20}$$

For microstretch and micropolar continua we can decompose the wryness tensor as:

$$\Gamma_{ABC} = \delta_{AB} \Gamma_C - \epsilon_{ABD} \Gamma_{DC}, \qquad \begin{cases} \Gamma_A = j^{-1} j_{|A} \\ \Gamma_{AB} = \frac{1}{2} \epsilon_{ACD} \chi^{kC}_{|B} \chi^D_k \end{cases} \tag{2.21}$$

The general non-linear compatibility conditions for a general microcontinuum are:

$$\epsilon^{KPQ} (D_{PL|Q} + D_{PR} \Gamma_{LRQ}) = 0$$
$$\epsilon^{KPQ} (\Gamma_{LMP|Q} + \Gamma_{LRQ} \Gamma_{RMP}) = 0 \tag{2.22}$$
$$D_{KL|M} - (\Gamma_{PKM} K_{LP} + \Gamma_{PLM} K_{KP}) = 0$$

For non-Euclidean geometries the above expressions need to be modified taking into account the Riemann tensor (see appendix B.5.1). Obviously, for microstretch or micropolar continuum these equations can be further simplified. For example, for a microstretch linear media the compatibility equations are only slightly different from those of classical continuum mechanics:

$$- \epsilon^{kpq} \frac{\partial \varepsilon_{pl}}{\partial x^q} + \gamma_{pp} \delta_{kl} - \gamma_{kl} = 0, \qquad \epsilon^{kpq} \frac{\partial \gamma_{lq}}{\partial x^p} = 0 \tag{2.23}$$

Where ε_{ij} and $\gamma_{kl} = \phi_{k|l}$ are the infinitesimal strain deformation and the infinitesimal micro-strain deformation.

2.3.6 Stress and balance principles in microcontinuum mechanics

In micropolar continuum mechanics, the *micro-structural contact forces* give rise to a Cauchy second-order tensor $\boldsymbol{\sigma} = \sigma^{ij}\ \boldsymbol{e}_i \otimes \boldsymbol{e}_j$ and, in addition, a couple stress tensor $\boldsymbol{\mu} = \hat{\mu}^{ij}\ \boldsymbol{e}_i \otimes \boldsymbol{e}_j$. The acting forces on a microcontinuum body can be represented by a force density field $\boldsymbol{b} = b_i\boldsymbol{e}^i$ and a couple density field $\boldsymbol{l} = l_i\boldsymbol{e}^i$. For a general micromorphic body, the formulation is slightly more complex; a third-order tensor $\hat{\boldsymbol{\mu}} = \mu^{ijk}\boldsymbol{e}_i \otimes \boldsymbol{e}_j \otimes \boldsymbol{e}_k$ replaces $\boldsymbol{\mu}$ and a second-order tensor field replace $\hat{\boldsymbol{l}}$ replaces $\boldsymbol{l}$. Eringen provides an intuitive justification for these new magnitudes in terms of the micro-structure of a material particle [31]. Intuitively, the magnitudes $\hat{\boldsymbol{\mu}}$ and $\hat{\boldsymbol{l}}$ are interpretable as the surface and volume averages a the particle (which contains several microparticles or "molecules"):

$$\mu^{ijk} = \left\langle \sigma'^{ij}\xi^k \right\rangle_{sup}, \qquad l_i^k = \left\langle b_i\xi^k \right\rangle_{vol} \tag{2.24}$$

where $\langle\cdot\rangle_{sup}$ and $\langle\cdot\rangle_{vol}$ represent the surface and volume averages in a particle (the average is taken over all the micro-particles contained in the particle). In this interpretation, the primed quantities refer to magnitudes of the micro-element contained in a particle. Eringen leaves undefined these quantities because, formally, it is sufficient to use the tensors $\boldsymbol{\sigma}$ and $\hat{\boldsymbol{\mu}}$ for all purposes (disregarding the notion of micro-particle). Given a coordinate system $\{x^A, \xi^B\}$ on $T\mathcal{S}$ we can define:

$$\hat{\boldsymbol{\mu}} := \boldsymbol{\sigma}' \otimes \boldsymbol{\xi}, \qquad \boldsymbol{l} := \boldsymbol{b}' \otimes \boldsymbol{\xi} \tag{2.25}$$

For the formulation of dynamic equations we need to introduce a new key concept: microinertia. In the same way that in continuum mechanics we need to substitute the notion of mass by a local magnitude, that we call *mass density* ρ. In microcontinuum mechanics we need to substitute the notion of *inertia tensor* of micro-structure, by a local magnitude representing it. This local magnitude is the *microinertia tensor*, a second-order tensor. The material and spatial representations of microinertia are given by:

$$\begin{aligned}
\rho_0 I^{AB} &:= \quad \left\langle \Xi^A \Xi^B \right\rangle_{vol} = \int_{\text{part}} \rho'_0 \Xi^A \Xi^B\ \mathbf{dV}' \\
\rho i^{ab} &:= \quad \left\langle \xi^a \xi^b \right\rangle_{vol} = \int_{\phi(\text{part})} \rho' \xi^a \xi^b\ \mathbf{dv}'
\end{aligned} \tag{2.26}$$

Formally, we assume that there are a scalar field $\rho_0(X, t)$ and a 2-tensor field

$\hat{\mathbf{I}} = I^{AB} \; \boldsymbol{E}_A \otimes \boldsymbol{E}_B$, representing the material density and the material microinertia. In can be proven that the mass conservation implies the existence of the corresponding spatial descriptions of ρ_0 and $\hat{\mathbf{I}}$, that is, the conservation of mass allows to define the scalar $\rho(x, t)$ and the 2-tensor field $\mathbf{i} = i^{ab} \; \boldsymbol{e}_a \otimes \boldsymbol{e}_b$.

The kinetic energy is computed as the sum of the translational kinetic energy and the "rotational" kinetic energy of the micro-structure. Thus, the total *kinetic energy per unit of mass* is given by:

$$
\begin{aligned}
e_K &= \tfrac{1}{2} \boldsymbol{v} \cdot \boldsymbol{v} + f(\boldsymbol{\nu} \otimes \boldsymbol{\nu}) \\
&= \tfrac{1}{2} g_{ab} v^a v^b + \tfrac{1}{2} g_{ab} i^{cd} \nu_d^a \nu_c^b \\
&= \tfrac{1}{2} g_{ab} \big(v^a v^b + i^{cd} \nu_d^a \nu_c^b \big)
\end{aligned}
\tag{2.27}
$$

Analogously, as the energy balance of section 2.3.6 we define the *principle of energy balance for microcontinua*:

Definition 2.3.9. *Consider a microcontinuum body $\hat{\mathcal{B}}$ in a state $\phi(\hat{\mathcal{B}}) \subset \mathrm{Lin}(\mathcal{S})$ and subject to applied forces represented by the force density $\boldsymbol{b}$: $\phi(\mathcal{B}) \to T\mathcal{S}$ and couple density $\boldsymbol{l} : \phi(\mathcal{B}) \to T_2^0 \mathcal{S}$. Assume the existence of the following continuous and differentiable fields: one scalar field representing mass density $\rho(x, t)$, a second-order tensor field representing the stresses $\boldsymbol{\sigma}$, and a third-order tensor field representing the couple stresses $\hat{\boldsymbol{\mu}}$:*
*We say that the **balance of energy** is satisfied provided that for every nice open set $\mathcal{U} \subset \hat{\mathcal{B}}$*

$$
\boxed{
\begin{aligned}
\frac{d}{dt} \int_{\phi_t(\mathcal{U})} \rho(e_K + u) \; \mathbf{dv} = {} &\int_{\phi_t(\mathcal{U})} \rho\big(b_k v^k + l_k^i \nu_i^k + h\big) \; \mathbf{dv} + \dots \\
&\dots + \int_{\partial \phi_t(\mathcal{U})} \big(\sigma_{ik} v^k + \mu_{ij}^k \nu_k^j + q_k\big) \; \mathbf{da}^i
\end{aligned}
}
$$

where $\boldsymbol{v} = v^k \boldsymbol{e}_k$ denotes the spatial velocity field and $\boldsymbol{\nu}$ denotes the the microgiration tensor (e_K, u are the kinetic energy and the internal energy per unit of mass, $\boldsymbol{q} = q^k \boldsymbol{e}_k$ represents the heat flux and h the heat generation).

To find the equilibrium equation for a microcontinuum body we need to define a microcontinuum analogue of the torque. This magnitude is called the *spin inertia* [per unit of mass], denoted $\boldsymbol{\zeta}$. It is related to the derivative of the angular momentum:

$$
\zeta^{ab} = \langle \ddot{\xi}^a \xi^b \rangle_{vol} = i^{bc}\big(\dot{\nu}_c^a + \nu_d^a \nu_c^d\big)
\tag{2.28}
$$

With this definition, it is a simple exercise to show that the following identity involving the material derivative holds:

$$\zeta^a_b \nu^b_a = \frac{1}{2} \frac{D}{Dt} \left(i^{ab} g_{cd} \nu^c_a \nu^d_b \right) \tag{2.29}$$

It can be proven that the previous principle entails the following local conservation laws:

Proposition 2.3.4. *Assuming: (a) that the balance of energy in integral form holds, (b) that the conservation of mass and micro-inertia hold, (c) the functions involved are differentiable, then the following differential equations hold:*

$$\boxed{\begin{array}{l} \rho \dot{\boldsymbol{v}} = \rho \boldsymbol{b} + \operatorname{div} \boldsymbol{\sigma} \\ \rho \boldsymbol{\zeta} = \rho \boldsymbol{l} + \boldsymbol{\sigma} - (\boldsymbol{\sigma}) + \operatorname{div} \hat{\boldsymbol{\mu}} \end{array}}$$

where $(\cdot)$ *denotes the symmetrization of a two tensor.*

Another useful differential equation for the formulation of microcontinuum constitutive is the "local form" of the energy balance principle 2.3.9:

$$\rho \dot{e} = \sigma^b_a (v^a_{|b} - \nu^a_b) + s^b_a \nu^a_b + \mu^{abc} \nu_{ab|c} + q^a_{|a} + \rho h \tag{2.30}$$

For a microstretch continuum some additional simplifications are possible. First, we define:

$$\mu^{abc} = \frac{1}{3} \mu^a g^{lm} - \frac{1}{3} \epsilon_{bcd} \mu^{ad}, \qquad l^b_a = \frac{l}{3} \delta^b_a - \frac{1}{2} \epsilon_{adc} g^{bd} l^c$$

$$\nu^b_a = \nu \delta^b_a - \epsilon_{adc} g^{bd} \nu^c \qquad \zeta^{ab} = \frac{\zeta}{3} - \frac{1}{2} \epsilon^{abc} \zeta_c \tag{2.31}$$

where g^{ab} are the components of the *inverse of the metric tensor* of $\mathcal{S}$, and $\mathbf{g}^\sharp = g^{ab} \boldsymbol{e}_a \otimes \boldsymbol{e}_b$. And α^{ab} are the components of the *spin inertia*. In Cartesian coordinates the equilibrium equations in propsition 2.3.4 can be written as:

$$\begin{array}{l} \rho(b^a - \dot{v}^a) + \sigma^{ac}_{|c} = 0 \\ \rho(l^a - \zeta^a) + \mu^{ab}_{|b} + \epsilon^a_{\ mn} \sigma^{mn} = 0 \\ \rho(l - \zeta) + \mu^b_{|b} + t - s = 0 \end{array} \tag{2.32}$$

2.4 Constitutive models for soft tissues

The aim of **constitutive theories** is to develop models for representing the real behavior of matter, being thermodynamically consistent as well as mathematically convenient. Constitutive theories of materials are at the heart of modern non linear continuum mechanics. As Noll and Coleman (1963) [18] showed there is a thermodynamical basis for arguing that every elastic material is indeed a **hyperelastic material** (also called Green-Elastic material). This means that for such material there exists a function called **Strain-Energy Density Function (SEDF)** from which elastic energy as well as stress-strain relations can be derived. Thermodynamically SEDF is a Helmholtz free-energy function W, which is defined per unit reference *volume* rather than per unit *mass*. This SEDF can be expressed as a function of deformation gradient or, equivalently, as a function of other strain measures (and the coordinates of points, if the material is heterogeneous). SEDF needs to satisfy some reasonable mathematical conditions in order to represent a physically reasonable material. The following short list is just a non exhaustive example of such conditions [51]:

- **Polyconvexity** is a condition required for the existence of global solutions (for an extensive discussion it can be seen) [16,72]. Polyconvexity of SEDF is weaker requeriment on SEDF than convexity. Ball established that a convex SEDF leads to unphysicall results, it also established some interesting existence results by requiring polyconvexity [6].

- **Objectivity/Covariance** (also called frame indifference condition), according to this condition, if two different observers, with different frames of reference, measure a physical magnitude the physical components of this magnitude are related by a change of frames/coordinates. Most authors, define mathematical objectivity as the invariance under rotation/orientation of coordinate axes (i.e. under rigid-solid movements or isometries), but frame indifference objectivity can be extended to arbitrary coordinate changes, in this form all the equations need to be covariant, i.e., invariant in form for different observers.

- **Invariance/Symmetry**, this means that under the action of the adequate subgroup of rotations upon the tensorial arguments of SEDF, the value of the scalar SEDF does not change. For example, for an isotropic material

the SEDF is invariant under the full group of rotations, but for a transversally isotropic material the SEDF is invariant only under rotations (whose rotation axis coincides with the normal direction to the plains of isotropy). Mathematically this implies that the SEDF needs to be a function of some scalars that are invariant under some subgroup of the orthonormal group $\mathbf{O}(3)$ [118]

- **Minimality**, for a material with a natural reference configuration or stress free configuration then the SEDF attains a minimum at this configuration. In addition, Ball (1977) [6] demonstrated that the solutions of some kinds of general non-linear elastic problems like *pure displacement problems* and *displacement-traction problems* are also a minimum of the energy functional.

In this section, attention is restricted to homogeneous materials (i.e., material properties are the same at all points). For this type of ideal material the SEDFΨ can be expressed only in terms of the deformation gradient $\mathbf{F}$ and the microdeformation gradient $\boldsymbol{\chi}$. For such a hyperelastic material, the stress tensor can be expressed as a derivative of the SEDF:

$$\mathbf{P} = \frac{\partial W(\mathbf{F}, \boldsymbol{\chi})}{\partial \mathbf{F}}, \quad \text{or} \quad P_{aA} = \frac{\partial W}{\partial F_{aA}} \tag{2.33}$$

where $\mathbf{P}$ is the **first Piola-Kirchhoff (or nominal) stress tensor**, and in a similar way the Cauchy stress tensor, i.e. $\boldsymbol{\sigma} = J^{-1}\mathbf{P}\mathbf{F}^T = \boldsymbol{\sigma}^T$, can be expressed in the following way:

$$\boldsymbol{\sigma} = J^{-1}\frac{\partial W(\mathbf{F}, \boldsymbol{\chi})}{\partial \mathbf{F}}\mathbf{F}^T, \quad \text{or} \quad \sigma^{ab} = J^{-1}F^b{}_A\frac{\partial W}{\partial F_{aA}} \tag{2.34}$$

Additional useful relationships are:

$$\mathbf{P} = 2\mathbf{F}\frac{\partial W(\mathbf{F}, \boldsymbol{\chi})}{\partial \mathbf{C}}, \quad \text{or} \quad P^a_A = F^a_B\frac{\partial W}{\partial C^A_B} \tag{2.35}$$

2.4.1 Constitutive classical models

Soft biological tissues are composed of fibrous components embedded with an isotropic ground substance. The distribution of elements usually determines an

overall anisotropic configuration.

Three classical constitutive models are summarized in this section: Yang *et al.* (2006), Natali-Gregersen (2009) and Holzapfel-Kroon-Gasser model (2000, 2008). The three models were developed for soft collagenous tissues. The models are increasing in complexity an reliability. It is a well established fact that empirically the stress-strain curve in uniaxial tests has a convex shape with highly increasing apparent Young modulus $E_{ap} = d\sigma/d\varepsilon > 0$ (being σ a measure related to axial tension and ε a measure of strain). Lu & Gregersen (2001) studied porcine esophagi and found that empirical curves adjust well to relations of type [69]:

$$S_L = A_L(e^{\beta_L E_L} - 1), \qquad S_t = A_t(e^{\beta_t E_t} - 1) \tag{2.36}$$

Where S_L, E_L are the first Piola-Kirchhoff) stress and the (Green) strain in the longitudinal direction of the esophageal tube, and S_L, E_L the same magnitudes in the transversal direction. The constants $A_L, A_t, \beta_L, \beta_t$ are mechanical properties of the model. Although a reasonably good fit with the data was found, this model does not seem well physically grounded, and no reason is provided for the occurrence of an "exponential law". In addition, this model does not take into account the near incompressibility of the esophageal tissue, and polyconvexity does not hold, and the SEDF from which is derived is not given.

All the other models supply this criticism: they are explicitly written in terms of the invariants of deformation tensors, showing the explicit symmetries/invariances and for the same reason the constitutive equations are objective.

Yang-Gregersen-Deng model [22, 114]
This model was originally devised by Deng *et al.* (1994) for arteries, but was subsequently applied for Yang *et al.* to esophageal tissue. This is one of the simplest "exponential" models used for soft tissue. The SEDF is an exponential of a quadratic polynomial in strains:

$$W(\mathbf{E}) = \frac{C}{2}e^{Q(E_{ij})} \tag{2.37}$$

where C is an elastic constant and the polynomial Q is:

$$Q(E_{ij}) = b_\theta E_{\theta\theta}^2 + b_z E_{zz}^2 + b_{\theta z} E_{\theta\theta} E_{zz} + c E_{\theta z}^2 \tag{2.38}$$

This model is quite simple and provides a slightly better fit to the experimental data than the Lu–Gregersen model previously mentioned. The stresses are given by:

$$
\begin{cases}
S_{zz} = C(b_z E_{zz} + b_{\theta z} E_{\theta\theta})e^{Q(E_{ij})} \\
S_{\theta\theta} = C(b_\theta E_{\theta\theta} + b_{\theta z} E_{zz})e^{Q(E_{ij})} \\
S_{\theta z} = Cc E_{\theta z} e^{Q(E_{ij})}
\end{cases}
\tag{2.39}
$$

For uniaxial tensile test in longitudinal (z direction) or transversal (θ direction) one has:

$$
\begin{cases}
S_L = S_{zz} = C\left(b_z - \dfrac{b_{\theta z}^2}{b_\theta}\right) E_L e^{Q(E_{ij})} = A_L E_L \exp(\beta_L E_L^2) \\
S_t = S_{\theta\theta} = C\left(b_\theta - \dfrac{b_{\theta z}^2}{b_z}\right) E_t e^{Q(E_{ij})} = A_t E_t \exp(\beta_t E_t^2)
\end{cases}
\tag{2.40}
$$

Where $A_L = C[b_z - (b_{\theta z}^2/b_\theta)]$, $A_t = C[b_\theta - (b_{\theta z}^2/b_z)]$, $\beta_L = A_L/C$, $\beta_t = A_t/C$. These relations allow to adjust the constants A_L, A_t, β_L, b_t by means of linear regression by taking logarithms:

$$
\begin{cases}
\ln\left(\dfrac{S_L}{E_L}\right) = \ln A_L + \dfrac{A_L}{C}(E_L^2) \Rightarrow \quad Y_L = \alpha_L + \beta_L X_L \\
\ln\left(\dfrac{S_t}{E_t}\right) = \ln A_t + \dfrac{A_t}{C}(E_t^2) \Rightarrow \quad Y_t = \alpha_t + \beta_t X_t
\end{cases}
\tag{2.41}
$$

It is interesting to note that uniaxial tensile tests are insufficient to compute all the constants of the model $b_z, b_\theta, b_{\theta z}, c, C$, in particular no information is obtained about c (this require tests with shearing). Worse still, the experimental $A_L, A_t, \beta_L, \beta_t$ from uniaxial tensile tests are insufficient even to determine the four parameters of the model $b_z, b_\theta, b_{\theta z}, C$ [the best we can have is $C = A_L/\beta_L = A_t/\beta_t$, $b_z = (A_L/A_t)b_\theta$, and $b_{\theta z}^2 = b_\theta(b_\theta(A_L/A_t) - \beta_L)]$. In addition, this model is not explicitly formulated in terms of invariants, and it is not clear how to generalize this model for incompressible materials.

Holzapfel-Kroon model [52, 59]

The article of Holzapfel, Gasser and Kroon (2000) develops a detailed constitutive model for arterial wall mechanics and compares it with other material models. This model has been taken as a basis in a certain number of other studies, including the generalization of Kroon and Holzapfel (2008). We will focus on the description of this last generalization (although it is interesting to consult [52] for a detailed theoretical justification). The model summarized here is an anisotropic incompressible hyperelastic constitutive model for arterial tissue (other studies have shown that the model is applicable to other collagenous soft tissues such as the esophagus walls). In this model the artery is modeled as a thick-walled nonlinearly hyperelastic circular cylindrical tube consisting of two layers corresponding to the media and adventitia (the solid mechanically relevant layers in healthy tissue). Each layer is treated as a fiber-reinforced material with the fibers corresponding to the collagenous component of the material and symmetrically disposed with respect to the cylinder axis. The strain energy density function (SEDF/HEDF) is defined by:

$$\Psi(\mathbf{C}) = U(J) + \bar{\Psi}(\mathbf{C}, \dots) \tag{2.42}$$

which is based on the kinematic assumption

$$\mathbf{C} = J^{2/3}\bar{\mathbf{C}}, \quad J = (\det \mathbf{C})^{1/2}, \quad \det \bar{\mathbf{C}} = 1 \tag{2.43}$$

of the right Cauchy-Green tensor $\mathbf{C}$, where J is the volume ration (or the "Jacobian") and $\bar{\mathbf{C}}$ is the modified right Cauchy-Green tensor. In equation 2.42 the function U describes the volumetric elastic response of the material. Holzapfel and Kroon consider the collagenous tissues as incompressible, as it is the case for arterial walls within the physiological range of deformation, implying $J = 1$. For this case, U serves as a penalty function which is motivated mathematically [52]. The mechanical response of collagenous tissues is very much dominated by the fibrous components, *i.e.* elastin and collagen. According to Holzapfel and Weizsäcker [53], the Kroon-Holzapfel model an additive decomposition of $\bar{\Psi}$ in a contribution due to elastin $\bar{\Psi}_{elas}$ and due to collagen $\bar{\Psi}_{coll}$, *i.e*:

$$\bar{\Psi} = \bar{\Psi}_{elast} + \bar{\Psi}_{coll} = \mu(\bar{I}_1 - 3) + \frac{k_1}{2k_2} \sum_{i=4,6} \left(\exp[k_2(\bar{I}_i - 1)^2] - 1 \right) \tag{2.44}$$

where $I_4 = \mathbf{C} : \boldsymbol{a} \otimes \boldsymbol{a} = C_{AB}a^A a^B$ and $I_6 = \mathbf{C} : \boldsymbol{b} \otimes \boldsymbol{b} = C_{AB}b^A b^B$, being $\boldsymbol{a}, \boldsymbol{b}$ unitary vectors appointing in dominant direction of fiber arrangements.

The term containing μ is the elastin term, and it seems to be of little significance for the data considered by Kroon and Holzapfel. For the collagenous part the model consider n discrete and distinct layers that form a laminate. Within a layer, labeled with index i, coherent bundles of straightened collagen fibers are perfectly aligned in the direction characterized by the angle ϕ_i, and defined with respect to a 2D in-plane reference coordinate system, as indicated in figure 2.16. The angles of the collagen fibers are defined according to
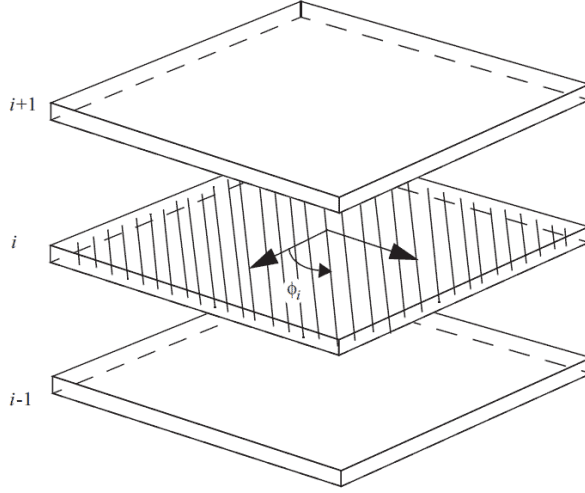
Figure 2.16. The structure of the tissue is assumed to be multi-layered consisting on n layers. Dominant arrangement for i is given by angle ϕ_i (after Kroon & Holzapfel, 2008) [59].

$$\phi_i = \frac{i-1}{n}\pi, \qquad 1 \le i \le n \tag{2.45}$$

and the fiber orientation are thus uniformly distributed over the whole azimuthal range. The value $n \ge 2$ provides the even number of tissue layers. Hence in this model the layers consists of bundles of collagen fibers with different mean alignments for each layer. The contribution to the strain energy of each collagen fiber layer is derived from the constitutive response of collagen under axial extension, which experimentally is of the form:

$$\psi_f = \frac{k}{8a}\left(\exp(a(\lambda^2-1)^2)-1\right), \qquad \lambda \ge 1, \tag{2.46}$$

where λ is the stretch acting on the collagen fibers, and $k \ge 0$ and $a > 0$ denote the mechanical properties. The exponent a describes the amount of of nonlinearity that the collagen fibers exhibit. It is assumed that the fibers can not sustain any load in compression implying that $\phi_f = 0$ for $\lambda < 1$. In order to introduce
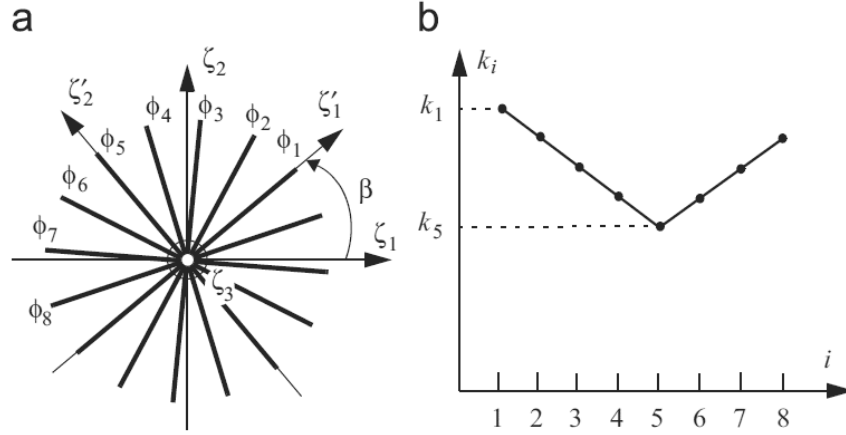
Figure 2.17. (a) Example of uniformly distributed collagen fibers illustrated for eight distinct tissue layers $n = 8$, (b) The principal directions $\{\boldsymbol{\zeta}'_i\}$ if the collagen fabric is rotated by an angle β with respect to the reference coordinate system $\{\boldsymbol{\zeta}_i\}$. The axis of rotation is $\boldsymbol{\zeta}_3$. Example of a stiffness distribution for the eight layers (after Kroon & Holzapfel, 2008) [59].

anisotropy in a convenient way, we assume that the in-plane principal directions 1 and 2 of the tissue are associated with the fiber directions characterized by through angles ϕ_1 and $\phi_{n/2+1}$, respectively. The coefficients k_i are then defined by two given stiffness k_1 and $k_{n/2+1}$ (associated with the respective directions ϕ_1 and $\phi_{n/2+1}$) according to

$$
\begin{aligned}
k_i &= k_1 + \frac{k_{n/2+1} - k_1}{n/2}(i-1), & 2 \le i \le n/2 \\
k_i &= k_{n/2+1} + \frac{k_1 - k_{n/2+1}}{n/2}(i - n/2 - 1), & n/2 + 2 \le i \le n
\end{aligned}
\tag{2.47}
$$

Note that for the case $n = 2$ no additional stiffness are required. The orientation of the principal coordinate system $\{\boldsymbol{\zeta}_i\}$ of the collagen fabric with respect to a reference coordinate system is defined by angle β (see figure 2.17). By using the constitutive equation 2.46 for the collagen the contribution $\bar{\psi}_{coll}$ to the strain energy due to collagen may then be formulated as

$$
\bar{\psi}_{coll} = \sum_{i=1}^{n} \frac{k_i}{8a} \left(\exp[a(\bar{I}_{4i} - 1)^2] \right), \quad \bar{I}_{4i} = \bar{\mathbf{C}} : \mathbf{A}(\phi_i, \beta)
\tag{2.48}
$$

where the index i denotes layer-specific entities, and $\mathbf{A}(\phi_i, \beta) = \boldsymbol{m} \otimes \boldsymbol{m}$ is a *structural tensor* (see section 2.5.1 for a general discussion of the concept), where $\boldsymbol{m} = (\cos(\phi_i + \beta), \sin(\phi_i + \beta), 0)^T$. We impose the requirements that $k_i \geq 0$ and $a > 0$. In addition, fibers will only contribute to the strain energy if $\bar{I}_{4i} \geq 1$, otherwise contribution is zero. Finally, using equations 2.44 and 2.45, it can be deduced that the isochoric part $\bar{psi}$ of the strain-energy function:

$$\bar{\psi} = \mu(\bar{I}_1 - 3) + \sum_{i=1}^{n} \frac{k_i}{8a} \left(\exp[a(\bar{I}_{4i} - 1)^2] \right) \tag{2.49}$$

It is straightforward to obtain the second Piola-Kirchhoff stress tensor $\mathbf{S}$:

$$\mathbf{S} = 2\frac{\partial \psi}{\partial \mathbf{C}} = 2\left(\frac{\partial U(J)}{\partial \mathbf{C}} + \frac{\partial \bar{\psi}_{elas}}{\partial \mathbf{C}} + \frac{\partial \bar{\psi}_{coll}}{\partial \mathbf{C}} \right) \tag{2.50}$$

Natali-Gregersen model [80]

The model of Natali, Carniel and Gregersen (2009), summarized here, is similar in many aspects to the Holzapfel-Kroon model, although it uses a large number of inveriants and tries to represent the interaction of the two main families of fiber arrangements in mucosa-submocosa layer. In addition, it is a little more complex and include a greater number of adjustable parameters. The Natali-Gregersen model is like the Holzapfel-Kroon model an anisotropic incompressible hyperelastic constitutive model. According to the theory of fiber-reinforced materials, the strain energy density function (SEDF) is defined by different contributions from the ground substance and fibrous components [51, 100]:

$$W(\mathbf{C}) = W_{iso}(\mathbf{C}) + W_f(\mathbf{C}, \mathbf{M}_i) \tag{2.51}$$

where $\mathbf{C}$ is the right Cauchy–Green strain tensor and $\mathbf{M}_i$ are the structural tensors (fabric tensors) depending on fibers organization. The high liquid content of ground substance defines an almost incompressible behavior and the isotropic contribution W_{iso} is split into volumetric U_{vol} and iso-volumetric $\tilde{W}_{iso}$ terms:

$$W_{iso}(\mathbf{C}) = U_{vol}(I_3) + \tilde{W}_{iso}(\tilde{I}_1, \tilde{I}_2) \tag{2.52}$$

$$U_{vol}(I_3) = \left[\frac{K_v}{2 + r(r+1)} \right] \left[(I_3^{1/2} - 1)^2 + I_3^{-r/2} + rI_3^{-1/2} - (r+1) \right] \tag{2.53}$$

$$\tilde{W}_{iso}(\tilde{I}_1, \tilde{I}_2) = \frac{C_1}{\alpha_1}\left(e^{\alpha_1(\tilde{I}_1-3)} - 1\right) + \frac{C_2}{\alpha_2}\left(e^{\alpha_1(\tilde{I}_2-3)} - 1\right) \tag{2.54}$$

where $\tilde{I}_1 = \mathrm{tr}(\tilde{\mathbf{C}})$, $\tilde{I}_2 = 1/2\left[\tilde{I}_1^2 - \mathrm{tr}(\tilde{\mathbf{C}})^2\right]$ are the two principal invariants of the iso-volumetric part of the right Cauchy–Green strain tensor, as $\tilde{\mathbf{C}} = J^{2/3}\mathbf{C}$ and the third invariant is related to the deformation Jacobian J, as $I_3 = J^2$. Constitutive parameters K_v and r are related to the tissue volumetric behavior and define the tangent volumetric modulus:

Parameters C_1 and C_2 specify the tissue shear stiffness as $G = 2(C_1 + C_2)$ while parameters α_1 and α_2 regulate the non-linearity of the material response, with reference to experimental results. On the other hand, the specific formulation of fibrous network term W_f depends on the fibrous components conformation and distribution (see [51] or [100], for a general explanation of the invariants $I_1, I_2, \ldots, I_9$ involved in the theory of fiber-reinforced materials.). Esophageal tissue, with particular regard to submucosa and muscularis externa, is characterized by fibrous elements mainly oriented along two principal directions $\boldsymbol{a}_0$ and $\boldsymbol{b}_0$ (see figure 2.18). The following formulation is adopted:
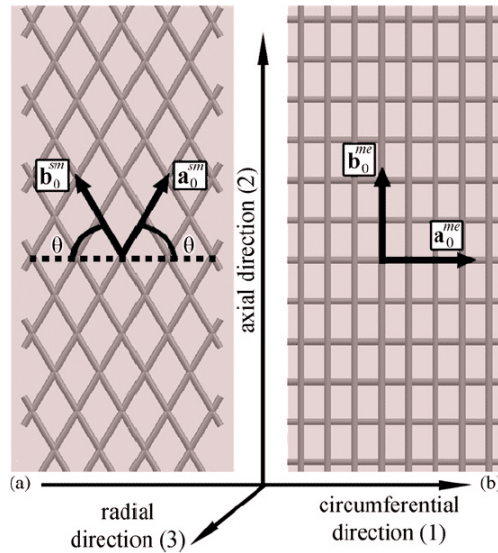
Figure 2.18. Planar representation of fiber arrangement in submucosa (a) and muscularis externa (b) (after Natali, 2009, [80]).

$$W_f(\mathbf{C}, \mathbf{M}_i) = W_f(\mathbf{C}, \boldsymbol{a}_0 \otimes \boldsymbol{a}_0, \boldsymbol{b}_0 \otimes \boldsymbol{b}_0) = W_f(I_4, I_5, I_6, I_7, I_8, I_9) = W_a(I_4) + W_b(I_6) + W_{ab}(I_8, I_9) \tag{2.55}$$

$$K^T = \frac{\partial^2 U}{\partial J^2} = \frac{K_v}{2 + r(r+1)}[2 + r(r+1)I_3^{-(r+2)/2}] \tag{2.56}$$

where:

$$\begin{cases} W_a(I_4) = \left[\dfrac{C_4}{\alpha_4^2}(e^{\alpha_4(I_4-1)}\alpha_4(I_4-1) - 1) \right] \\[2ex] W_b(I_6) = \left[\dfrac{C_6}{\alpha_6^2}(e^{\alpha_6(I_6-1)}\alpha_6(I_6-1) - 1) \right] \\[2ex] W_{ab}(I_8, I_9) = C_{89}(I_8 - I_9)^2) \end{cases} \tag{2.57}$$

The fourth and sixth invariants $I_4 = \mathbf{C} : (\boldsymbol{a}_0 \otimes \boldsymbol{a}_0) = \boldsymbol{a}_0 \cdot \mathbf{C}\boldsymbol{a}_0 = C_{ij}a_0^i a_0^j = \lambda_{\boldsymbol{a}_0}^2, I_6 = \mathbf{C} : (\boldsymbol{b}_0 \otimes \boldsymbol{b}_0) = \boldsymbol{b}_0 \cdot \mathbf{C}\boldsymbol{b}_0 = C_{ij}b_0^i b_0^j = \lambda_{\boldsymbol{b}_0}^2$ depend on the tissue stretch along fiber directions $\boldsymbol{a}_0$ and $\boldsymbol{b}_0$ (namely, $\lambda_{\boldsymbol{a}_0}$ and $\lambda_{\boldsymbol{b}_0}$). The fifth an seventh invariants are similar but use the square of the Cauchy tensor: $I_5 = \mathbf{C}^2 : (\boldsymbol{a}_0 \otimes \boldsymbol{a}_0), I_7 = \mathbf{C}^2 : (\boldsymbol{b}_0 \otimes \boldsymbol{b}_0)$, these invariants specify the fiber contribution to the overall tissue mechanical response, when complex strain conditions are applied, such as shearing. With regard to esophagus, Natali *el al.*(2009) suggest to neglect the contribution of the fifth and the seventh invariants due to the weakness of the fiber-matrix interaction. Finally the eighth and ninth invariants $I_8 = (\boldsymbol{a}_0 \cdot \boldsymbol{b}_0)[\mathbf{C} : (\boldsymbol{a}_0 \otimes \boldsymbol{b}_0)], I_9 = (\boldsymbol{a}_0 \cdot \boldsymbol{b}_0)^2$ specify the influence of mutual interactions between the two fiber families [51, 64].

For obtaining the [first Piola] stress tensor we will use equation 2.35, then we obtain:

$$\mathbf{P} = \mathbf{P}_{vol} + \tilde{\mathbf{P}}_{iso} + \mathbf{P}_a + \mathbf{P}_b + \mathbf{P}_{ab} \tag{2.58}$$

$$\mathbf{P}_{vol} = 2\mathbf{F}\frac{\partial U_{vol}}{\partial \mathbf{C}} = \frac{K_v}{2 + r(r+1)}[2J(J-1) - rJ^{-r} + rJ]\mathbf{F}^{-T} \tag{2.59}$$

$$\tilde{\mathbf{P}}_{iso} = 2\mathbf{F}\frac{\partial \tilde{W}_{iso}}{\partial \mathbf{C}} = C_1 e^{\alpha_1(\tilde{I}_1 - 3)}\left(2J^{-2/3}\mathbf{F} - \frac{2\tilde{I}_1}{3}\mathbf{F}^{-T}\right) \tag{2.60}$$

$$\mathbf{P}_a = 2\mathbf{F}\frac{\partial W_a}{\partial \mathbf{C}} = \frac{C_4}{\alpha_4}e^{\alpha_4(I_4-1)}\mathbf{F}(\boldsymbol{a}_0 \otimes \boldsymbol{a}_0) \tag{2.61}$$

$$\mathbf{P}_b = 2\mathbf{F}\frac{\partial W_b}{\partial \mathbf{C}} = \frac{C_6}{\alpha_6}e^{\alpha_4(I_6-1)}\mathbf{F}(\boldsymbol{b}_0 \otimes \boldsymbol{b}_0) \tag{2.62}$$

$$\mathbf{P}_{ab} = 2\mathbf{F}\frac{\partial W_{ab}}{\partial \mathbf{C}} = C_{89}\sqrt{I_9}(I_8 - I_9)\mathbf{F}(\boldsymbol{a}_0 \otimes \boldsymbol{b}_0 + \boldsymbol{b}_0 \otimes \boldsymbol{a}_0) \tag{2.63}$$

For uniaxial tensile test the deformation gradient $\mathbf{F}$ can be represented by a diagonal matrix with eigenvalues $\lambda_1, \lambda_2, \lambda_3$. If 1 and 2 denote longitudinal and transversal directions then λ_1, λ_2 are the relevant variables for measuring strain in the uniaxial testing (being λ_3 the stretch in the radial direction, *i.e.* the reduction of thickness). Histological evidence suggests to take:

$$\boldsymbol{a}_0^{sm} = (\cos\theta, \sin\theta, 0), \qquad \boldsymbol{b}_0^{sm} = (-\cos\theta, \sin\theta, 0) \tag{2.64}$$

for the layer composed of submucosa and mucosa, and

$$\boldsymbol{a}_0^{me} = (1, 0, 0), \qquad \boldsymbol{b}_0^{me} = (0, 1, 0) \tag{2.65}$$

for muscularis externa. Thus, the stress term $\mathbf{P}_{ab}$ disappears for muscularis externa because the fiber directions $\boldsymbol{a}_0^{me}$ and $\boldsymbol{b}_0^{me} = (0, 1, 0)$ are orthogonal and therefore $I_9 = 0$ (see figure 2.18). Note the above equations define the first Piola–Kirchhoff stress tensor as a function of the invariants $\tilde{I}_1, I_3, I_4, I_6, I_8, I_9$ that, in turn, are functions of all the principal stretches $\lambda_1, \lambda_2, \lambda_3$, so the stretches that are not measured directly (in particular λ_3) can be evaluated by analytical methods; we have:

$$\begin{cases} P_{ii}(\lambda_i^{exp}, \lambda_j, \lambda_k) = \dfrac{F_t}{A_0} \\ P_{jj}(\lambda_1, \lambda_2, \lambda_3) = 0 \qquad i \notin \{j, k\} \end{cases} \tag{2.66}$$

Where $i = 1$ (longitudinal tests) or $i = 2$ (transversal tests), accounting for the experimental value λ_i^{exp}, the solution of the system 2.66 leads to the other componets of stretch λ_j, λ_k.

Remark. Although the above classical constitutive models fit the data reasonably, are empirically satisfactory and are well developed; no physical reason is given in the literature for the occurrence of *exponential functions* [99]. One of the theoretical results of this dissertation is the construction an explanation for its occurrence based on statistical mechanics.4.2.1■.

2.4.2 Constitutive microcontinuum models

Up to now, the use of microcontinuum models in biomechanics is mainly limited to the linear microcontinuum elasticity. This theory is adequate, for example, for small deformations and a number of authors have used this kind of approaches for studying the hard tissue of the bones. Its use for soft tissue is less developed although we can find some interesting works [55, 70]. More over, there are works using microcontinuum theory of fluids [94]. We restrict here to the general microcontinuum constitute theory, summarized in [31].

A general constitutive model for a thermoelastic microcontinuum is a functional relation among the "independent" variables and the "dependent" variables. The independent variables are:

$$\mathcal{I}(x,t) = \{\mathbf{D}(x,t), \mathbf{K}(x,t), \hat{\mathbf{\Gamma}}(x,t), \nabla\theta(x,t), \dot{\theta}(x,t), \theta(x,t), \hat{\mathbf{I}}(x,t), x, t\} \quad (2.67)$$

that its, the macrodeformation tensor, the microdeformation tensor, the wryness tensor, the temperature gradient, the rate of change of the temperature, the temperature, the microinertia tensor, the point location and the time. The set of dependent variable is:

$$\mathcal{D}(x,t) = \{\boldsymbol{\sigma}(x,t), \hat{\boldsymbol{\mu}}(x,t), \mathbf{s}(x,t), \boldsymbol{q}(x,t), e(x,t)\} \quad (2.68)$$

The balance laws form a system of 20 partial differential equations and one inequality (for entropy production). Given the external loads $\boldsymbol{b}, \hat{\boldsymbol{l}}$ and the heat generation h, there are 67 unknowns $\rho, \boldsymbol{v}, \mathbf{j}, \boldsymbol{\nu}, \boldsymbol{\sigma}, \hat{\boldsymbol{\mu}}, \mathbf{s}, \boldsymbol{q}, e, \eta$ and θ (density, velocity, traceless microinertia, microgyration, stress, couple stress, symmetric tensor, heat flux, total energy, entropy and temperature). Clearly then, the system is highly indeterminate. Forty-seven independent additional equations are needed for the determination of motions and temperatures of a micromorphic body. It is assumed that the dependent set $\mathcal{D}$, at (x,t) is a functional of the independent variable set. Symbolically:

$$\mathcal{D}(x,t) = \mathcal{F}[\mathcal{I}(x,t)], \qquad x \in \mathcal{S}, \ t \in \mathbb{R} \quad (2.69)$$

This functional is assumed to be coherent with the *material-frame indifference axiom* or more in general *covariance axiom*. For a usual elastic theory further requirements are necessary for example the *locality axioms* or the *memory-*

independent material restriction. We assume here the usual locality and time-independence requirements; then the above equation can be simplified to $\mathcal{D}(x,t) = \mathcal{F}[\mathcal{I}]$. For a viscoelastic continuum, we need to remove the time-independence and assume a relation of type $\mathcal{D}(x,t) = \mathcal{F}[\mathcal{I}(t-t')]$ with $t' \in \mathbb{R}^+$. As discussed at the beginning of this dissertation for practical purposes we can ignore the viscoelastic effects in the type of problems addressed in this research.

To formulate the constitutive elastic laws, we need the *local* second law of thermodynamics:

$$\rho\dot{\eta} - \nabla_k\left(\frac{q^k}{\theta}\right) - \frac{\rho h}{\theta} \geq 0 \tag{2.70}$$

where η is the entropy by unit of mass, $\boldsymbol{q} = q^k\boldsymbol{e}_k$ the heat flux, θ the absolute temperature, and h the heat generation. Introducing the *Helmholtz energy density function* (HEDF)

$$\psi = e - \theta\eta$$

and eliminating h from the last equation and the *local energy balance* (equation 2.30), we obtain the *generalized Clausius-Duhem* inequality:

$$-\rho(\dot{\psi} + \eta\dot{\theta}) + \sigma^{ab}a_{ab} + \mu^{abc}b_{abc} + s^{ab}c_{kl} + \frac{q^k\theta_{|k}}{\theta} \geq 0 \tag{2.71}$$

where the following abbreviations have been used:

$$\begin{aligned} a_{ab} &= g_{ac}(v^c_{|b} - \nu^c_b), \qquad 2c_{ab} = g_{ac}\nu^c_b + g_{bc}\nu^c_a \\ b_{abc} &= g_{ad}(\nu^d_{b|c}) \end{aligned} \tag{2.72}$$

Postulating that the HEDF is a function of the independent variables $\psi = \psi(\mathbf{D}, \mathbf{K}, \mathbf{\Gamma}, \nabla\theta, \theta, x)$, the time derivative of ψ is given by:

$$\dot{\psi} = \frac{\partial\psi}{\partial D_{AB}}\dot{D}_{AB} + \frac{\partial\psi}{\partial K_{AB}}\dot{K}_{AB} + \frac{\partial\psi}{\partial\Gamma_{ABC}}\dot{\Gamma}_{ABC} + \frac{\partial\psi}{\partial\theta_{|A}}\dot{\theta}_{|A} + \frac{\partial\psi}{\partial\theta}\dot{\theta} + \frac{\partial\psi}{\partial\dot{\theta}}\ddot{\theta} \tag{2.73}$$

Computing the expressions for $\dot{D}_{AB}$, $\dot{K}_{AB}$ and $\dot{\Gamma}_{ABC}$, we have:

$$\dot{D}_{AB} = a_{ab}x^a_{|A}\bar{\chi}^b_B, \qquad \dot{K}_{AB} = c_{ab}\chi^a_A\chi^b_B, \qquad \dot{\Gamma}_{ABC} = b_{abc}\bar{\chi}^a_A\chi^b_B x^c_{|C} \tag{2.74}$$

where $\bar{\boldsymbol{\chi}} = \boldsymbol{\chi}^{-1}$.

Substituing these derivatives into equation 2.71, we obtain:

$$
-\rho\left(\frac{\partial\psi}{\partial\theta}+\eta\right)\dot{\eta}+\left(\sigma^{ab}-\rho\frac{\partial\psi}{\partial D_{AB}}x^a_{|A}\bar{\chi}^b_B\right)a_{ab}+
$$
$$
+\left(\mu^{abc}-\rho\frac{\partial\psi}{\partial\Gamma_{ABC}}\bar{\chi}^a_A\chi^b_B x^c_{|C}\right)b_{klm}+\left(s^{ab}-2\rho\frac{\partial\psi}{\partial K_{AB}}\chi^a_A\chi^b_B\right)c_{kl}-
$$
$$
-\rho\frac{\partial\psi}{\partial\theta_{|A}}\dot{\theta}_{|A}-\rho\frac{\partial\psi}{\partial\dot{\theta}}\ddot{\theta}+\frac{q^k\theta_{|k}}{\theta}\geq 0
$$

(2.75)

This inequality is linear in $\ddot{\theta}, a_{ab}, b_{abc}, c_{ab}$ and $\dot{\theta}_{|A}$. It must remain in one sign for *all independent variations* of these quantities. But this is impossible unless:

$$
\sigma^{ab}=\rho\frac{\partial\psi}{\partial D_{AB}}x^a_{|A}\bar{\chi}^b_B,\quad s^{ab}=2\rho\frac{\partial\psi}{\partial K_{AB}}\chi^a_A\chi^b_B\quad \mu^{abc}=\rho\frac{\partial\psi}{\partial\Gamma_{ABC}}\bar{\chi}^a_A\chi^b_B x^c_{|C}
$$
$$
\eta=\frac{\partial\psi}{\partial\theta}\qquad\qquad \frac{\partial\psi}{\partial\theta_{|A}}=0,\qquad\qquad \frac{\partial\psi}{\partial\dot{\theta}}=0
$$
$$
-\rho\eta\dot{\theta}+\frac{q^k\theta_{|k}}{\theta}\geq 0
$$

(2.76)

The above equations are the most general possible constitutive laws for a micromorphic continuum. We can particularize them for a microstretch continuum, defining $j=\det\boldsymbol{\chi}$ then the stress tensor take the special forms:

$$
D_{AB}=j^{-2}x^a_{|B}\chi_{aB},\quad K_{AB}=j^2\delta_{AB},\quad \Gamma_{ABC}=j^{-2}\chi^a_A\chi_{aB|C}
$$

(2.77)

These tensors are possible candidates for strain measures, but the are coupled and they do not constitute an independent set. For simplify computations it is useful to define $\tilde{\boldsymbol{\chi}}=j^{-1}\boldsymbol{\chi}$ and then redefine the macrodeformation, the microdeformation and the wryness tensors as:

$$
\begin{aligned}
\tilde{D}_{AB}&=x^a_{|B}\tilde{\chi}_{aB}=jD_{AB}, & \tilde{K}_{AB}&=j^2\delta_{AB}=K_{AB}\\
\Gamma^A_B&=\tfrac{1}{2}\epsilon^{ACD}\hat{\chi}^a_{C|B}\hat{\chi}_{aD}, & \Gamma_A&=j^{-1}j_{|A}
\end{aligned}
$$

(2.78)

Obviously, we have the decomposition $\Gamma_{ABC}=\Gamma_C\delta_{AB}-\epsilon_{ABE}\Gamma^E_C$. Then repeating the procedure used for 2.76, we obtain for a microstretch continuum the following

constitutive equations:

$$\sigma^{ab} = \rho \frac{\partial \psi}{\partial \tilde{D}_{AB}} x^a_{|A} \tilde{\chi}^b_B, \qquad s - t = 3\rho j \frac{\partial \psi}{\partial j}$$

$$\mu^{ab} = \rho j^{-2} \frac{\partial \psi}{\partial \Gamma^B_A} x^a_{|A} \tilde{\chi}^{Bb} \quad \mu^a = \rho \frac{\partial \psi}{\partial \Gamma_A} x^a_{|A} \tag{2.79}$$

[We have omitted the purely thermodynamic restrictions]. These equations are the key equations for deriving the constitutive laws from a proposed HEDF. They will be used in section 4.5.

2.5 Representation of anisotropy

As previously discussed, constitutive equations are easier to represent by means of a Strain-Energy Density Function (SEDF). This SEDF is a scalar function whose arguments are different tensors (strain tensor, micro-strain tensor, etc.) In the isotropic case, the SEDF for a material needs to be a function of invariants under geometrical transformations of the whole three dimensional orthogonal group $\mathbf{O}(3)$ (formed by three dimensional rotations $\mathbf{SO}(3)$, reflections and spatial inversions, see section A.3 for a definition). The above fact is a straightforward consequence of the representation theory for tensor functions; this section discusses the anisotropic case more extensively. In particular, complete and irreducible forms for anisotropic tensor functions are treated. These representations allow general consistent invariant forms for nonlinear constitutive equations and specify the number and type of the scalar variables involved Zheng (1994) [118, p. 545]. These representation have proved to be even more pertinent in attempts to model mechanical behavior of anisotropic materials, since invariant conditions predominate and the number and type if independent scalar variables cannot be found by simple arguments.

For introducing some elementary ideas, consider for example an elastic material for which the SEDF (here denoted by W) exists and is expressible as a scalar-valued function of a strain tensor (e.g. the Green deformation tensor) $\mathbf{E}$ or its six independent components $E_{xx}, E_{yy}, E_{zz}, E_{xy} = E_{yx}, E_{yz} = E_{zy}, E_{zx} = E_{xz}$. If the material is isotropic, then the symmetry imposes the restriction that W is expressible as a function of three principal traces $\mathrm{tr}\mathbf{E}, \mathrm{tr}\mathbf{E}^2, \mathrm{tr}\mathbf{E}^3$ (or equivalently,

the three principal invariants $I_1^{\mathbf{E}}, I_2^{\mathbf{E}}, I_3^{\mathbf{E}}$ of $\mathbf{E}$:

$$W = W(\operatorname{tr} \mathbf{E}, \operatorname{tr} \mathbf{E}^2, \operatorname{tr} \mathbf{E}^3) \tag{2.80}$$

For a transversely isotropic material with the preferred direction $\boldsymbol{n}$, the material symmetry imposes the restrictions that W depends on five invariants in the form:

$$W = W(\operatorname{tr} \mathbf{E}, \operatorname{tr} \mathbf{E}^2, \operatorname{tr} \mathbf{E}^3, \mathbf{n} \cdot \mathbf{E}\boldsymbol{n}, \boldsymbol{n} \cdot \mathbf{E}^2\boldsymbol{n}) \tag{2.81}$$

rather than the six components of the strain tensor. The material symmetry, *i.e.*, the isotropy is precisely and automatically satisfied in 2.80 or 2.81.

The material symmetry (isotropy, transverse isotropy, orthotropy, crystal symmetries, etc.) imposes definite restrictions on the forms of the tensor functions in constitutive relations. These restrictions are precisely one aspect treated by the representation theory which specifies the type and number of independent scalar variables involved in constitutive relations to be observed in experiments. Representations for tensor functions are thus valuable and even indispensable form modeling of nonlinear constitutive laws, particularly when the material is anisotropic and when the mechanical response of the material depends on more than one tensor argument (as it happens in micro-continuum mechanics). The theory of representation for tensor functions is well established since the 1990s, including a number of essential theorems and a large amount of complete and irreducible representations for both isotropic and anisotropic tensor functions. The modern developments in both the general approach to nonlinear constitutive equations and in representation theorems date largely from the work of Rivlin and Reiner (1945, 1948) [90] on finitely strained isotropic compressible hyper-elastic materials. Since the work of Rivlin and Ericksen (1955) [28, 91], the representation theory for tensor polynomials has been extensively developed, as described by Spencer (1971, 1987).

2.5.1   Theory of representation for tensor functions

The theory of representations proposed by Rivlin and Ericksen is a theory of representations of tensor polynomials, and corresponds to the assumption that the tensor functions in the constitutive relations are polynomials, or that they can be approximated with sufficient accuracy by tensor polynomials of arbitrarily

high degree. This assumption is a matter of mathematical convenience. It may be even misleading if the constitutive equations are not analytic. But this "defect" is partly removed by the significant works of Pipkin and Wineman (1963) and Wineman and Pipkin (1964) [87,111]. They proved that complete representations for tensor polynomials can be regarded as complete representations for general tensor functions.

Numerous isolated instances by Cauchy (1850) [13], Rivlin and Ericksen (1955), Rivlin (1955) [28,91], Pipkin and Rivlin (1959) [88] and Noll (1967) [81], of complete and irreducible representations for isotropic tensor fucntions could be found in the literature (note that an irreducible representation is a nonzero representation that has no proper closed sub-representations). A new period was opened by the works of Boehler (1978, 1979) [7,8] to deal with anisotropic tensor functions and constitutive equations of anisotropic material. In these works the elegant concept of *structural tensors* or *structural tensors* (Lokhin & Sedov, 1963 [66]; Boehler 1978-79) which characterize the anisotropy was extended to join the so called *principle of isotropy of space* that an anisotropic tensor function is expressible as an isotropic one with the structural tensors as additional tensor agencies (see Liu (1982), [65], see Holzapfel-Kroon and Natali models of section 2.4.1, where structural tensors were used). By this principle the known isotropic tensor function representations can be used to immediately yield representations for anisotropic functions. Along this line, constitutive laws of transversely isotropic, orthotropic and clinotropic materials for complex irreversible mechanical phenomena such as yielding, failure, creep and damage can be formulated in terms of invariants and structural tensors. Furthermore, we can see three potential additional significant benefits of above Boehler's idea in formulating constitutive equations of anisotropic materials:

- First, this concept allows constitutive equations to be formally expressed in isotropic forms irrespective of the actual anisotropy of materials in consideration.
- Second, the effects of anisotropy in the constitutive equation become more clear via the structural tensors.
- Third, the constitutive equation has a coordinate free-form, however, it is a tensorial type law.

The modern theory of representation for tensor functions address the following fundamental problems:

- Could all kinds of anisotropy be described and classified?
- Weather every anisotropy could be characterized in terms of enough simple tensor(s) or not?
- Assert the existence of complete tensor function representations in finite forms.
- Develop effective and simple new methods of determining not only complete but also irreducible representations for anisotropic tensor functions.

Zheng (1994) summarized important mathematical results concerning these fundamental problems [118]. Among these results are the *Zheng-Boehler classification theorem*, the *structural tensor theorem* and the *isotropicization theorem*. We begin with some basic definitions:

> **Definition 2.5.1.** *Any function whose arguments are tensors and whose values are scalars is called a **tensor function**. The tensorial arguments will be referred simply as **agencies**. The tensor functions with any finite number of tensor agencies $\mathbf{S}^{(1)}, \ldots, \mathbf{S}^{(A)}$ will be denoted $\varphi(\mathbf{S}^{(a)})$, and the set of all such tensor functions as Φ.*

The next definitions allowsto formalize the notion of change of reference frame by means of transformations of $\mathbf{O}(n)$ (rotations, reflections or combinations of both). The set of all these transformations forms the Lie group $\mathbf{O}(n)$ (see section A.3 for an overview of Lie groups):. We begin with the concept of tensorial representation of the Lie group $\mathbf{O}(n)$:

> **Definition 2.5.2.** *A **tensorial representation** of the matrix Lie group $\mathbf{O}(n)$ of type (r, s) over the inner product vector space V is a mapping $\langle \cdot \rangle : \mathbf{O}(n) \to T_{r+s}^{r+s} V$, given an orthonormal basis the components are:*
>
> $$\langle \mathbf{Q} \rangle = Q_{i_1}^{m_1} \cdots Q_{i_r}^{m_r} Q_{n_1}^{j_1} \cdots Q_{n_s}^{j_s}$$
>
> *This representation allows to define a mapping $T_s^r V \to T_s^r V$ given by $\mathbf{T} \mapsto \langle \mathbf{Q} \rangle \mathbf{T}$, using components, we have:*
>
> $$\langle \mathbf{Q} \rangle T_{j_1 \ldots j_s}^{i_1 \ldots i_r} = Q_{i_1}^{m_1} \cdots Q_{i_r}^{m_r} Q_{n_1}^{j_1} \cdots Q_{n_s}^{j_s} T_{j_1 \ldots j_s}^{i_1 \ldots i_r}$$
>
> *where $T_{j_1 \ldots j_s}^{i_1 \ldots i_r}$ are the components of a tensor of type (r, s) over V. The tensor $\langle \mathbf{Q} \rangle \mathbf{T}$ is called the **transformed tensor** or the "rotated tensor".*

A transformation such as $\mathbf{Q}$ relates the change in orientation of the frame bases used by two different observers. The above formula for a vector $\boldsymbol{v}$ is simply the ordinary matrix vector product $\langle\mathbf{Q}\rangle\boldsymbol{v} := \mathbf{Q}\boldsymbol{v}$, for a linear application or $(0,2)$-tensor $\mathbf{A}$ the above formula is $\langle\mathbf{Q}\rangle\mathbf{A} := \mathbf{Q}\mathbf{A}\mathbf{Q}^T$, and for a general $(0,n)$-tensor $(\langle\mathbf{Q}\rangle\mathbf{T})_{ij\ldots k} := Q_i^m Q_j^n \cdots Q_k^p T_{mn\ldots p}$

As we discussed in section 2.4 about constitutive theory, the SEDF is a scalar function of the strain tensor (and in microcontinuum theory, the tensors defining the different types of deformation). For an anisotropic materials, the mechanical properties measured by different observers need to be related by a kind of tensor transformation such as the examined in definition 2.5.2. The following definition refers to the changes of such a scalar function (SEDF or other similar functions) under rotations or reflections of the group $\mathbf{O}(n)$:

> **Definition 2.5.3.** *An **action the orthogonal group** $\mathbf{O}(n)$ **on the set of tensor functions** Φ is a mapping $\mathbf{O}(n) \times \Phi \to \Phi$, such that*
>
> $$(\mathbf{Q}, \varphi(\mathbf{S}^{(a)})) \mapsto \varphi(\langle\mathbf{Q}\rangle\mathbf{S}^{(a)})$$
>
> *where the adequate representation type (r,s) is used for each $\mathbf{S}^{(a)}$.*
> *A transformation of $\mathbf{O}(n)$ is called a **symmetry transformation** of φ if:*
>
> $$\varphi(\langle\mathbf{Q}\rangle\mathbf{S}^{(a)}) = \varphi(\mathbf{S}^{(a)})$$
>
> *In this case it is said that φ is invariant under $\mathbf{Q}$.*
> *The set of all symmetry transformations of φ form the **symmetry group of** φ.*

It can be proven that the *symmetry group of a tensor function* is a *point group*, *i.e.* a subgroup of the full orthogonal group $\mathbf{O}(n)$. A tensor function is said to be *isotropic* if its symmetry group is the full orthogonal group itself; *hemitropic* if its symmetry group is the group of rotations $\mathbf{SO}(n)$; otherwise, *anisotropic*. Relative to a point group $\mathcal{G}$, we refer to tensor polynomial functions as *invariants* if their symmetry groups include this $\mathcal{G}$. For example,

- the scalar product $\boldsymbol{u} \cdot \boldsymbol{v}$ of any two vectors and the trace $\mathrm{tr}(\mathbf{A})$ of any second-order tensor are isotropic invariants.[10]

[10]When the metric tensor of the manifold is not Euclidean, there are differences between

- the mixed product $[\boldsymbol{u}, \boldsymbol{v}, \boldsymbol{w}] := (\boldsymbol{u} \times \boldsymbol{v}) \cdot \boldsymbol{w}$ is a hemitropic invariant.

Finally, we can introduce the notion of tensor representation for a given symmetry group. This is a fundamental object in the formulation of constitutive laws, in particular, a constitutive law for a certain type of anisotropic hyperelastic material is a function of the invariants contained in the tensor representation:

> **Definition 2.5.4.** *A **complete representation** for a symmetry group* $\mathcal{G}$
> *and a set of agencies* $\mathbf{S}^{(a)}$ *is a set* $\{I_i\}$ *of invariants relative to* $\mathcal{G}$ *such that any polynomial tensor function with symmetry group* $\mathcal{G}$ *can be expressed as:*
>
> $$\varphi(\mathbf{S}^{(a)}) = \tilde{\varphi}(I_1, I_2, \ldots, I_N)$$
>
> *A complete representation is also **irreducible** if none of the invariants in the representation is expressible as a single-valued function or polynomial of the remainders, thus, if any proper subset of the representation fails to be a representation.*

For example, an isotropic tensor function whose only argument is a vector $\boldsymbol{v}$ admits a unique representation in terms of only one scalar, namely $\boldsymbol{v} \cdot \boldsymbol{v}$, *i.e.* $\varphi(\boldsymbol{v}) = \tilde{\varphi}(\boldsymbol{v} \cdot \boldsymbol{v})$ [this the only possible functional form for φ in order to be a scalar invariant tensor function].

2.5.2 Isotropic tensor functions

The isotropic problems have had most priority in theoretical and applied mechanics. Since the isotropic materials possess the simplest form comparing with those of anisotropic materials. In addition, the isotropicization theorem allows to reduce anisotropic cases by adding the anisotropic structural tensors to the formulation.

The complete and irreducible representations for three-dimensional isotropic of any finite number of second-order tensors and vectors were achieved by Wang (1970, 1971) [109,110] and Smith (1971) [97] and simplified by Zheng (1993) [117]. The results are shown in table 4.1. The table shows complete and irreducible

---

three types of second-order tensors (of types (1,1), (2,0) and (0,2), thus the trace is: $\text{tr}_g(\mathbf{A}) = g^{ij} A_{ij} = g_{ij} A^{ij} = A_i^i$

lists of isotropic invariants necessary for representing isotropic and hemitropic tensor functions, *i.e* functions with symmetry groups $\mathbf{O}(3)$ and $\mathbf{SO}(3)$, any tensor functions with that symmetry groups need to be a function of the given invariants. In all tables for representations in this section the following abbreviations are employed; the symmetric 2-tensors are denoted:

$$\mathbf{A} = \mathbf{A}_i, \quad \mathbf{B} = \mathbf{A}_j, \quad \mathbf{C} = \mathbf{A}_k$$

where $i, j, k \in \{1, \ldots, N\}$ and $i < j < k$. The antisymmetric 2-tensors are denoted:

$$\mathbf{W} = \mathbf{W}_p, \quad \mathbf{V} = \mathbf{W}_q, \quad \mathbf{U} = \mathbf{W}_r$$

where $p, q, r \in \{1, \ldots, P\}$ and $p < q < r$. The vectors are denoted:

$$\boldsymbol{v} = \boldsymbol{v}_m, \quad \boldsymbol{u} = \boldsymbol{v}_n, \quad \boldsymbol{w} = \boldsymbol{v}_l$$

where $m, n, l \in \{1, \ldots, M\}$ and $m < n < l$. Note that for classical continuum mechanics the usual deformation tensors are symmetric (and some types of stress tensors). But in microcontinuum mechanics neither macrodeformation tensor is symmetric nor microdeformation tensor is symmetric. For this reason we need to explore symmetric and antisymmetric parts:

$$(\mathbf{A})_S := (\mathbf{A}) = \frac{\mathbf{A} + \mathbf{A}^T}{2}, \qquad [\mathbf{A}]_a := [\mathbf{A}] = \frac{\mathbf{A} - \mathbf{A}^T}{2}$$

Numerous isolated instances of representation theorems for isotropic tensor functions can be found in the literature before Wang's and Smith general results. They are representations theorems:
(i) for ordinary tensor functions of vectors $\boldsymbol{v}_1, \ldots, \boldsymbol{v}_M$ due to Cauchy (1850):

$$\varphi = \varphi(\boldsymbol{v}_i \cdot \boldsymbol{v}_j), \quad \text{for all pairs } i, j. \tag{2.82}$$

(ii) for scalar-valued and tensor-valued tensor functions of single second-order symmetric tensor $\mathbf{A}$:

$$\begin{aligned} \mathbf{B} &= \varphi_0 \mathbf{I} + \varphi_1 \mathbf{A} + \varphi_2 \mathbf{A}^2 \\ \varphi_i &= \varphi_i(\operatorname{tr} \mathbf{A}, \operatorname{tr} \mathbf{A}^2, \operatorname{tr} \mathbf{A}^3) \end{aligned} \tag{2.83}$$

where the φ's are of the form. Equation 2.82 show that the only possibility to form a scalar function with vector arguments is a function which consists uniquely

Table 2.3. Invariants for isotropic/hemitropic tensor functions.

Agencies	Isotropy	Hemitropy
$\mathbf{A}$	$\operatorname{tr}\mathbf{A}, \operatorname{tr}\mathbf{A}^2, \operatorname{tr}\mathbf{A}^3$	
$\mathbf{A}, \mathbf{B}$	$\operatorname{tr}\mathbf{AB}, \operatorname{tr}\mathbf{A}^2\mathbf{B}, \operatorname{tr}\mathbf{AB}^2, \operatorname{tr}\mathbf{A}^2\mathbf{B}^2$	
$\mathbf{A}, \mathbf{B}, \mathbf{C}$	$\operatorname{tr}\mathbf{ABC}$	
$\mathbf{W}$	$\operatorname{tr}\mathbf{W}^2$	
$\mathbf{A}, \mathbf{W}$	$\operatorname{tr}\mathbf{AW}^2, \operatorname{tr}\mathbf{A}^2\mathbf{W}^2, \operatorname{tr}\mathbf{A}^2\mathbf{W}^2\mathbf{AW}$	
$\mathbf{A}, \mathbf{B}, \mathbf{W}$	$\operatorname{tr}\mathbf{ABW}, \operatorname{tr}\mathbf{A}^2\mathbf{BW}, \operatorname{tr}\mathbf{AB}^2\mathbf{W}^2, \operatorname{tr}\mathbf{AW}^2\mathbf{BW}$	
$\mathbf{W}, \mathbf{V}$	$\operatorname{tr}\mathbf{WV}$	
$\mathbf{A}, \mathbf{W}, \mathbf{V}$	$\operatorname{tr}\mathbf{AWV}, \operatorname{tr}\mathbf{AW}^2\mathbf{V}, \operatorname{tr}\mathbf{AWV}^2$	
$\mathbf{W}, \mathbf{V}, \mathbf{U}$	$\operatorname{tr}\mathbf{WVU}$	
$\mathbf{v}$	$\mathbf{v}\cdot\mathbf{v}$	$\mathbf{v}\cdot\mathbf{v}$
$\mathbf{A}, \mathbf{v}$	$\mathbf{v}\cdot\mathbf{Av}, \mathbf{v}\cdot\mathbf{A}^2\mathbf{v}$	$\mathbf{v}\cdot\mathbf{Av}, \mathbf{v}\cdot\mathbf{A}^2\mathbf{v}, [\mathbf{v}, \mathbf{Av}, \mathbf{A}^2\mathbf{v}]$
$\mathbf{A}, \mathbf{B}, \mathbf{v}$	$\mathbf{v}\cdot\mathbf{ABv}$	$\mathbf{v}\cdot\boldsymbol{\epsilon}[\mathbf{AB}], \mathbf{v}\cdot\boldsymbol{\epsilon}[\mathbf{A}^2\mathbf{B}],$ $\mathbf{v}\cdot\boldsymbol{\epsilon}[\mathbf{AB}^2], [\mathbf{v}, \mathbf{Av}, \mathbf{Bv}]$
$\mathbf{W}, \mathbf{v}$	$\mathbf{v}\cdot\mathbf{W}^2\mathbf{v}$	$\mathbf{v}\cdot\boldsymbol{\epsilon}\mathbf{W}, \mathbf{v}\cdot\mathbf{A}^2\mathbf{v}, [\mathbf{v}, \mathbf{Av}, \mathbf{A}^2\mathbf{v}]$
$\mathbf{A}, \mathbf{W}, \mathbf{v}$	$\mathbf{v}\cdot\mathbf{AWv}, \mathbf{v}\cdot\mathbf{A}^2\mathbf{Wv}, \mathbf{v}\cdot\mathbf{WAW}^2\mathbf{v}$	$\mathbf{v}\cdot\mathbf{AWv}, \mathbf{v}\cdot\boldsymbol{\epsilon}[\mathbf{AW}], \mathbf{v}\cdot\boldsymbol{\epsilon}[\mathbf{AW}^2]$
$\mathbf{W}, \mathbf{V}, \mathbf{v}$	$\mathbf{v}\cdot\mathbf{WVv}, \mathbf{v}\cdot\mathbf{W}^2\mathbf{Vv}, \mathbf{v}\cdot\mathbf{WV}^2\mathbf{v}$	$\mathbf{v}\cdot\boldsymbol{\epsilon}[\mathbf{WV}]$
$\mathbf{u}, \mathbf{v}$	$\mathbf{v}\cdot\mathbf{u}$	$\mathbf{v}\cdot\mathbf{u}$
$\mathbf{A}, \mathbf{v}, \mathbf{u}$	$\mathbf{v}\cdot\mathbf{Au}, \mathbf{v}\cdot\mathbf{A}^2\mathbf{u}$	$\mathbf{v}\cdot\mathbf{Au}, [\mathbf{v}, \mathbf{u}, \mathbf{Av}], [\mathbf{v}, \mathbf{u}, \mathbf{Au}]$
$\mathbf{A}, \mathbf{B}, \mathbf{v}, \mathbf{u}$	$\mathbf{v}\cdot(\mathbf{AB}-\mathbf{BA})\mathbf{u}$	—
$\mathbf{W}, \mathbf{v}, \mathbf{u}$	$\mathbf{v}\cdot\mathbf{Wu}, \mathbf{v}\cdot\mathbf{W}^2\mathbf{u}$	$\mathbf{v}\cdot\mathbf{Wu}$
$\mathbf{A}, \mathbf{W}, \mathbf{v}, \mathbf{u}$	$\mathbf{v}\cdot(\mathbf{AW}+\mathbf{WA})\mathbf{u}$	—
$\mathbf{W}, \mathbf{V}, \mathbf{v}, \mathbf{u}$	$\mathbf{v}\cdot(\mathbf{WV}-\mathbf{VW})\mathbf{u}$	—
$\mathbf{v}, \mathbf{u}, \mathbf{w}$	—	$[\mathbf{v}, \mathbf{u}, \mathbf{w}]$

in the norms of the vectors and/or inner products of the vectors. The result in equation 2.83 is known as the *Rivlin-Ericksen's theorem* for isotropic solids.

2.5.3 Anisotropic tensor functions

A subgroup of the Orthogonal group $\mathbf{O}(3)$ is referred as a *point group*. As numbers measure size, groups measure symmetry. A fundamental problem arises whether or not every point group describes a possible real material symmetry Zheng and Boehler (1994) [119] established some useful results about this question:

> **Theorem 2.5.1.** *Concerning the symmetry group of a tensor function:*
> (i) *The symmetry group of a polynomial tensor function of any finite number of tensor agencies can be only a compact point group (the compact subgroups are precisely the Lie subgroups).*
> (ii) Generalized Wineman-Pipkin's theorem. *For any finite number of tensor agencies and relative to any compact point group, a complete representation for polynomal tensor functions can play as complete representation for tensor functions.*
> (iii) Zheng-Boehler's classification theorem. *Any compact three-dimensional point group is conjugate of one of the following groups: the axial groups* $\mathrm{C}_n, \mathrm{S}_{2n}, \mathrm{C}_{nh}, \mathrm{C}_{nv}, \mathrm{D}_n, \mathrm{D}_{nd}, \mathrm{D}_{nh}$, *the polyhedral groups:* $\mathrm{T}, \mathrm{T}_d, \mathrm{T}_h, \mathrm{O}, \mathrm{O}_h, \mathrm{I}, \mathrm{I}_h$, *the infinite axial groups* $\mathrm{C}_\infty, \mathrm{C}_{\infty h}, \mathrm{D}_\infty, \mathrm{C}_{\infty v}, \mathrm{D}_{\infty h}$ *and the complete groups* $\mathbf{SO}(3), \mathbf{O}(3)$ *and any non-compact three-dimensional group point group is conjugate to a group which is dense in one of the infinite groups (the axial infinite groups or the complete groups)*

The part (i) can be made more general, if $\Psi(\mathbf{S}^{(a)})$ is a non-polynomial tensor function and the induced function Ψ^* of any orthogonal tensor $\mathbf{Q}$:

$$\Psi^*(\mathbf{S}^{(a)}) = \Psi(\langle\mathbf{Q}\rangle\mathbf{S}^{(a)}) \tag{2.84}$$

is continuous in the full orthogonal group, then the symmetry group of $\Psi(\mathbf{S}^{(a)})$ must be a compact group. This extends the results to all continuous tensorial functions, from the result obtained for polynomials.

The theorem 2.5.1 classifies all types of material symmetry groups, but in the elastic behavior not all the above symmetries are distinguishable. A consequence of the *Zheng-Boehler's classification theorem* and the *structural tensor theorem* (see below theorem 2.5.2) is that the all possible symmetries of linear physical properties by a pth-order tensor in three dimensions are the symmetries of the table 2.4.

Table 2.4. Possible symmetry groups of a pth-order tensor in three dimensions

$p = 2l$ (even order)	$p = 2l + 1$ (odd order)
$C_i, C_{3i}, C_{5i}, \ldots, C_{(p-1)i},$ $D_{3d}, D_{5d}, D_{7d}, \ldots, D_{(p-1)d},$ $C_{2h}, C_{4h}, C_{6h}, \ldots, C_{ph}; C_{\infty h},$ $D_{2h}, D_{4h}, D_{6h}, \ldots, D_{ph}; D_{\infty h},$ $T_h(\text{if } p \geq 4), O_h(\text{if } p \geq 4),$ $I_h(\text{if } p \geq 6), \mathbf{O}(3)(\text{if } p \geq 2)$	$C_1, C_2, C_3, \ldots, C_q; C_\infty$ $D_1, D_3, D_4, \ldots, D_p; D_\infty$ $C_{2v}, C_{3v}, C_{4v}, \ldots, C_{pv}; C_{\infty v},$ $C_{2i}, C_{4i}, C_{6i}, \ldots, C_{(p-1)i},$ $D_{2d}, D_{4d}, D_{6d}, \ldots, D_{(p-1)d},$ $C_{1h}, C_{3h}, C_{5h}, \ldots, C_{ph},$ $D_{3h}, D_{5h}, D_{7h}, \ldots, D_{ph},$ $T(\text{if } p \geq 3), T_d(\text{if } p \geq 3),$ $O(\text{if } p \geq 5), I(\text{if } p \geq 7)$ $\mathbf{SO}(3)(\text{if } p \geq 3)$

A representation of some the symmetry groups described in the above theorem are represented in tables 2.5 and 2.6. In this tables two-color partition (a tessellation) is showed, this partition is invariant under rotations and reflections of a given group. A two-color partition on the sphere which is invariant under a given point group $\mathcal{G} \subset \mathbf{O}(3)$, with the property that no finer partition is invariant under $\mathcal{G}$ is called the **"invariant domain"** of $\mathcal{G}$.

Table 2.5. Invariant domains of three-dimensional polyhedral point groups.

T_d (order 24)	O_h (order 48)	I_h (order 120)
Tetrahedral group	Octahedral group	Icosahedral group
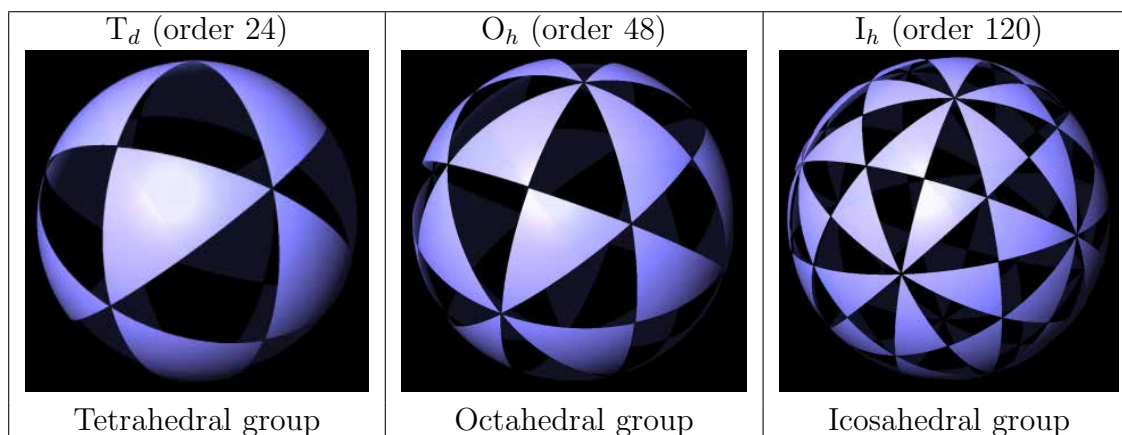
Table 2.6. Invariant domains of three-dimensional axial point groups.
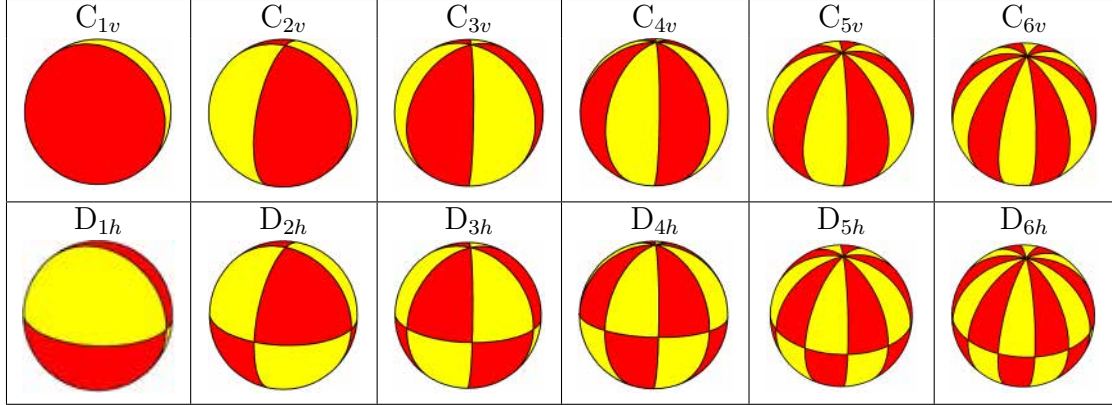
Table 2.7. Invariants for symmetry groups TR_4, TR_2 and TR_5.

Agencies	Transversal isotropy type $TR_4 = \mathrm{D}_{\infty h}$	Transversal isotropy type $TR_2 = \mathrm{C}_{\infty v}$	Transversal isotropy type $TR_5 = \mathrm{D}_\infty$
$\mathbf{A}$	$\operatorname{tr}\mathbf{A}, \operatorname{tr}\mathbf{A}^2, \operatorname{tr}\mathbf{A}^3, \mathbf{k}\cdot\mathbf{Ak}, \mathbf{k}\cdot\mathbf{A}^2\mathbf{k}$		
$\mathbf{A},\mathbf{B}$	$\operatorname{tr}\mathbf{AB}, \operatorname{tr}\mathbf{A}^2\mathbf{B}, \operatorname{tr}\mathbf{AB}^2, \mathbf{k}\cdot\mathbf{ABk}$		
$\mathbf{W}$	$\operatorname{tr}\mathbf{W}^2, \mathbf{k}\cdot\mathbf{W}^2\mathbf{k}$		
$\mathbf{A},\mathbf{W}$	$\operatorname{tr}\mathbf{AW}^2, \operatorname{tr}\mathbf{A}^2\mathbf{W}^2, \operatorname{tr}\mathbf{A}^2\mathbf{W}^2\mathbf{AW}, \mathbf{k}\cdot\mathbf{AWk}, \mathbf{k}\cdot\mathbf{A}^2\mathbf{Wk}, \mathbf{k}\cdot\mathbf{WAW}^2\mathbf{k}$		
$\mathbf{W},\mathbf{V}$	$\operatorname{tr}\mathbf{WV}, \mathbf{k}\cdot\mathbf{WVk}, \mathbf{k}\cdot\mathbf{W}^2\mathbf{Vk}, \mathbf{k}\cdot\mathbf{WV}^2\mathbf{k},$		
$\mathbf{v}$	$\mathbf{v}\cdot\mathbf{v}, (\mathbf{v}\cdot\mathbf{k})^2$	$\mathbf{v}\cdot\mathbf{v}, \mathbf{v}\cdot\mathbf{k}$	$\mathbf{v}\cdot\mathbf{v}, (\mathbf{v}\cdot\mathbf{k})^2$
$\mathbf{A},\mathbf{v}$	$\mathbf{v}\cdot\mathbf{Av}, \mathbf{v}\cdot\mathbf{A}^2\mathbf{v},$ $(\mathbf{k}\cdot\mathbf{v})(\mathbf{k}\cdot\mathbf{Av})$	$\mathbf{v}\cdot\mathbf{Av}, \mathbf{k}\cdot\mathbf{Av},$ $\mathbf{k}\cdot\mathbf{A}^2\mathbf{v}$	$\mathbf{v}\cdot\mathbf{Av}, \mathbf{v}\cdot\mathbf{A}^2\mathbf{v},$ $[\mathbf{k},\mathbf{v},\mathbf{Ak}], [\mathbf{k},\mathbf{v},\mathbf{A}^2\mathbf{k}]$ $[\mathbf{v},\mathbf{Av},\mathbf{A}^2\mathbf{v}]$
$\mathbf{W},\mathbf{v}$	$\mathbf{v}\cdot\mathbf{W}^2\mathbf{v},$ $(\mathbf{k}\cdot\mathbf{v})(\mathbf{k}\cdot\mathbf{Wv}),$ $(\mathbf{k}\cdot\mathbf{Wv})(\mathbf{k}\cdot\mathbf{W}^2\mathbf{v})$	$\mathbf{v}\cdot\mathbf{Wv},$ $\mathbf{v}\cdot\mathbf{W}^2\mathbf{v}$	$[\mathbf{k},\mathbf{v},\mathbf{Wk}], [\mathbf{k},\mathbf{v},\mathbf{W}^2\mathbf{k}]$ $(\mathbf{k}\cdot\mathbf{v})(\mathbf{k}\cdot\mathbf{Wv}),$ $\mathbf{v}\cdot\boldsymbol{\epsilon}[\mathbf{W}]$
$\mathbf{v},\mathbf{u}$	$\mathbf{v}\cdot\mathbf{u}, (\mathbf{v}\cdot\mathbf{k})(\mathbf{u}\cdot\mathbf{k})$	$\mathbf{v}\cdot\mathbf{u}, (\mathbf{v}\cdot\mathbf{k})(\mathbf{u}\cdot\mathbf{k})$ $[\mathbf{k},\mathbf{v},\mathbf{u}]$	$\mathbf{v}\cdot\mathbf{u}, (\mathbf{v}\cdot\mathbf{k})(\mathbf{u}\cdot\mathbf{k})$ $[\mathbf{k},\mathbf{v},\mathbf{u}](\mathbf{k}\cdot\mathbf{v})$ $[\mathbf{k},\mathbf{v},\mathbf{u}](\mathbf{k}\cdot\mathbf{u})$
$\mathbf{A},\mathbf{v},\mathbf{u}$	$\mathbf{v}\cdot\mathbf{Au}, \mathbf{v}\cdot\mathbf{A}^2\mathbf{u},$ $\mathbf{v}\cdot(\mathbf{k}\otimes\mathbf{Ak}-\mathbf{Ak}\otimes\mathbf{k})\mathbf{u}$	$\mathbf{v}\cdot\mathbf{Au}$	$\mathbf{v}\cdot\mathbf{Au}, [\mathbf{v},\mathbf{u},\mathbf{Au}]$ $[\mathbf{v},\mathbf{u},\mathbf{Av}]$
$\mathbf{W},\mathbf{v},\mathbf{u}$	$\mathbf{v}\cdot\mathbf{Wu}, \mathbf{v}\cdot\mathbf{W}^2\mathbf{u},$ $\mathbf{v}\cdot(\mathbf{k}\otimes\mathbf{Wk}-\mathbf{Wk}\otimes\mathbf{k})\mathbf{u}$	$\mathbf{v}\cdot\mathbf{Wu}$	$\mathbf{v}\cdot\mathbf{Wu}$
$\mathbf{v},\mathbf{u},\mathbf{w}$	—	—	$[\mathbf{v},\mathbf{u},\mathbf{w}]$

The two lists in table 2.4 imply that for classical elasticity (where strain tensor and stress tensors are second-order tensors) we have the following types of anisotropy:

- **Isotropy and hemitropy**. A tensor function is isotropic if it is invariant under transformations "rotations" and "reflexitons" (invariant under the action of $\mathbf{O}(3)$), and hemitropic it is invariant only under "rotations" (invariant under the action of $\mathbf{SO}(3)$).

- **Transversal isotropy/hemitropy**. This type of anisotropy when there is a preferred direction. Unidirectional fiber composite is a typical example of transversely isotropic material with the fiber direction as the preferred direction, where the constitutive relations are invariant under rotations about the preferred direction. Muscle should be considered as transversally isotropic material rather than an isotropic one. There are five subtypes of transverse isotropy, one for each of the following symmetry groups: $TR_1 = C_\infty$, $TR_2 = C_{\infty v}$, $TR_3 = C_{\infty h}$, $TR_4 = D_{\infty h}$, $TR_5 = D_\infty$ (respectively *rotational symmetry, rotational symmetry with parallel reflection planes* (parallel to the preferred direction), *rotational symmetry with reflection normal plane* (normal to the preferred direction), *full transverse isotropy* and *transverse hemitropy*). The transversal isotropic/hemitropic invariants are summarized in tables 2.7 and 2.8 (in tables, $\mathbf{k}$ represents the structural vector).
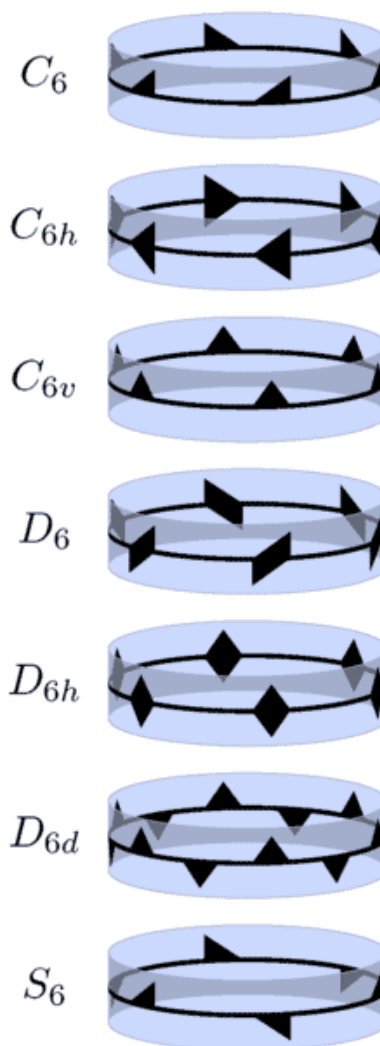
Figure 2.19. Invariant geometries under the axial groups: rotational or cyclic group C_6, cyclic group with horizontal reflection C_{6h}, pyramidal group or cyclic group with horizontal reflections C_{6v}, dihedral group D_6, prismatic group D_{6h}, anti-prismatic group D_{6v}, cyclic group with inversion S_6, (after A. Kepert, Wikimedia, 2006)

- **Orthotropy**. There are three subtypes of properly orthotropic materials with symmetry groups: $OR_1 = C_{2v}, OR_2 = D_2, OR_3 = D_{2h}$. Some authors do not distinguish properly between orthotropy and transversal isotropy, and consider the later one a subtype of the former one. Here, we will use the term "orthotropy" in a proper sense, and consider transversal symmetries other type. Some cross-ply laminates are orthotropic, whose material symmetry can be described as OR_3. Rolled sheet steels possess a plastic-induced orthotropy in the rolling direction, the transverse direction and the direction of the thickness. The orthotropic invariants are summarized in table 2.9 (in the table, $\mathbf{k}$ and $\mathbf{M}$ represent the structural tensors for OR_i).
- **Clinotropy**. Crystals in the monoclinic system and composite reinforced with families of fibers in two non-orthogonal and mechanically non-equivalent directions are referred as "clinotropic" materials. There are thre subtypes of materials called monoclinic clinotropic materials (with symmetry groups $CL_1^m = C_{2h}, CL_2^m = C_{1h}, CL_3^m = C_2$), and two additional subtypes called triclinic clinotropic materials (with symmetry groups $CL_1^t = C_i, CL_2^t = C_1$).

Table 2.8. Invariants for symmetry groups TR_1 and TR_3.

Agencies	Transversal isotropy type $TR_3 = C_{\infty h}$	Transversal isotropy type $TR_1 = C_\infty$
$\mathbf{A}$	$\operatorname{tr} \mathbf{A}, \operatorname{tr} \mathbf{A}^2, \operatorname{tr} \mathbf{A}^3, \mathbf{k} \cdot \mathbf{Ak}, \mathbf{k} \cdot \mathbf{A}^2\mathbf{k}, [\mathbf{k}, \mathbf{Ak}, \mathbf{A}^2\mathbf{k}]$	
$\mathbf{A}, \mathbf{B}$	$\operatorname{tr} \mathbf{AB}, \operatorname{tr} \mathbf{A}^2\mathbf{B}, \operatorname{tr} \mathbf{AB}^2, \operatorname{tr} \mathbf{A}^2\mathbf{B}^2, \mathbf{k} \cdot \boldsymbol{\epsilon}[\mathbf{AB}], \mathbf{k} \cdot \boldsymbol{\epsilon}[\mathbf{A}^2\mathbf{B}], [\mathbf{k}, \mathbf{Ak}, \mathbf{Bk}]$	
$\mathbf{W}$	$\operatorname{tr} \mathbf{W}^2, \mathbf{k} \cdot \boldsymbol{\epsilon}[\mathbf{W}]$	
$\mathbf{A}, \mathbf{W}$	$\operatorname{tr} \mathbf{AW}^2, \mathbf{k} \cdot \mathbf{AWk}, \mathbf{k} \cdot \boldsymbol{\epsilon}[\mathbf{AW}], \mathbf{k} \cdot \boldsymbol{\epsilon}[\mathbf{AW}^2]$	
$\mathbf{W}, \mathbf{V}$	$\operatorname{tr} \mathbf{WV}, \mathbf{k} \cdot \boldsymbol{\epsilon}[\mathbf{WV}]$	
$\mathbf{v}$	$\mathbf{v} \cdot \mathbf{v}, (\mathbf{v} \cdot \mathbf{k})^2$	$\mathbf{v} \cdot \mathbf{v}, \mathbf{k} \cdot \mathbf{v}$
$\mathbf{A}, \mathbf{v}$	$\mathbf{v} \cdot \mathbf{Av}, \mathbf{v} \cdot \mathbf{A}^2\mathbf{v}, [\mathbf{k}, \mathbf{v}, \mathbf{Av}], [\mathbf{k}, \mathbf{v}, \mathbf{A}^2\mathbf{v}], (\mathbf{v} \cdot \mathbf{k})[\mathbf{k}, \mathbf{v}, \mathbf{A}^2\mathbf{k}]$	$\mathbf{v} \cdot \mathbf{Av}, \mathbf{k} \cdot \mathbf{Av}, [\mathbf{k}, \mathbf{v}, \mathbf{Av}], [\mathbf{k}, \mathbf{v}, \mathbf{Ak}]$
$\mathbf{W}, \mathbf{v}$	$\mathbf{v} \cdot \mathbf{W}^2\mathbf{v}, [\mathbf{k}, \mathbf{v}, \mathbf{Wv}], [\mathbf{k}, \mathbf{v}, \mathbf{W}^2\mathbf{v}], (\mathbf{v} \cdot \mathbf{k})(\mathbf{k} \cdot \mathbf{Wv})$	$\mathbf{v} \cdot \boldsymbol{\epsilon}[\mathbf{W}], \mathbf{k} \cdot \mathbf{Wv}$
$\mathbf{u}, \mathbf{v}$	$\mathbf{v} \cdot \mathbf{u}, [\mathbf{k}, \mathbf{u}, \mathbf{v}],$	$\mathbf{v} \cdot \mathbf{u}$
$\mathbf{A}, \mathbf{v}, \mathbf{u}$	$\mathbf{v} \cdot \mathbf{Au}, \mathbf{k} \cdot (\mathbf{v} \times \mathbf{Au} - \mathbf{u} \times \mathbf{Av})$	—
$\mathbf{W}, \mathbf{v}, \mathbf{u}$	$\mathbf{v} \cdot \mathbf{Wu}, \mathbf{k} \cdot (\mathbf{v} \times \mathbf{Wu} - \mathbf{u} \times \mathbf{Wv})$	—

Table 2.9. Invariants for symmetry groups OR_3, OR_1 and OR_2.

Agencies	Transversal isotropy type $OR_3 = D_{2h}$	Transversal isotropy type $OR_1 = C_{2v}$	Transversal isotropy type $OR_2 = D_2$
A	$\operatorname{tr}\mathbf{A}, \operatorname{tr}\mathbf{A}^2, \operatorname{tr}\mathbf{A}^3, \operatorname{tr}\mathbf{MA}, \operatorname{tr}\mathbf{M}^2\mathbf{A}, \operatorname{tr}\mathbf{MA}^2, \operatorname{tr}\mathbf{M}^2\mathbf{A}^2$		
A, B	$\operatorname{tr}\mathbf{AB}, \operatorname{tr}\mathbf{A}^2\mathbf{B}, \operatorname{tr}\mathbf{AB}^2, \operatorname{tr}\mathbf{MAB}$		
A, B, C	$\operatorname{tr}\mathbf{ABC}$		
W	$\operatorname{tr}\mathbf{W}^2, \operatorname{tr}\mathbf{MW}^2, \operatorname{tr}\mathbf{M}^2\mathbf{W}^2, \operatorname{tr}\mathbf{M}^2\mathbf{W}^2\mathbf{MW}$		
A, W	$\operatorname{tr}\mathbf{AW}^2, \operatorname{tr}\mathbf{MAW}, \operatorname{tr}\mathbf{M}^2\mathbf{AW}, \operatorname{tr}\mathbf{MA}^2\mathbf{W}$		
A, B, W	$\operatorname{tr}\mathbf{ABW}$		
W, V	$\operatorname{tr}\mathbf{WV}, \operatorname{tr}\mathbf{MWV}, \operatorname{tr}\mathbf{MW}^2\mathbf{V}, \operatorname{tr}\mathbf{MWV}^2$		
A, W, V	$\operatorname{tr}\mathbf{AWV}$		
W, V, U	$\operatorname{tr}\mathbf{WVU}$		
v	$\mathbf{v}\cdot\mathbf{v}, \mathbf{v}\cdot\mathbf{Mv}, \mathbf{v}\cdot\mathbf{M}^2\mathbf{v}$	$\mathbf{v}\cdot\mathbf{v}, \mathbf{v}\cdot\mathbf{Mv}, \mathbf{k}\cdot\mathbf{v}$	$\mathbf{v}\cdot\mathbf{v}, \mathbf{v}\cdot\mathbf{v}, \mathbf{v}\cdot\mathbf{Mv},$ $\mathbf{v}\cdot\mathbf{M}^2\mathbf{v},$ $[\mathbf{v},\mathbf{Mv},\mathbf{M}^2\mathbf{v}]$
A, v	$\mathbf{v}\cdot\mathbf{Av}, \mathbf{v}\cdot\mathbf{A}^2\mathbf{v},$ $\mathbf{v}\cdot\mathbf{MAv}$	$\mathbf{v}\cdot\mathbf{Av}, \mathbf{k}\cdot\mathbf{Av},$ $\mathbf{k}\cdot\mathbf{A}^2\mathbf{v}$ $\mathbf{k}\cdot(\mathbf{AM}-\mathbf{MA})\mathbf{v}$	$\mathbf{v}\cdot\mathbf{Av}, \epsilon[\mathbf{MA}],$ $\epsilon[\mathbf{M}^2\mathbf{A}], \epsilon[\mathbf{MA}^2]$
W, v	$\mathbf{v}\cdot\mathbf{W}^2\mathbf{v}, \mathbf{v}\cdot\mathbf{MWv},$ $\mathbf{v}\cdot\mathbf{M}^2\mathbf{Wv}$	$\mathbf{v}\cdot\mathbf{MWv}, \mathbf{k}\cdot\mathbf{Wv},$ $\mathbf{k}\cdot\mathbf{W}^2\mathbf{v},$ $\mathbf{k}\cdot(\mathbf{MW}+\mathbf{WM})\mathbf{v}$	$\mathbf{v}\cdot\mathbf{MWv}, \mathbf{v}\cdot\epsilon[\mathbf{W}],$ $\mathbf{v}\cdot\epsilon[\mathbf{MW}],$ $\mathbf{v}\cdot\epsilon[\mathbf{MW}^2]$
v, u	$\mathbf{v}\cdot\mathbf{u}, \mathbf{v}\cdot\mathbf{Mu}$ $\mathbf{v}\cdot\mathbf{M}^2\mathbf{u}$	$\mathbf{v}\cdot\mathbf{u}, \mathbf{v}\cdot\mathbf{Mu}$	$\mathbf{v}\cdot\mathbf{u}, \mathbf{v}\cdot\mathbf{Mu}$ $[\mathbf{v},\mathbf{u},\mathbf{Mu}], [\mathbf{v},\mathbf{u},\mathbf{Mv}]$

2.5.4 Structural tensor theorem and isotropicization theorem

For any point group $\mathcal{G} \subset \mathbf{O}(3)$, if there are tensors $\mathbf{M}_1,\ldots,\mathbf{M}_S$ such that any orthogonal transformation $\mathbf{Q}$ belongs to $\mathcal{G}$ if and only if:

$$\langle\mathbf{Q}\rangle\mathbf{M}_1 = \mathbf{M}_1, \ldots, \langle\mathbf{Q}\rangle\mathbf{M}_S = \mathbf{M}_S$$

we say that the tensors $\mathbf{M}_1,\ldots,\mathbf{M}_S$ characterize $\mathcal{G}$. In other words the tensors $\mathbf{M}_i$ are **structural tensors**. Formally, we can write that a set of tensors $\{\mathbf{M}_1,\ldots,\mathbf{M}_S\}$ is *structural* if for this set the following proposition is true:

$$(\forall i : \langle\mathbf{Q}\rangle\mathbf{M}_i = \mathbf{M}_i) \Leftrightarrow \mathbf{Q} \in \mathcal{G} \tag{2.85}$$

In correspondence with the Zheng-Boehler's classification theorem, the same authors established the following **structural tensor theorem** [119] and Zheng established the **isotropicization theorem** [118]. We quote both results as part of the same result:

Theorem 2.5.2. *Concerning the symmetry group of a tensor function:*
(i) Structural tensor theorem. Let $\mathcal{G}$ a two- or three-dimensional point group. Then (a) if $\mathcal{G}$ is compact, $\mathcal{G}$ can be characterized by single (even irreducible) tensor. (b) if $\mathcal{G}$ can be characterized by a finite number of tensors, then $\mathcal{G}$ is compact; and (c) if $\mathcal{G}$ is non-compact, $\mathcal{G}$ cannot be characterized by a finite number of tensors of finite orders.
(ii) Isotropicization theorem. An anisotropic tensor function in three-dimensional space of any finite number of tensor agencies relative to a compact point group is expressible as an isotropic tensor function of the original tensor agencies and the structural tensors.

Mathematically, let $\varphi(\mathbf{S}_a)$ be an anisotropic tensor function of tensor agencies $\mathbf{S}_1, \ldots, \mathbf{S}_A$ relative to a compact point group characterized by structural tensors $\mathbf{M}_1, \ldots, \mathbf{M}_S$. Then, there exists an isotropic tensor function $\varphi_{iso}(\mathbf{S}_a, \mathbf{M}_s)$ of $\mathbf{S}_1, \ldots, \mathbf{S}_A; \mathbf{M}_1, \ldots, \mathbf{M}_S$ so that:

$$\varphi(\mathbf{S}_a) = \varphi_{iso}(\mathbf{S}_a, \mathbf{M}_s) \tag{2.86}$$

The importance of isotropicization theorem can be seen in deriving complete and irreducible representations for anisotropic tensor functions as well as isotropic functions involving higher order tensor, and in formulating constitutive laws in unified and consistent forms [118].

It is interesting to note that the non-compact groups (which are infinite groups contained but dense in some compact infinite groups) do not admit a finite representation in terms of structural tensors. This seems an undesirable property considered unphysical for many authors. These non-compact subgroups note being closed are not Lie subgroups (For this reason, it is interesting to use the theory of topological groups not simply the theory of groups for classifying symmetries).

As a final comment we can remark that the reality of crystal classes, transverse isotropies, hemitropy and isotropy are well-known. In addition, the two

kinds of three-dimensional point group in the icosahedral system are of increasing importance in describing the symmetry of quasi-crystals and viruses [49, 106]. For every other non-crystallographic finite point group, Zheng and Boehler exampled real or ideal laminates (which can be generally referred as quasi-isotropic composites) such that their macroscopic material symmetry correspond to this point group [119]. The density of a non-compact point group in a certain continuous or mixed continuous group and the observation of the physical reality of materials in continuum physics point of view have lead to the fundamental proposal of Zheng and Boehler: *The description of the symmetry of a continuous medium or any physical property of this medium by a non-compact point group is an unreality.* This can be included as an additional principle that seems to be a general property of matter. Thus Zheng (1994) introduced the following so-called **principle of symmetry of continuum**:

> ***Principle of symmetry of continuum*** *Compact point groups describe and classify all kind of real and ideal material symmetry and physical symmetry, while the description of the symmetry of a continuous medium by a non-compact point group is not physical realistic.*

Assuming this principle some authors call compact point groups as *material point groups* as a broader category than crystallographic point groups. In particular, since a mechanical symmetry group includes the central inversion $-\mathbf{1}$, as a direct consequence of the principle of symmetry of continuum and the classification theorem, we can classify all kinds of mechanical symmetry in three-dimensional spaces, as shown in table 2.10. In the tables of structural tensors the following notations is used: $\mathbf{R}(\theta\boldsymbol{n})$ denotes a rotation of θ (radians) around the axis $\boldsymbol{n}$; $\boldsymbol{i},\boldsymbol{j},\boldsymbol{k}$ is the canonical basis in $\mathbb{R}^3$; the vectors: $\boldsymbol{c} = \boldsymbol{i} + \boldsymbol{j} + \boldsymbol{k}/\sqrt{3}$, $\boldsymbol{l} = \boldsymbol{i}\cos\zeta - \boldsymbol{k}\sin\zeta$ with $\tan\zeta = (3 - \sqrt{5}/4)$; $\mathbf{R_i}$ a reflection; and the polyhedral structural tensors:

$$\begin{aligned}
\mathbf{T}_h &= \boldsymbol{i}^2 \otimes \boldsymbol{j}^2 - \boldsymbol{k}^2 \otimes \boldsymbol{i}^2 + \boldsymbol{j}^2 \otimes \boldsymbol{k}^2 - \boldsymbol{k}^2 \otimes \boldsymbol{j}^2 + \boldsymbol{k}^2 \otimes \boldsymbol{i}^2 - \boldsymbol{i}^2 \otimes \boldsymbol{k}^2 \\
\mathbf{O}_h &= \boldsymbol{i}^4 + \boldsymbol{j}^4 + \boldsymbol{k}^4 \\
\mathbf{I}_h &= \boldsymbol{a}_1^6 + \boldsymbol{a}_2^6 + \cdots + \boldsymbol{a}_6^6
\end{aligned}$$

where $\boldsymbol{a}_6 = \boldsymbol{k}$ and $\sqrt{5}\boldsymbol{a}_m = \boldsymbol{k} + 2(\cos(2\pi m/5)\boldsymbol{i} + \sin(2\pi m/5)\boldsymbol{j})$ and the abbreviation $\boldsymbol{w}^n$ for any real or complex vector $\boldsymbol{w}$ denotes the nth-order real or complex tensor:

$$\boldsymbol{w}^n := \underbrace{\boldsymbol{w} \otimes \cdots \otimes \boldsymbol{w}}_{n}$$

The nth-order basic structural tensors $\mathbf{P}_n (n = 1, 2, \dots)$ is defined as:

$$\mathbf{P}_n = \mathrm{Re}(\boldsymbol{i} + i\boldsymbol{j})^n$$

where $i = \sqrt{-1}$, $\mathrm{Re}(\cdot)$ denotes "real part of". The first term in the list are: $\mathbf{P}_1 = \boldsymbol{i}$, $\mathbf{P}_2 = \boldsymbol{i} \otimes \boldsymbol{i} - \boldsymbol{j} \otimes \boldsymbol{j}$, $\mathbf{P}_3 = \boldsymbol{i} \otimes \boldsymbol{i} \otimes \boldsymbol{i} - (\boldsymbol{i} \otimes \boldsymbol{j} \otimes \boldsymbol{j} + \boldsymbol{j} \otimes \boldsymbol{i} \otimes \boldsymbol{j} + \boldsymbol{j} \otimes \boldsymbol{j} \otimes \boldsymbol{i})$, etc.

Table 2.10. Classification of three-dimensional mechanical symmetries

Mechanical symmetries	Group generators (all include $-\mathbf{1}$)	Structural tensors	Symmetries of linear elasticity
$\mathrm{C}_{ni}(n = 3, 5, 7, \dots)$	$\mathbf{R}(2\pi/n\boldsymbol{k})$	$\mathbf{P}_n \otimes \boldsymbol{k}, \epsilon\boldsymbol{k}$	$\mathrm{C}_i, \mathrm{C}_{3i}$
$\mathrm{D}_{nd}(n = 3, 5, 7, \dots)$	$\mathbf{R}(2\pi/n\boldsymbol{k}), \mathbf{R_j}$	$\mathbf{P}_n \otimes \boldsymbol{k}$	C_{3d}
$\mathrm{C}_{nh}(n = 2, 4, 6, \dots)$	$\mathbf{R}(2\pi/n\boldsymbol{k})$	$\mathbf{P}_n, \epsilon\boldsymbol{k}$	$\mathrm{C}_{2h}, \mathrm{C}_{4h}, \mathrm{C}_{6h}$
$\mathrm{D}_{nh}(n = 2, 4, 6, \dots)$	$\mathbf{R}(2\pi/n\boldsymbol{k}), \mathbf{R_i}, \mathbf{R_j}$	$\mathbf{P}_n$	$\mathrm{D}_{2h}, \mathrm{D}_{4h}, \mathrm{D}_{6h}$
$\mathrm{C}_{\infty h}$	$\mathbf{R}(\theta\boldsymbol{k})$	$\epsilon\boldsymbol{k}$	$\mathrm{C}_{\infty h}$
$\mathrm{D}_{\infty h}$	$\mathbf{R}(\theta\boldsymbol{k}), \mathbf{R_i}, \mathbf{R_j}$	$\boldsymbol{k} \otimes \boldsymbol{k}$	$\mathrm{D}_{\infty h}$
T_h	$\mathbf{R}(2\pi/3\boldsymbol{c}), \mathbf{R_i}$	$\mathbf{T}_h$	T_h
O_h	$\mathbf{R}(2\pi/3\boldsymbol{c}), \mathbf{R}(\pi/2\boldsymbol{i}), \mathbf{R_j}$	$\mathbf{O}_h$	O_h
I_h	$\mathbf{R}(2\pi/5\boldsymbol{l}), \mathbf{R}(2\pi/3\boldsymbol{i}), \mathbf{R_j}$	$\mathbf{I}_h$	—
$\mathbf{O}(3)$	$\mathbf{R}(\theta\boldsymbol{k}), \mathbf{R}(\psi\boldsymbol{i})$	1	$\mathbf{O}(3)$

3

Data and methods

3.1 Introduction

The study of the mechanical behavior of the esophageal wall under forced dilation requires a constitutive model of large deformations to be realistic. All models include functional relations among measurable magnitudes and additional parameters (called *mechanical properties*). These mechanical properties characterize the specific mechanical behavior of each sample; thus, the determination or estimation of the mechanical properties for a specific individual is required in order to predict the result of a procedure of forced dilation under specific load conditions.

A relative straightforward procedure for determining the mechanical properties of a soft tissue sample is to conduct some experiments under different conditions (a uniaxial tensile test in both longitudinal and transversal directions, inflation tests, etc.). The results of these experiments can be compared with the predictions of different models. This comparison leads to the estimation of the mechanical properties which produce the best fit between the predictions of the model and the obtained results.

For this study, we have used the uniaxial tests for determining the mechanical properties of the samples (the statistical analysis of these data allow us to have some knowledge of the average mechanical behavior of a typical esophagus, and to study the effect of some anthropometric factors like age, sex and body mass index). For the experiments, thirty-two samples of esophageal tissue were harvested from seventeen different donors. In addition, some complementary tests have been made on animal tissues, including inflation tests for comparison. All experiments in this study are *in vitro* experiments, this implies that some special conditions present *in vivo* situations are absent in the experiments. For example residual stress in esophageal wall need to be indirectly estimated as explained below.

This chapter describes the preparation of the samples, the pre-processing, the uniaxial and inflation tests, the processing of the data (forces, displacements, pressures, etc.), and the computational issues related to the post-processing of the data. Regarding the force, the digitalized data were provided by the testing machine, and the displacement of selected points were obtained by digital motion tracking with an auxiliary optical capture system.

3.2 Specimens for experimentation

3.2.1 Description of swine specimens

The first part of our testing was made using swine samples, and the obtained data were used for adjusting a restricted microcontinuum model. These results were published in *Annals of Biomedical Engineering* (henceforth ABME) [99]. The main reason for using these samples was to test the procedure; no human samples were needed for adjusting the technical requirements for our further testing.

All these swine samples were collected from 5- to 8-month-old piglets. Their esophagi were conserved after sacrifice in an animal farm (this farm is outside the facilities of the biomechanics laboratory of the UPC). Then the transportation to the UPC facilities was done in isothermal hermetical bags with a temperature of about 2°C to 5°C in saline solution inside a refrigerator. In the manipulation of all the samples, the instructions of the protocol of bio-safety of the University of Virginia (UVA) was followed.

From each swine specimen at least two samples could be obtained (in some cases three samples were obtained). For each sample a uniaxial tensile test was conducted. For computing mechanical properties, only twelve uniaxial tensile tests were selected (these tests included: two-layered sample tests (both longitudinal and transversal) and one-layered samples (again, for longitudinal and transversal directions). In addition, three inflation tests were conducted with three different swine intact esophagi. These last tests provided an interesting qualitative information about anatomical failure of an esophagus fixed to an internal pressure condition, but the numerical data are less useful than the uniaxial tensile tests.

3.2.2 Description of human specimens

Samples from seventeen donors were harvested, but only fifteen of them were suitable for testing. The manipulation of human specimens requires higher biomedical health and safety standards because all samples are treated as potentially infectious by default, according to the UVA protocol (while laboratory tests are not available providing negative results). On the other hand, swine specimens do not present some of the biomedical hazards potentially present in human samples. The anthropometric data of the human specimens are summarized in table 3.1.

As shown in the table 3.1, the mean *age* is 62.7 ± 16.3 y.o. (58.3 ± 16.5 y.o. for males, and 75.0 ± 7.7 y.o. for females), and the mean *body Mass Index* (BMI) is 33.6 ± 8.7 kg/m^2 (32.0 ± 9.6 for males, and 37.5 ± 4.7 for females). In addition, eight samples of porcine esophagi were used for some complementary tests. The swine specimens were extracted from 5 to 8 month-old piglets, no bio-metrical data are provided given that no statistical computation with those variables was performed.

3.2.3 Preparation of specimens

The used procedure for both types of samples is similar. On the first stage of this research, twelve *swine esophagi* were used. On the second stage, once the testing procedure was well established, seventeen *human esophagi* were used. All human specimens used for this study were obtained by means of a collaboration agree-

Table 3.1. Main anthropometric data of the specimens.

Specimen Number	Sex	Age [year]	Weight [kg]	Height [m]	BMI [kg/m^2]
839	♂	64	131	1.69	45.9
855	♂	66	160	1.76	51.7
856	♂	85	72	1.68	25.5
880	♂	61	—	1.55	—
911	♂	64	90	1.70	31.1
912	♂	32	88	1.67	31.6
954	♂	45	72	1.62	27.4
957	♂	68	70	1.57	28.4
961	♂	30	90	1.67	32.3
964	♂	69	60	1.70	20.8
966	♂	57	80	1.77	25.5
879	♀	68	99	1.52	42.8
906	♀	85	70	1.48	32.0
907	♀	70	76	1.46	35.7
953	♀	77	88	1.49	39.6

ment between the UPC and the IMLC (*Institut de Medicina Legal de Catalunya*).
. In all cases specimens were obtained according to the established protocols by
the Ethics Committee of this public institute.[1]

For each human specimen, an informed consent form was given to the relatives
of the potential donor. The obtained samples were processed according to this
protocol:

- **Identification**. All samples were identified by a code preserving anonymity
  of the donor. For each donor clinical data were collected: age, sex, height,
  weight and cause of death.
- **Preservation**. All samples were put in a saline solution and maintained at
  low temperature before testing it. All samples were tested in least fifteen
  hours after the extraction from the body.
- **Examination**. Each sample was examined in order to check integrity and
  absence of scratches produced during the extraction procedure.
- **Cutting**. Residues of visceral fat were completely removed carefully by
  means of a scalpel and two samples of the same length were obtained from

---

[1]On the other hand, the swine samples were collected in a nearby farm.

each specimen (both proximal and distal parts were measured in length).

- **Weighing**. The weight of each sample was measured before and after testing (in some cases a reduction of the weight of 5-15%, due to a loss of fluid in the sample by stretching was registered).

- **Marking**. In order to improve the optical process of motion tracking (used for computation of stretching and deformation) a matrix pattern of black dots were marked on the surface of the samples (an example can be seen in figure 3.1).
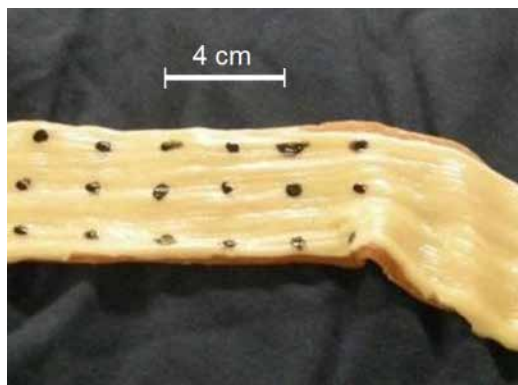
Figure 3.1. A swine sample showing the regular pattern, each sample was about 5×15 cm.

All specimens came from individuals with no known digestive diseases, and without risk in their medical histories and no esophageal pathologies. All samples were harvested in the following 24 hours after the decease. For each esophagus at least two segments of the tissue were obtained (we refer to them as the *distal* and the *proximal* parts), exceptionally for some individuals three segments were obtained (*distal, medial*, and *proximal*). The ages of all donors fall in the range 30-85 years old. A typical sample of the two segment is shown in figure 3.2:

For the preparation of all samples, surgical instrumental has been used and the UVA bio-safety protocol was followed. For human tissue samples the security and hygienic measures were much stricter than those for the animal samples, in order to prevent infections. The separation of layers was possible for all the swine esophagi except for some that were left apart. For the separation of layers, surgical scissors and a scalpel were used. The separation of both layers requires a series of consecutive cuts of the fibers joining the layers. For the *marking*, some essays were made to find an adequate substance. The main problem was that fresh tissue is normally wet and a conventional adhesive or ink is not suitable
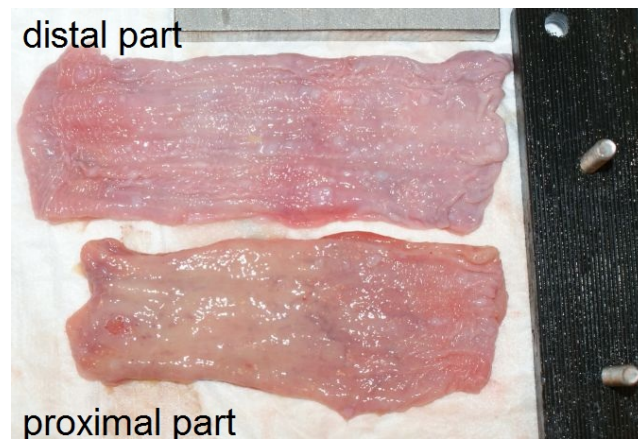
Figure 3.2. The two segments (distal and proximal) of the sample 964 [donor: male, 69 y.o.], the shown faces are in both cases is mucosa.

for the marking. In addition, an adequate contrast with the natural color of the tissue was required in order to have good results in motion tracking. Table 3.2 summarizes the inconvenient drawbacks found with some substances in the marking:

Table 3.2. Observed behavior of substances intended for marking.

Substance/ Pigment	Evaluation	Observations
Ink	Deficient	Humidity of the tissue disperses ink, resulting in cloudy streams
Aerosol paint	Deficient	Humidity of the tissue disperses ink, resulting in cloudy streams
Permanent marker	Very deficient	The marks are too weak, after some uses the marker is moistened
Enamel paint	Satisfactory	The marks are visible, if there is no abrasion in the surface, marks are stable

3.3 Experiments

3.3.1 Uniaxial tensile tests

Uniaxial tensile tests are commonly used for characterization of materials. An uniaxial test applies an increasing force on a segment of the esophagus in order

to achieve an homogeneous state of deformation. Relative displacement of the clamps is registered for each value of the applied force. Assuming that the segment is homogeneous the mechanical properties can be computed from these data (if the material is not completely homogeneous, an average is obtained instead). By computing strain and stress, the stress-strain curves can be plotted. Every test is conducted until the tearing of the tissue and cleavages are observed in the sample. Only the initial part of the data was used for the computation of the mechanical properties. In addition, the maximum stress (tearing stress) was computed from the final part.
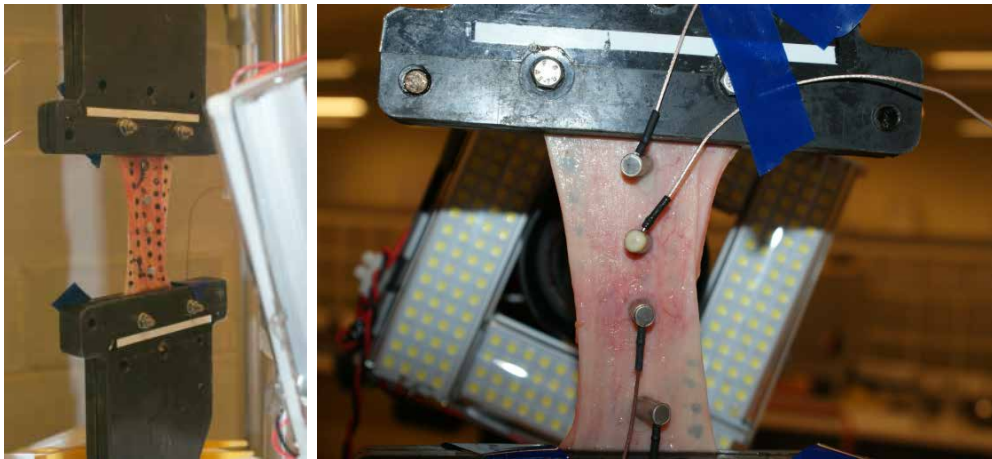
Figure 3.3. Experimental setting for the uniaxial tensile tests. *Right*: sample in place for testing, with clamps and acoustic sensors, the upright face is the *muscularis externa* layer. *Left*: detail of the acoustic sensors in the close-up face is the *mucosa* layer.

Stress is deduced from the applied forces measured by the load cell coupled to the testing machine (MTS-BIONIX 858). The load cell measures the changes in electric resistance of some elements; these changes can be associated to the deformation of the cell and thus the stress in the cell. The measurement of the load cells is converted into a digital signal that is recorded by a PC. The homogeneity of the tissue has been found to be an acceptable hypothesis given that the strain field measured by motion tracking is uniform. This fact can be profitably used in the computation of the stress. For the computations, the first Piola-Kirchhoff stress is used instead of the Cauchy stress (this makes measuring the cross sectional area unnecessary).

The geometric measures of the samples obtained from the specimens are summarized in table 3.3. For each sample the *lumen perimeter* and the *effective*

length (distance between edge of clamps) have been measured (the length of the sample includes the effective length and the supplementary fixation length inside the clamps). The thickness was directly computed for some samples (those with a "c" in the table) for the rest, the thickness was indirectly estimated (those with an "e" in the table). The cross area is computed according to the lumen perimeter and the thickness. The cross area is the main geometric measure affecting the computations and is computed according to:

$$\text{cross area} = \text{lumen perimeter} \times \text{thickness}$$

The cross area is involved in the computation of the first Piola-Kirchhoff stress (see section 3.4.1). Regarding the thickness, for the samples in which a direct computation of thickness was used the computation proceeds in two steps. The first step is to compute the frontal area, although it can be approximately computed by

$$\text{frontal area} = \text{lumen perimeter} \times \text{length}$$

we used a direct computation using a CAD program that determined exactly the frontal area in pixels^2, and then this areas was converted into cm^2. From this exact frontal area the mean thickness is computed from weight, density and total frontal area as:

$$\text{mean thickness} = \frac{\text{weight}}{\text{frontal area} \times \text{density}}$$

In the table of geometric dimensions, "c" in "type of thickness" indicates direct computation and "e" indicates indirect estimation. The mean effective length for the samples was 73.0 ± 24.1 mm, the mean lumen perimeter was 44 ± 5.9 mm and the thickness 4.15 ± 0.89 mm (for proximal parts 4.21 ± 0.90 mm and 4.11 ± 0.99 mm for distal parts, the difference is statistically significant with p-value $< 0,0002$, distal part is 14% thicker than proximal part).

Table 3.3. Main geometric dimensions for the samples.

Sample Number	Part	Lumen perimeter [mm]	Effective Length [mm]	Type of thickness	Cross area [mm²]	Frontal area [mm²]
839	dist	46.8	70.5	e	3302	194.4
839	med	38.1	28.9	e	1102	158.1
839	prox	38.1	28.9	e	1102	158.1
855	dist			e		
855	prox			e		
856	dist	48.3	73.3	e	3544	200.7
856	prox	43.1	93.3	e	4020	179.0
879	dist	43.4	41.6	e	1805	180.3
879	prox	36.7	37.5	e	1376	152.5
880	dist	54.8	94.2	e	5163	227.7
880	prox	46.1	68.6	e	3162	191.5
906	dist	51.3	93.0	e	4774	213.1
906	prox	41.0	86.5	e	3550	170.3
907	dist	41.5	104.8	e	4346	172.1
907	prox	31.4	59.4	e	1863	130.3
911	dist	52.2	86.0	e	4489	216.7
911	prox	43.9	42.7	e	1873	182.2
912	dist	48.0	92.1	e	4423	199.4
912	prox	41.5	88.3	e	3661	172.2
953	dist			c		
953	prox			c		
954	dist	41.9	85.1	c	3567	228.9
954	prox	35.9	86.4	c	3102	171.1
957	dist	49.7	89.1	c	4431	199.5
957	prox	42.0	45.9	c	1931	132.0
961	dist	—	—	—	—	—
961	prox	53.0	107.6	c	5705	199.2
964	dist			c		
964	prox	47.1	61.8	c	2908	158.8
966	dist	45.9	87.6	c	4023	153.0
966	prox	—	—	—	—	—
Average		44.2	73.0	—	3169	173.6
St. Dev		5.9	24.1	—	1445	44.9

3.3.2 Inflation tests

Some complementary tests of inflation were carried out with swine samples. The aim of these tests was to determine what type of failure could be detected in a forced dilation.
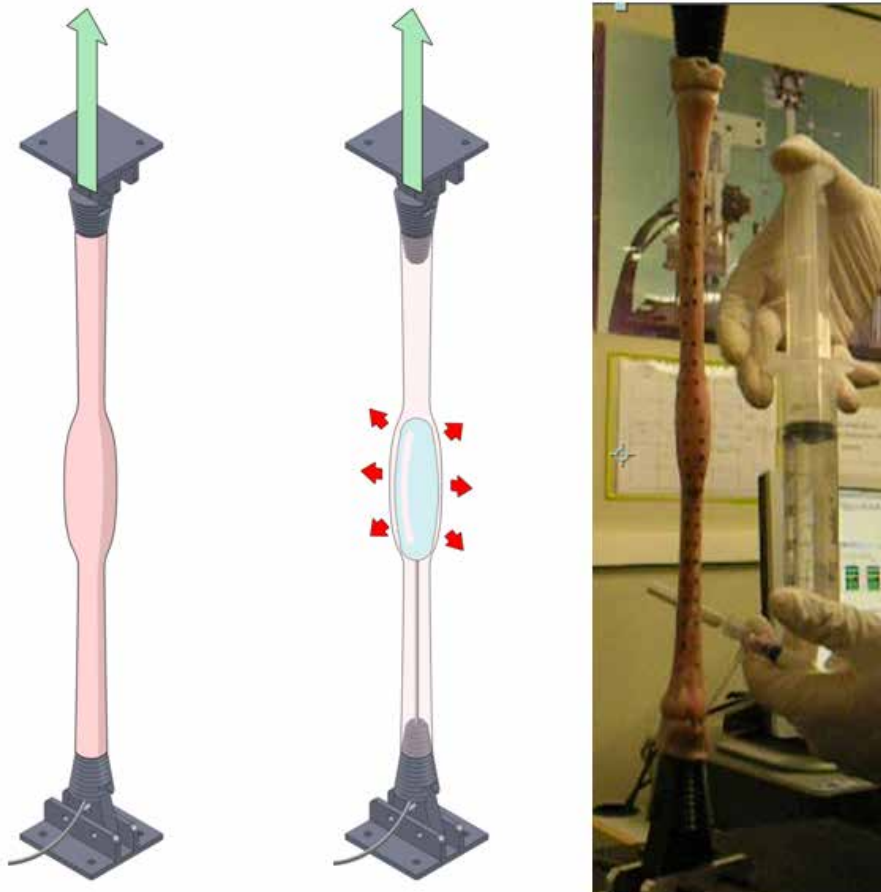
Figure 3.4. Experimental setting for the inflation tests. *Right*: The sample in place for testing, with conical clamps. *Center*: The location of the gastric balloon . *Left*: A photograph of the real test.

For the testing, gastric balloons of the same type used in forced dilations were used. For inflating the balloons, an incompressible fluid was used to measure exactly the change in the volume of the gastric balloons. Our procedure differs from the usual forced dilation in one point: we used water (an incompressible fluid) instead of air (a compressible one). In the usual procedure the pressure of the air is controlled, but not the volume. By controlling the amount of fluid,

it is easy to know the diameter reached by the gastric balloon, and thus, it is possible to estimate the strain in the lumen of the esophagus (the pressure in the balloon is not directly related to the direct contact pressure of the balloon and the esophageal wall, a fact hardly mentioned in the medical literature).

For this type of tests, we used clamps of type II (frustoconical clamps) and an intact tubular portion of esophagus. In each end, a frustoconical clamp was inserted. Two or three cable ties were used to fix the end of the esophagus to each frustoconical clamp. Then 100 ml of water were injected into the gastric balloon, until the central part of the balloon got a diameter 26 mm. At this point, the breaking of some capillary could be observed. The tests were conducted with esophagus in an axially relaxed situation, and with the esophagus pre-stressed. The results were similar; therefore, it seems that longitudinal strain/stress does not affect the mural strength of esophagus.

3.3.3 Motion tracking

The strains were computed from optical means of **motion tracking** . Motion tracking (video tracking) is a process for locating a moving object (or multiple objects) over time using a camera. For this purpose, a set of marks on the surface of the sample was the target of the motion tracking. All tests were videotaped and the video was processed with the help of a software program that follows each mark optically on the surface of the sample. The software is able to compute the position of each mark over time (indeed a position/number of frame is obtained for each mark).

This technique has also been used in other studies of biomechanical properties [39]. For the swine esophagus tests, a digital camera at a fixed resolution of 640×480 pixels was used and for the human esophagus tests we used a resolution of 400x250 pixels. In both cases, the samples of esophagus, marked with a regular net of dots were tracked by motion capture algorithms (see figure 3.5).

- **Pre-processing**. Recorded sequences of images were transferred to a computer for the tracking motion procedure. First, the sequences were trimmed and synchronized with the stress data recorded in the testing machine. The luminance of the frames was also modified to create a higher contrast between the esophagus tissue and the matrix of dots.
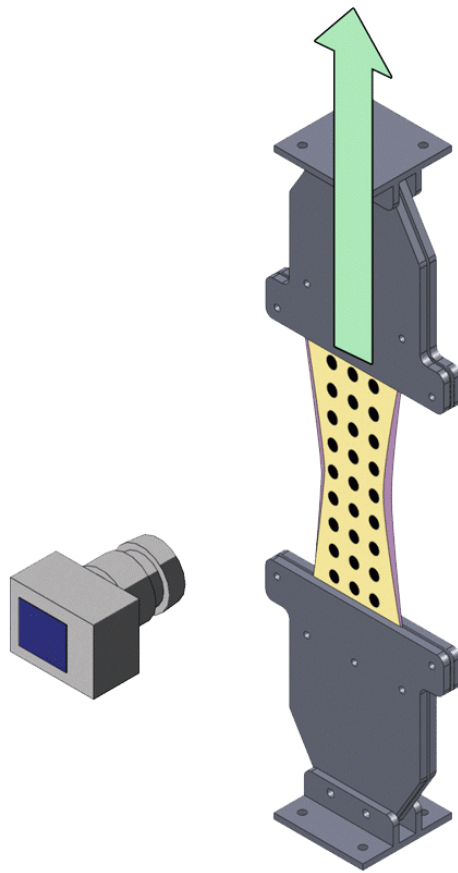
Figure 3.5. General setting for motion tracking: the sample is held between clamps, for each instant of time the camera captures a close-up of the sample.
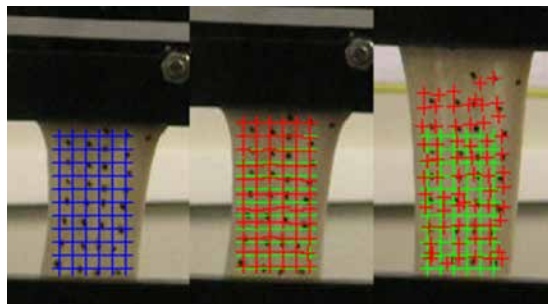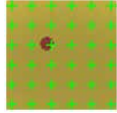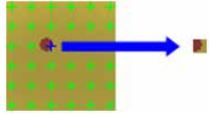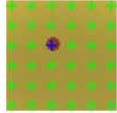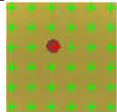
Figure 3.6. In *blue*, the initial grid used for computing strain; in *red*, the computed new positions, and in *green*, the initial position. The difference between red and green crosses is the displacement.

Table 3.4. Detailed explanation of the algorithm of motion tracking.

Explanation	Graph
Original image in $t = k$	
Original image with superimposed grid	
Scanning of the window around a point (blue)	
Next image in $t = k + 1$ with grid (brown dot moves to the right)	
Pixels are compared in each window near the blue dot. A dot is found that matches with the established criterion	
From the matching window, the new postion of the dot (red) is established	

- **Processing**. Once the frame rate was reduced and the luminance was modified, the strain was determined with a Matlab script (Christoph Eberl, Robert Thompson, Daniel Gianola; Group of Kevin J. Hemker, John Hopkins University) [17]. Essentially, a rectangular grid of 6 by 10 points was defined over the first reference frame. Each of these defined points was surrounded by a window of 25 square pixels. In every frame step, this software compares the hue and the luminance of each frame with the following one (figure 3). When the 90% of the pixels in a window matched, the center of this window would become the new position of the point. This procedure was repeated until the end of the image sequence. Table 3.4 summarizes the phases of the processing.
- **Post-processing**. The distance between every pair of marks were used to calculate the strain data. The result is a plot of the global strain versus time.

The figure 3.6 shows how the computation of position as the sample is stretched.

Usually, most of the points are correctly tracked; when it is not the case incorrectly tracked points need to be eliminated in the post-processing.

3.3.4 Clamp design

An important technical issue was the design of the clamps used for both types of tests: the uniaxial tensile tests and the inflation tests. The clamps were made out of non-porous polymeric material (Nylon 6). There are two main reasons: (1) a porous material would have produced adherence and local dehydration in the sample, (2) in addition, being less rigid the polymeric material allows a better fit to the soft tissue.

The clamps used for all tests were specifically designed for the occasion. The preliminary computations from the geometry of the clamps demonstrated that they are much stiffer than the tested soft tissue. The thickness and dimensions were adjusted in order to ensure that deformations of the clamps are completely negligible and the application of pressures and forces is fairly uniform. Two types of clamps were used:

- **Uniaxial tensile test clamps (type I)**. The first type are planar clamps for holding rectangular samples of esophagi obtained by cutting the esophagus longitudinally (see figure 3.7).
- **Inflation test clamps (type II)**. The second type are frustoconical clamps to hold tubular samples of esophagus. It was required that this type of clamps allowed the insertion of a gastric balloon inside the esophagus. Each clamp allowed the adjustment of different diameters of esophagus (see figure 3.8).

An important issue in both types of clamps was to ensure that biological samples did not creep over the surface of the clamps. Preventing the creeping of the tissue was specially difficult because of the existence of water and moisture in the tissue; which in some cases acted as lubricant. To avoiding any sliding, both types of clamps were provided with a fluted surface in the area of contact with the samples. Some preliminary testing, forced to select the right pressure of the clamp on the samples and to add some additional drills to increase the number of bolts near the edge of the samples was necessary. The final design resulted satisfactory for the type I used in uniaxial tensile tests and no human sample had

(a)   (b)
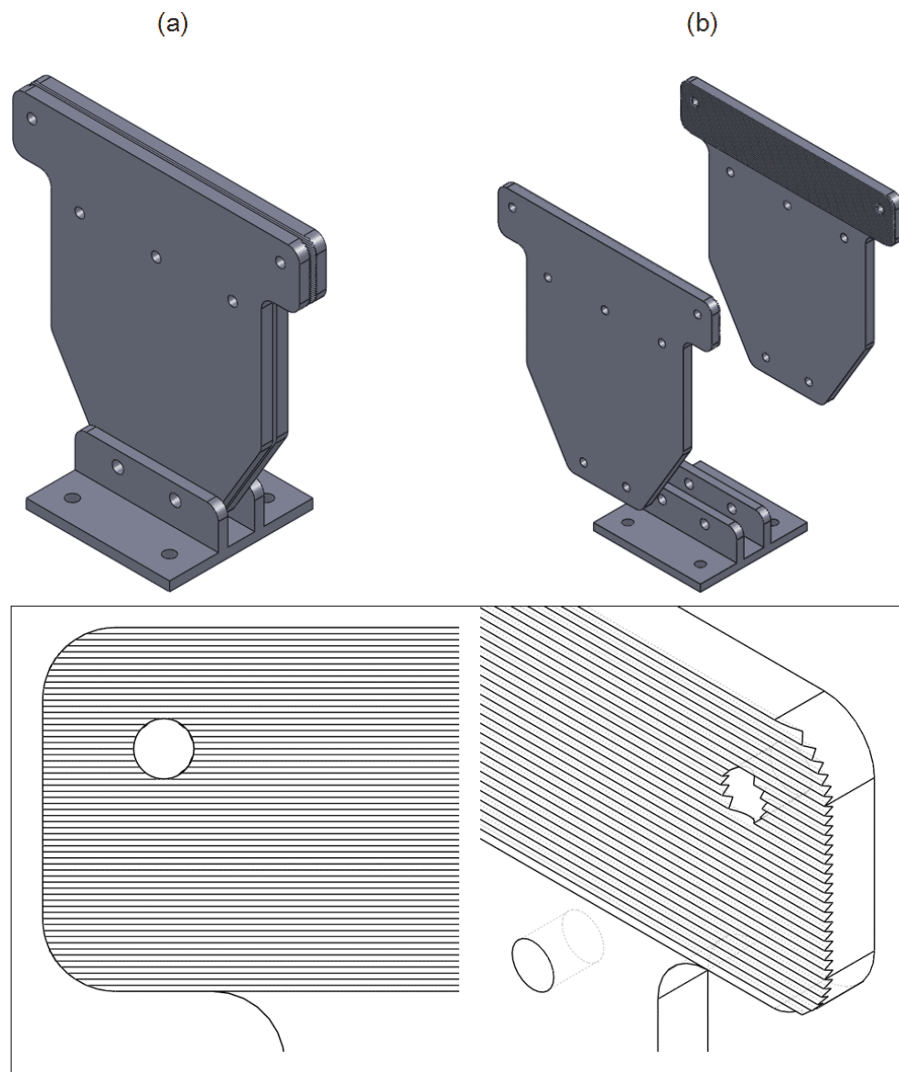
Figure 3.7. Planar clamps for uniaxial tensile tests: *Top* (a) the pair of clamps in position for holding the sample, (b) Exploded assembly. *Bottom* Details of the fluted surface.

to be discarded for this factor. For the type II the result was not that good and the inflation tests were conducted only with a low axial stress (just for holding the esophagus a slightly tight, without slackness). Anyway, the main task could be fulfilled even for clamps of type II.

As it can be observed in figure 3.7, the planar clamps are formed by two sets of twin plates, each set is located at the ends of the rectangular sample of tissue.
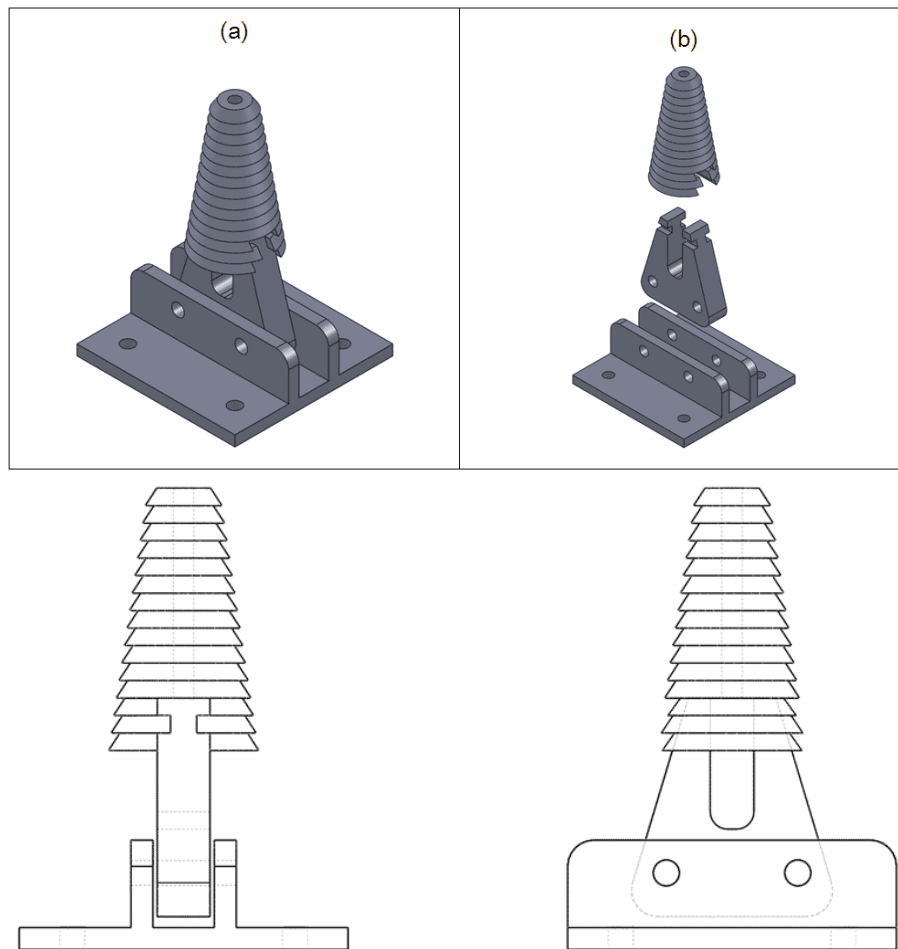
Figure 3.8. Frustroconical clamps for inflation tests: *Top* (a) one frustoconical clamps assembled, (b) Exploded assembly. *Bottom* Constructive details of the frustoconical clamp.

As it has previously been stated, each pair of plates can press hard on the sample by a set of bolts surrounding the end of the sample. This pressure ensures no significant sliding and thus the strain measures are correct (if there is some sliding present, the strain measure would be distorted). The fluted area includes small grooving of about 1 mm in width with a sawtooth shape.

For the inflation tests the two frustoconical clamps which insert in a tubular intact sample were designed. These clamps are shown in figure 3.8. An important detail is that there is a central drill in the clamps through which a deflated gastric balloon can be inserted. The tube of the balloon connects it with the exterior of the intact esophagus and allows us to inflate the balloon once inserted. Then the

frustoconical clamps enclose the tubular cavity of the esophagus. The esophagus is hold to the clamps by means of some plastic pull ties that press the tissue against the exterior surface of the frustoconical shape.

3.4 Computational issues

This section describes the mathematical aspects needed for the strain computation and the fitting of strain-stress curves. Although nowadays there is commercial software for doing this task, in our case these tasks were done only semi-automatically. The basic ideas behind the methods are interesting and they deserve some attention in form of a brief exposition.

3.4.1 Stress and strain computation

In uniaxial tensile tests, the testing machine provides measurements of force. This force is presumably applied quite uniformly at the edges of the sample. The traction vector is easily computed from the forces provided by the testing machine. We will use the nominal traction vector or **first Piola-Kirchoff traction vector**, instead of the true traction vector or **Cauchy traction vector**. The difference between the two in this case is mainly due to the shrinkage of the transversal area. For a uniaxial tensile test (in Cartesian coordinates, and assuming near incompressibility of the tissue), the Cauchy stress $\boldsymbol{\sigma}$ tensor and the first Piola-Kirchhoff stress tensor $\mathbf{P}$ are given by:

$$
(\sigma^a{}_b) = \begin{bmatrix} p\lambda & 0 & 0 \\ 0 & 0 & 0 \\ 0 & 0 & 0 \end{bmatrix}, \qquad (P^{aA}) = \begin{bmatrix} p & 0 & 0 \\ 0 & 0 & 0 \\ 0 & 0 & 0 \end{bmatrix} \tag{3.1}
$$

where $p = F/A_0$ is the nominal stress (the total force divided by the initial area), and $\lambda > 1$ the longitudinal stretch. Obviously, the Cauchy stress is greater because of the effect of the shrinkage of the transversal area. The Piola-Kirchhoff stress is a little bit simple because it only requires the initial area and the applied force.

For the computation of strains, the displacements provided by the motion

tracking algorithm are used. We use the **Green-Lagrange strain tensor** as a measure of strain. This tensor is related to the coordinate by means of:

$$E_{AB} = \frac{1}{2}\left(\frac{\partial x^a}{\partial X^A}\frac{\partial x^b}{\partial X^B}\delta_{ab} - \delta_{AB}\right) \tag{3.2}$$

where $x^a(t, X^A)$ are the spatial coordinates of the point occupying the position $x^a = X^A$ for $t = 0$. The 2-tensor given by equation 3.2 represents the strain field, a tensorial field over the initial configuration. But a practical difficulty needs to be addressed: experimental measures only refer to a finite collection of points, not the complete field. Therefore, the strain field can be obtained only by interpolations of this finite set of points. A linear interpolation was used; in this case there is no need of quadratic or cubic interpolation (the linear approximation was found sufficiently approximate in practice). The motion tracking provides the displacements of an orthogonal matrix of $m \times n$ points, being h the distance between each pair of adjacent point (and in both directions). There are two possibilities for the strain computation: the *method of the averaging of pairs* and *the method of the slope.*

Method of the averaging of pairs
This method is based on the finite differences for approximating derivatives of displacements, *i.e.* strains can be calculated approximating the strain in the line joining a pair of points with the ratio of differences of displacements divided by distances between the pair points. This method is quite simple and was used for some samples (that were also computed with the second method). The use of finite differences is explained and described in many standard references (see, for example, [5]).

Considering an orthogonal net of points of coordinates $(X_{i,j}, Y_{i,j})$ where $(i,j) \in \{1,\ldots,m\} \times \{1,\ldots,n\}$, if the point are near enough, we can approximate the derivative of the displacements by expressions like the following:

$$\frac{\partial x^a(X_{i,j}, Y_{i,j}, t)}{\partial X} \approx \frac{x^a_{i+1,j} - x^a_{i,j}}{X_{i+1,j} - X_{i,j}} \tag{3.3}$$

$$\frac{\partial x^a(X_{i,j}, Y_{i,j}, t)}{\partial Y} \approx \frac{x^a_{i,j+1} - x^a_{i,j}}{Y_{i,j+1} - Y_{i,j}} \tag{3.4}$$

Where $x_{i,j} = x_{i,j}^1 = \phi^a(X_{i,j}, Y_{i,j}, t)$ and $y_{i,j} = x_{i,j}^2 = \phi^a(X_{i,j}, Y_{i,j}, t)$. So, the strains are algebraic combinations of expressions of this form, so we can approximate strain by ratios of differences in coordinates.

Method of the slopes

The method of slopes is similar but instead of computing differences between pairs of points, it uses all the points simultaneously in order to achieve the best fit in the least-squares sense. Although, conceptually more complex, computationally is not much more complicate than the method of averaging pairs. The fact of using all the points for each instant reduces significantly the "noise" in the computed strain.

For computing $\partial x^a / \partial X^B$ at time t, one takes the variables $x_{i,j}^a = \phi^a(X_{i,j}^B, t)$ and compute the regression:

$$x_{ij}^a = \beta_{\{A\}}^{\{a\}}(t) X_{ij}^A + \epsilon_{ij} \tag{3.5}$$

Then it is obtained with a very good approximation that:

$$\frac{\partial x^a}{\partial X^A} = \beta_{\{A\}}^{\{a\}}(t) \tag{3.6}$$

These coefficients are all what is required for computing the strain components:

$$E_{AB} = \frac{1}{2}\left(\sum_{a=1}^{2} \beta_{\{A\}}^{\{a\}} \beta_{\{B\}}^{\{a\}} - \delta_{AB}\right) \tag{3.7}$$

3.4.2 Curve fitting

The curve fitting is in general a mathematical problem that involves determining material parameters in incompressible isotropic elastic strain–energy functions on the basis of a non-linear least squares optimization. The non-linear character of the problem makes it mandatory the use of numerical methods for solving the least squares optimization. The basic theory for this type of numerical problems was initially developed by Levenberg (1944) [63], while working at the Frankford Army Arsenal. It was rediscovered by Marquardt (1963) [71] who worked as a statistician at DuPont and independently by Girard, Wynn and Morrison [40, 78, 112]. This studies are the base of the currently called the *Levenberg–Marquardt algorithm* (LMA) described in [89], which has been further generalized [77].

The basic description of the LM algorithm is as follows. In this section, $\|\cdot\|$ shall denote the ordinary Euclidean norm, the following explanation is based on [67]. Let f be an assumed functional relation which maps a parameter vector $\mathbf{p} \in \mathbb{R}^n$ to an estimated measurement vector $\hat{\mathbf{x}} = f(\mathbf{p}) \in \mathbb{R}^n$. An initial parameter estimates $\mathbf{p}_0$ and a measured vector $\mathbf{x}$ are provided and it is desired to find the vector $\hat{\mathbf{p}}$ that best satisfies the functional relation f, *i.e.* it minimizes the squared distance $\mathbf{d}^T\mathbf{d}$ with $\mathbf{d} = \mathbf{x} - \hat{\mathbf{x}}$. The basis of the LM algorithm is a linear approximation in the neighborhood of $\mathbf{p}$. For a small $\|\boldsymbol{\delta}_{\mathbf{p}}\|$, a Taylor series expansion leads to the approximation

$$f(\mathbf{p} + \boldsymbol{\delta}_{\mathbf{p}}) \approx f(\mathbf{p}) + \mathbf{J} \cdot \boldsymbol{\delta}_{\mathbf{p}} \tag{3.8}$$

where $\mathbf{J} = (\partial f^i / \partial x^j)$ is the Jacobian matrix. Like all non-linear optimization methods, LM is iterative: Initiated at the starting point $\mathbf{p}_0$, the method produces a series of vectors $\mathbf{p}_1, \mathbf{p}_2, \dots$ which converge towards a local minimizer for $\hat{\mathbf{p}}$. Hence, at each step, it is required to find the $\boldsymbol{\delta}_{\mathbf{p}}$ that minimizes the quantity $\|\mathbf{x} - f(\mathbf{p} + \boldsymbol{\delta}_{\mathbf{p}})\| \approx \|\mathbf{d} - \mathbf{J} \cdot \boldsymbol{\delta}_{\mathbf{p}})\|$. The sought $\boldsymbol{\delta}_{\mathbf{p}}$ is thus the solution to a linear least-squares problem: the minimum is attained when $\mathbf{d} - \mathbf{J} \cdot \boldsymbol{\delta}_{\mathbf{p}})$ is orthogonal to the column space of $\mathbf{J}$. This leads to $\mathbf{J}^T(\mathbf{d} - \mathbf{J} \cdot \boldsymbol{\delta}_{\mathbf{p}}) = 0$ which yields $\boldsymbol{\delta}_{\mathbf{p}}$ as the solution of the so-called normal equations [43]:

$$\mathbf{J}^T\mathbf{J} \cdot \boldsymbol{\delta}_{\mathbf{p}} = \mathbf{J}^T\mathbf{d} \tag{3.9}$$

The matrix $\mathbf{J}^T\mathbf{J}$ on the left side of 3.9 is the approximate Hessian, *i.e.* an approximation to the matrix of second order derivatives. The LM algorithm actually solves a slight variation of this equation, known as the augmented normal equations

$$\mathbf{N} \cdot \boldsymbol{\delta}_{\mathbf{p}} = \mathbf{J}^T\mathbf{d} \tag{3.10}$$

where the off-diagonal elements of $\mathbf{N}$ are identical to the corresponding elements of $\mathbf{J}^T\mathbf{J}$ and the diagonal elements are given by $N_{ii} = \mu + [\mathbf{J}^T\mathbf{J}]_{ii}$ for some $\mu > 0$. The strategy of altering the diagonal elements of $\mathbf{J}^T\mathbf{J}$ is called *damping* and μ is referred to as the damping term. If the updated parameter vector $\mathbf{p} + \boldsymbol{\delta}_{\mathbf{p}}$ with $\boldsymbol{\delta}_{\mathbf{p}}$ computed from 3.10 leads to a reduction in the error distance $\mathbf{d}$,

the update is accepted and the process repeats with a decreased damping term. Otherwise, the damping term is increased, the augmented normal equations are solved again and the process iterates until a value of $\boldsymbol{\delta_p}$ that decreases error is found. The process of repeatedly solving 3.10 for different values of the damping term until an acceptable update to the parameter vector is found corresponds to one iteration of the LMA.

In LMA, the damping term is adjusted at each iteration to assure a reduction in the error distance $\mathbf{d}$. If the damping is set to a large value, matrix $\mathbf{N}$ in 3.10 is nearly diagonal and the LM update step $\boldsymbol{\delta_p}$ is near the steepest descent direction. Moreover, this magnitude is reduced in this case. Damping also handles situations where the Jacobian is rank deficient and $\mathbf{J}^T\mathbf{J}$ is therefore singular [62]. In this way, LMA can defensively navigate a region of the parameter space in which the model is highly nonlinear. If the damping is small, the LMA step approximates the exact quadratic step appropriate for a fully linear problem. LMA is adaptive because it controls its own damping: it raises the damping if a step fails to reduce $\mathbf{d}$; otherwise, it reduces the damping. In this way LMA is capable to alternate between a slow descent approach when being far from the minimum and a fast convergence when being at the minimum's neighborhood. The LMA terminates when at least one of the following conditions is met:

- The magnitude of the gradient of $\mathbf{d}^T\mathbf{d}$, *i.e.* $\mathbf{J}^T\mathbf{d}$ on the right side of 3.9, drops below a threshold $\mathbf{d}_1$
- The relative change in the magnitude of $\boldsymbol{\delta_p}$ drops below a threshold $\mathbf{d}_2$
- The error $\mathbf{d}^T\mathbf{d}$ drops below a threshold $\mathbf{d}_3$
- A maximum number of iterations is completed

Explicit pseudo-codes for the algorithm can be found in [38, 67]

Input: A vector function $f : \mathbb{R}^m \to \mathbb{R}^n$ with $n \geq m,$;
a measurement vector $\mathbf{x} \in \mathbb{R}^n$;
and an initial parameter estimate $\mathbf{p}_0 \in \mathbb{R}^m$
Output: A vector $\hat{\mathbf{p}} \in \mathbb{R}^m$ minimizing $\|\mathbf{x} - f(\mathbf{p})\|^2$
initialization:
k:=0; ν=2; $\mathbf{p} = \mathbf{p}_0$;
$\mathbf{A} := \mathbf{J}^T \mathbf{J}; \mathbf{d} := \mathbf{x} - f(\mathbf{p}); \mathbf{g} = \mathbf{J}^T \mathbf{d}$;
stop:=$(\|\mathbf{g}\|_\infty \leq \epsilon_1); \mu := \tau * \max_{i=1,\dots m} A_{ii}$;
while (not stop) and $(k < k_{\max})$ **do**
    k:=k+1;
    repeat
        Solve$(\mathbf{A} + \mu\mathbf{I})\boldsymbol{\delta}_\mathbf{p} = \mathbf{g}$;
        if $\|\boldsymbol{\delta}_\mathbf{p}\| < \epsilon_2 \|\mathbf{p}\|$ **then**
            stop:=true;
        else
            $\mathbf{p}_{new} = \mathbf{p} + \boldsymbol{\delta}_\mathbf{p}$;
            $\rho := (\|\mathbf{d}\|^2 - \|\mathbf{x} - f(\mathbf{p}_{new})\|^2)/(\boldsymbol{\delta}_\mathbf{p}^T(\mu\boldsymbol{\delta}_\mathbf{p} + \mathbf{g}))$;
            if $\rho > 0$ **then**
                $\mathbf{A} := \mathbf{J}^T \mathbf{J}; \mathbf{d} := \mathbf{x} - f(\mathbf{p})$;
                stop:=$(\|\mathbf{g}\|_\infty \leq \epsilon_1)$ or $(\|\mathbf{d}\|^2 \leq \epsilon_3)$;
                $\mu := \mu * \max(\frac{1}{3}, 1 - (2\rho - 1)^3); \nu := 2$;
            else
                $\mu := \mu * \nu; \nu := 2 * \nu$;
            end
        end
    until $\rho > 0$ or (stop);
end
$\hat{\mathbf{p}} := \mathbf{p}$;

Algorithm 1: Levenberg–Marquardt algorithm (LMA) non-linear least squares algorithm

In this study the strain-stress relations for uniaxial tensile tests have been derived from the SEDF/HEDF. Some interesting technical details about the fitting hyperelastic models to experimental data can be found in Ogden *et al.* (2004) [83]. The work of Ogden highlights, in particular, (a) the relative errors generated in

the fitting process and (b) the occurrence of multiple sets of optimal material parameters for the same data sets. This multiplicity can lead to very different numerical solutions for a given boundary-value problem (a well known fact in non-linear elastostatics). Some commercial software incorporates efficient sub-rutines based on the algorithm 1 just given.

Nōbis prīme est virtūs perspicuitās; prōpria verba, rectus ordō, nōn in longum dīlāta conclūsiō: nihil neque dēsit, neque superfluat...

Quintilianus (AD 35-AD 95),
Institutio Oratoriæ

4

Results

4.1 Experimental results

Stress-strain curves are the main experimental evidence for prediciting failure of the esophagus wall. In addition, in this research the inflation tests showed that, in some cases, the occurrence of bleeding occurs even when no damage is detectable in the esophagus wall; possibly the probability of hemorrhaging episodes can not be assessed from *in vitro* tests, because of the absence of blood preassure and circulation. The inflation test also showed that the ripping of some blood vessels leads to early hemorrhage episodes. We will concentrate in this section on stress-strain curves. First, we will address the procedure for obtaining the curves; second, we will examine the results of the best fitting for the Lu-Gregersen model (2001) and the Yang-Gregersen model (2006), which were reviewed in section 2.4.1.

To obtain the stress-strain curves it is necessary to "synchronize" the information from two different sources:

1. **Computation of displacements by motion tracking**. From these data, the curves $\varepsilon(t)$ are obtained following the methodology explained in section 3.4.1. For each sample a computation time of about 15 hours is required to obtain all the displacements.

2. **Data of load cell in the testing machine**. The load cell produces a digital list of instants of time, and for each instant a measure of force and a measure of voltage are provided. Then, the curves $\sigma(t)$ are obtained.
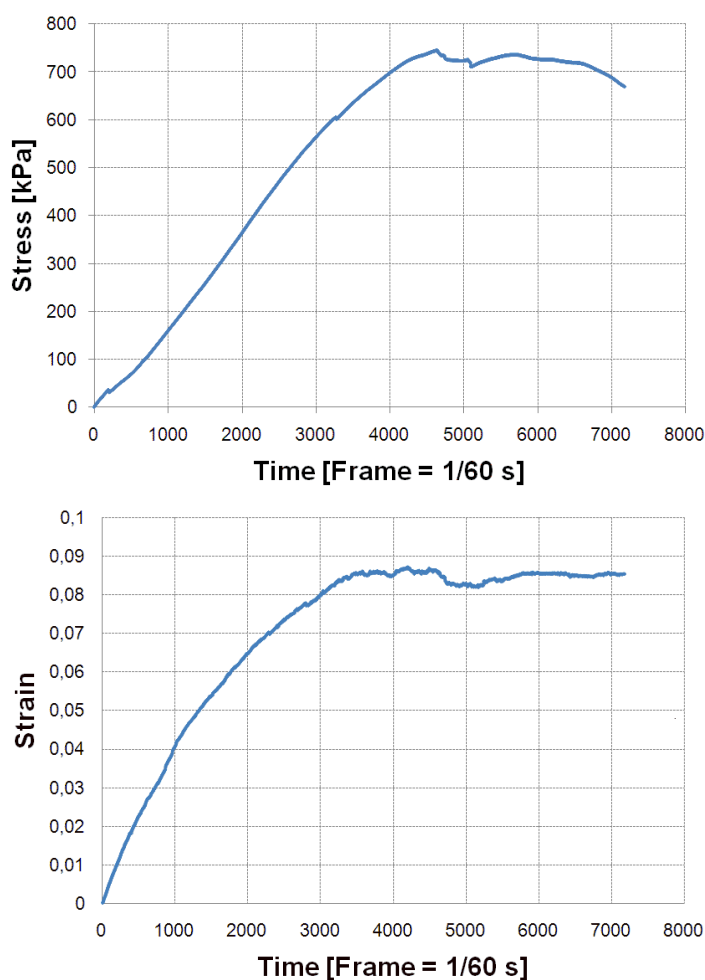
Figure 4.1. Stress-time and strain-time curves (sample 839 proximal). *Top*: Stress-time curve *Bottom*: Strain-time curve.

In this processes it is very important to synchronize the instant $t = 0$ for both types of data in order to achieve good results. In our case we used a

switch off to achieve a correct synchronization. The switch off produces a voltage dop and simultaneously a "black out" in the recorded video, in this way the video signal and the measures of force and voltage of the testing machine are easily synchronized. This type of data allows us to compute for each sample the mechanical properties (*i.e.* the elastic constants) that characterize the particular sample according to the constitutive model used. The figure 4.1 shows both types of measures after synchronization. Note that the final form of the stress-strain is not obvious from the graphs (note that $\varepsilon = \varepsilon(t), \sigma = \sigma(t)$ can be seen as a parametric form of the stress-strain curves shown above, see section 4.1.1)

The following section shows the obtained curves for all samples. As it has been stated, the uniaxial tensile test also provides information for the cleaving-ripping stress and the maximum attainable strain (i.e., "maximum" stress and strain). In all cases, the ripping was due to the stress in the region between clamps. This shows that the design of the clamps was effective in avoiding inconvenient stress concentrations in the clamp edge. In some cases of porcine samples a delamination of the two layers of the esophagus was observed. This effect is not present in the human samples (this is consistent with the observed fact that porcine esophagi permit a separation of the two layers in a much easier way).

4.1.1 Stress-Strain curves for human samples

All the stress-strain curves obtained show two important characteristics:

1. All the curves are not only monotonically increasing, but also have a convex shape.

2. The effective tangent longitudinal modulus (*i.e*, the "Young's modulus") increases as stress increases.

This type of curves has been found for all types of collagenous soft tissue. The second characteristic (2) suggests that an "exponential law" is adequate. Informally, this implies that the effective tangent longitudinal modulus is proportional to stress multiplied by some functions of the strain.

Some of the experimental stress-strain curves (in gray color) show low to medium level of white noise (this can be due to vibration of the sample or low

contrast in the sample surface, etc.). The noise is particularly high for samples 856 prox, 911 prox, 953 dist (see figures 4.4, 4.8, 4.10). Other samples are very clear and with no significant noise (see the non-zigzaging curves in the same figures). Despite the apparent irregularities in some curves, all of them can be adjusted to the models with a good fitting (see section 4.1.2).
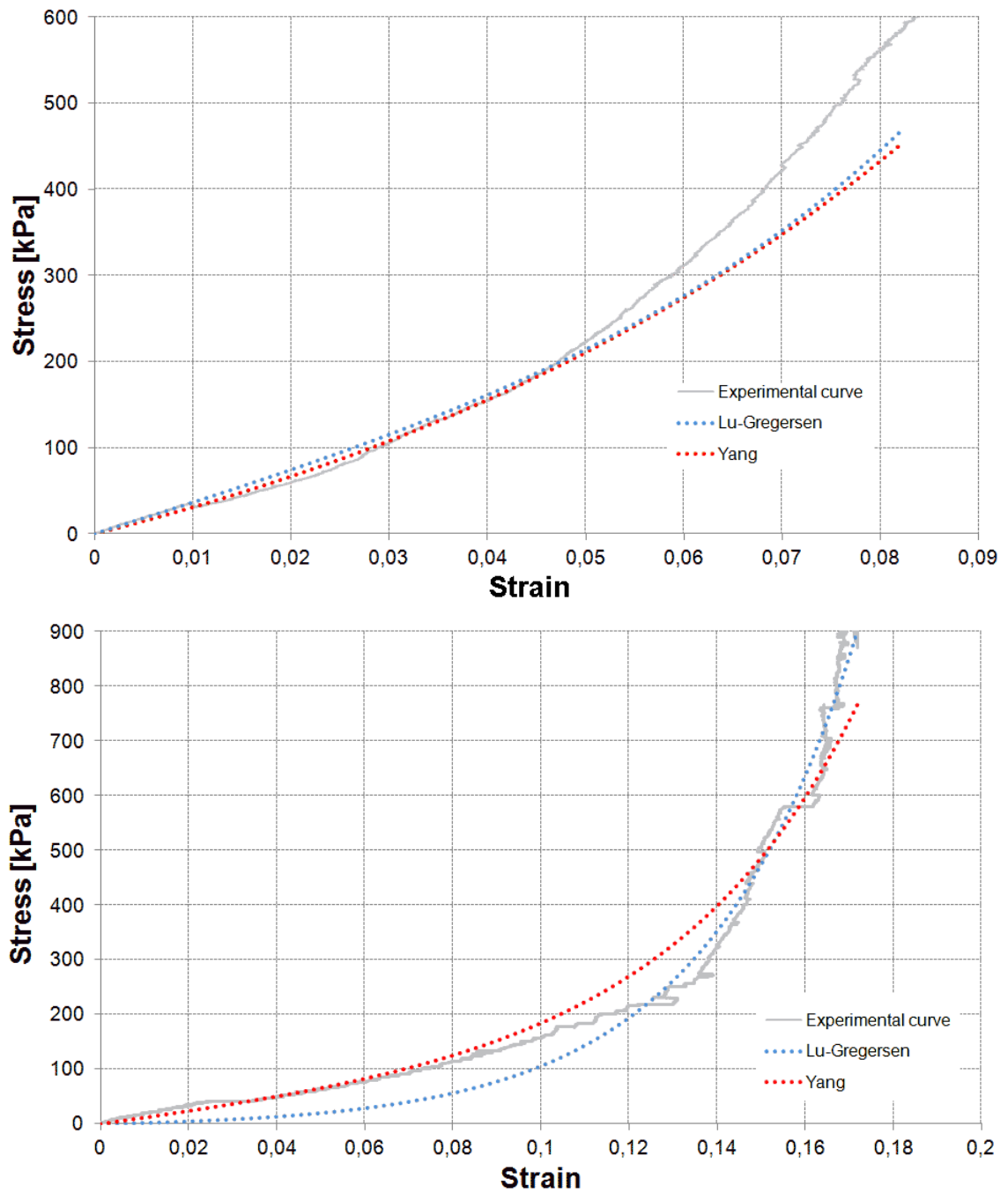
Figure 4.2. Stress-Strain curves from donor 839. *Top*: proximal, male, 64 y.o., BMI 45.9 *Bottom*: another similar sample from the same donor.
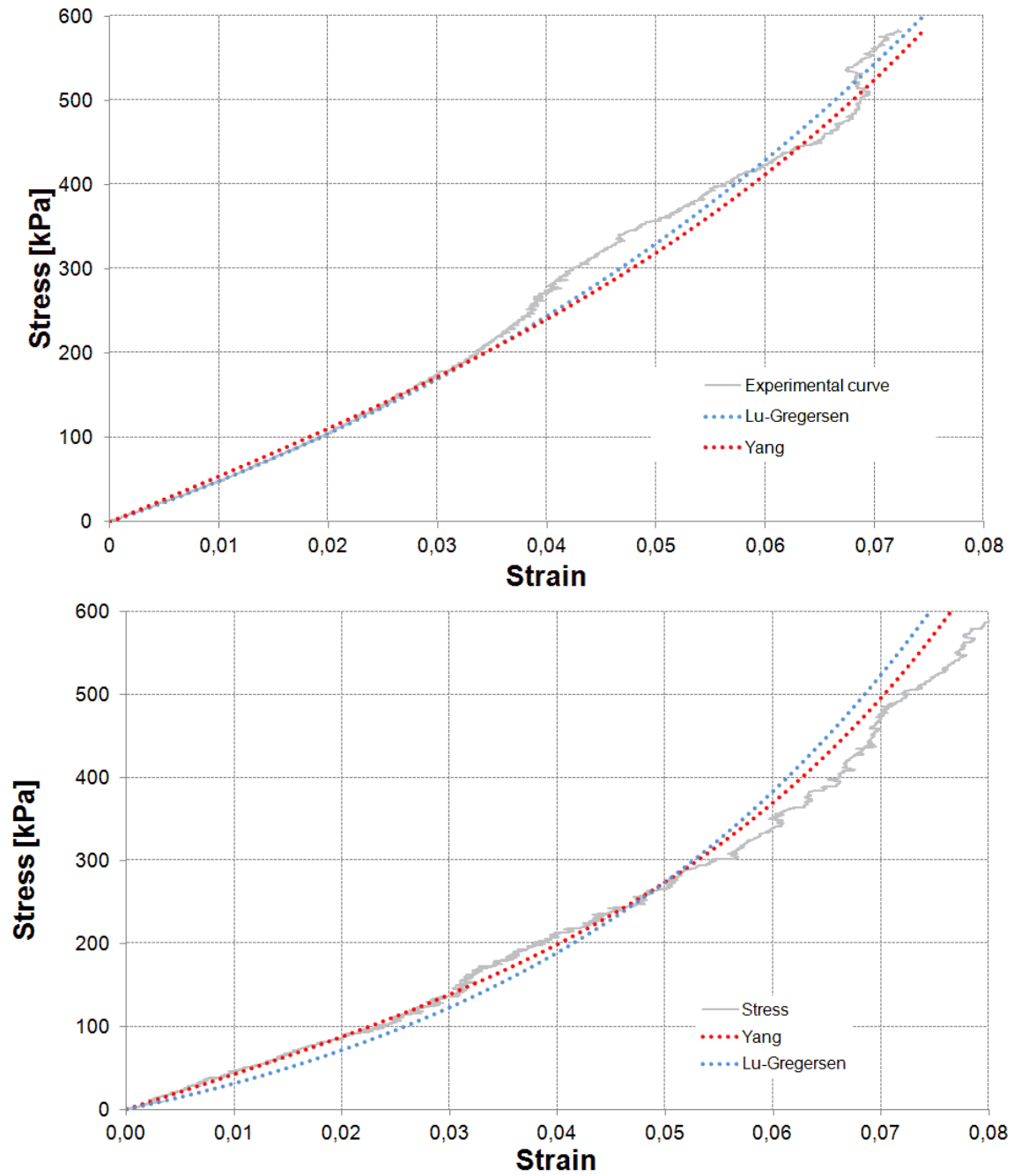
Figure 4.3. Stress-Strain curves from donors 839 and 855. *Top*: distal, male, 64 y.o., BMI 45.9 *Bottom*: male, distal, 66 y.o, BMI 51.7.
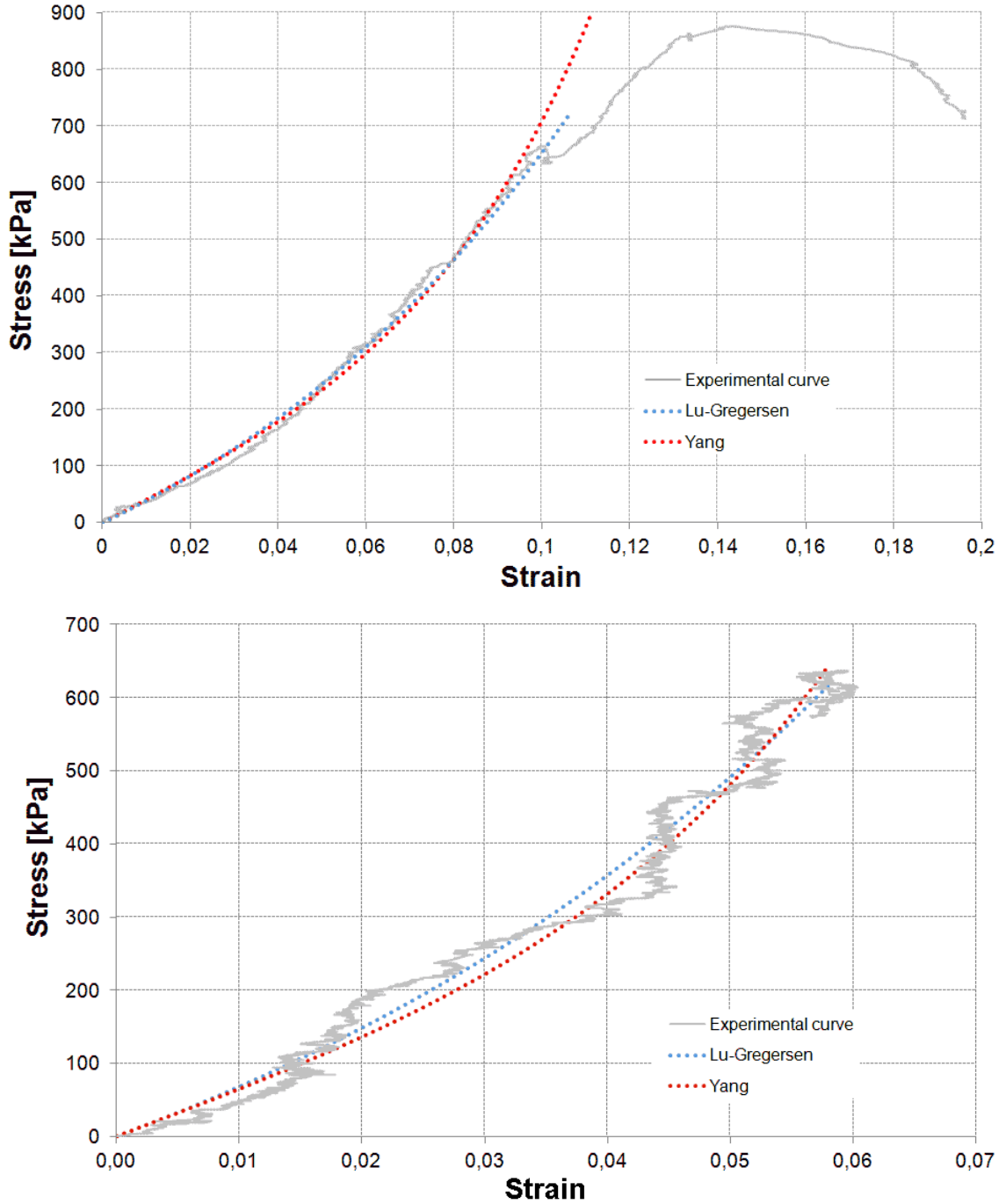
Figure 4.4. Stress-Strain curves from donor 856. *Top*: proximal, male, 85 y.o., BMI 25.5 *Bottom*: distal, same donor.
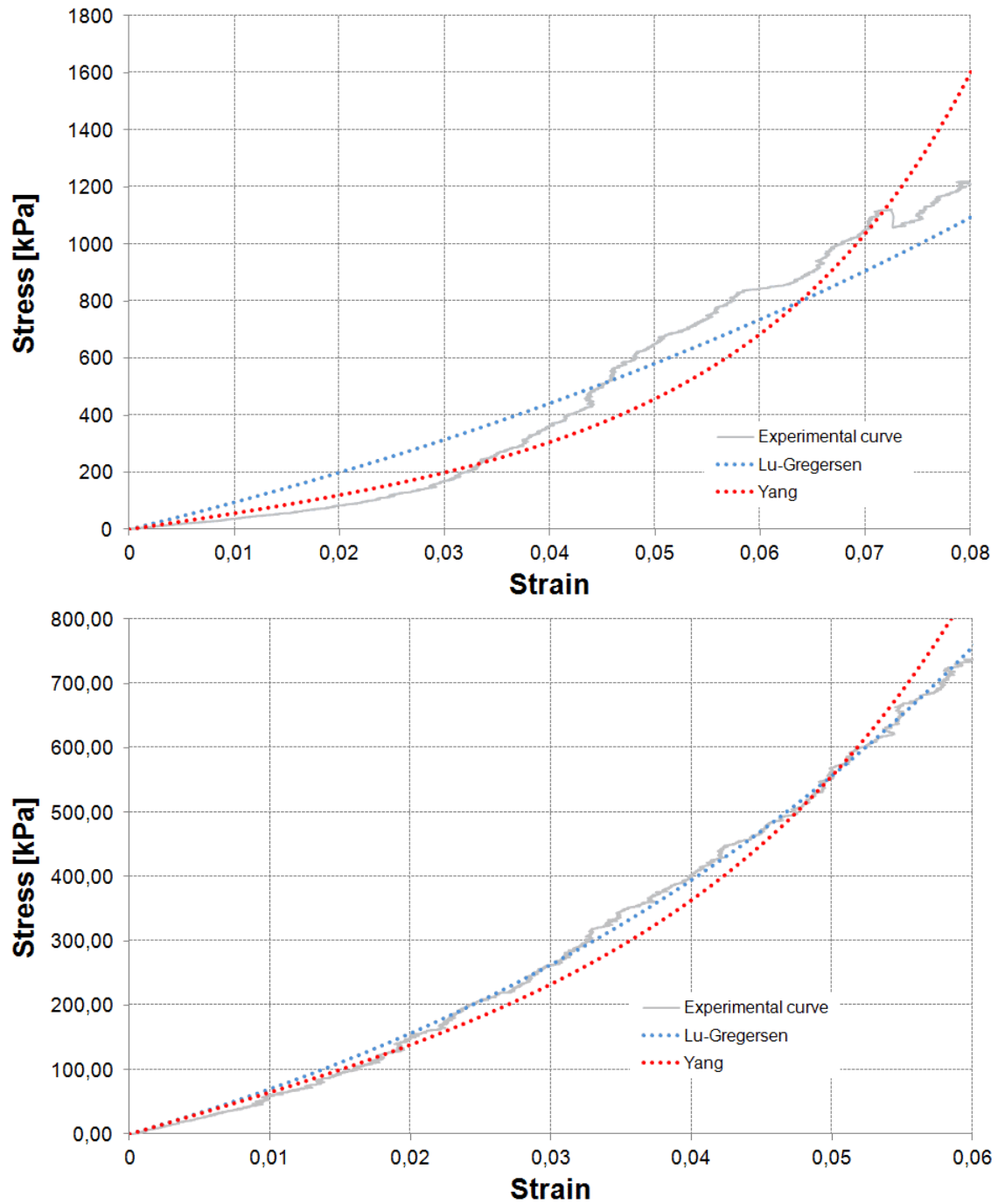
Figure 4.5. Stress-Strain curves from donor 879. *Top*: proximal, female, 68 y.o., BMI 42.8 *Bottom*: distal, same donor.
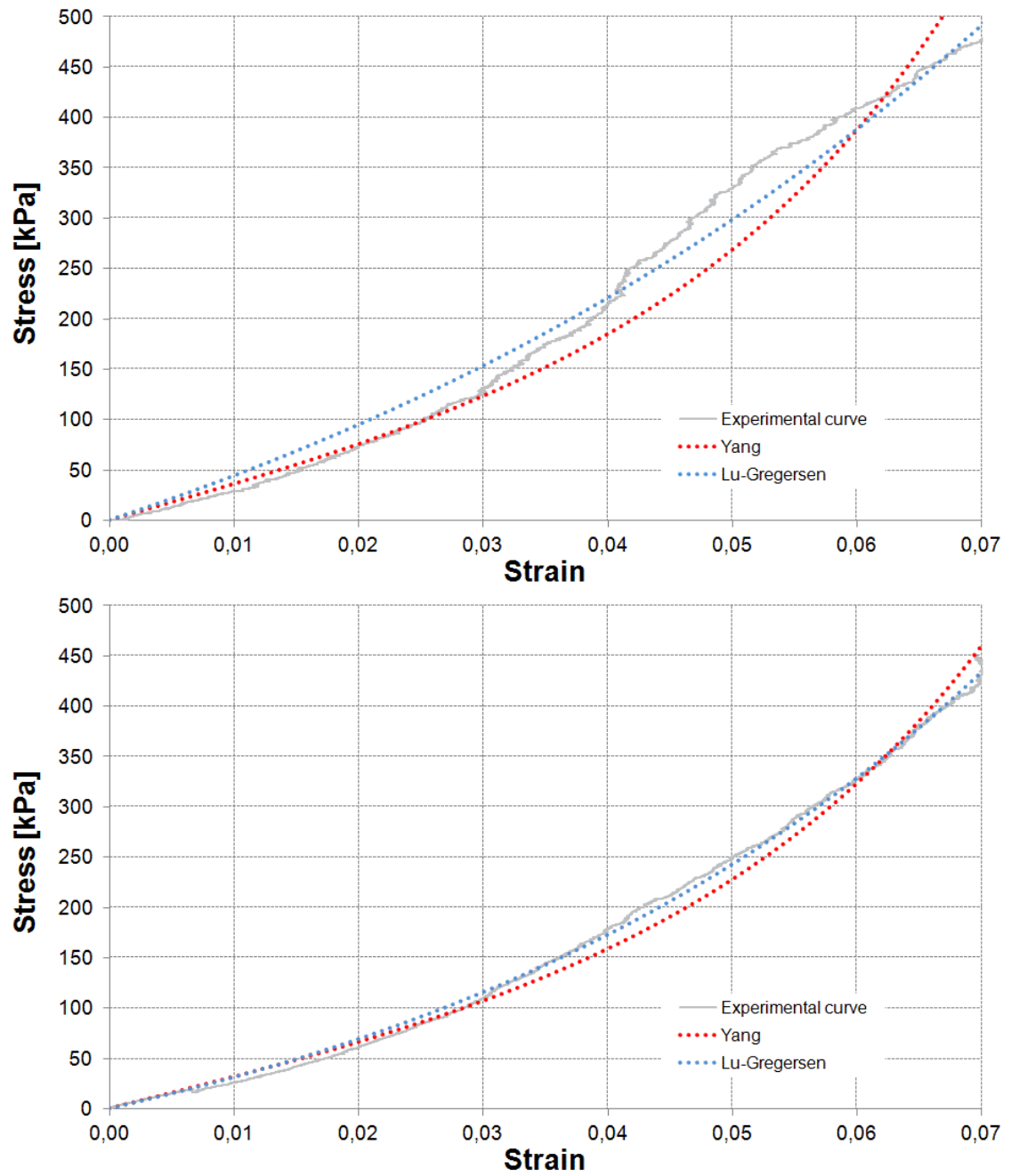
Figure 4.6. Stress-Strain curves from donor 880. *Top*: proximal, male, 61 y.o., *Bottom*: distal, same donor.
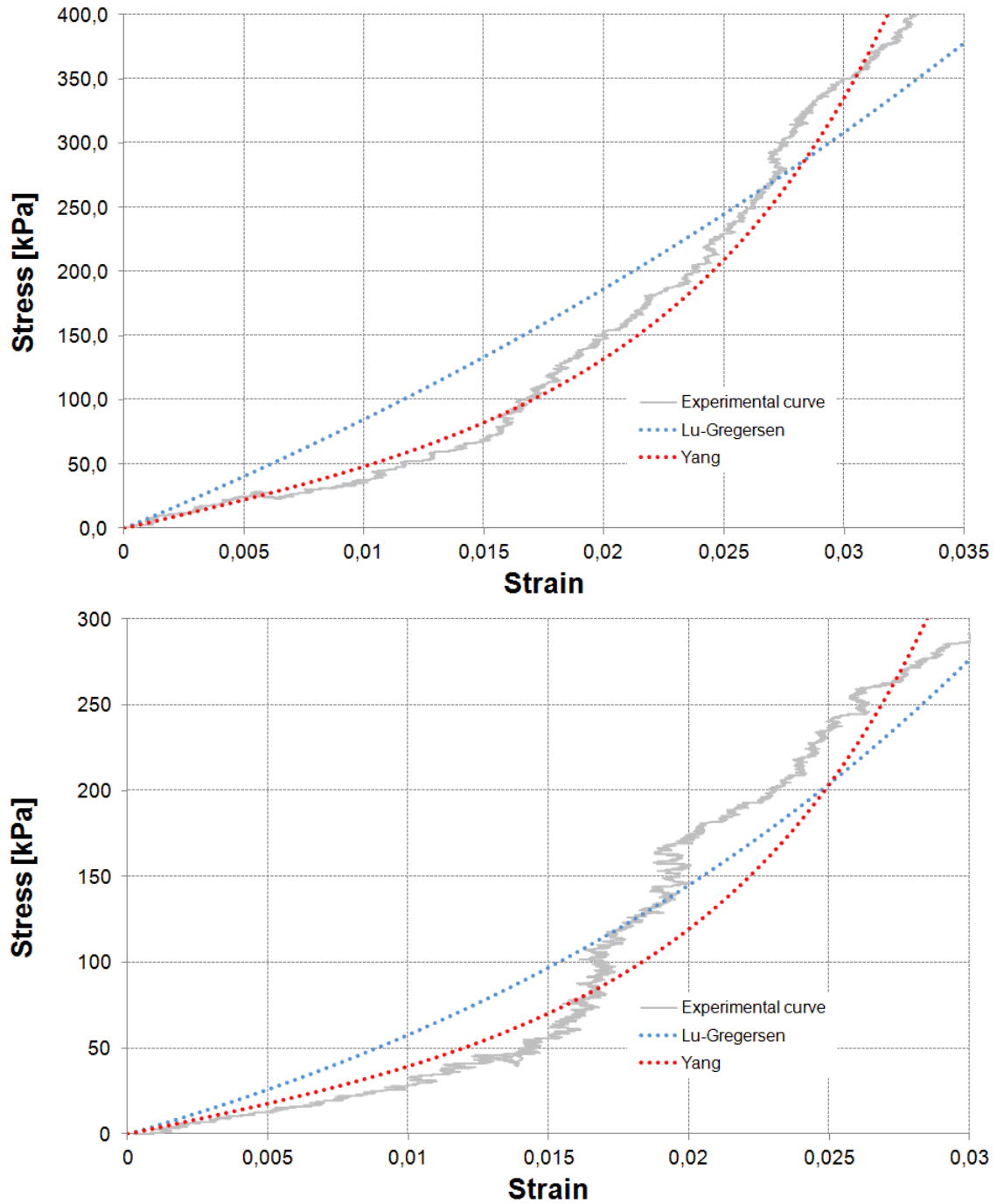
Figure 4.7. Stress-Strain curves from donor 907. *Top*: proximal, female, 70 y.o., BMI 35.7 *Bottom*: distal, same donor.
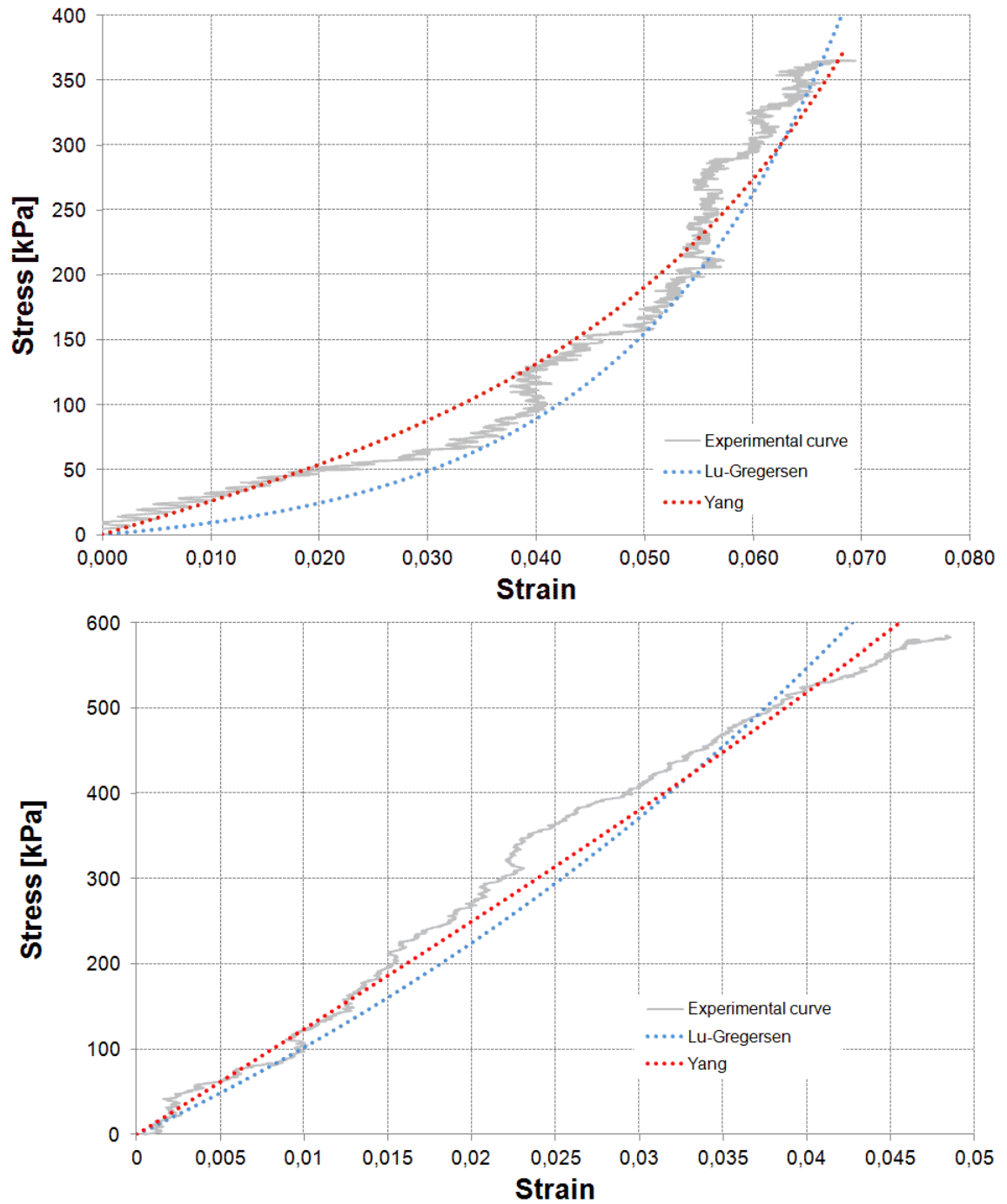
Figure 4.8. Stress-Strain curves from donor 911. *Top*: proximal, male, 90 y.o., BMI 31.1 *Bottom*: distal, same donor.
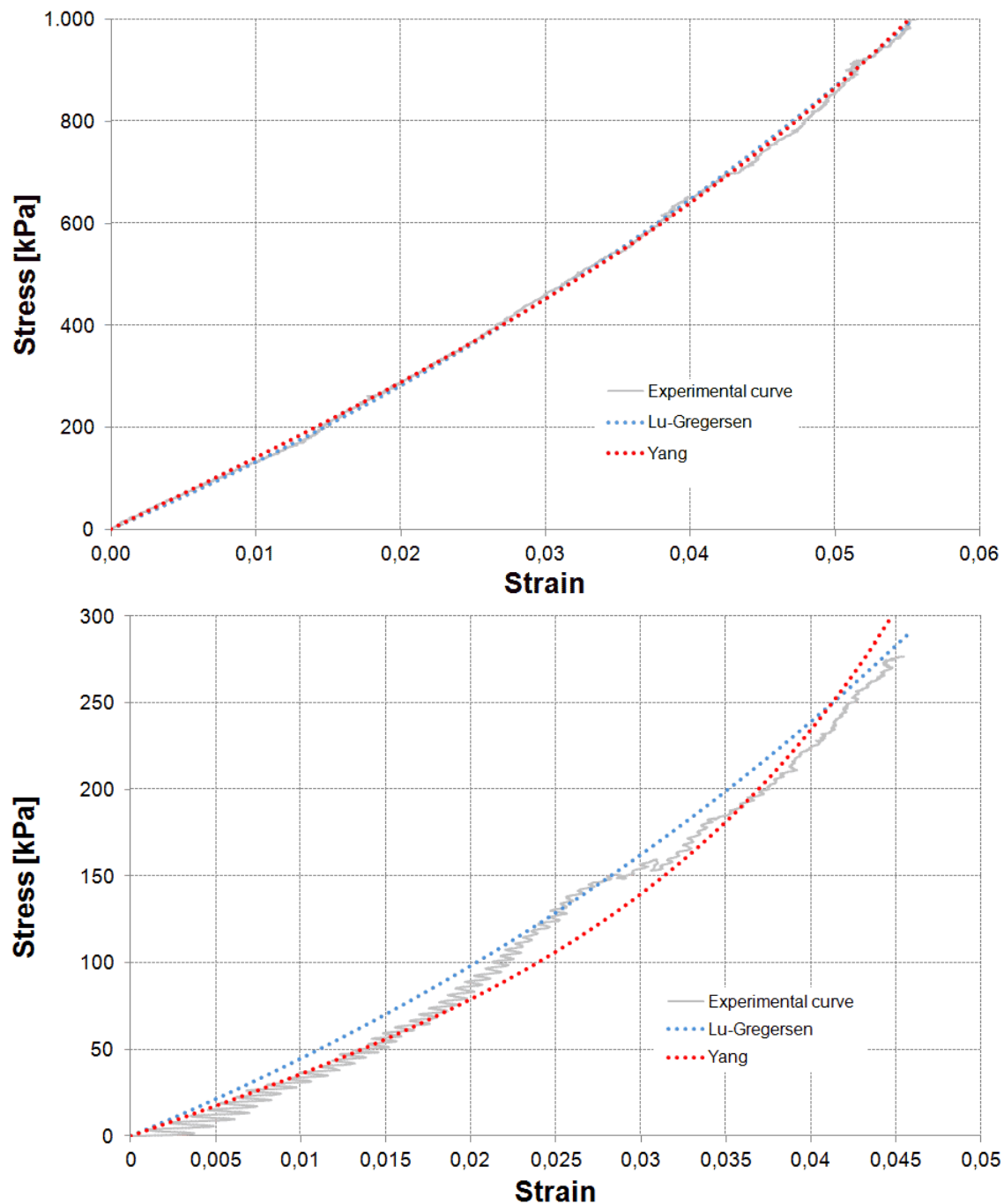
Figure 4.9. Stress-Strain curves from donor 912. *Top*: proximal, male, 32 y.o., BMI 31.6 *Bottom*: distal, same donor.
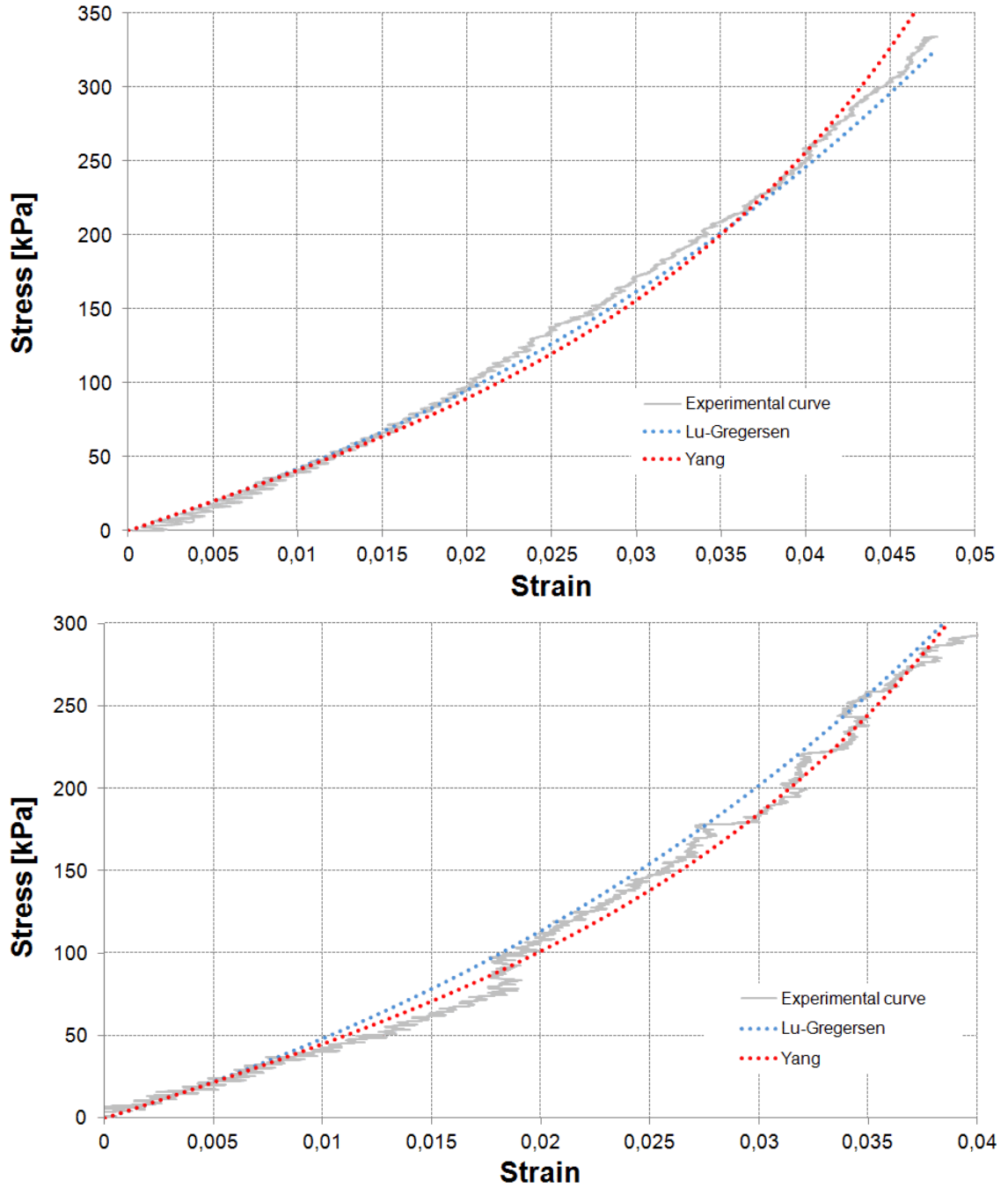
Figure 4.10. Stress-Strain curves from donor 953. *Top*: proximal, female, 77 y.o., BMI 39.6 *Bottom*: distal, same donor.
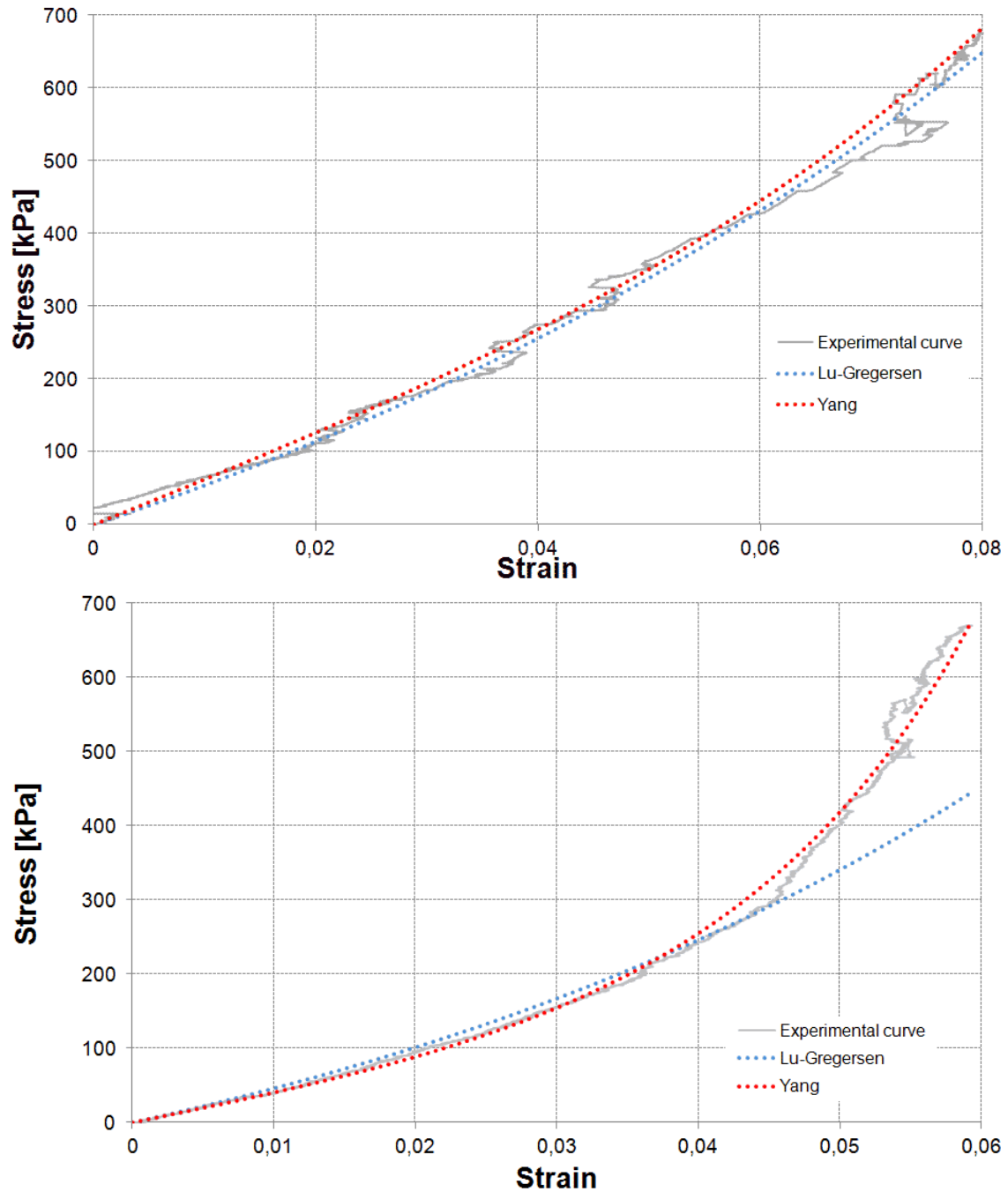
Figure 4.11. Stress-Strain curves from donor 954. *Top*: proximal, male, 45 y.o., BMI 27.4 *Bottom*: distal, same donor.
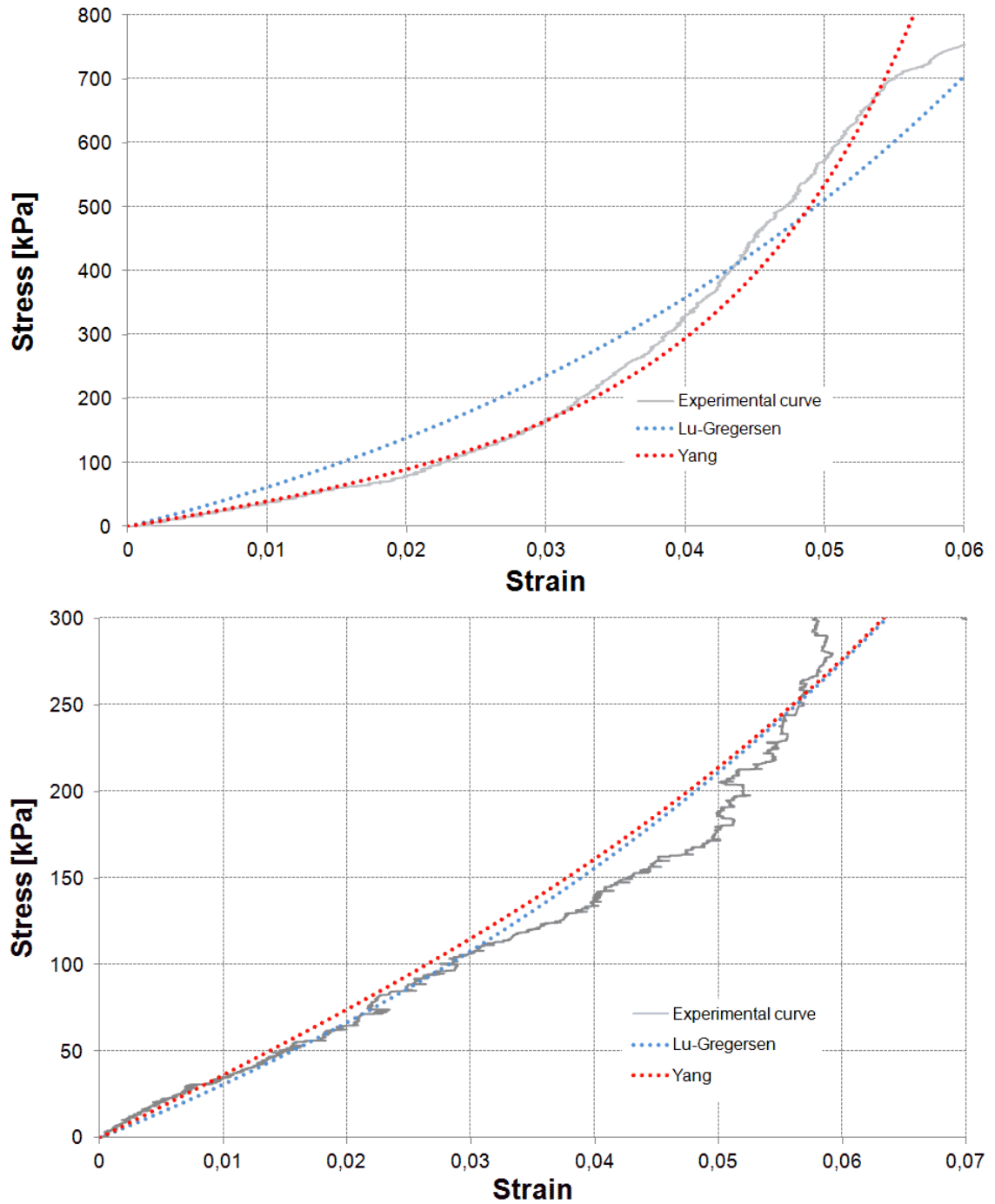
Figure 4.12. Stress-Strain curves from donors 906 and 961: *Top*: 906, proximal, female, 85 y.o., BMI 32.0 *Bottom*: 961, male, proximal, 30 y.o, BMI 32.3.
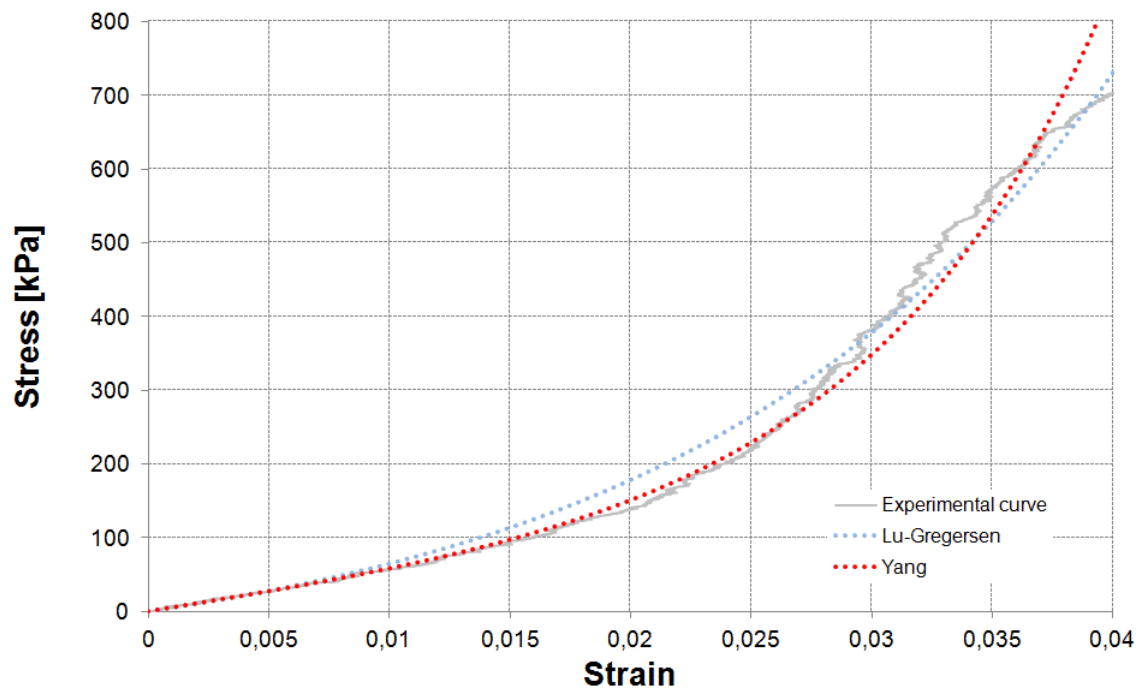
Figure 4.13. Stress-Strain curves from donor 966: distal, male, 57 y.o., BMI 25.5.

4.1.2 Comparison with previously proposed models

The experimental data are compared with two previously proposed models: the Lu-Gregersen model and the Yang-Gregersen-Deng model, summarized in section 2.4.1. The experimental fit with most of the samples is very good (see table 4.1).

Table 4.1. Fitted elastic constants for Lu-Gregersen and Yang-Deng models.

Sample		Lu-Gregersen			Yang-Deng		
Number	Type	A_L [kPa]	β_L	r	A_L [kPa]	β_L	r
839	dist	320.4	14.18	0.9954	5007	66.8	0.9953
839	med	199.2	14.45	0.9997	3212	126.8	0.9966
839	prox	*6.07	29.16	0.9901	1172	*45.3	0.9777
855	dist	91.0	25.01	0.9967	4208	107.0	0.9961
856	dist	364.1	17.08	0.9872	6373	165.4	0.9843
856	prox	365.2	10.27	0.9967	4098	55.0	0.9967
879	dist	301.2	20.39	0.9991	6337	224.8	0.9914
879	prox	*934.7	9.699	0.9911	5556	200.6	0.9547
880	dist	137.1	20.40	0.9993	3113	153.1	0.9970
880	prox	288.2	14.24	0.9932	3537	167.9	0.9680
906	prox	239.7	22.87	0.9788	3799	415.0	0.9913
907	dist	114.1	41.05	0.9756	3442	*1381	0.8909
907	prox	432.4	17.94	0.9819	4351	*1051	0.9848
911	dist	392.3	18.05	0.9800	*12376	*30.7	0.9920
911	prox	14.50	49.18	0.9858	2534	164.3	0.9828
912	dist	226.8	17.99	0.9976	3469	328.5	0.9903
912	prox	*944.9	13.05	0.9993	*13920	87.8	0.9994
953	prox	138.7	29.99	0.9964	4351	389.9	0.9961
954	dist	399.1	17.95	0.9740	3928	303.3	0.9959
954	prox	480.5	10.69	0.9965	6200	*50.0	0.9963
957	dist	49.8	50.07	0.9869	3018	844.8	0.9918
957	prox	565.0	17.97	0.9859	10871	246.4	0.9909
961	prox	199.2	14.45	0.9369	3619	67.4	0.9331
964	dist	89.4	18.01	0.9867	—	—	—
964	prox	95.2	41.57	0.9921	3038	*922.8	0.9956
966	dist	84.8	56.60	0.9941	5348	*864.1	0.9966
[geometric] mean		182.3	21.6	—	4040	211.2	—
superior limit		427.3	34.85	—	5244	541.1	—
inferior limit		77.8	13.37	—	3113	82.4	—

All samples show good adjustment (An 80% of the samples have a correlation coefficient $r > 0.98$). This means that, numerically, these models are quite good for our experimental data. Much more complex models (such as the Kroon-Holzapfel and Natali-Gregersen models) can provide even a better fit according to some studies [38]. Possibly, at least in some cases, the computational complexity might not be suitable for some applications.

4.1.3 Analysis of mechanical properties for human samples

The elastic mechanical properties of the Lu-Gregersen model $A_L^{(L)}, \beta_L^{(L)}$ and the Yang-Deng model $A_L^{(Y)}, \beta_L^{(Y)}$ computed in the previous section show a great variability. The logarithmic average or geometric mean has been computed excluding the the extreme values, marked with an asterisk (*). This logarithmic average is computed by:

$$\ln \mu_M = \frac{1}{n} \sum_{i=1}^{n} \ln M_i \tag{4.1}$$

where $M_i \in \{A_{L,i}^{(L)}, \beta_{L,i}^{(L)}, A_{L,i}^{(Y)}, \beta_{L,i}^{(Y)}\}$. A covariance analysis shows that these four parameter are far from being independent the covariance matrix is given by:

$$\begin{array}{c|cccc} & A_L^{(L)} & \beta_L^{(L)} & A_L^{(Y)} & \beta_L^{(L)} \\ \hline A_L^{(L)} & 1 & -0,631 & +0,698 & -0,268 \\ \beta_L^{(L)} & -0,631 & 1 & -0,320 & +0,621 \\ A_L^{(Y)} & +0,698 & -0,320 & 1 & -0,241 \\ \beta_L^{(Y)} & -0,268 & +0,621 & -0,241 & 1 \end{array} \tag{4.2}$$

As we can see the $A_L^{(L)}$ and $A_L^{(Y)}$ are positively correlated, the same is true for $\beta_L^{(L)}$ and $\beta_L^{(Y)}$. Interestingly the A_L's are negatively correlated with the β_L's. To characterize each sample we search of a set of statistically independent parameters. For this purpose we performed a *Principal Component Analysis* (PCA), with the covariance matrix 4.4 as starting point. This analysis provided four explicative factors or "principal components" (PC), the first principal component explained a 60.3% of the variance, and the second one a 24.5% (the third and fourth factors are less important). Therefore, the first and second factors together explain about a 85% of the variance and are useful for characterize approximately a sample. The cumulative importance of the different principal components is shown in figure 4.14.
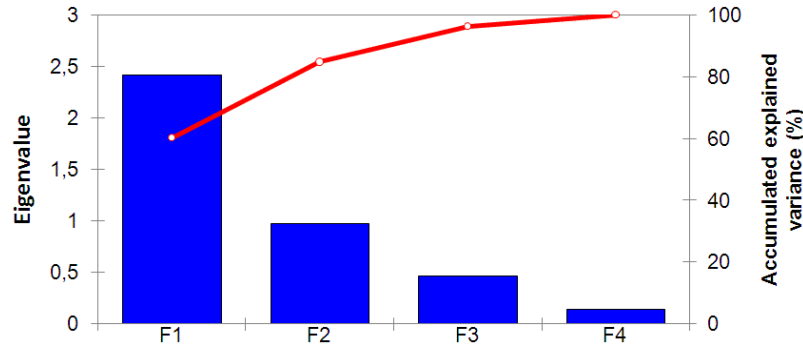
Figure 4.14. Accumulated explained variance for principal factors of mechanical properties

Table 4.2. Principal Component Analysis for mechanical properties

Specimen	Type	1st PC	2nd PC	Age [y.o.]	BMI $[\mathrm{kg \cdot m^{-2}}]$	Gender
839	dist	0.7791	−0.6934	64	45.9	♂
839	med	0.1408	−1.0975	64	45.9	♂
839	prox	−1.1265	−1.5233	64	45.9	♂
855	dist	−0.3602	−0.8290	66	51.7	♂
856	prox	0.8585	−0.1176	85	25.5	♂
856	prox	0.9134	−0.9205	85	25.5	♂
879	dist	0.5043	−0.0248	68	42.8	♀
879	prox	2.2954	0.4648	68	42.8	♀
880	dist	−0.2910	−1.0038	61	—	♂
880	prox	0.3555	−0.8333	61	—	♂
906	prox	−0.3563	−0.1835	85	32.0	♀
907	dist	−2.5709	1.7795	70	35.7	♀
907	prox	−0.3701	1.2217	70	35.7	♀
911	dist	1.9782	0.8280	64	31.1	♂
911	prox	−1.8535	−0.5060	32	31.6	♂
912	dist	−0.1364	−0.5508	32	31.6	♂
912	prox	3.6198	1.9259	77	39.6	♂
953	dist	−0.5677	−0.6451	77	39.6	♀
953	prox	−0.7631	−0.0885	45	27.4	♀
954	dist	0.3599	−0.2490	45	27.4	♂
954	prox	1.4938	−0.3510	68	28.4	♂
957	dist	−2.5278	0.8826	68	28.4	♂
957	prox	1.8891	1.1956	30	32.3	♂
961	prox	0.2737	−1.1283	69	20.8	♂
964	prox	−2.1638	0.8674	69	20.8	♂
966	dist	−2.3739	1.5799	57	25.5	♂
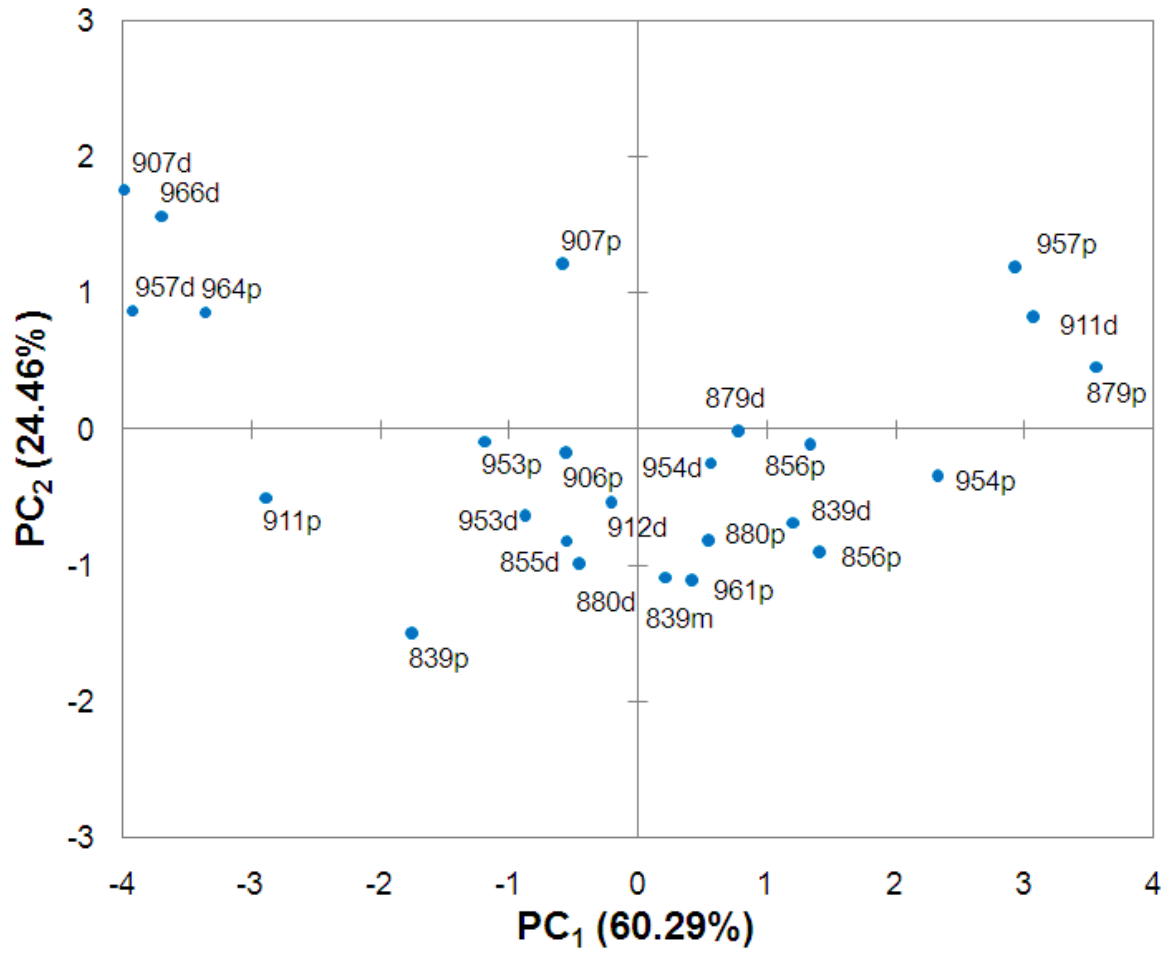
Figure 4.15. Distribution of the elastic parameters for the samples on the space of principal components PC_1 and PC_2.

The values of the principal components (PC_1 and PC_2) for the samples is given in table 4.3. The correlation of the anthropometric variables with these principal factors are low:

Table 4.3. Correlations of principal components and anthropometric variables

	Age	BMI	Gender (1= female)
PC_1	+0,1218	+0,1985	−0,1041
PC_2	+0,0105	−0,2092	+0,2257

This means that the anthropometric variables (Age, Body Mass Index (BMI) and Gender) do not seem to be very relevant for explaining the observed variation in mechanical properties. We know that the mechanical properties are well explained by the two variables, the principal components PC_1 and PC_2, but these variables are not well correlated with the age, the BMI or the gender. For understanding the relation of the principal components with the mechanical properties $A_L^{(L)}, \beta_L^{(L)}, A_L^{(Y)}$ and $\beta_L^{(Y)}$, we show in figure 4.16 the correlations of the principal components with the mechanical properties.
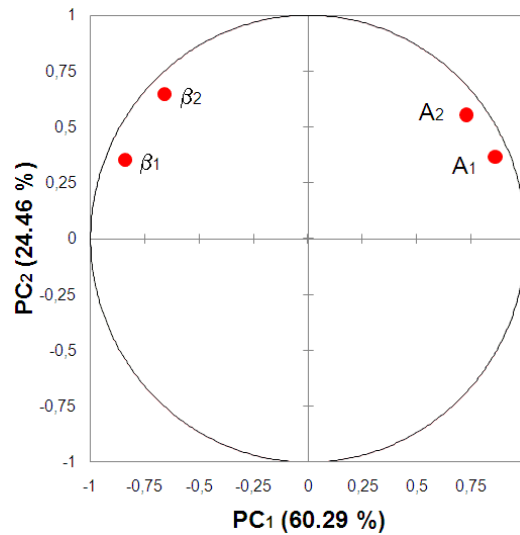
Figure 4.16. Correlation of the principal components PC_1 and PC_2 with mechanical properties. The horizontal axis represents the correlations of the $A_1 = A_L^{(L)}, \beta_1 = \beta_L^{(L)}, A_2 = A_L^{(Y)}$ and $\beta_2 = \beta_L^{(Y)}$ with PC_1. The vertical axis represents the correlations with PC_2.

The mechanical properties can be related with the PC_1 and PC_2 by means of:

$$
\begin{aligned}
A_L^{(L)} &= \quad +0.5556 \cdot PC_1 \quad +0.3700 \cdot PC_2 \\
\beta_L^{(L)} &= \quad -0.5409 \cdot PC_1 \quad +0.3543 \cdot PC_2 \\
A_L^{(Y)} &= \quad +0.4693 \cdot PC_1 \quad +0.5695 \cdot PC_2 \\
\beta_L^{(Y)} &= \quad -0.4238 \cdot PC_1 \quad +0.6515 \cdot PC_2
\end{aligned}
\tag{4.3}
$$

The properties of the PC analysis imply that, the above "linear coefficients" are related to the correlations:

$$
\text{linear coefficient} = \frac{\text{correlation}}{\sqrt{n \times \text{weight of factor}}}
$$

where the "weight factor" are 60.29% and 24.46% for PC_1 and PC_2, $n = 4$ is the number of principal components, and the correlations (the same depicted in figure 4.16) are:

	$A_L^{(L)}$	$\beta_L^{(L)}$	$A_L^{(Y)}$	$\beta_L^{(Y)}$
PC_1	+0.8613	−0.8400	+0.7287	−0.6581
PC_2	+0.3660	+0.3505	+0.5534	+0.6444

$$\tag{4.4}$$

In our study, two other mechanical properties were measured for the human samples: the maximum stress and the maximum strain before fiber breaking (after the breaking of some fibers there is a decrease in the force measure, notice the breaking of some fibers does not imply complete failure). These magnitudes are called here FB-stress and FB-strain. The FB-stress σ_{bf} and FB-strain ε_{bf} are positively correlated ($r = +0.6069$), the values for each sample are shown in table 4.4. The influence of the anthropometric variables (Age, BMI and Gender) data was investigated for both magnitudes σ_{bf} and ε_{bf}. For computing if the effect of the anthropometric variables were significant some regression analyses and principal component analyses were carried out.

Table 4.4. Mechanical properties associated for initial fiber breaking

Sample	Type	FB-strain ε_{bf}	FB-Stress σ_{bf} [kPa]	Age [y.o.]	BMI $[\text{kg} \cdot \text{m}^{-2}]$	Gender
839d	dist	0.076	613.8	64	45.9	♂
839m	med	0.086	669.6	64	45.9	♂
839p	prox	0.178	1155	64	45.9	♂
855d	dist	0.082	781.9	66	51.7	♂
856p	dist	0.057	781.9	85	25.5	♂
856p	prox	0.101	664.4	85	25.5	♂
879d	dist	0.064	737.7	68	42.8	♀
879p	prox	0.080	1219	68	42.8	♀
880d	dist	0.070	449.2	61		♂
880p	prox	0.075	515.2	61		♂
906p	prox	0.072	840.0	85	32.0	♀
907d	dist	0.038	367.6	70	35.7	♀
907p	prox	0.035	460.6	70	35.7	♀
911d	dist	0.048	584.7	64	31.1	♂
911p	prox	0.068	365.0	64	31.1	♂
912d	dist	0.045	276.4	32	31.6	♂
912p	prox	0.056	1099	32	31.6	♂
953d	dist	0.048	284.1	77	39.6	♂
953p	prox	0.041	295.4	77	39.6	♀
954d	dist	0.059	669.5	45	27.4	♀
954p	prox	0.081	681.0	45	27.4	♂
957d	dist	0.026	158.8	68	28.4	♂
957p	prox	0.048	835.8	68	28.4	♂
961p	prox	0.066	353.3	30	32.3	♂
964d	dist	0.030	71.1	69	20.8	♂
964p	prox	0.038	409.6	69	20.8	♂
966d	dist	0.044	717.4	57	25.5	♂

A significant correlation was found between the FB-strain (ε_{bf}) and the body mass index (BMI). To analyze the correlation of ε_{bf} and the anthropometric variables three regression models were examined:

$$\varepsilon_{bf} = \alpha_0 + \alpha_1 \cdot \text{Age} + \alpha_2 \cdot \text{BMI} + \alpha_3 \cdot \text{Gender} \quad \text{(Model 1)}$$
$$\varepsilon_{bf} = \alpha_0 + \alpha_2 \cdot \text{BMI} \quad \text{(Model 2)} \quad (4.5)$$
$$\varepsilon_{bf} = \alpha_2 \cdot \text{BMI} \quad \text{(Model 3)}$$

Model 1 is the best adjusted model, *i.e.* the model with higher correlation $r =$

0.529, the regression analysis showed that only α_2 is statistitistical significant (with a p-value $< 0,013$). Then two the other models were considered: model 2 is the a complete linear model with the only significant variable (BMI) and model 3 is an incomplete linear model. The values of the coefficients for the three model and the significance analysis is summarized in table 4.5.

Table 4.5. Influence of anthropometric parameters in $\varepsilon_{\mathrm{bf}}$

Model	Coefficient	Value	SD	t-Student	p-value
1	α_0	$-1.98 \cdot 10^{-3}$	$3.27 \cdot 10^{-2}$	-0.061	—
	α_1	$+8.98 \cdot 10^{-5}$	$3.77 \cdot 10^{-4}$	$+0.238$	—
	α_2	$+1.89 \cdot 10^{-3}$	$6.93 \cdot 10^{-4}$	$+2.730$	(0.013)
	α_3	$-1.78 \cdot 10^{-2}$	$1.31 \cdot 10^{-2}$	-1.365	—
2	α_0	$+4.22 \cdot 10^{-3}$	$2.41 \cdot 10^{-2}$	$+0.175$	—
	α_2	$+1.72 \cdot 10^{-3}$	$6.90 \cdot 10^{-4}$	$+2.488$	(0.021)
3	α_2	$+1.85 \cdot 10^{-3}$	$1.57 \cdot 10^{-4}$	11.73	(< 0.0001)

From the table 4.5 it is clear that the effect of BMI is significant in all three models; this means that there is a verified tendency: the higher the BMI, the larger the FB-strain of their esophagi. This can be clearly observed in figure 4.17 where the model 2 is plotted along with the data.
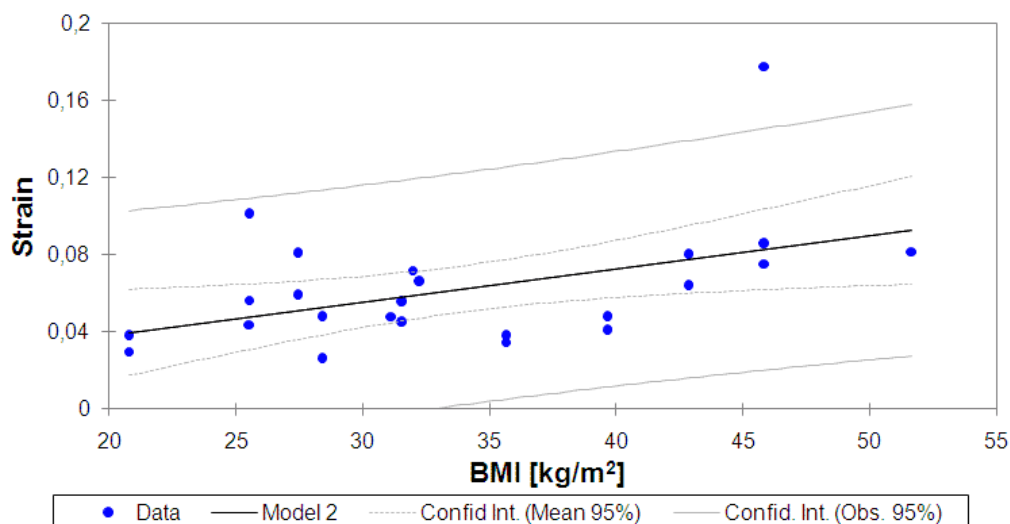
Figure 4.17. Effect of Body Mass Index on the fiber breaking strain. The dots are the data for the samples along with the standard confidence intervals of 95%.

For the FB-stress σ_{bf} the positive effect of BMI is present, but it is not significant (except for model 3 or incomplete variants of model 1 and 2). The effect of

BMI on σ_{bf} is plotted in figure 4.18 where the model 3 is plotted along with the data.
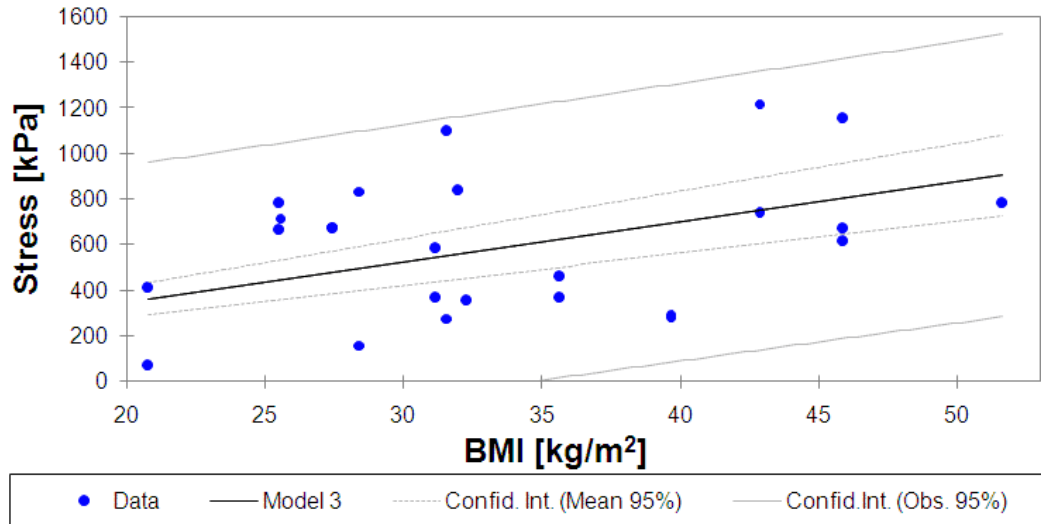
Figure 4.18. Effect of Body Mass Index on the fiber breaking stress. The dots are the data for the samples along with the standard confidence intervals of 95%.

4.1.4 Stress-Strain curves for swine samples

The curves for swine samples were qualitatively similar to those of humans (see figure 4.20). Interestingly, the swine samples allowed an easier separation of the two layers, and on the other hand, the data for mucosa-submucosa tests and muscularis externa test could be compared.
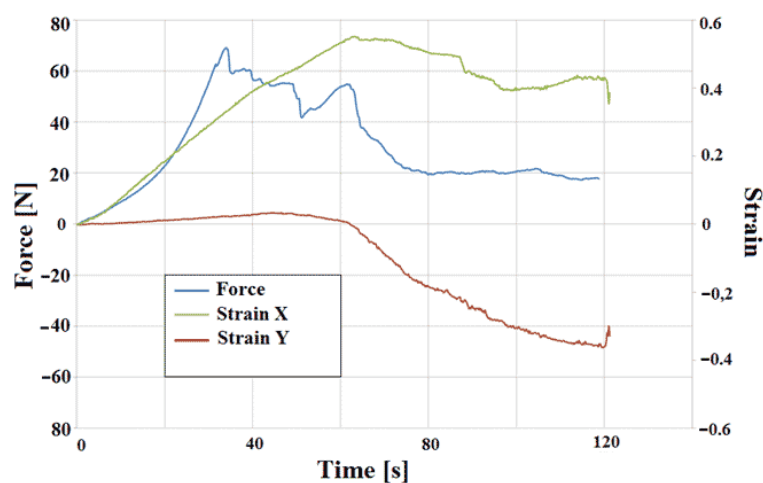
Figure 4.19. Force-time response and strain-time relations (for sample 13), once synchronization is made (X is the direction of the force). After final failure, the computed strains are only the result of a calculation from motion tracking; not the real strains.
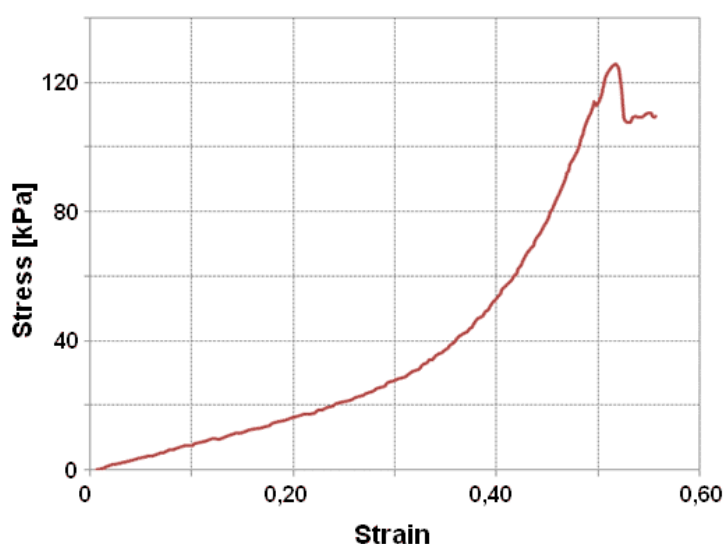
Figure 4.20. A typical computed stress-strain curve (sample 13).

4.2 Theoretical results

Besides the empirical findings previously described, three main theoretical results have been obtained:

- **A theoretical justification for exponential laws in soft tissue mechanics**. Although broadly used in the literature, no explanation other than empirical adequacy is given for the "exponential constitutive laws". Here, an encouraging theoretical result has been obtained using statistical mechanics: if it is assumed that in a soft tissue there are fibers of different lengths (and some of them slack if the strain is sufficiently low), one expects that, by increasing the strain, an increasing number of fibers get tense; this implies that by increasing the strain, the rigidity increases due to the addition of fibers in tension. To the best of my knowledge, this would be the first non-heuristic argument for expecting the occurrence of an "exponential law" for soft tissue.

- **An exact distribution for the residual stress**. Residual stress has been briefly mentioned in section 2.2; its exact distribution has been computed using the tools of Riemann geometry (see section 4.2.2). Other authors had found linear approximations to this distribution, but here, we have found the exact *non-linear distribution*.

- **The necessary conditions for the existence and stability of the solutions of a microstretch elasticity problem**. We examined here the necessary conditions for the propagation of elastic waves and related restrictions for the elastic tensor. This could be considered a generalization of some mathematical results in elasticity for microcontinuum continua.

Some other additional minor mathematical results are explained in detail in the next sections. For example, the mathematical *structure for the group of configurations* of a microstretch continuum or to find the scalar tensor functions which is invariant under the symmetry group D_{2h} (the dihedral group) used in the proposed model.

4.2.1 Statistical mechanics of collagenous tissues

Statistical mechanics is a branch of Physics that applies probability theory for dealing with systems that are formed by a large amount of particles or elements which interact among them. In statistical mechanics only the overall behavior of the whole system is investigated (and the information directly concerning individual particles or elements is ignored). A typical case extensively studied in statistical mechanics is the case of a gas formed typically by 10^{21} molecules. Obviously, the individual behavior of a particular molecule is not relevant, but temperature, pressure and other properties are relevant for the overall behavior of the system. The matter is that statistical mechanics allows to predict the physical magnitudes of a gas by averaging over all molecules. If we have a large population of particles or identical elements interacting weakly, statistical mechanics provides a framework for relating the microscopic properties of the elements to the macroscopic bulk properties of the material, thereby explaining thermodynamics as a result of the classical mechanical descriptions of statistics and mechanics at the microscopic level.

Statistical mechanics provides an interpretation of macroscopic thermodynamic quantities such as work, heat, free energy, and entropy in terms of microscopic elements. Statistical mechanics, like thermodynamics, is governed by the *second law of thermodynamics* through the medium of entropy. The important difference is that entropy in thermodynamics is only known empirically, whereas in statistical mechanics, it is a function of the distribution of the system on its micro-states. The use of statistical mechanics is widespread to obtain constitutive equations. For example, the Swiss physical chemist Werner Kuhn successfully derived a thermal equation of state for rubber molecules using Boltzmann's formula, which has since come to be known as the entropy model of rubber. Other early uses of statistical mechanics in constitutive theory were Kuhn & Grün (1942, 1946) [60, 61], James & Guth (1943) [56], and Flory (1953, 1956) [36].

In this section a theoretical explanation for the "exponential laws", discussed in section 2.4.1, is developed. The point of departure is that the tissue is formed by a large number of interwoven collagenous fibers inside an elastin matrix. It is supposed that the criss-crossed disposition of the collagen fibers inside the elastin matrix produces an interaction among them by which the deformation is distributed among all the tissue. That is, the collagenous tissue is considered as a complex system of identical weakly interacting fibers that can be addressed by

the *canonical ensemble* formalism of statistical mechanics. A short account of the formalism of the statistical mechanics used here can be found in Zemansky & Dittman (1997) [116] or in Pathria (1996) [86]. According to the principles of statistical mechanics, the actual equilibrium state observed in a system is the macro-state which maximizes the entropy subject to two constrains (the conservation of the number of particles or micro-elements, and the conservation of energy). As the work of Ludwig Boltzmann (1877) suggested, and was stated explicitly by Max Planck (1900) the entropy is related to the probability of a macro-state, and thus the number of micro-states (a specific microscopic arrangement of fibers) compatible with that macro-state, by the equation:

$$S = k_B \ln \Omega, \qquad \text{where} \qquad \Omega = \frac{g_1^{N_1}}{N_1!} \frac{g_2^{N_2}}{N_2!} \dots \qquad (4.6)$$

where k_B is the Boltzmann constant, g_i the number of possible ways to fill the state i, and N_i the number of fibers in state i (it is important to highlight that a state of the whole system is called *macro-state*, but a state of an individual fiber or element is referred as *micro-state* or just *state*). The constrains for the number of fibers and for the total energy are:

$$\begin{cases} \sum_i N_i = N = \text{const.} \\ \sum_i N_i \mathcal{E}_i = U = \text{const.} \end{cases} \qquad (4.7)$$

Where N is the total number of fibers, U the internal energy of the system, and $\mathcal{E}_i$ is the typical deformation energy stored in a fiber in the strain-state i.

Given a deformation energy, and a fixed number of fibers; the problem of finding the distribution of occupation numbers $\{N_1, N_2, \dots\}$ for fibers in each possible strain-state by maximizing the entropy in 4.6 subject to the constrains in 4.7 can be solved by using the method of the Lagrange multipliers (with two multipliers A and β). The solution of this problem is the Boltzmann distribution of the corresponding canonical ensemble:

$$N_i = A g_i e^{-\beta \mathcal{E}_i} \qquad (4.8)$$

By computing the sum of all these occupation numbers, we can eliminate the

first multiplier:

$$\sum_i N_i = A \sum_i g_i e^{-\beta \mathcal{E}_i} = N \quad \Rightarrow \quad A = \frac{N}{\sum_i g_i e^{-\beta \mathcal{E}_i}} \tag{4.9}$$

The second multiplier for a system for a conventional system is related to the thermodynamical temperature. For a hydrostatic system, it can be computed that:

$$\beta = \frac{1}{k_B} \left(\frac{\partial S}{\partial U} \right)_V \tag{4.10}$$

Thus given the well know thermodynamic relation: $T = (\partial U/\partial S)_V$ we have the relation between the second multiplier and the "temperature" of the system: $\beta = 1/k_B T$ (although in this case, the "statistical" is only a parameter related to the relation among entropy and energy, it can not be identified with the environment temperature). Indeed we will see that being the possible strain-energy of a fiber bounded form above, this implies that the second multiplier needs to be negative (a similar situation is found in a few physical systems which exhibit "negative temperature"). Before proceeding to develop this argument, we define a fundamental tool called *partition function Z* given by:

$$Z = \sum_i g_i e^{-\beta \mathcal{E}_i}, \qquad Z = \int_\Sigma e^{-\beta \mathcal{E}(\mathbf{s})} g(\mathbf{s}) \, d^n \mathbf{s} \tag{4.11}$$

where the first form is used when the possible energies for the micro-state of the elements form a discrete set, the second one is used for systems with a continuous spectrum. The variable $\mathbf{s} \in \mathbb{R}^n$ is taken over the space of possible states. The partition function of a system is important because it is directly related to the Helmholtz Free-Energy Density Function Ψ (HEDF) and to the internal energy or Strain-Energy Density Function W (SEDF) by:

$$\Psi = -\frac{1}{\beta} \ln Z, \qquad W = -\frac{\partial Z}{\partial \beta} \tag{4.12}$$

Returning to equations 4.8 and 4.9, we will assume that a fiber in its natural state is slack and most of the strain is due to the lost of this slackness (fiber

realignment before suffering stretch). In addition, we will assume that only a fraction of the fibers has axial stretch different from zero; even for moderate strains, most fibers will have experienced low stretch in longitudinal direction. For most of the fibers that are in tension, it seems reasonable to assume that energy of deformation can be approximated by a low order polynomial in deformation, that is:

$$\mathcal{E}_i = \mathcal{E}_{0,i} + C^{ab}\varepsilon_{ab} + C^{abcd}\varepsilon_{ab}\varepsilon_{cd} \qquad (4.13)$$

where C^{abcd} represents the [contravariant] components of the elastic tensor (due the arbitrariness of the origin of energy scale we can choose $\mathcal{E}_{0,i} = 0$, and other physical reasons imply $C^{ab} = 0$). The partition function for a system of fibers with global strain ε_f is:

$$Z = g_0 e^{\mathcal{E}(0)} + \int_0^{\varepsilon_f} g(\varepsilon)e^{-\beta\mathcal{E}(\varepsilon)} \, d\varepsilon \qquad (4.14)$$

The first term represents the fraction of fibers that are completely slack when the total strain is ε_f. The integral represents the fibers in different states of stress ranging from 0 to ε_f. Taking into account that $\mathcal{E}(0) = 0$ and using the second mean value theorem for integrals for monotonically increasing functions, we can rewrite the previous expression as:

$$Z = g_0 + e^{-\beta\mathcal{E}(\varepsilon_f)} \int_0^{\varepsilon_0} g(\varepsilon) \, d\varepsilon = g_0 + e^{-\beta\mathcal{E}(\varepsilon_f)} \int_0^{\varepsilon_0} g(\varepsilon)d\varepsilon = g_0 + g_f e^{-\beta\mathcal{E}(\varepsilon_f)} \quad (4.15)$$

We can achieve the same qualitative result by simply assuming that there are two groups of fibers: slacking fibers and a group of uniformly stretched fibers. By computing the Helmholtz free-energy density function (HEDF) according to equation 4.12, we obtain:

$$\Psi_{col} = -\frac{1}{\beta}\ln Z = -\frac{1}{\beta}\ln\left(g_0 + g_f e^{-\beta\mathcal{E}(\varepsilon_f)}\right) = -\frac{\ln g_0}{\beta} - \frac{1}{\beta}\ln\left(1 + \frac{g_f}{g_0}e^{-\beta\mathcal{E}(\varepsilon_f)}\right) \quad (4.16)$$

We can rewrite this equation in a different form, in order to compare it with the expressions in section 2.4.1. Using the Taylor series for logarithm:

$$
\begin{aligned}
\tilde{\Psi}_{col} := \Psi_{col} + \frac{\ln g_0}{\beta} = \quad & -\frac{1}{\beta}\ln\left(1 + k_g e^{-\beta\mathcal{E}(\varepsilon_f)}\right) \\
\approx & -\frac{k_g e^{-\beta\mathcal{E}(\varepsilon_f)}}{\left(1 + k_g e^{-\beta\mathcal{E}(\varepsilon_f)}\right)\beta} \\
\approx & -\frac{k_g e^{-\beta\mathcal{E}(\varepsilon_f)}}{(1 + k_g)\beta}
\end{aligned}
\tag{4.17}
$$

where $k_g := g_f/g_0$. Then we have proved that for moderate stress the statistical mechanics predicts an exponential law. This exponential law in 4.17 is directly comparable with expressions in section 2.4.1. In all of these models the exponential is positive and so is the total HEDF, obviously this is only possible if $\beta < 0$ (which in other systems plays the rôle of the absolute temperature), as we will argue below there are good physical reasons related to the behavior of the entropy of the fibers that imply that in our case β is a negative number, and therefore, the statistical mechanics justifies the proposed phenomenological models containing "exponential" laws. The other terms are in accordance with the results, according to our model $k_g > 0$ (because it is related to the ratio of two probabilities) and thus this implies the mechanical stability of the system $\partial^2\tilde{\Psi}_{col}/\partial\varepsilon_f^2 \geq 0$

As it was previously mentioned, the system analyzed here differs significantly from a conventional thermodynamical system, in one important point (although a full discussion of systems with "negative temperatures" is beyond the scope of this dissertation, some brief comments comparing our system to them is in order). This will help to understand intuitively that the requirement of $\beta < 0$ is not only necessary but also natural for the system of tense and slack collagenous fibers in a soft tissue. Most conventional thermodynamic systems are energetically unbounded from above. For example in a classical gas, every molecule has an infinite number of energy-states available (if the velocity increases the energetic state of the molecule increases). This property implies that by supplying more and more energy to a classical gas the entropy increases with the energy, therefore we have $1/T = (\partial S/\partial U)_V > 0$, thus the thermodynamic "temperature" of the system is positively defined. This situation is completely the inverse in systems with energy-states bounded from above. Given a deformation of the soft tissue

the maximum strain of a fiber is bounded by the total strain. Indeed, when we stretch a piece of tissue only a fraction of the fibers are in tension, because the fibers are not straight. Only when the stretching of the tissue is high enough most fibers are straightened out and are in tension. The work of the exterior forces increases the elastic energy, but reduces the disalignment and reduces entropy. This situation implies that for a soft tissue the Lagrange multiplier β is negative:

$$\beta_{\text{soft-tissue}} = \left(\frac{\partial S}{\partial U}\right)_{\varepsilon} < 0 \tag{4.18}$$

The subindex ε refers to the thermodynamic restriction that the path along which we take the derivative is one with constant strain ε. This situation is analogous to the "exotic" systems such as the system of nuclear spins at very low temperature, the lasers, and other systems which can exhibit effective negative Kelvin temperatures. [116, p. 544].

4.2.2 About residual stress

The intact state is the shape that adopts the esophagus with no applied load. It has been demonstrated that this load-free intact state is not a stress-free state. An approximate distribution of the residual stress is found at the end of this section (see figure 4.24), the objective of this section is to compute the exact distribution of residual stretches along a cross-section of esophagus. It is interesting to note that the existence of residual stresses is very common in a lot of anatomic structures and tissues. In fact, the existence of residual stress, as it was explained in section 2.2, is a consequence of the stress-driven growth and remodeling of tissues. Rodriguez *et al.* (1994) proposed a continuum formulation for growth of elastic tissues [93] in which the shape of an unloaded tissue changes according to a magnitude analogous to the deformation gradient tensor. The work of Rodriguez *et al.* suggests that a complete kinematic formulation for growth requires a constitutive law for stress in the tissue. Since growth may in turn be affected by stress in the tissue, such a formulation involves a symmetric growth-rate tensor and the stress tensor. There are different evidences to show the presence of the residual stresses. The most obvious evidence is the opening angle of dissected ring of esophagus. Indeed, this effect provides the key factor for computing the residual stretch. In figure 4.21, it can be observed that when

a ring section is cut the part in tension (outer part) pulls out and the part in compression (inner part) pushes in; the result is an opening angle. The same effect has been observed for esophageal tissues [45, 115].
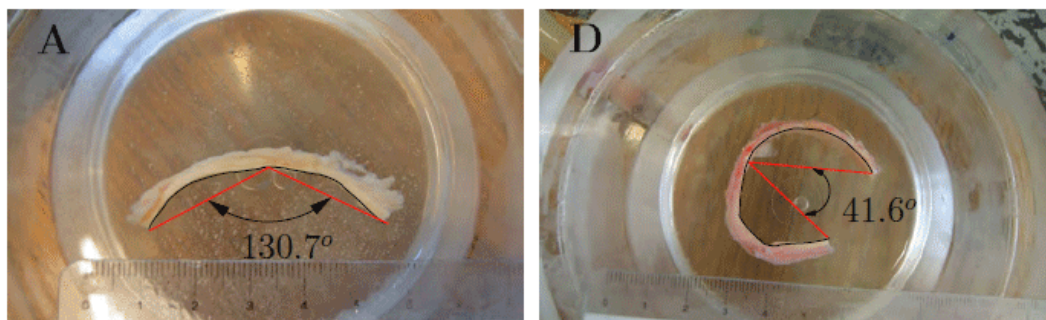
Figure 4.21. The opening angle for samples of aortic artery tissue, the black line indicates the position of intima layer. (*Left*) Normal aortic tissue, with typical angle $\alpha = 131°$, (*Right*) Abnormal aortic tissue from a donor with Marfan's syndrome $\alpha = 42°$ (images from Garcia-Herrera, 2008), [38]

From a geometrical point of view, the existence of residual stress implies that it is not possible to achieve a stress-free shape in Euclidean space. It is interesting that the intact shape can be isometrically mapped to a three-dimensional Riemannian manifold $\varphi : \mathbb{R}^3 \hookrightarrow Y$ with curvature different from zero (in turn, the Nash-Kuiper theorem and the Nash embedding theorem for Riemannian manifolds imply that this three-dimensional non-Euclidean manifold can be $\mathcal{C}^k$-embedded ($k > 3$) in a Euclidean space of dimension $n \leq m(m + 1)(3m + 11)/12$, where $m = 3$, for simple states of residual stress this bound probably can be reduced significantly).

The general theory for dealing exactly with residual stress can be found in Lu (2012), this formulation requires unavoidably the use of Riemann manifolds for representing the initial non-natural state [68]. This formulation assigns a Riemann metric tensor to the tissue an effective (see B.5.1) different from the Euclidean metrics (or distance). This metric tensor $G = G_{AB}dX^A dX^B$ (*i.e.* non-degenerated, 2-tensor, positively-defined over the tangent bundle) allows to define a non-Euclidean or Riemann distance over the tissue. For the compressed parts of the tissue the Euclidean length along a virtual curve inside the tissue will be shorter than the effective Riemann distance given by the metric tensor describing residual stress. For tensed parts with (stretch higher than one) the Euclidean length is larger than the effective Riemann distance. Thus, we can predict the

residual stress from the difference between the Riemann metric tensor and the Euclidean metric tensor. For a direction of parallel to the unitary vector $\mathbf{n} = (n^1, n^2, n^3)$:

$$\sigma_{res} = (G_{AB} - \delta_{AB})n^A n^B \tag{4.19}$$

Trivially, for an unstressed part of the body one has $G_{AB} = \delta_{AB}$
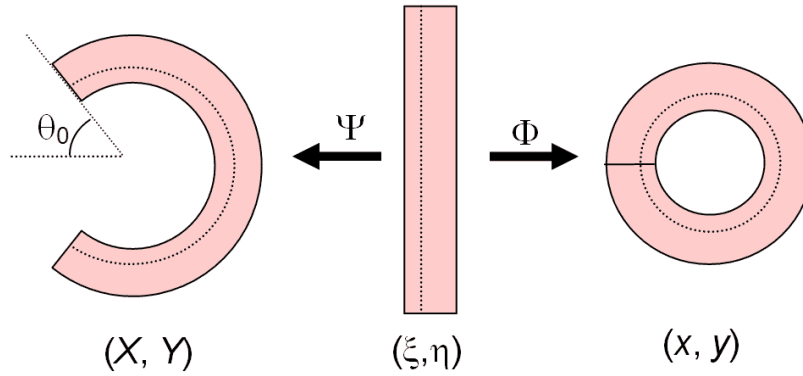
Figure 4.22. The stress-free state (*left*), a non-stress-free fictitious/virtual state (*center*), and the load-free intact state (*right*)

To account for the residual stresses and strains, we need to compute the distortion of distances in the intact state, according to the proposal of Lu (2012) [68]. If we assume that the state depicted on the left side of figure 4.22 is a *free-stress state*, the natural distances are given by the Euclidean metric tensor:

$$g = g_{\alpha\beta}dX^\alpha \otimes dX^\beta = \delta_{\alpha\beta}dX^\alpha \otimes dX^\beta = dX \otimes dX + dY \otimes dY$$

The transformation Ψ and Φ are given by:

$$\begin{cases} (X,Y) = \Psi(\xi,\eta) = \left((R+\xi)\cos\dfrac{\eta}{2\pi r}, (R+\xi)\sin\dfrac{\eta}{2\pi r} \right) \\ (x,y) = \Phi(\xi,\eta) = \left((r+\xi)\cos\dfrac{\eta}{2\pi r}, (r+\xi)\sin\dfrac{\eta}{2\pi r} \right) \end{cases} \tag{4.20}$$

where r is the the radius of neutral axis in the intact configuration (dotted line in the figure 4.22, on the left side) and R the radius of the same material

line on the right side (dotted line). The dotted line has the same length in all the three figures. This implies that $r\pi = R(\pi - \theta_0)$. The inverse functions are:

$$\begin{cases} (\xi, \eta) = \Psi^{-1}(X, Y) = \left(\sqrt{X^2 + Y^2} - R, 2\pi r \arctan \dfrac{Y}{X} \right) \\ (\xi, \eta) = \Phi^{-1}(x, y) = \left(\sqrt{x^2 + y^2} - r, 2\pi r \arctan \dfrac{y}{x} \right) \end{cases} \quad (4.21)$$

The diffeomorphism between the stress-free state on the right and the intact state to the left is given by $\Lambda = \Psi \circ \Phi^{-1}$:

$$(X, Y) = \Lambda(x, y) := \Psi \circ \Phi^{-1}(x, y) = \left(\left[\frac{R - r}{\sqrt{x^2 + y^2}} + 1 \right] x, \left[\frac{R - r}{\sqrt{x^2 + y^2}} + 1 \right] y \right) \quad (4.22)$$

Using this change of coordinates, we have the following relation among covectors (1-forms in the cotangent bundle, see appendix B.3)

$$\begin{cases} dX = \dfrac{\partial X}{\partial x} dx + \dfrac{\partial X}{\partial y} dy \quad \Lambda_x^X dx + \Lambda_y^X dy \\ dY = \dfrac{\partial Y}{\partial x} dx + \dfrac{\partial Y}{\partial y} dy \quad \Lambda_x^Y dx + \Lambda_y^Y dy \end{cases} \quad (4.23)$$

and therefore the metric tensor expressed in the (x, y) coordinates is:

$$g = g_{\alpha\beta} dx^\alpha dx^\beta =$$
$$[(\Lambda_x^X)^2 + (\Lambda_x^Y)^2] dx \otimes dx + [\Lambda_x^X \Lambda_y^X + \Lambda_x^Y \Lambda_y^Y] dx \otimes dy + \quad (4.24)$$
$$[\Lambda_x^X \Lambda_y^X + \Lambda_x^Y \Lambda_y^Y] dy \otimes dx + [(\Lambda_y^X)^2 + (\Lambda_y^Y)^2] dy \otimes dy$$

By computing explicitly the Λ_j^J functions, we obtain:

$$g = (dx \otimes dx + dy \otimes dy) + \frac{(R - r)^2 + 2(R - r)\sqrt{x^2 + y^2}}{(x^2 + y^2)^2} (y dx + x dy) \otimes (y dx + x dy) \quad (4.25)$$

The first part is an Euclidean tensor, and the second part gives the deviations

from the Euclidean distances due to residual strains. For practical computations of distances around the lumen of esophagus, it is useful to do the same computation in "cylindrical type" coordinates:

$$
\begin{cases}
(P,\Theta) = \hat{\Psi}(\xi,\eta) = \left(\xi + R, \dfrac{\eta}{R}\right), & (\xi,\eta) = \hat{\Psi}^{-1}(P,\Theta) = (P - R, R\Theta) \\[2mm]
(\rho,\theta) = \hat{\Psi}(\xi,\eta) = \left(\xi + r, \dfrac{\eta}{r}\right), & (P,\Theta) = \hat{\Phi}^{-1}(\rho,\theta) = (\rho - r, r\theta)
\end{cases}
\tag{4.26}
$$

The Euclidean metrics in cylindrical coordinates is (P,Θ) is $g = dP \otimes dP + P^2 d\Theta \otimes d\Theta$. If the coordinate change $(P,\Theta) \mapsto (\rho,\theta)$ (given by $\hat{\Lambda} = \hat{\Psi} \circ \hat{\Phi}^{-1}$), we have the metric tensor in the new coordinates:

$$
g = d\rho \otimes d\rho + \left(\rho + r\frac{\theta_0}{\pi - \theta_0}\right)^2 \left(1 - \frac{\theta_0}{\pi}\right)^2 d\theta \otimes d\theta
\tag{4.27}
$$

Given this form, we can check that the neutral axis $\rho = r$ has the same original length:

$$
L_r = \hat{L}(r) \quad \int_0^{2\pi} \sqrt{\left(\frac{\partial \rho}{\partial \theta}\right)^2 + \left(\rho + \frac{r\theta_0}{\pi - \theta_0}\right)^2 \left(1 - \frac{\theta_0}{\pi}\right)^2 \left(\frac{\partial \theta}{\partial \theta}\right)^2} \, d\theta =
$$
$$
= \int_0^{2\pi} \left(r + \frac{r\theta_0}{\pi - \theta_0}\right)\left(1 - \frac{\theta_0}{\pi}\right) d\theta = \qquad 2\pi r
$$

It can also be checked that the inner part has been shrunk (compressed) and that the exterior part has been stretched out (see figure 4.23), *i.e.* the perimeter fibers outside the neutral axis $(\rho > r)$ are longer in the intact configuration. On the other hand, the fibers inside the neutral axis $(\rho < r)$ are shorter. For seeing this, we compute the initial length of a circumference of the intact configuration with $\rho = \rho_0$:

$$
\hat{L}(\rho_0) = 2\pi \left[\rho_0 \left(1 - \frac{\theta_0}{\pi}\right) + r\frac{\theta_0}{\pi}\right] = 2\left[\rho_0 \left(\pi - \theta_0\right) + r\theta_0\right]
$$

Clearly, we have:

$$
\lambda(\rho) = \frac{2\pi\rho}{\hat{L}(\rho)} = \begin{cases} < 1 & \text{for } \rho < r \\ > 1 & \text{for } \rho > r \end{cases}
$$
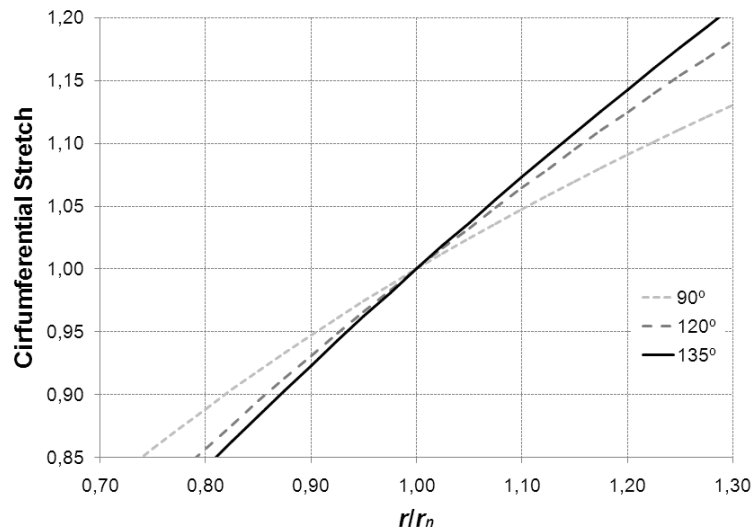
Figure 4.23. Circumferential stretches as a function of the ratio r/r_n, being r the radius and r_n the radius of the neutral axis.).

Therefore the metric tensor given by 4.27 satisfies the conditions for representing the initial geometry. In the past, other approximate approaches, such as Navier-Kirchhoff hypothesis, were used to determine the distribution of residual stress, see for example figure 4.24. It is obvious that the Navier-Kirchhoff is a only a linear approximation to the exact formulas found in this section. This result corroborates the powerful possibilities associated to the use of Riemannian geometry.
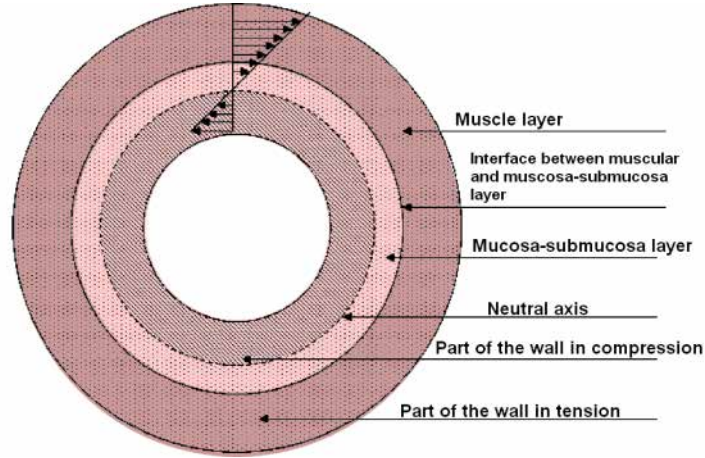
Figure 4.24. Gregersen & Liao (2008) postulate that as a first approximation the Navier-Kirchhoff hypothesis is valid for residual stresses in an esophageal ring, and they use this fact to compute of the neutral axis (figure adapted from Gregersen & Liao, [46]).

4.2.3 Other additional theoretical results

In section 2.3.5, it was explained that a configuration is an element of one group of the form $\hat{\mathscr{C}}_{\hat{\mathcal{B}}} \subset \mathscr{C}_{\mathcal{B}} \times \mathbf{GL}^+(n)$, where $\mathscr{C}_{\mathcal{B}}$ can be identified with a certain group of diffeomorphisms, characterizing the macro-deformation; and a subgroup of $\mathbf{GL}^+(n)$, characterizing the micro-deformation (see definition 2.3.7). For the case of a microstretch continuum, the additional degrees of freedom include a reorientation of the microstructure (mathematically, a rotation or member of $\mathbf{SO}(3)$) and a uniform compression/stretch of the microstructure (mathematically, a homothety or homogeneous dilation of ratio j). Obviously, the group representing the configurations of the microstructure of a microstretch continuum needs to include homotheties and rotations as subgroups, the following group $\mathcal{G}_{ms} \subset \mathbf{GL}^+(3)$ satisfies this condition:

$$\mathcal{G}_{ms} = \left\{ \mathbf{g} \in \mathbf{GL}(3) \mid \mathbf{g}^T\mathbf{g} = \mathbf{g}\mathbf{g}^T = k\mathbf{1}, k > 0 \right\} \tag{4.28}$$

here, "ms" stands for "microstretch". We will prove that a member of this group $g \in \mathcal{G}_{ms}$ can be uniquely rewritten as a product of one rotation and one homothety, that is: $\forall \mathbf{g} \in \mathcal{G}_{ms}$, *there are* $\mathbf{g}_1 = j\mathbf{1}$ *and* $\mathbf{g}_2 \in \mathbf{SO}(3)$, *such that* $\mathbf{g} = \mathbf{g}_1\mathbf{g}_2$, where $j \in \mathbb{R}$ and $\mathbf{1}$ identity matrix or unit element in the General Linear

Group. This last factorization is the right-hand factorization, analogously one can find a left-hand factorization $\mathbf{g} = \mathbf{g}_4\mathbf{g}_3$ with $\mathbf{g}_3 = j'\mathbf{1}$ and $\mathbf{g}_4 \in \mathbf{SO}(3)$. For doing this we will prove that $\mathcal{G}_{ms}$ is the semidirect product of $\mathbf{SO}(3)$ and $\mathbb{R}^+$, that is, $\mathcal{G}_{ms} = \mathbf{SO}(3) \rtimes \mathbb{R}^+$. Then the right- and left-hand factorization follow from the following theorem of group theory:

Theorem 4.2.1. *Let G be a group whose identity element is e, N a normal subgroup of G (i.e., $N \triangleleft G$) and H a subgroup of G. Then the following statements are equivalent:*
(i) $G = NH$ and $N \cap H = \{e\}$.
(ii) $G = HN$ and $H \cap N = \{e\}$.
(iii) Every element of G can be written in a unique way as a product of an element of N and an element of H.
(iv) Every element of G can be written in a unique way as a product of an element of H and an element of N.
(v) The natural embedding $H \to G$, composed with the natural projection $G \to G/N$, yields an isomorphism between H and the quotient group G/N.
(vi) There exists a homomorphism $G \to H$ which is the identity on H and whose kernel is N.
(vii) The group G is the semidirect product $G = N \rtimes H$.

We will prove that statement (vi) is true for $\mathcal{G}_{ms}$ then the right- and left-hand factorizations are statements (iii) and (iv). First of all we need to prove that $N = \mathbf{SO}(3)$ is a normal subgroup of $\mathcal{G}_{ms}$, that is, we need to prove that for all $\mathbf{g} \in \mathcal{G}_{ms}$, we have $\mathbf{g}N\mathbf{g}^{-1} \subset N$. Let $\mathbf{n}$ an element of $\mathbf{SO}(3)$ and let $\mathbf{g} \in \mathcal{G}_{ms}$, then we need to prove that for all $\mathbf{n}$, $\mathbf{g}\mathbf{n}\mathbf{g}^{-1} \in \mathbf{SO}(3)$. From the definition of the microstretch group $\mathcal{G}_{ms}$:

$$\mathbf{g}^T\mathbf{g} = \mathbf{g}\mathbf{g}^T = k\mathbf{1} \Rightarrow \quad \det(\mathbf{g})^2 = k > 0, \text{ and } \mathbf{g}^{-1} = \mathbf{g}^T/\det(\mathbf{g})^2$$

Now, we compute the transpose and the inverse of $\mathbf{g}\mathbf{n}\mathbf{g}^{-1}$:

$$(\mathbf{g}\mathbf{n}\mathbf{g}^{-1})^{-1} = (\mathbf{g}^{-1})^{-1}\mathbf{n}^{-1}\mathbf{g}^{-1} = \mathbf{g}\mathbf{n}^T\mathbf{g}^{-1}$$
$$(\mathbf{g}\mathbf{n}\mathbf{g}^{-1})^T = (\mathbf{g}^{-1})^T\mathbf{n}^T\mathbf{g}^T = (\mathbf{g}^T/\det(\mathbf{g})^2)^T\mathbf{n}^T(\mathbf{g}^{-1}\det(\mathbf{g})^2) = \mathbf{g}\mathbf{n}^T\mathbf{g}^{-1}$$

Then we have proved that $(\mathbf{g}\mathbf{n}\mathbf{g}^{-1})^{-1} = (\mathbf{g}\mathbf{n}\mathbf{g}^{-1})^T$ with $\det\mathbf{g} > 0$ and, therefore, $\mathbf{g}\mathbf{n}\mathbf{g}^{-1} \in \mathbf{SO}(3)$, then $\mathbf{SO}(3)$ is a normal subgroup of $\mathcal{G}_{ms}$. Now we consider the

homomorphism $h : \mathcal{G}_{ms} \to H$, defined by $\mathbf{g} \mapsto h(\mathbf{g}) = \det(\mathbf{g})\mathbf{1}$ where

$$H = \{\mathbf{A} \in \mathbf{GL}(3)| \ \mathbf{A} = a\mathbf{1}, a > 0\} \tag{4.29}$$

The ker $h = N = \mathbf{SO}(3)$. This proves (vi) and we thus have as consequences (iii), (iv) and (vii) [and the other statements]. This implies we can represent every element of the group $\mathcal{G}_{ms}$ as a pair $(\mathbf{R}, j) \in \mathbf{SO}(3) \times \mathbb{R}^+$ with the operation group:

$$(\mathbf{R}_1, j_1) \circ (\mathbf{R}_2, j_2) = (\mathbf{R}_1\mathbf{R}_2, j_1 j_2) \tag{4.30}$$

Obviously, the morphism $h_{iso} : \mathbf{SO}(3) \times \mathbb{R}^+ \to \mathcal{G}_{ms}$ defined by $(\mathbf{R}, j) \mapsto (j\mathbf{1})\mathbf{R}$ is an isomorphism. This is a formal proof that allows to say that for a microstretch continuum in $\mathbb{R}^3$ the need can use as degrees of freedom $(\boldsymbol{u}, \mathbf{R}, j)$, a vector field, an $\mathbf{SO}(3)$-valued field, and a scalar field. This was informally stated by some authors see table 2.2, but to the best of my knowledge no formal proof had been published.

4.3   Simulation of esophageal perforation

4.3.1   Software used and geometry

This section summarizes some characteristics of the analysis of the mechanical behavior of esophagus using the *Finite Element Method* (FEM) to solve the equations that describe completely the problems of forced dilatation. As it can be deduced from the previous chapters and sections, the quantitative and numerical investigation of the mechanical behavior of esophagus during forced dilatation treatments requires a non-linear analysis of soft tissue. Being time-dependent problems, it is necessary to perform time-dependent analyses, although as it has been discussed that the viscoelastic effects in practice are not important given the time scale and the characteristics of the treatments.

To perform numerical simulations with FEM, it is required a software code with the adequate characteristics. A software than can be used for simulating the classical constitutive models is the software LS-DYNA created by Livermore Software Technology Corp. - LSTC. This software has been extensively used for biomechanical analyses of crash accidents and other interesting biomechanical

problems. Regarding the type of algorithm for integrating in time, LS-DYNA allows us to perform both types of analyses: implicit analyses (with convergence to an equilibrium state in each computation step) and explicit analyses (this result for the studied cases a saving of time, because has a shorter time of computation and require less adjustments). All tests showed that the results for explicit analyses were acceptable and for this reason it has been the preferred type of analysis. For the classical constitutive models LS-DYNA fulfills all the requirements. For the microcontinuum models, no widely commercial software implement all the requeriments. Some authors have developed their own codes for simulation [42, 95].

X-ray computed tomography (CT) data were used for the creation of a reliable geometry. Most of the software available generates images and three-dimensional reconstructions adequate for the visualization but not for the generation of a useful FE model. For this reason, a lot of additional work is needed in order to convert the CT data in a geometry suitable for FE computations. This additional work involves the creation of external surfaces with a software that allows non-parametric edition for surfaces was used. This means that the surfaces do not correspond to geometrical conditions controlled by specific values and thus, heuristic manipulation is allowed to obtain well defined surfaces representing adequately the biological organs. The used software codes are mainly Blender (developed by the Blender Foundation, first release 1995, last version 2.68 / July 18, 2013) y Zbrush (developed by Pixologic Inc). Although these codes were not specifically developed for biomedical image processing, they proved to be very useful for the generation of geometries from CT data. Other software codes such as Catia or Solidworks proved to be less useful for generating adequate surfaces.

4.3.2 Rigid dilator simulation

These simulations reproduce the effect of semi-flexible rod commonly used for esophageal dilatation. For this simulation a complete geometry of esophagus created form CT data is used. This complete geometry will reproduce the effect of the actual curvature disposition of the esophagus inside the body. The semi-flexible rod has a length of 429 mm and a diameter of 9 mm. Some additional, simulations with diameter 15 mm were performed, nevertheless, a hight rate of premature perforation was observed.

The boundary conditions are null displacement for the proximal and distal

Figure 4.25. The geometries used for the human esophagus (in red) and the semil-flexibe rod used as a dilator (in green).

end rings and unilateral boundary condition of place for simulating the contact between the rod and the inner surfaces of mucosa layer[1]. The motion of the rod is completely prescribed with time and the necessary force for overcoming resistance of esophageal tissue is computed. Figure illustrates the evolution of stress in time.
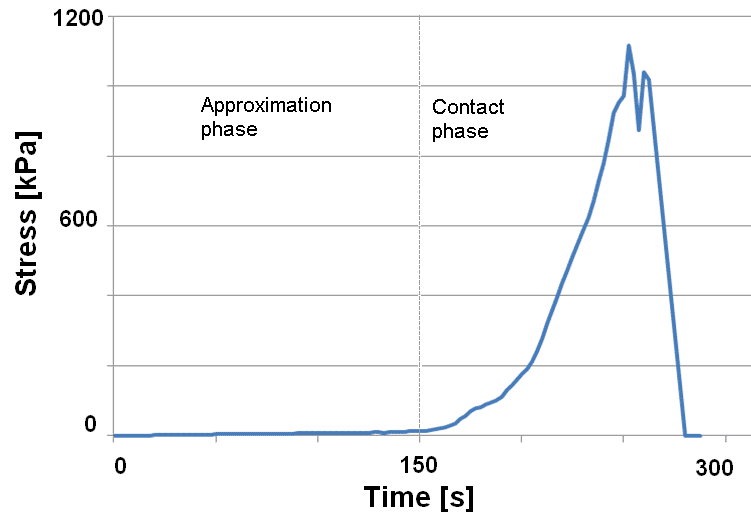
Figure 4.26. Maximum first principal stress induced by the semi-flexible dilator on the esophagus according to the simulation.

The condition of tearing/perforation is defined when the principal stress over-comes a fixed stress threshold (probably this is the least realistic detail of the simulations and genuinely microcontinuum constitutive models can be helpful). The three following images show the predicted type of cleavage of this elasto-tearing model. It is interesting to note that in a number of cases the tearing is produced outside the contact area; it suggests that the tearing mechanism is not mainly due to pressure associated with dilatation.

---

[1]Unilateral boundary condition of place is explained in detail in Ciarlet (1988) [16, p.207]

Figure 4.27. Area of tearing/ripping for the semi-flexible rod dilator: *Right* For a 15 mm dilator the most frequent tearing mode is one in which the contact area with the tip of the dilator is critical, *Left* For a 9 mm dilator frequently the critical area is not that where the dilator exerts greater pressure.

4.3.3 Balloon catheter simulation

Another common procedure for forced dilatation is to introduce a balloon catheter, *i.e.* a catheter provided with an inflatable part. The expansion of the inflatable part presses against the esophageal wall producing the tearing of some fibers and a greater lumen. This simulation uses the airbag system implemented in LS-Dyna code. In this case, the whole geometry is formed only by a small piece of tubular esophagus, containing the stenotic narrowing (figure 4.28 shows the geometry used in this case).

4.4 Published articles on mechanical properties of esophageal tissue

Some of the results explained in this dissertation were published in an article in *Annals of Biomedical Engineering*: "A micro-continuum model for mechanical properties of esophageal tissue: experimental data and constitutive analysis" [99]. The first part of the paper deals with the experimental methodology here explained. The second part proposes a micropolar elasticity constitutive model. The paper used data of the available of swine samples. The article is included at the end of this document.
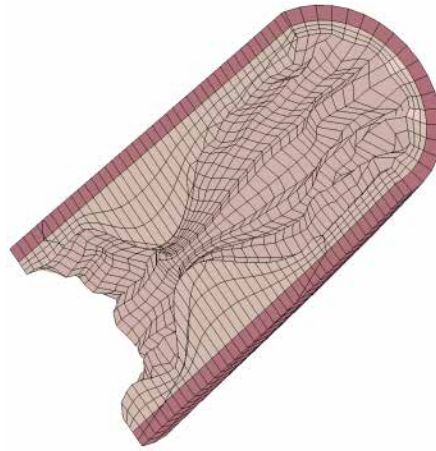
Figure 4.28. A virtual stenosis used for simulating the effect of a balloon catheter. The exterior part represents the muscularis externa layer and the muscular parameters are assigned to the material properties of that part, the internal part is the mucosa-submucosa layer (with the corresponding mechanical properties assigned).
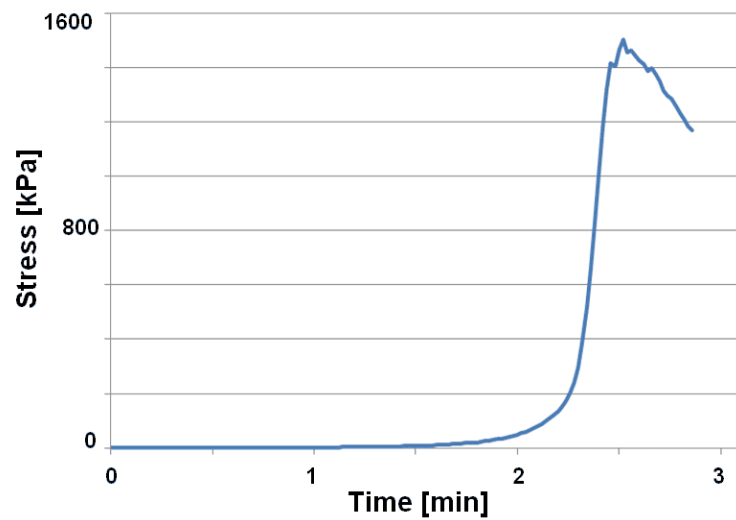
Figure 4.29. Maximum first principal stress induced by the balloon catheter on the esophagus according to the simulation.

4.5 The proposed model

This section proposes a new constitutive model. In many aspect the model is similar to that found in the literature but there are a number of key innovations, conceptually important:

- The **functional form of the "exponential terms"** are introduced in the form suggested by expression 4.17. This form was derived from a model of weakly interacting collagenous fibers using the tools of statistical mechanics. In most proposed models by other authors no other justification is given for the exponential terms, except the empirical adequacy, but this is a theoretically unsatisfactory because there are slightly different forms that adjust the data equally well. For example Lu-Gregersen and Yang-Deng models contain exponential terms with different functional forms, although both fit to the data similarly.

- The **anisotropy** of the tissue implies that the material symmetry group is a proper subgroup of $\mathbf{O}(3)$. The histological analysis of esophageal tissues found in literature show that both layers of esophagus seem to be formed by fibers mainly directed along two directions [80]. The existence of two privileged directions in tissue also excludes the *transversal isotropic/hemitropic* groups TR_i as possible symmetry groups (see figure 4.30).

- The **helix shape of the collagen fiber** in esophagus (see figure 4.30) introduces a **chiral asymmetry** that excludes the point groups containing reflections as adequate for representing the material symmetry of the esophageal tissue. This observation seems to have been unnoticed by most authors, and no reference to the physical implications has been found in the literature.

- The model includes the requirement of the **covariant constitutive theory** of Marsden and Hughes [72], and the generalizations of Lu [68] for extend this theory to the case with presence of **residual stress**. The computed Riemann metric of section 4.2.2 is incorporated in functional form of the model according to the prescriptions of the Marsden-Hughes-Lu theory.

- The last innovation is the **microcontinuum approach** for representing the micro-structure. The collagenous fibers can rotate be reoriented (3 degrees of freedom) in the tissue and in addition at each point can be stretched (1 degree of freedom). Thus the right type of microcontinuum is clearly a microstretch continuum.

The proposed model is a microstretch orthotropic incompressible hyperelastic constitutive model with large deformations. The material symmetry group is the dihedral group D_{2h} representing the subtype O_3 of orthotropic symmetry
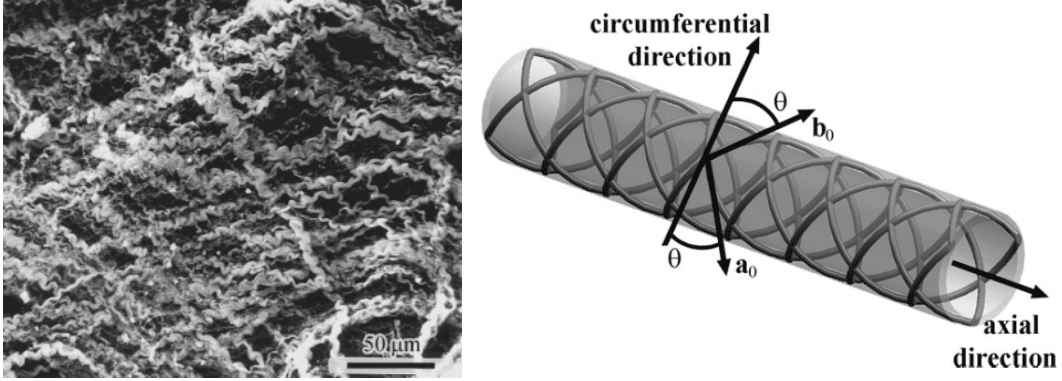
Figure 4.30. Distribution fo collagenous fibers within submucosa: *Left* electron micrograph (after Ottani *et al.* [84]) *Right* schematic fiber arrengement (after Natali *et al.* [80])

(*i.e.* the orthotropic symmetry compatible with chiral asymmetries). In this model the esophagus is consdered as a thick-walled nonlinearly hyperelastic circular cylindrical tube composed by two homogenous layers (mucosa-submucosa and muscularis externa). Each layer is treated as a fiber-reinforced material with the fibers corresponding to the collagenous component of the material and symmetrically disposed with respect to the cylinder axis. The strain energy density function (HEDF) is defined as:

$$\Psi(\mathbf{C}, \mathbf{G}_s, \mathbf{K}, \boldsymbol{\Gamma}) = \Psi_{vol}(J, G) + \bar{\Psi}_{iso}(\bar{\mathbf{C}}, \mathbf{G_s}) + \bar{\Psi}_f(\bar{\mathbf{C}}, \mathbf{G}_s, \mathbf{K}, \boldsymbol{\Gamma}) \qquad (4.31)$$

which is based on the kinematic assumption

$$\mathbf{C} = J^{2/3}\bar{\mathbf{C}}, \quad J = (\det \mathbf{C}), \quad \det \bar{\mathbf{C}} = 1 \qquad (4.32)$$

This initial decomposition similar to the decomposition used in the *Kroon-Holzapfel model* and the *Natali-Gregersen model*. We have include the the microdeformation tensor $\mathbf{K}$ and the wryness tensor $\boldsymbol{\Gamma}$ for accounting the changes in the microstructure and the metric $\mathbf{G}_s$ for accounting for the initial residual stress, being the scalar $G = \det \mathbf{G}_s$. We proceed to explain in detain the three terms $\Psi_{vol}, \bar{\Psi}_{iso}$ and $\bar{\Psi}_f$.

The term $\Psi_{vol}(J, G)$ accounts for the incompressibility of the material. It contributes to the second Piola-Kirchhoff with a term of the form $\mathbf{S} = Jp\mathbf{C}^{-1}$, where $p = (\partial \Psi_{vol}(J, G)/\partial J)$. For this function different functional forms have been proposed by different authors in the absence of residual stress. Ogden

proposed the general form [82]:

$$\Psi_{vol}(J) = \frac{1}{\beta^2}(\beta \ln J + J^{-\beta} - 1) \tag{4.33}$$

The experiments carried out are not sufficient for determining the functional form. Nevertheless, the physical restrictions imply that $\Psi_{vol}(J,G) = \tilde{\Psi}(J/G)$, and that $\tilde{\Psi}(1) = 0, \tilde{\Psi}''(1) \geq 0$. Ciarlet and Geymonat analyzed the general requirement conditions for polyconvexity and proposed a general form [17]:

$$\Psi_{vol}(J) = c(J-1)^2 + d\ln J \tag{4.34}$$

Natali on the base of an empirical study proposed another form (see equation 2.53). In this proposed model we will select a modified form proposed for Ciarlet because it clearly satisfies the physical requirements and can approximate well the other forms, so for practical purposes is a suitable form (further theoretical results and experimentation are needed to solve completely this issue). The selected form including the presence of residual stress:

$$\Psi_{vol}(J,G) = c\left(\frac{J}{G} - 1\right)^2 + d\ln\frac{J}{G} \tag{4.35}$$

For the term $\bar{\Psi}_{iso}(\bar{\mathbf{C}}, \mathbf{G}_s)$ in conventional continuum theories, most authors use a function depending on $(I_1 - 3)$ where $I_1 = \operatorname{tr} \bar{\mathbf{C}}$. The term is numerically important only for low strain. For this reason we here follow the proposal of Holzapfel and will adopt a simple linear functional form:

$$\bar{\Psi}_{iso}(\bar{\mathbf{C}}, \mathbf{G}_s) = \mu(\tilde{I}_1 - 3) \tag{4.36}$$

where μ is an elastic constant associated to the elastic properties the elastin matrix of collagenous tissues and $\tilde{I}_1 = \operatorname{tr}(\bar{\mathbf{C}}\mathbf{G}_s^{-1})$

The last term is the most important term for moderate and large strains and represents the contribution of collagen fibers and the micro-structure. From the *isotropicization theorem* 2.5.2 it follows that the most general form for this term is $\bar{\Psi}_f(\bar{\mathbf{C}}, \mathbf{G}_s, \mathbf{K}, \mathbf{\Gamma}) = \varphi(\bar{\mathbf{C}}\mathbf{G}_s^{-1}, \mathbf{K}, \mathbf{\Gamma}, \mathbf{M})$ where $\mathbf{M} = \boldsymbol{i} \otimes \boldsymbol{i} - \boldsymbol{j} \otimes \boldsymbol{j}$. Accordingly the equation 4.17 deduced from statistical mechanics we will select the functional

form:

$$\bar{\Psi}_f(\bar{\mathbf{C}}, \mathbf{G}_s, \mathbf{K}, \mathbf{\Gamma}) = -\frac{1}{\beta} \sum_i \ln\left(1 + k_{g,i} e^{-\beta \mathcal{E}_i(\bar{\mathbf{C}}, \mathbf{G}_s, \mathbf{K}, \mathbf{\Gamma})}\right) \tag{4.37}$$

The sum in i is extended over the two families of collagenous fibers, denoted a and b ($i \in \{a, b\}$. The constants $k_{g,i}, \beta$ are the model parameters (or mechanical properties to be determined for each sample). The above equation is similar to the form used in the Kroon-Holzapfel and the Natali-Gregersen models when no microrotation or microdilation is present ($\mathbf{K} = 0, \mathbf{\Gamma} = 0$) and no residual stress is present ($\mathbf{G}_s = \mathbf{I}^\flat$). The problem now is to select the correct form for $\mathcal{E}_i$. Most authors use for $\mathcal{E}_i$ a tensor function which is a quadratic polynomial in the components of $\bar{\mathbf{C}}$ for classical constitutive models [59, 80, 114]. Thus we will use the most general polynomial in the components of $\bar{\mathbf{C}}\mathbf{G}_s^{-1}, \boldsymbol{\gamma}$ which is invariant under the group $O_3 = D_{2h}$. To find such a polynomial is a mathematical problem solvable with the theory of tensor representations developed by Zheng (1994) [118]. Before finding the explicit form, we introduce explicitly the microstretch deformation tensors

$$\begin{aligned}
K_{AB} &= (2j - 1)\delta_{AB}, & \Gamma_{ABC} &= \delta_{AB}\Gamma_C - \epsilon_{ABD}\Gamma_{DC} \\
\Gamma_{AB} &= \gamma_{ab}\delta_A^a \delta_B^b, & \Gamma_A &= 3j_{|a}\delta_A^a \\
\gamma_{ab} &= \phi_{a|b}
\end{aligned} \tag{4.38}$$

The covector $\boldsymbol{\phi} = (\phi_1, \phi_2, \phi_3)$ and the scalar j are the additional four degrees of freedom for a microstretch continuum. The covector $\boldsymbol{\phi}$ represent the reorientation in space of the dominant direction of collagen fibers at a point and j is the microdilation. With these definitions, the two scalar tensor polynomials $\mathcal{E}_a$ and $\mathcal{E}_b$ are:

$$\begin{aligned}
\mathcal{E}_a &= I_{4a} + \sum_{k=1}^2 \lambda_k I_{k,\phi}, & \mathcal{E}_b &= I_{4b} + \sum_{k=1}^2 \lambda_k I_{k,\phi} \\
I_{4a} &= a^A \bar{C}_{AB} G_s^{BC} a_C & I_{4b} &= b^A \bar{C}_{AB} G_s^{BC} b_C \\
I_{1,\phi} &= \frac{j^2}{2}\gamma_{a|a}^2 & I_{1,\phi} &= \frac{j^2}{2}\gamma_{a|b}\gamma_{b|a}
\end{aligned} \tag{4.39}$$

The final functional form $\Psi(\mathbf{C}, \mathbf{G}_s, \mathbf{K}, \mathbf{\Gamma})$ is a combination of invariants of the orthotropic group $O_3 = D_{2h}$, the constants $k_{g,a}, k_{g,b}, \beta, \lambda_1, \lambda_2$ are the model parameters (or mechanical properties to be determined for each sample). The dependence in the microstretch, through $I_{1,\phi}$ and $I_{1,\phi}$, part was selected according to the findings in the published article about this microcontinuum models for soft tissue [99]. An additional term $I_{3,\phi} = j_{|a}\gamma_{a|b}\gamma_{b|c}j_{|c}$ could be included but it needs to be investigated if it is empirically adequate.

The relation between strain and stress can be derived from equations 2.35. For the first Piola-Kirchhoff stress tensor we have:

$$\mathbf{P} = \mathbf{P}_{vol} + \mathbf{P}_{iso} + \mathbf{P}_f \tag{4.40}$$

where $\mathbf{P}_{vol}, \mathbf{P}_{iso}$ and $\mathbf{P}_f$ can be derived from the functional forms for $\Psi_{vol}(J, G)$, $\bar{\Psi}_{iso}(\bar{\mathbf{C}}, \mathbf{G_s})$ and $\bar{\Psi}_f(\bar{\mathbf{C}}, \mathbf{G}_s, \mathbf{K}, \mathbf{\Gamma})$. This three parts has clear physical meanings:

- The first part is $\mathbf{P}_{vol} = p\mathbf{F}^{-T}$ and represents the effect due the water in the tissue that makes it virtually incomprehensible.

- The second $\mathbf{P}_{iso}$ represents the effect elastin matrix and it is only important for small strain and does not contribute to the anisotropy in the tissue.

- The third part $\mathbf{P}_f$ represents the effect of the collagen fibers. It characterizes the anisotropy of the tissue and contains the effect of the micro-stucture associated with the local stretching of collagen fibers or its reorientation inside the tissue.

The couple stresses and the micropresure due to the micro-structure can be found form equation 2.79. For the scalar micropressure s (energy conjugate of the microdilation j), we have:

$$
\begin{aligned}
s - \sigma_a^a &= 3\rho j \frac{\partial \Psi_f}{\partial j} \\
&= 3\rho j^2 \sum_i \left(\frac{k_{g,i} e^{-\beta \mathcal{E}_i}}{1 + k_{g,i} e^{-\beta \mathcal{E}_i}} \right) \left[\lambda_1 (\phi_{|a}^a)^2 + \lambda_2 \phi_{|b}^a \phi_{|a}^b \right]
\end{aligned} \tag{4.41}
$$

For couple stress tensor $m^{abc} = m^a \delta^{bc}/3 - \epsilon^{bcd} m_{ad}/2$, we derive Ψ_f with respect to $j_{|a}$ and γ_{ab}:

$$
\begin{aligned}
m_a &= 3\rho \frac{\partial \Psi_f}{\partial j_{|a}} = 0 \\
m^{ab} &= \rho \frac{\partial \Psi_f}{\partial \gamma_{ab}} = \frac{\rho j^2}{2} \sum_i \left(\frac{k_{g,i} e^{-\beta \mathcal{E}_i}}{1 + k_{g,i} e^{-\beta \mathcal{E}_i}} \right) \left[\lambda_1 \delta^{ab} + \lambda^2 (\phi^{a|b} + \phi^{b|a}) \right]
\end{aligned} \tag{4.42}
$$

5

Conclusions

5.1   Introduction

In this research the mechanical behavior of human esophagus has been examined. Experimental and numerical work have been carried out. In addition, some theoretical questions have been addressed and solved. The experimental tests of the elastic behavior included uniaxial tensile tests and inflation tests. The theoretical results include an analysis of residual stresses and a theoretical justification of the occurrence of "exponential laws" in soft tissue. These two features are incorporated in the final proposed constitutive model.

The experimental work has confirmed the expected *non-linear* and *anisotropic behavior* of soft-tissue. The tensile tests allowed to obtain parameters that characterize the mechanical behavior (elastic constants, strain and stress before the detectable breaking of collagenous fibrils). The results were compared with anthropometric variables (age, body mass index, gender) and some significant correlations were found with these variables. For example the body mass index seems contribute moderately to the elastic resistance by increasing the before-fiber-

breaking strain ($p < 0,05$) [also an increase in the before-fiber-breaking stress, but it is no so significant]. The effect of age seems to be to stiffen the wall (a positive correlation has been found), but effect is not significant for the set of examined samples. The statistical tests also confirm that the mechanical properties are significantly different for the transversal and the longitudinal directions.

The value of the mechanical properties for porcine esophageal tissue is similar to the values found in the literature (for swine esophageal tissue, [45,69,114,115]). The typical values of mechanical properties for human esophagus have been determined for different models from the experimental data (this involved extensive numerical computations to find the best fit). Less accurate data are available in the literature for human esophageal tissue and no adequate data were found for an extensive comparison. Nevertheless, a characterization of the range of the variation of some mechanical properties for human esophageal tissue has been obtained (these data are new and, therefore, it is planned to publish them because of its interest). Although the testing only involved esophageal tissue from donors with with no severe digestive diseases, the obtained values for the mechanical properties are a point of departure, they can be used in numerical simulations involving abnormal conditions such as stenosis or achalasia as a first approximation. Interestingly, the inflation tests showed that bleeding occurs at relatively low strains compared with the failure strain, thus the medical complications can arise without perforation of the wall.

The hypothesis that microcontinuum theories can be useful for soft tissue has been confirmed. Some of the typical characteristics of the stress-strain curves can be derived on the basis of assuming the influence of micro-structure, part of the research concerning the influence of micro-structure was published in *Annals of Biomedical Engineering* that explains this in detail.

Some numerical simulations have been carried out, showing that the failure can arise outside the zone of contact of the dilator and the esophagus wall. This suggests that pressure detectors on the detector can not predict the failure in the absence of a complete mechanical model. Some examples in the scientific literature show that computational models can improve medical procedures and treatments [23, 103]. Thus, the characterization of esophageal tissue of mechanical properties can be used for predicting the likely results of forced dilatation procedure when combined with finite element (FE) computations [23, 98]. The results of this study provide a computational model that is likely to have a similar

impact.

For the problem of residual stresses, the data in the literature were used for improve the law that governs their distribution along the esophageal wall. In particular, the tools of Riemann geometry were applied to the existent data suggesting that the residual stress is distributed according a non-linear law (some previous proposal in the literature used a linear law that is only an approximation to the real distribution).

5.2 Contributions

This dissertation contains the following original contributions:

- **Experimental methodology** A new and simple experimental methodology has been developed, and many practical problems were solved in an original way. Comparable values to that of the literature for many mechanical properties were obtained with the new methodology.The main experimental innovations are in the preparation of samples and measurement of some critical magnitudes of samples.

- **Range of variation of mechanical properties** The range variation of elastic properties (for different conventional models) has been determined for a good number of human samples ($n > 25$). The analytical form of the obtained data, as a parameters in models, makes these obtained data suitable for simulation (some studies for human esophagus in literature are limited to numerical values, and do not provide a complete constitutive model). In addition, other anelastic properties constants were determined.

- **Influence of BMI and other anthropometric variables** The mechanical properties found for the set of samples were analyzed statistically. A significant effect of the body mass index (BMI) has been found for the maximum attainable strain before detectable fibril breaking. Although the amount of the total variance explained by BMI is small $r = 0.469$ (being other factors unidentifiable factors important), the effect of BMI is clearly significant, as was established in the regression analysis.

- **Influence of micro-structure** This dissertation includes one of the firsts applications of microcontinuum theory for investigating the mechanical properties of soft tissues.

- **Simulations of forced dilations**. Numerical simulations of the esophageal wall for two different dilatation procedures were carried out. Interestingly, some simulations suggested the occurrence of the mechanical failure at locations strictly outside the area of contact of dilator and the esophageal (this is not a general result, it is only a suggestive finding).

- **A new non-linear model of residual stress**. The existence of residual stress in esophageal wall is a well established fact. Some authors had proposed a linear distribution for accounting that is appropriate for practical purposes, a more geometrical analysis in this dissertation suggested that the true distribution is non-linear (the previously proposed linear laws are only a good approximation to the non-linear distribution found here).

- **Theoretical justification of exponential laws for soft tissue**. An original deduction using statistical mechanics was developed for modeling a large collection of collagenous fiber that interact weakly. This model established a precise functional form according to the hypothesis of the model. Many proposed models exhibit a functional form that approximate to the functional form predicted by our model.

- **A constitutive model is proposed** A new constitutive model is proposed which incorporates exponential terms in a theoretically justified way. The residual stresses are introduced in a geometrical way. The group of symmetry of fiber disposition was investigated and incorporated in the functional form. In addition, additional terms accounting for the micro-structure of the tissue are added to the model in a consistent way according to the symmetry group.

5.3 Limitations

The main identified limitations of this study are:

- **Great variability**. Mechanical properties show a great variation in the

samples. The reasons are twofold, part of this variation is due to experimental uncontrollable conditions. On the other hand, each individual has his own genetic endowment; some unseen factors related to the clinical history of each individual may also explain part of the variation. In the present study it is unknown which part of the observed variation is due to each of these factors. For this reason, only a probabilistic analysis is possible.

- **In vivo vs. in vitro differences**. All esophagi have been maintained for a short time at a low temperature and in contact with saline solution after their extraction. But it is known that *in vivo* position the esophagi are subject to residual stress even in the absence of exterior loads that in part are lost *in vitro* condition. This is particularly clear by the fact that the *in vivo* normal position the esophagus is a tube with the inner part subject to slight compression and its outer part subject to slight traction.

- **Dynamic testing/Viscosity**. The proposed model is valid for low deformation rate $\dot{\varepsilon} < 10^{-2}$, although in practice for the forced dilations this is not a serious limitation. The scope of this research was limited to forced dilatations for this reason viscoelastic effects were negligible. For broader applications the consideration of viscoelastic effects would be of some interest.

- **Other simplifications**. For the fitting of parameters some geometrical simplifications have been done, for example in computations only the average thickness is considered. No biaxial testing has been performed to determine independently the influence of the first and the second algebraic invariants, as in the classical experiments of Treolar [104] and Rivlin and Saunder [92].

- **Restricted scope**. All human samples examined in this work are from previously healthy patients which did not present any severe digestive disease. The present research does not allow to make any statement about the differences between normal and abnormal conditions in esophageal tissues. It would be interesting in future work to systematically investigate abonormal conditions.

- **Dissected parts**. This research has not examined regional differences inside distal or proximal parts. It has been detected that the distal part show a slightly thicker walls. But the variation along the esophagus is not

well know for the sample, except for the distinction between distal/proximal parts. A systematic study considering independently the differente layers of esophageal wall would be desirable.

- **Growing**. The effect of growing and its characterization for esophageal wall is important in patients subject to successive medical procedures of dilatation. It is expected that a first medical treatment could modify locally the properties of the tissue.

5.4 Future work

Almost every limitation cited in previous section is a potentially fruitful area of future research. Some other additional factors that are not limitations of the present research deserve systematic research for themselves. There is a certain number of obvious extensions and generalizations of this research that are interesting for future work:

Tearing models, acoustic emission and the Extreme Value Theory. When tensile tests were conducted, acoustic emission sensors were attached to the tissue, and measures of fiber break were obtained. This procedure allowed to obtain detailed information about fiber breaking. A fiber breaking is a micromechanical phenomenon and has no macroscopic observable effect. It was observed that when a great amount of fiber breakings concentrated in a region some seconds after these breakings a cleavage appeared in the soft tissue. This evidence supply some basis for formulating a model for the ripping/tearing of soft tissue. For this purpose, the implications of the Extreme Value Theory (EVT) need to be investigated. Precisely the EVT emerged from the pioneering work of L. H. C. Tippet[1]. Tippet was interested in predicting the breaking of textiles, then he observed that the effect of the "weakest thread" was determinant in the strength of tissues. In collaboration with R. A. Fisher, Tippett published the first important result in EVT [35]; the Fisher–Tippett distribution is named after them. Later this EVT result was generalized by E. Gumbel (1935) [48] and B. V. Gnedenko [41], the main result of EVT is the useful Fisher–Tippett–Gnedenko theorem (summarized in A.4). The implications of the EVT for tissue tearing, given the evidence of the

---

[1]L. H. C. Tippet worked at the Shirley Institute an institution, established in 1920, this intstitutition depended on the the British Cotton Industry Research Association

acoustic emission, are clear (currently EVT is regularly applied to assess risk of earthquakes, tsunamis, hydrological risk and situations were extreme values are involved, but the theory started with problems not dissimilar to the tearing of a soft tissue).

Pathological conditions in esophagus. Many of the forced dilations procedures are conducted in patients with some pathological conditions. In some of these pathologies, the tissue is expected to have altered mechanical properties at some points. It would be interesting to investigate systematically the mechanical differences between the the normal and abnormal conditions, from the point of view of the mechanical properties.

A

Appendix: Functional analysis and Lie Groups

Since differential calculus in normed vector spaces are widely used in this dissertation, in this appendix some basic results concerning differential mappings are reviewed. These results are needed for the mathematical formulation of part of this dissertation.

A.1   Fréchet derivative

In this section, all vector spaces considered are real. This section reproduces some results on Fréchet derivatives. The approach is based mainly in Ciarlet [16], but for a more detailed accounts, one can consult Avez [4], Cartan [11] and Schwartz [96]. Given two normed vector spaces X and Y, let

$$\mathscr{L}(X;Y), \quad \text{or simply } \mathscr{L}(X) \text{ if } X = Y, \tag{A.1}$$

denote the vector space formed by all continuous linear mappings $A : X \to Y$. Equipped with the norm

$$\|A\| := \sup_{x \in X, x \neq 0} \frac{\|Ax\|_Y}{\|x\|_X} \tag{A.2}$$

the space $\mathscr{L}(X; Y)$ becomes itself a normed vector space, which is complete if the space Y is complete. If $X = Y = \mathbb{R}^n$, an element $\mathbf{A} \in \mathscr{L}(\mathbb{R}^n; \mathbb{R}^n)$ is identified with the matrix that represents it (in a certain base), and if both spaces are equipped with the Euclidean vector norm $|\cdot|$, the associated norm of the matrix $\mathbf{A}$ is the *spectral norm*, also denoted $|\cdot|$. When $Y = \mathbb{R}$, the space

$$X' := \mathscr{L}(X; \mathbb{R}) \tag{A.3}$$

is called the topological **dual space** of the space X. For notational brevity, let us agree that whenever the notation

$$f : \Omega \subset X \to Y \tag{A.4}$$

is used in this section, it means that X and Y are normed vector spaces (whose norms are denoted by the same symbol $\|\cdot\|$ whenever no confusion should arise), that Ω is an open subset of the space X, and that f is a mapping defined on the set Ω, with values in the space Y. A mapping $f : \Omega \subset X \to Y$ is **differentiable** *at a point* $a \in \Omega$ if there exists an element $f'(a)$ of the space $\mathscr{L}(X; Y)$ such that

$$\boxed{f(a + h) = f(a) + f'(a)h + o(h)} \tag{A.5}$$

where the notation $o(h)$ means that

$$o(h) = \|h\|\epsilon(h) \qquad \text{with } \lim_{h \to 0} \epsilon(h) = 0 \text{ in } Y. \tag{A.6}$$

Of course, only points $(a + h)$ that belong to the set Ω should be considered in the above relation; since the set Ω is open by assumption, the set of admissible vectors h contains a ball centered at the origin in the space X. If a mapping

f is differentiable at $a \in \Omega$, it is easy seen that f is continuous at a and that the element $f'(a) \in \mathscr{L}(X;Y)$ is called the **Fréchet derivative**, or simply the **derivative**, of the mapping f at the point a. If $X = \mathbb{R}$ and x denotes the generic point of $\mathbb{R}$, the derivative is also noted:

$$f'(a) = \frac{\mathrm{d}f(a)}{\mathrm{d}x}. \tag{A.7}$$

If a mapping $f : \Omega \subset X \to Y$ is differentiable at all points of the open set Ω, it is be *differentiable in* Ω. If the mapping

$$f' : x \in \Omega \subset X \to f'(x) \in \mathscr{L}(X;Y), \tag{A.8}$$

which is well defined in this case, is continuous, the mapping f is said to be *continuously differentiable in* Ω or simply of class $\mathscr{C}^1$. We denote by

$$\mathscr{C}^1(\Omega;Y), \text{ or simply } \mathscr{C}^1(\Omega) \text{ if } Y = \mathbb{R}, \tag{A.9}$$

the space of all continuously differentiable mappings from Ω into Y. Consider for example an *affine continuous mapping*

$$f : x \in X \to f(x) = Ax + b \text{ with } A \in \mathscr{L}(X;Y) \text{ and } b \in Y. \tag{A.10}$$

Since $f(a + h) = f(a) + Ah$ for all $a, h \in X$, such a mapping is continuously differentiable in X, with $f'(x) = A$ for all $x \in \Omega$, i.e., the mapping f' is constant in this case. Conversely it can be shown (using the mean value theorem) that, if $f'(x) = A \in \mathscr{L}(X;Y)$ for all $x \in \Omega$ and if in addition the open set Ω is *connected*, there exists a vector $b \in Y$ such that $f(x) = Ax + b$ for all $x \in \Omega$.

If the space Y is a product $Y = Y_1 \times \cdots \times Y_m$ of the normed vector spaces Y_i, a mapping $f : \Omega \subset X \to Y$ is defined by *m component mappings* $f_i : \Omega \subset X \to Y_i$, and it is easily seen that the mapping f differentiable at a point if and only if each mapping f_i is differentiable at the same point. In this case, the derivative $f'(a) \in \mathscr{L}(X;Y)$ can be identified with the element $(f'_1(a), \ldots, f'_n(a))$ of the product space $\mathscr{L}(X;Y_1) \times \cdots \times \mathscr{L}(X;Y_m)$.

Consider next the case where the space X is a product $X = X_1 \times \cdots \times X_n$ of vector spaces. Given a point $a = (a_1, \ldots, a_n)$ of an open subset Ω of the space X, there exists for each j and open set subject Ω_j of the space X_j containing the point a_j such that the open set $\Omega = \Omega_1 \times \cdots \times \Omega_n$ is contained Ω. If for some index j the *partial mapping*:

$$f(a_1, \ldots, a_{j-1}, \cdot, a_{j+1}, \ldots, a_n) : \Omega_j \subset X_j \to Y \tag{A.11}$$

is differentiable at the point $a_j \in \Omega_j$, its derivative

$$\partial_j f(a) \in \mathscr{L}(X_j; Y) \tag{A.12}$$

is called the jth **partial derivative** of the mapping f at the point a. If x_j denotes a generic point of the space X_j, the partial derivatives are also noted:

$$\partial_j f(a) = \frac{\partial f(a)}{\partial x_j}. \tag{A.13}$$

Remark. The notation $\partial f/\partial \mathbf{A}$ is also used in a different setting, to denote ∎.

If a mapping $f : \Omega \subset X = X_1 \times \cdots \times X_n$ is differentiable ate a point $a \in \Omega$, it is easy to see that the n partial derivatives $\partial_j f(a)$ exist and that

$$f'(a)h = \sum_{j=1}^{n} \partial_j f(a)h_j \quad \text{for all } h = (h_1, \ldots, h_n) \in X_1 \times \cdots \times X_n \tag{A.14}$$

Using the mean value theorem, it can be shown that *conversely, if the partial derivatives are defined and continous on Ω, the equivalence*:

$$f \in \mathscr{C}^1(\Omega; Y) \Leftrightarrow \partial_j f \in \mathscr{C}^0(\Omega; \mathscr{L}(X_j; Y)), \ 1 \le j \le n \tag{A.15}$$

holds, where $\mathscr{C}^0(E; F)$ denotes in general the set of all continuous mappings from a topological space E into a topological space F. Let X_1, X_2, Y be normed vector spaces. A mapping $B : X_1 \times X_2 \to Y$ is *bilinear* if it satisfies

$$B(\alpha_1 x_1 + \alpha_1' x_1', x_2) = \alpha_1 B(x_1, x_2) + \alpha_1' B(x_1', x_2),$$
$$B(x_1, \alpha_2 x_2 + \alpha_2' x_2') = \alpha_2 B(x_1, x_2) + \alpha_2' B(x_1, x_2') \tag{A.16}$$

for all $x_1, x_1' \in X_1, x_2, x_2' \in X_2, \alpha_1, \alpha_1', \alpha_2, \alpha_2' \in \mathbb{R}$. If it is in addition *continuous*, i.e., if and only if

$$\|B\| := \sup_{\substack{(x_1, x_2) \in X_1 \times X_2 \\ x_1 \neq 0, x_2 \neq 0}} \frac{\|B(x_1, x_2)\|_Y}{\|x_1\|_{X_1} \|x_2\|_{X_2}} < +\infty \tag{A.17}$$

it is differentiable in the space $X_1 \times X_2$, since (by the bilinearity) $B(a_1 + h_1, a_2 + h_2) = B(a_1, a_2) + B(h_1, a_2) + B(a_1, h_2) + B(h_1, h_2)$, and sice (by continuity)

$$\|B(h_1, h_2)\| \leq \|B\| \|h_1\|_{X_1} \|h_2\|_{X_2} \leq \|B\| (\max\{\|h_1\|_{X_1} \|h_2\|_{X_2}\})^2 \tag{A.18}$$

The derivative and the partial derivatives are thus respectively given by

$$B'(a_1, a_2)(h_1, h_2) = B(h_1, a_2) + B(a_1, h_2),$$
$$\partial_1 B(a_1, a_2)h_1 = B(h_1, a_2), \quad \partial_2 B(a_1, a_2)h_2 = B(a_1, h_2) \tag{A.19}$$

If $X_1 = X_2 = X$, a similar computation shows that the mapping $f : x \in X \to B(x, x) \in Y$ is also differentiable, with $f'(a)h = B(a, h) + B(h, a)$ for all $a, h \in X$ If in addition the bilinear mapping: $B : X \times X \to Y$ is *symmetric*, i.e., the vectors

$$f'(a)h = \lim_{\theta \to 0} \frac{f(a + \theta h) - f(a)}{\theta} = \frac{\mathrm{d}}{\mathrm{d}\theta} f(a + \theta h)\Big|_{\theta=0} \in Y \tag{A.20}$$

are computed for arbitrary vectors h of the space X. Such a vector $f'(a)h \in Y$ is called a **directional derivative**, or a **Gâteaux derivative**, *in the direction of the vector h.*

In varius instances, like that shown in the following section, the mapping to be differentiated is itself composed of simpler mappings whose derivatives are

known. In this case, the following result is particularly useful:

Proposition A.1.1. *Let X, Y and Z be normed vector spaces, let U and V be open subsets of the spaces X and Y respectively, let $f : U \subset X \to V \subset Y$ be a mapping differentiable at a point $a \in U$ and let $g : V \subset Y \to Z$ be a mapping differentiable at the point $f(a) \in V$. Then the composite mapping $g \circ f : U \subset X \to Z$ is differentibable at the point $a \in U$ and:*

$$\boxed{(g \circ f)'(a) = g'(f(a))f'(a)}$$

A.2   Algebraic invariant and its derivatives

Constitutive models are formulated in terms of an scalar function (SEDF/HEDF) of the algebraic invariants of a tensor. An algebraic invariant is a polynomial function of the components of the tensor takes the same value in any basis (*i.e.* an invariant combination of tensorial components). The computation of the invariants and its derivatives is needed for computations of stresses and the derivation of stress-strain relations.

A.2.1   Definition of algebraic invariants

Given a (1,1)-tensor $\mathbf{C}$ over $\mathbb{R}^3$ with components C^i_j and eigenvalues λ_i, we define the three main algebraic invariants as:

Definition A.2.1. *The **invariants** of a symmetric matrix $\mathbf{C}$ (in an inner product space or a Riemann manifold) are defined by:*

$$I_1(\mathbf{C}) = \operatorname{tr}(\mathbf{C}), \quad I_2(\mathbf{C}) = \det(\mathbf{C})\operatorname{tr}(\mathbf{C}^{-1}), \quad I_3(\mathbf{C}) = \det(\mathbf{C})$$

The following proposition gives useful explicit expressions in terms of eigenvalues:

Proposition A.2.1. *The invariants of $\mathbf{C}$ are related to the coefficients in the characteristic polynomial $P(\lambda)$ of $\mathbf{C}$ as follows:*

$$P(\lambda) = \lambda^3 - I_1(\mathbf{C})\lambda^2 + I_2(\mathbf{C})\lambda - I_3(\mathbf{C})$$

In therms of the eigenvalues $\lambda_1, \lambda_2, \lambda_3$, we have:

$$I_1(\mathbf{C}) = \lambda_1 + \lambda_2 + \lambda_3, \quad I_2(\mathbf{C}) = \lambda_1\lambda_2 + \lambda_3\lambda_1 + \lambda_2\lambda_3, \quad I_3(\mathbf{C}) = \lambda_1\lambda_2\lambda_3$$

(these are the elementary symmetric functions of $\lambda_1, \lambda_2, \lambda_3$). Moreover, the following formula for I_2 holds:

$$I_2(\mathbf{C}) = \frac{1}{2}[(\operatorname{tr}\mathbf{C})^2 - \operatorname{tr}(\mathbf{C}^2)]$$

For constitutive theory, we have the following key result:

Proposition A.2.2. *The following statements are equivalent:*
(a) A scalar function f of $\mathbf{C}$ is invariant under orthogonal transformations.
(b) f is a function of the invariants of $\mathbf{C}$.
(c) f is a symmetric function of the principal eigenvalues of $\mathbf{C}$.

For anisotropic materials the following additional partial "invariants" are needed:

These partial "invariants" are not invariants under the action of any change of basis. Unlike true invariants, that are invariant under any action of the rotation group $\mathbf{SO}(3)$ (indeed, under the action of any element of $\mathbf{GL}(3)$):

$$I_i(\mathbf{C}) = I_i(\mathbf{Q}\mathbf{C}\mathbf{Q}^T), \qquad \forall \mathbf{Q} \in \mathbf{SO}(3) \tag{A.21}$$

the partial invariants are invariant only under the action of a subgroup $\mathcal{G} \subset \mathbf{SO}(3)$, *i.e.* the above equation are valid only for $\mathbf{Q} \in \mathcal{G}$

A.2.2 Derivatives of algebraic invariants

The interest of **derivatives of invariants** is that in constitutive theory one has expression of the type:

$$\mathbf{S} = 2\frac{\partial W}{\partial \mathbf{C}} \tag{A.22}$$

where the las derivative can be computed by using the *chain rule* defined on the previous section:

$$\frac{\partial W}{\partial \mathbf{C}} = \frac{\partial W}{\partial I_1}\frac{\partial I_1}{\partial \mathbf{C}} + \frac{\partial W}{\partial I_2}\frac{\partial I_2}{\partial \mathbf{C}} + \frac{\partial W}{\partial I_3}\frac{\partial I_3}{\partial \mathbf{C}}$$

Derivative of I_1

The mapping $I_1 : \mathbb{M}^n \to \mathbb{R}$ is linear and continuous, it is differentiable over the space real matrices $\mathbb{M}^n = M_{n \times n}(\mathbb{R})$ with:

$$I_1'(\mathbf{A})\mathbf{H} = I_1(\mathbf{H}) = \text{tr}(\mathbf{H}) \tag{A.23}$$

In components:

$$\frac{\partial I_1}{\partial C_j^i} = \frac{\partial C_k^k}{\partial C_j^i} = \delta_i^k \delta_k^j = \delta_i^j \tag{A.24}$$

Thus, $I_1'(\mathbf{A})\mathbf{H} = \delta_i^j H_j^i = H_j^j = \text{tr}(\mathbf{H})$

Derivative of I_3

The mapping $I_3 : \mathbb{M}^3 \to \mathbb{R}$ is a polynomial of degree $n = 3$ with respect to the n^2 elements of the matrix, it is continuously differentiable over the space $\mathbb{M}^3$. If the matrix $\mathbf{A}$ is invertible, we can write:

$$
\begin{aligned}
I_3(\mathbf{A} + \mathbf{H}) \quad &= \det(\mathbf{A} + \mathbf{H}) = \det(\mathbf{A})\det(\mathbf{I} + \mathbf{A}^{-1}\mathbf{H}) \\
&(\det \mathbf{A})(1 + \text{tr}(\mathbf{A}^{-1}\mathbf{H}) + o(\mathbf{H}))
\end{aligned}
$$

the last equality is deduced from the relation

$$\det(\mathbf{I} + \mathbf{E}) = 1 + \text{tr}\mathbf{E} + \{\text{monomials of degree } \geq 2\}$$

which itself follows form the definition of the determinant. We have thus proved that:

$$I_3'(\mathbf{A})\mathbf{H} = \det(\mathbf{A})\text{tr}(\mathbf{A}^{-1}\mathbf{H})\text{tr}\{(\text{Cof } \mathbf{A})^T\mathbf{H}\} \tag{A.25}$$

where the Cof $\mathbf{A}$ is the cofactor matrix. The components of the cofactor matrix is given by Cof $\mathbf{A} := (\det \mathbf{A})\mathbf{A}^{-T}$. This proof is valid, even for $n \geq 3$ with minimal changes we can compute I_n. Using components we have:

$$\frac{\partial I_3}{\partial C_j^i} = I_3(\mathbf{A}^{-T})_i^j \tag{A.26}$$

Derivative of I_2

For the mapping $I_2 : \mathbb{M}^n \to \mathbb{R}$ we will compute the derivative as an application of the chain rule, we compute the derivative of the mapping $\mathbf{A} \mapsto I_2(\mathbf{A}) = \det(\mathbf{A})\mathrm{tr}(\mathbf{A}^{-1})$. We can write $I_2 = I_3 \cdot (I_1 \circ f)$, where $\mathbf{A} \mapsto f(\mathbf{A}) = \mathbf{A}^{-1}$, we obtain:

$$I_2'(\mathbf{A})\mathbf{H} = (I_3'(\mathbf{A})\mathbf{H})(I_1 \circ f)(\mathbf{A}) + I_3(\mathbf{A})I_1'(f(\mathbf{A}))f'(\mathbf{A})\mathbf{H}$$

Since the matrix $(\mathbf{I} + \mathbf{A}^{-1}\mathbf{H})$ is invertible for $\|\mathbf{H}\| < \|\mathbf{A}^{-1}\|^{-1}$, with

$$(\mathbf{I} + \mathbf{A}^{-1}\mathbf{H})^{-1} = \mathbf{I} - \mathbf{A}^{-1}\mathbf{H} + o(\mathbf{H})$$

we can write:

$$\begin{aligned} f(\mathbf{A} + \mathbf{H}) &= (\mathbf{A} + \mathbf{H})^{-1} = (\mathbf{I} + \mathbf{A}^{-1}\mathbf{H})^{-1}\mathbf{A}^{-1} \\ &= \mathbf{A}^{-1} - \mathbf{A}^{-1}\mathbf{H}\mathbf{A}^{-1} + o(\mathbf{H}) \end{aligned}$$

and hence $f'(\mathbf{A})\mathbf{H} = -\mathbf{A}^{-1}\mathbf{H}\mathbf{A}^{-1}$, using the expression of I_1, I_3, we thus obtain:

$$\begin{aligned} I_2'(\mathbf{A})\mathbf{H} &= \det(\mathbf{A})\left[\mathrm{tr}(\mathbf{A}^{-1}\mathbf{H})\mathrm{tr}(\mathbf{A}^{-1}) - \mathrm{tr}(\mathbf{A}^{-1}\mathbf{H}\mathbf{A}^{-1})\right] \\ &= \mathrm{tr}[(\mathrm{Cof}\ \mathbf{A})^T((\mathrm{tr}\mathbf{A}^{-1})\mathbf{I} - \mathbf{A}^{-1})\mathbf{H}] \end{aligned} \tag{A.27}$$

With minimal changes the above derivation is valid of I_{n-1}. A shorter proof in components (not generalizable for $n \geq 2$) is:

$$\begin{aligned} \frac{\partial I_2}{\partial C_j^i} &= \frac{1}{2}\frac{\partial}{\partial C_j^i}(C_k^k C_l^l - C_l^k C_k^l) \\ &= \frac{1}{2}(\delta_i^k \delta_k^j C_l^l + C_k^k \delta_i^l \delta_l^j - C_l^k \delta_i^l \delta_k^j - C_k^l \delta_i^k \delta_l^j) \\ &= \frac{1}{2}(\delta_j^i I_1 + I_1 \delta_j^i - 2C_i^j) = I_1 \delta_i^j - C_i^j \end{aligned} \tag{A.28}$$

The equation A.22 can be rewritten in terms of the derivatives of I_1, I_2 and I_3 as:

$$\mathbf{S} = 2\frac{\partial \Psi(\mathbf{C})}{\partial \mathbf{C}} = 2\left[\left(\frac{\partial \Psi}{\partial I_1} + I_1\frac{\partial \Psi}{\partial I_2}\right)\mathbf{I} - \frac{\partial \Psi}{\partial I_2}\mathbf{C} + I_3\frac{\partial \Psi}{\partial I_2}\mathbf{C}^{-1}\right] \tag{A.29}$$

or in components:

$$S_A^B = 2\frac{\partial \Psi}{\partial C_B^A} = 2\left[\left(\frac{\partial \Psi}{\partial I_1} + I_1\frac{\partial \Psi}{\partial I_2}\right)\delta_A^B - \frac{\partial \Psi}{\partial I_2}C_A^B + \frac{\partial \Psi}{\partial I_3}I_3(C^{-1})_A^B\right] \tag{A.30}$$

A.3   Lie Groups

A rigorous description of the material symmetries of the materials and the description requires the use of symmetry groups. A symmetry group is usually understood as a *Lie group* (a mathematical group that is also a topological space). In addition, the Lie groups are used to describe the effect deformation of the micro-structure as the the action of a Lie group on the appropriate fiber bundle (see section B.8, for a review of fiber bundles; and definition 2.3.8 for the description of the use of Lie groups in the motion of a microcontinuum solid). For these reasons, we will make a brief review of Lie groups and actions of Lie groups on manifolds which are needed for applications in elasticity. For further details on the topics of this section reference [1] can be consulted.

> **Definition A.3.1.** *A finite-dimensional **Lie group** is a smooth manifold $\mathcal{G}$ that is a group and for which the group operations of multiplications, $(\cdot) : \mathcal{G} \times \mathcal{G} \to \mathcal{G}$, $(g,h) \mapsto g \cdot h$, and inversion $()^{-1} : \mathcal{G} \to \mathcal{G}$, $g \mapsto g^{-1}$ are smooth. The identity of the group will be designed by e.*

Most of the well known examples of Lie gropus are defined as matrix groups. Some examples of matrix Lie groups are:

- **General Linear group GL(n).** The group of linear isomorphisms of $\mathbb{R}^n \to \mathbb{R}^n$ (*i.e.*, the group of invertible linear mappings), called General Linear group, is denoted by $\mathbf{GL}(\mathbb{R}^n)$ or $\mathbf{GL}(n)$ which is a Lie group of dimension n^2. It is a smooth manifold, being an open set of $\mathbb{R}^{n^2}$ and the group operations are smooth since the formulas for the product and inverse of matrices are smooth rational functions in the matrix components.

- **Special Linear group SL(n).** The linear mappings with determinant equal to 1, is a subgroup of $\mathbf{GL}(n)$, called Special Linear group, which is denoted by $\mathbf{SL}(\mathbb{R}^n)$ or $\mathbf{SL}(n)$.

- **Orthogonal group O(n).** The set of linear mappings that are isometries $\mathbb{R}^n$ form different subgroup of $\mathbf{GL}(n)$, called Orthogonal linear group, which is denoted by $\mathbf{O}(\mathbb{R}^n)$ or $\mathbf{O}(n)$.

- **Special Orthogonal group SO(n).** The set of rotations in the vector space $\mathbb{R}^n$ are a subgroup of $\mathbf{O}(n)$ and $\mathbf{SL}(n)$, called Special Orthogonal linear group, which is denoted by $\mathbf{SO}(\mathbb{R}^n)$ or $\mathbf{SO}(n)$.

We have the following chains of inclusions:

$$\begin{array}{ccccc} \mathbf{SO}(n) & \subset & \mathbf{O}(n) & \subset & \mathbf{GL}(n) \\ \mathbf{SO}(n) & \subset & \mathbf{SL}(n) & \subset & \mathbf{GL}(n) \end{array}$$

In addition, we have the intersection of groups $\mathbf{SO}(n) = \mathbf{O}(n) \cap \mathbf{SL}(n)$ and the semidirect product $\mathbf{GL}(n) = \mathbf{SL}(n) \rtimes \mathbb{R}^+$ (*i.e.* $g \in \mathbf{GL}(n)$, that is, it is possible to write $g = \bar{g} \rtimes \det(g)$ where $\bar{g} = g/\det(g) \in \mathbf{SL}(n)$, and $\mathbf{SL}(n) \lhd \mathbf{GL}(n)$). The set of elements of the General Linear group with positive determinant form a group: *i.e.* $\mathbf{GL}^+(n)$ and $\mathbf{SL}^+(n)$ are Lie groups.

Anisotropic materials have symmetry groups that are proper subgroups of $\mathbf{O}(n)$, these subgroups are called **point groups**, a term used mainly in crystallography. For each point of a solid, the type of material symmetry or type of anisotropy is characterized by one such group. The symmetry group can be a continuous point group or a discrete point group. In more than one dimension discrete point groups come in infinite families, but from the *crystallographic restriction theorem* and one of *Bieberbach's theorems*, each number of dimensions has only a finite number of point groups that are symmetric over some lattice or grid with that number. These are the crystallographic point groups. The above fact allows to characterize all the possible types of anisotropic behavior for a homogeneous material.

> **Definition A.3.2.** *A **Lie subgroup** $\mathcal{H}$ of a $\mathcal{G}$ is a subgroup of $\mathcal{G}$ for which the inclusion mapping $i : \mathcal{H} \hookrightarrow \mathcal{G}$ is an immersion (see section B.3.5), that is, $i(\mathcal{H})$ is an immersed submanifold of $\mathcal{G}$.*

It can be demonstrated that a topologically closed subgroup $\mathcal{H}$ of a Lie group $\mathcal{G}$ is a closed manifold and in particular is a Lie subgroup. Obviously every discrete point group is a Lie subgroup. Note that not every subgroup of $\mathbf{O}(n)$ is

closed (for example, the elements all the rotations of rational angle in the plane are a non-closed subgroup of $\mathbf{SO}(n)$).

A.4 Fisher–Tippett–Gnedenko theorem

The main result of the EVT is the Fisher–Tippett–Gnedenko theorem. Let $X_1, \ldots, X_n$ be a sequence of independent and identically distributed variables with distribution function F and let $M_n = \max(X_1, \ldots, X_n)$ denote the maximum. The exact asymptotic distribution of the maximum M_n can be derived:

$$\begin{aligned} \Pr(M_n \leq z) \quad &= \Pr(X_1 \leq z, \ldots, X_n \leq z) \\ &= \Pr(X_1 \leq z) \cdots \Pr(X_n \leq z) = (F(z))^n \end{aligned} \tag{A.31}$$

The associated *indicator function* $I_n = I(x_n > z)$ is a *Bernoulli process* with a success probability $p(z) = (1 - F(z))$ that depends on the magnitude ¡math¿z¡/math¿ of the extreme event. The number of extreme events within n trials thus follows a *binomial distribution* and the number of trials until an event occurs follows a geometric distribution with expected value and standard deviation of the same order $O(1/p(z))$. The Fisher–Tippett–Gnedenko theorem is the following:

> **Theorem A.4.1.** *Let $X_1, \ldots, X_n$ be a sequence of independent and identically distributed variables with distribution function F and let*
>
> $$M_n = \max(X_1, \ldots, X_n)$$
>
> *denote the maximum. If there exist sequences of constants $a_n > 0$ and $b_n \in \mathbb{R}$ such that*
>
> $$\Pr\{(M_n - b_n)/a_n \leq z\} \to G(z) \propto \exp\left[-(1 + \zeta z)^{-1/\zeta}\right]$$
>
> *as $n \to \infty$ where ζ depends on the tail shape of the distribution.*

B

Appendix: Manifolds, Tensors, and Covariant derivative

B.1 Types of magnitudes

The quantitative description of the physical world requires the use of physical magnitudes. A physical magnitude is a number (or an array of numbers) which represents an observation by an observer. Different observers can use different ways for representing the same reality, i. e. different observers will have different measures of the physical properties (due to the frame dependency of the components). The assumed *objectivity of physical world* will imply that the different measures (or set of numbers used for representing some property) from different observers can be related in a systematic way (see proposition B.4.1). Thus, the objectivity of the physical world implies that there are some mathematical transformation relating the measures of different observers, in other words, *intersubjectivity of measures* is a logical consequence of objectivity of the physical world. The converse of this affirmation is not a logical deduction, but is justified

by induction: if there are intersubjectivity of measures for a physical property we will assume there is an objectivity of this property. From a mathematical point of view, we have different types of magnitudes:

- **Scalar magnitudes**. The properties described by scalar magnitudes can be represented by a single number, that is equal for all observers (and thus it represents an invariant number). Examples of this type of magnitude are mass, density, temperature or pressure. Mathematically, scalar magnitudes are tensors of 0th order or 0-tensors.

- **Vector magnitudes**. The more complex properties requiring to specify orientation, direction and magnitude are frequently represented by Euclidean vectors. Examples of this type of magnitude are velocity, acceleration, etc. Mathematically, vectors are first order tensors or 1-tensors (indeed, as we will see, there are two types of "[polar] vectors": contravariant 1-tensors, called simply *vectors*, and covariant 1-tensors, called 1-forms; pseudo-vectors or axial vectors such as torque, angular moment or magnetic field are not true vectors, and tensorially they can be represent as the dual of Hodge of a higher order tensor).

- **[Proper] tensor magnitudes**. Other magnitudes describing a complex relation between directions in the neighborhood of a point and vectors require higher order tensors. In classical mechanics, we have some 2-tensor like the inertia tensor, the different types of stress tensors, and the different types deformation tensors. Tensors of order higher than 2 are less frequent, but in elasticity one have an important case the elastic tensor or tensor of elastic constants for an anisotropic solid. (as in the case of 1-tensors in curvilinear coordinates we need to distinguish between covariant, contravariant and mixed

(In quantum physics an additional type is required *spinorial magnitudes* but classically these types can be ignored because the symmetry group of the space is not required to be simply connected groups, and thus there is no need for using universal covering groups. Therefore, we do not need additional spinorial magnitudes).

For specifying a physical magnitude, an observer needs to measure (or to compute) the "components" of a tensor that describes mathematically the magnitude. For a k-tensor in a space of d dimensions an observer needs to specify d^k numbers; these numbers are referred to as the "components". Naturally, this set of

"components" are referred to a *system of coordinates*. For this reason the mathematical transformations relating different measures from different observers are indeed *changes of coordinates* in a general sense. The following will supply the formal details explaining that tensors are indeed multi-linear applications over the tangent bundle of the "physical space", and the systems of coordinates are indeed different ways of choosing vectorial bases over this tangent bundle.

Some additional technical details on the issues studied in this appendix can be found in [72] (general use of manifolds in elasticity) and [50] (fiber bundles).

B.2 Curvilinear coordinates

In order to work out expressions form magnitudes in general coordinates we define general systems of coordinates (in section B.6.2, the Christoffel symbols which are needed for defining accelerations and covariant derivatives in general coordinates will be defined).

> **Definition B.2.1.** *A **coordinate system** on $\mathbb{R}^3$ is a set $\{x^\alpha\}, \alpha = 1, 2, 3$ is a C^∞ mapping (x^1, x^2, x^3) from an open set $\mathcal{U}_z \subset \mathbb{R}^3$ to $\mathbb{R}^3$ such that: (i) the range is an open set $\mathcal{U}_x \subset \mathbb{R}^3$, and*
> *(ii) the mapping $(z^1, z^2, z^3) \mapsto (x^1(z^1, z^2, z^3), x^2(z^1, z^2, z^3), x^3(z^1, z^2, z^3))$ of $\mathcal{U}_z$ to $\mathcal{U}_x$ has a C^∞ inverse, whose components are denoted $z^i(x^1, x^2, x^3)$ The coordinate lines are curves $c_1(t), c_2(t), c_3(t)$ whose components in Euclidean coordinates are $z^i(c_1(t)) = z^i(t, x^2, x^3)$, where x^2 and x^3 are fixed. Similar definition hold for $c_2(t)$ and $c_3(t)$. The tangents to these curves are the coordinate basis vectors; thus*
>
> $$\boldsymbol{e}_a = \frac{\partial z^i}{\partial x^a} \hat{\boldsymbol{i}}_i$$
>
> *where $\hat{\boldsymbol{i}}_i$ $(i = 1, 2, 3)$ are the standard basis vectors in $\mathbb{R}^3$. Note that $\boldsymbol{e}_a \in \mathbb{R}^3$ and is a function of (x^1, x^2, x^3); that is, $\boldsymbol{e}_a : \mathcal{U}_x \to \mathbb{R}^3$. We always use the* [**Einstein**] **summation convention**: *summation on repeated indices is understood.*

For example, cylindrical coordinates define a coordinate system in the whole $\mathbb{R}^3$. Because the condition (ii) in definition B.2.1, the Jacobian of the transforma-
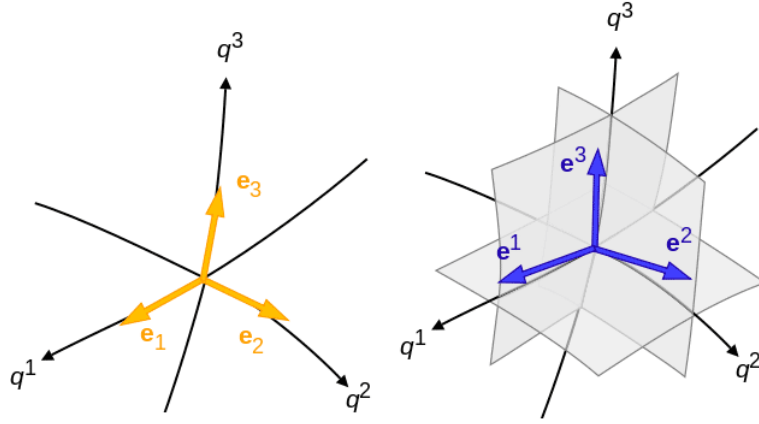
Figure B.1. Curvilinear coordinates in $\mathbb{R}^3$, intersection of three *coordinate lines* at one point, the tangent vectors depicted at the point correspond to the basis vectors at that point (elements of the tangent bundle).

tion $z^i \mapsto x^a(z^i)$ is nonsingular, so $\{\boldsymbol{e}_a\}$ is a basis of $\mathbb{R}^3$ for each (x^1, x^2, x^3). For this reason the spherical coordinates (ρ, θ, φ) only define a coordinate system in $\mathbb{R}^3$ minus an axis (namely where $\theta = 0$, because for this value the Jacobian would be null).

If $c(t)$ is a curve in $\mathbb{R}^3$ the tangent vector. If the trajectory is represented by a curve parametrized by time then the tangent vector is precisely the velocity (if arc length is used instead the vector is the unit tangent vector). We shall use the special notation ϕ_E^i, and so on, for the Euclidean components of ϕ and other magnitudes. Thus, the [Euclidean] *material velocity* is given by:

$$
\begin{aligned}
\boldsymbol{V}(X,t) = \boldsymbol{V}_t(X) = \quad & V_E^j(X,t)\hat{\boldsymbol{i}}_j \\
(V_E^1(X,t), V_E^2(X,t), V_E^3(X,t)) = \quad & \left(\frac{\partial \phi_E^1}{\partial t}(X,t), \frac{\partial \phi_E^2}{\partial t}(X,t), \frac{\partial \phi_E^3}{\partial t}(X,t) \right)
\end{aligned}
$$

$\boldsymbol{V}(X,t)$ can be regarded as an element of the tangent space and $\boldsymbol{V}(\cdot, t)$ is a vector field that is a section of the tangent bundle (see B.3.2). In the same vein, the Euclidean coordinates of the acceleration are:

$$
A_E^i(X,t) = \frac{\partial V_E^i}{\partial t}(X,t) = \frac{\partial^2 \phi_E^i}{\partial t^2}(X,t)
$$

Proposition B.2.1. *Let $\phi(X,t)$ be a $\mathscr{C}^1$ motion of an elastic body $\mathcal{B}$ and let $\boldsymbol{V}$ be the material velocity (see definition 2.3.8 for these two concepts). Let*

$\{x^i\}$ *be a general coordinate system on* $\mathbb{R}^3$ *and let* $\phi^i(X,t) := x^i(\phi(X,t))$. *Then:*

$$V^i(X,t) = \frac{\partial \phi^i(X,t)}{\partial t}$$

where $V^i(X,t)$ *are the components of* $\boldsymbol{V}$ *relative to* $\boldsymbol{e}_i$ *at the point* $\phi(X,t)$ *with coordinates* $x^i(\phi^i(X,t))$.

▶*Proof* Consider $((\partial/\partial t)\phi^i)\boldsymbol{e}_i$ [where ϕ^i stands for $\phi^i(X,t) = x^i(\phi(X,t))$ and where $\boldsymbol{e}_i$ stands for $\boldsymbol{e}_i(x^i(\phi(X,t)))$. We have:

$$\begin{aligned}
\left(\frac{\partial}{\partial t}\phi^a\right)\boldsymbol{e}_a &= \quad \frac{\partial x^a}{\partial z^i}\frac{\partial \phi^i_E}{\partial t}\boldsymbol{e}_a = \frac{\partial x^a}{\partial z^i}V^i_E\frac{\partial z^j}{\partial x^a}\hat{\boldsymbol{i}}_j \\
&= \delta^j_i V^i_E\hat{\boldsymbol{i}}_j = V^i_E\hat{\boldsymbol{i}}_j = \boldsymbol{V} = V^a\boldsymbol{e}_a
\end{aligned}$$

since $\partial x^a/\partial z^i$ and $\partial z^i/\partial x^a$ are inverse matrices. ■

The following proposition shows that the velocity vector is a 1-tensor with the usual transformation for 1-tensor. Suppose that $\bar{x}^i$ is another coordinate system with, say, the same domain $\mathcal{U}_x$. By composition we can form the change of coordinate functions $\bar{x}^i(x^j)$ and $x^i(\bar{x}^j)$. The transformation property of $\boldsymbol{V}$ is worked out next; one says $\boldsymbol{V}$ transforms "like a vector". We let $\bar{V}^a$ denote the components of $\boldsymbol{V}$ in the basis $\bar{\boldsymbol{e}}_a$ associated with $\{\bar{x}^a\}$:

Proposition B.2.2. $\bar{V}^a = (\partial \bar{x}^a/\partial x^b)V^b$, *where* $\bar{V}^a$ *stands for* $\bar{V}^a(X,t)$, *and so forth.*

▶*Proof* By the chain rule and B.2.1,

$$\bar{V}^a = \frac{\partial}{\partial t}\bar{\phi}^a = \frac{\partial \bar{x}^a}{\partial x^b}\frac{\partial}{\partial t}\phi^b = \frac{\partial \bar{x}^a}{\partial x^b}V^b$$

An alternative proof is obtained by noting that $\bar{\boldsymbol{e}}_a = (\partial x^b/\partial \bar{x}^a)\boldsymbol{e}_b$ ■

To work out the components of the acceleration in a general coordinate system we recall a few notations from calculus on $\mathbb{R}^n$ (and Fréchet derivative in other Banach spaces in A.1). For a function $f : \mathbb{R}^n \to \mathbb{R}^m$, the Fréchet derivative of f at the point x_0 will be denoted indistinctly by $f'(x_0)$ or $Df(x_0)$. Notice that the standard definition is independent of the coordinates and only the norm and the linear structure of the involved Banach spaces are used. The usual calculus

rules hold for the Fréchet derivative on $\mathbb{R}^n$, for example, the chain rule states that $D(g{\circ}f)(x_0) = Dg(f(x_0)){\circ}Df(x_0)$; the second "$\circ$" stands for composition of linear maps (thus, matrix multiplication in $\mathbb{R}^m$). The *inverse function theorem* and the *implicit function theorem* remain valid even in infinite-dimensional Banach spaces with minimal variations with respect the results in Euclidean spaces.

B.3 Manifolds, vector fields, one-forms and pull-backs

Intuitively a manifold is a topological space which is locally homeomorphic to an Euclidean space. Manifolds admit a tangent space and locally it is possible to "approximate" a small neighborhood by a convex set of the tangent space (in every point on the surface of the calm sea, the surface is very close to an Euclidean plane for practical purposes although the surface of the Earth is not plane).

This section initiates with a general definition of manifold and then the special case of open sets in $\mathbb{R}^3$ is considered. The basic guidelines and manifold terminology is the one used in this dissertation. Many of the definitions and concepts are considered in further detail in references [72].

Definition B.3.1. *A **smooth** **n-manifold** (or a manifold modeled on $\mathbb{R}^n$) is a set $\mathcal{M}$ such that: (1) For each $P \in \mathcal{M}$ there is a subset $\mathcal{U} \subset \mathcal{M}$ containing P, and a one-to-one mapping, called a **chart** or **coordinate system**, $\{x^\alpha\}$ from $\mathcal{U}$ onto an ope set $\mathcal{V} \subset \mathbb{R}^n$; x^α will denote the components of this mapping ($\alpha = 1, 2, \ldots, n$).*
(2) If x^α and $\bar{x}^\alpha$ are two mappings, the change of coordinate functions $\bar{x}^\alpha(x^1, \ldots, x^n)$ are C^∞
If $\{\tilde{x}^\alpha\}$ maps a set $\mathcal{U} \subset \mathcal{M}$ one-to-one onto an open set in $\mathbb{R}^n$, and if thee change of coordinate functions with the given coordinate functions are C^∞, then $\{\tilde{x}^\alpha\}$ will also be called a chart or coordinate system.

For instance, an open set $\mathcal{M} \subset \mathbb{R}^n$ is a manifold. We take the Cartesian coordinates $\{Z^I\}_{I=1,\ldots,n}$, and the the identity map to define the manifold structure. By allowing all possible coordinate system that are C^∞ functions of the Z^I, we can enlarge our set of coordinate systems. Thus, a manifold embodies the idea

of allowing general coordinate systems, it allow us to consider curved object like surfaces (two manifolds) in addition to open sets of Euclidean space. The manifold $\mathcal{M}$ becomes a topological space by declaring the sets $\mathcal{U}$ the open sets of the topology.

For continuum mechanics both the initial configuration of the body $\mathcal{B}$ (the set that contains all the particles of the body) and the containing space $\mathcal{S}$ are special cases of manifolds. But many applications *require* this generality, such as shell, liquid crystals and bodies with micro-structure. Many authors explicitly consider $\mathcal{B}$ as a set of $\mathbb{R}^3$ with compact closure and directly assume that $\mathcal{S} = \mathbb{R}^3$, this is sufficient if there is no micro-structure for example.

For a manifold that is explicitly contained in Euclidean space it is trivial to define the tangent space, even though an important mathematical discovery made at the turn of the 20th century was that one could define a tangent to a manifold without using a containing Euclidean space. Unfortunately, the abstraction necessary to do this causes seems sometimes unnatural. Here we consider that every manifold indeed can be considered embedded in an Euclidean space, and we use this fact to define the tangent space directly:

Definition B.3.2. *Let $\mathcal{M} \subset \mathbb{R}^n$ be an open set and let $P \in \mathcal{M}$. The **tangent space** to $\mathcal{M}$ at P; this tangent space is denoted by $T_P\mathcal{M}$. The **tangent bundle** of $\mathcal{M}$ is the disjoint union:*

$$T\mathcal{M} = \bigsqcup_{x \in \mathcal{M}} T_x\mathcal{M} = \bigcup_{x \in \mathcal{M}} \{x\} \times T_x\mathcal{M} = \bigcup_{x \in \mathcal{M}} \{(x, y) \mid y \in T_x\mathcal{M}\}$$

*consisting of pair (P, v) of base points P and tangent vectors at P. The map π (or $\pi_{\mathcal{M}}$ if there is no danger of confusion) from $T\mathcal{M}$ to $\mathcal{M}$ mapping a tangent vector (P, v) to its base point P is called **projection**. We may identify $T_P\mathcal{M} = \{P\} \times \mathbb{R}^n$ as set order to keep the different tangent spaces distinguished, or denote tangent vectors by $v_P = (P, v)$ to indicate the point P which is meant.*

The tangent bundle is one of the most simple types of fiber bundles (see section B.8). A fiber bundle can be considered as a manifold in which each point bears attached a fiber (usually a linear space, see figures B.3 and B.4 for a graphic intuition about them). A *vector field* is an assignment $\boldsymbol{V} : \mathcal{M} \to T\mathcal{M}$ that assigns

each point of the base manifold a vector of the tangent space at that point, thus,
a vector field can be viewed as a section of the tangent bundle (see definitions
B.4.1 and B.8.2). Once the tangent bundle of a manifold is defined, one makes it
into a manifold by introducing the coordinates of vectors as in definition B.3.1.
For the special case in which $\mathcal{M} = \mathcal{B}$ is an open subset of $\mathbb{R}^n$ this is easy. We
define the coordinate system induced by a coordinate chart on $\mathcal{M}$:

Definition B.3.3. *Let $\mathcal{B} \subset \mathbb{R}^n$ be an open set and $T\mathcal{B} \approx \mathcal{B} \times \mathbb{R}^n$ be its tangent
bundle. Let $\{X^A\}$ be a coordinate system on $\mathcal{B}$. The corresponding **coor-
dinate system induced on** $T\mathcal{B}$ is defined by mapping $\boldsymbol{W}_X = (X, \boldsymbol{W})$ to
$(X^A(X), W^A)$, where $x \in \mathcal{B}$ and $W^A = (\partial X^A/\partial Z^I)W_E^I$ are the components
of $\boldsymbol{W}$ in the coordinate system $\{X^A\}$, as explained in section B.2.*

For $\mathcal{B} \subset \mathbb{R}^3$, then $T\mathcal{B}$ is a six-dimensional manifold. In general if $\mathcal{B}$ is an
$n-$manifold, $T\mathcal{B}$ is a $2n-$manifold. In Euclidean space we know what is meant by
a $\mathscr{C}^r$ map. A mapping of manifols is $\mathscr{C}^r$ it it is $\mathscr{C}^r$ expressed in local coordinates:

Proposition B.3.1. (a) *Let $\mathcal{B} \subset \mathbb{R}^n$ be an open set and let $f : \mathcal{B} \to \mathbb{R}$ be a
$\mathscr{C}^1$ function. Let $\boldsymbol{W}_X = (X, \boldsymbol{W} \in T_X\mathcal{B}$. Let $\boldsymbol{W}_X[f]$ denote the derivative
of f at X in the direction $\boldsymbol{W}_X$, i.e., $\boldsymbol{W}_X[f] = Df(X) \cdot \boldsymbol{W}$. If $\{X^A\}$
is any coordinate system on $\mathcal{B}$, then $\boldsymbol{W}_X[f] = (\partial f/\partial X^A)W^A$, where it is
understood that $\partial f/\partial X^A$ is evaluated at X*
(a) *If $c(t)$ is a $\mathscr{C}^1$ curve in $\mathcal{B}$, $c(0) = X$, and $\boldsymbol{W}_X = (X, \boldsymbol{W}) = (X, c'(0))$ is
the tangent to $c(t)$ at $t = 0$, then, in any coordinate system $\{X^A\}$,*

$$W^A = \frac{dc^A}{dt}, \qquad where \quad c^A(t) = X^A(c(t))$$

▶*Proof*

(a) $Df(X) \cdot \boldsymbol{W} = \dfrac{\partial f}{\partial Z^I}W_E^I = \dfrac{\partial f}{\partial X^A}\dfrac{\partial X^A}{\partial Z^I}W_E^I = \dfrac{\partial f}{\partial X^A}W^A$

(b) $\dfrac{dc^A(t)}{dt} = \dfrac{\partial X^A}{\partial Z^I}W_E^I = W^A$, evaluated at $c(t)$. ∎

Following standard practice, we let $c'(0)$ stand for both $(X, c'(0))$ and $c'(0) \in$
$\mathbb{R}^n$, when there is no danger of confusion. The above proposition gives a corre-
spondence between the "transformation of coordinate" definition and the other

methods of defining the tangent space. Observe that the mapping $f \mapsto \boldsymbol{W}_X[f]$ is a *derivation*; *i.e.*, it satisfies

$$\boldsymbol{W}_X[f+g] = \boldsymbol{W}_X[f] + \boldsymbol{W}_X[g] \qquad \text{(sum rule)}$$

$$\boldsymbol{W}_X[fg] = f\boldsymbol{W}_X[g] + g\boldsymbol{W}_X[f] \qquad \text{(product rule)}$$

In a coordinate system $\{X^A\}$ the basis vectors $\boldsymbol{E}_A = (\partial Z^I/\partial X^A)\hat{\boldsymbol{\imath}}_I$ are written in some textbooks $\partial/\partial X^A$, since for any function f, $\boldsymbol{E}_A[f] = \partial f/\partial X^A$. The following definition lifts any mapping between manifolds to a mapping between tangent bundles:

> **Definition B.3.4.** *Let $\mathcal{B} \subset \mathbb{R}^n$ be an open set and let $\mathcal{S} = \mathbb{R}^m$. If $\phi : \mathcal{B} \to \mathcal{S}$ is $\mathcal{C}^1$, the **tangent map** of ϕ is defined as follows:*
>
> $$T\phi : T\mathcal{B} \to T\mathcal{S}, \qquad \text{where} \quad T\phi(X, \boldsymbol{W}) = (\phi(X), D\phi(X) \cdot \boldsymbol{W})$$
>
> *For $X \in \mathcal{B}$, we let $T_X\phi$ denote the restriction of $T\phi$ to $T_X\mathcal{B}$, so $T_X\phi$ becomes the linear map $D\phi(X)$ when the base point is dropped.*
> *For completely general manifolds $\mathcal{M}$ and $\mathcal{N}$ and $\phi : \mathcal{M} \to \mathcal{N}$, the tangent map can be defined in terms of tangent vectors to curves, if $[c]_m$ is a tangent vector of a curve c through $m \in \mathcal{M}$ at this point the tangent map is simply defined as:*
> $$T\phi([c]_m) = [\phi \circ c]_{\phi(m)}$$

Notice that according to the previous definition, the following diagram commutes:

$$
\begin{array}{ccc}
T\mathcal{B} & \xrightarrow{\ T\phi\ } & T\mathcal{S} \\
\downarrow{\scriptstyle \pi_{\mathcal{B}}} & & \downarrow{\scriptstyle \pi_{\mathcal{S}}} \\
\mathcal{B} & \xrightarrow{\ \phi\ } & \mathcal{S}
\end{array}
\qquad (\text{B.1})
$$

The tangent mapping is in some sense the generalization of Jacobian matrix to manifold calculus. The next proposition is the essence of the fact that $T\phi$ makes intrinsic sense on manifolds:

> **Proposition B.3.2.** (a) *If $c(t)$ is a curve in $\mathcal{B}$ and $\boldsymbol{W}_X = c'(0)$, then*
>
> $$T\phi \cdot \boldsymbol{W}_X = \left. \frac{d}{dt}\phi(c(t)) \right|_{t=0}$$

(the base points X of $\boldsymbol{W}_X$ and $T\phi \cdot \boldsymbol{W}_X$, being understood).

(b) If $\{X^A\}$ is a coordinate chart on $\mathcal{B}$ and $\{x^a\}$ is one on $\mathcal{S}$, then, for
$\boldsymbol{W} \in T_X\mathcal{B}$

$$T(\phi \cdot \boldsymbol{W}_X)^a = \frac{\partial \phi^a}{\partial X^A} W^A$$

that is, in coordinate charts on $\mathcal{B}$ of $T_X\mathcal{B}$ is the Jacobian matrix of ϕ evaluated at X.

▶*Proof*

(a) By the chain rule, $\frac{d}{dt}\phi(c(t))\Big|_{t=0} = D\phi(X) \cdot c'(0)$.

$$
\begin{aligned}
D\phi(X) \cdot \boldsymbol{W} \quad &= \frac{\partial \phi^i_E}{\partial Z^i} W^I_E \hat{\boldsymbol{i}}_i \\
&= \frac{\partial \phi^a}{\partial Z^i} \frac{\partial z^i}{\partial x^a} W^I_E \hat{\boldsymbol{i}}_i \quad \text{(chain rule)} \\
&= \frac{\partial \phi^a}{\partial X^A} \left(\frac{\partial X^A}{\partial Z^I} W^I_E \right) \left(\frac{\partial z^i}{\partial x^a} \hat{\boldsymbol{i}}_i \right) \quad \text{(chain rule)} \\
&= \frac{\partial \phi^a}{\partial X^A} W^A \boldsymbol{e}_a
\end{aligned}
$$

(b)

∎

In addition, it can be proven that $T\phi$ is a tensor. Note the following transformation rule:

$$\frac{\partial \bar{\phi}^a}{\partial \bar{X}^A} = \frac{\partial X^B}{\partial \bar{X}^A} \frac{\partial \bar{\phi}^b}{\partial X^B} \frac{\partial \bar{x}^a}{\partial x^b}$$

The chain rule can be expressed in terms of tangent mappings as follows:

Proposition B.3.3. *Let $\phi : \mathcal{B} \to \mathcal{S}$ and $\psi : \mathcal{S} \to \mathcal{V}$ be $\mathcal{C}^r$ maps of manifolds $(r \geq 1)$. Then $\psi \circ \phi$ is a $\mathcal{C}^r$ mapping and $T(\psi \circ \phi) = T\psi \circ T\phi$*

The proof of the above result is routine. This "T" formulation keeps track of the base points automatically.

Before proceeding with the formulation, it is interesting to introduce some additional terminology about mappings between manifolds, for future reference.

Definition B.3.5. (a) *A map $f : \mathcal{M} \to \mathcal{N}$ for which $T_m f$ is one-to-one at each $m \in \mathcal{M}$ is called an **immersion**. For an immersion for each $m \in \mathcal{M}$*

there is a neighborhood U such that $f(U) \subset N$ that is a submanifold of $\mathcal{N}$.

*(b) An immersion is said to be an **embedding** if it is a homeomorphism onto its image in the induced topology. Thus and embedding is a one-one immersion.*

*(c) A map $f : \mathcal{M} \to \mathcal{N}$ is said to be **proper** if the inverse image $f^{-1}(K)$ of any compact set $K \subset \mathcal{N}$ is compact. It can be shown that a proper one-one immersion is an embedding.*

*(d) A map $f : \mathcal{M} \to \mathcal{N}$ is said to be a $\mathscr{C}^r$ **diffeomorphism** if it is a one-one $\mathscr{C}^r-$ map and the inverse $f^{-1} : \mathcal{N} \to \mathcal{M}$ is a $\mathscr{C}^r$ map.*

Now, we define two mappings that allow to relate physical magnitudes expressed in material (initial) ans spatial (final) configurations: the *push-forward map* and the *pull-back map*. For motivating the formal definitions, we recall some uses of the push-forward and pull-back maps in elasticity theory. The relation among stress tensors and strain tensors are definable by means of these maps:

- The **second Piola-Kirchhoff stress tensor S** is the pull-back of the **Cauchy stress tensor $\boldsymbol{\sigma}$** (or equivalently the Cauchy stress tensor is the push-forward of the second Piola-Kirchhoff stress tensor).
- The [full-covariant] **right Cauchy-Green tensor $\mathbf{C}^\flat$** (sometimes referred to as the **Green deformation tensor**) is the pull-back of the **metric tensor g** of the space where the motion of the elastic body takes place.
- The [full-contravariant] **left Cauchy-Green tensor $\mathbf{b}^\sharp$** (sometimes referred to as the **Finger deformation tensor**) is the push-forward of the **inverse metric tensor $\mathbf{G}^{-1}$** of the original geometry of the body.
- The **Green-Lagrange strain tensor E** is the pull-back of the **Euler-Almansi strain tensor e**.
- The components **deformation gradient** are the components of the restriction of the tangent map (Jacobian matrix) of the motion (which we assume is an diffeomorphism). It allows to relate the matrix components of the above pairs of tensors.

See equations B.13 and B.14 for the justification of some of the above claims.

Returning to the formal definitions, we first define the pull-back and the push-forward for vector fields. A formal definition is given in definition B.8.2, but more informally, a vector field $\boldsymbol{V}$ is an assignment $\boldsymbol{V} : \mathcal{M} \to T\mathcal{M}$ such that $\boldsymbol{V}(X) \in T_X \mathcal{M}$ for all $X \in \mathcal{M}$. A vector field is indeed a tensor field of type (1,0)

as it can be seen in definition B.4.1. Then the pull-back and the push-forward of
a vector field are defined:

> **Definition B.3.6.** Pull-back and Push-forward of a vector field. *If $\boldsymbol{V}$ is a
> vector field $\boldsymbol{V} : \mathcal{M} \to T\mathcal{M}$, $\phi : \mathcal{M} \to \mathcal{N}$ is a regular $\mathscr{C}^1$ diffeomorphism and
> $\boldsymbol{v}$ is another vector field $\boldsymbol{v} : \mathcal{N} \to T\mathcal{N}$ then:*
> *(a) If ϕ is a regular map, then $\phi_* \boldsymbol{V} = T\phi \circ \boldsymbol{V} \circ \phi^{-1}$, a vector field on $\phi(\mathcal{M})$
> is called the **push-forward** of $\boldsymbol{V}$ by ϕ*
> *(b) If ϕ^{-1} exists and is a regular map, then $\phi^* \boldsymbol{v} = T(\phi^{-1}) \circ \boldsymbol{v} \circ \phi$, a vector
> field on $\phi(\mathcal{M})$ is called the **push-forward** of $\boldsymbol{V}$ by ϕ*

In addition, the pull-back and the push-forward can be defined for 1-form
field [a tensor field of type (0,1)] and, in fact, for any type of tensor. Recall
that a 1-form at $m \in \mathcal{M}$ is a linear mapping $\boldsymbol{\alpha}_m : T_m\mathcal{M} \to \mathbb{R}$; the vector space
of all 1-forms is denoted as $T_m^*\mathcal{M}$. The *cotangent bundle* $T^*\mathcal{M}$ is the disjoint
union $T^*\mathcal{M} = \bigsqcup_{m \in \mathcal{M}} T_m^*\mathcal{M}$. A 1-form field is a cross-section of this bundle, *i.e*
an assignment $\boldsymbol{\alpha} : \mathcal{M} \to T^*\mathcal{M}$ such that $\boldsymbol{\alpha}(X) \in T_m^*\mathcal{M}$ for all $X \in \mathcal{M}$. Then the
pull-back and push-forward of an 1-form field are defined by:

> **Definition B.3.7.** Pull-back and Push-forward of a 1-form field. *If $\boldsymbol{\beta}$ is a
> 1-form field $\boldsymbol{\beta} : \mathcal{N} \to T\mathcal{N}$, and $\phi : \mathcal{M} \to \mathcal{N}$ is a $\mathscr{C}^1$ map then:*
> *(a) If ϕ is a $\mathscr{C}^1$ map and $\boldsymbol{\beta}$ is a 1-form on $\mathcal{N}$, then $\phi_* \boldsymbol{\beta}$ is a one form on $\mathcal{M}$
> defined by $(\phi^* \boldsymbol{\beta})_X \cdot \boldsymbol{W}_X = \boldsymbol{\beta}_{\phi(X)} \cdot (T\phi \cdot \boldsymbol{W}_X)$ for $X \in \mathcal{M}$ and $\boldsymbol{W}_X \in T_X\mathcal{M}$ is
> called the **pull-back** of $\boldsymbol{\beta}$ by ϕ. In contrast to vector fields, the pull-back of
> a 1-form does not use the inverse of ϕ, so does not require ϕ to be regular.*
> *(b) If ϕ is regular, it is possible to define the **push-forward** of a 1-form $\boldsymbol{\alpha}$
> on $\mathcal{M}$ by $\phi_* \boldsymbol{\alpha} = (\phi^{-1})^* \boldsymbol{\alpha}$.*

The coordinate expression for the pull-back is $(\phi^* \boldsymbol{\beta})_A = (\partial \phi^a / \partial X^A) \beta_a$. For a
completely general tensor field the pull-back and the push-forward are formally
defined in the next section (definition B.4.2)

We conclude this section with another fundamental mathematical object in
manifolds analysis, the *connection*. A connection allows to define the notion of
parallel transport along a curve and the concept of *material derivative*:

Definition B.3.8. *A **connection** on a manifold $\mathcal{M}$ is an operation ∇ : $\mathcal{X} \times \mathcal{X} \to \mathcal{X}$ (where $\mathcal{X}$ is the set of vector fields on $\mathcal{M}$) that associates to each pair of vector fields $\boldsymbol{X}, \boldsymbol{Y}$ on $\mathcal{M}$ a third vector filed denoted $\nabla_{\boldsymbol{X}} \boldsymbol{Y}$ and called the **covariant derivative** of $\boldsymbol{Y}$ along $\boldsymbol{X}$, such that:*
(i) $\nabla_{\boldsymbol{X}} \boldsymbol{Y}$ is linear in each of the two arguments $\boldsymbol{X}, \boldsymbol{Y}$.
(ii) $\nabla_{f\boldsymbol{X}} \boldsymbol{Y} = f \nabla_{\boldsymbol{X}} \boldsymbol{Y}$ for scalar functions f.
(iii) $\nabla_{\boldsymbol{X}}(f\boldsymbol{Y}) = f \nabla_{\boldsymbol{X}} \boldsymbol{Y} + (\boldsymbol{X}[f])\boldsymbol{Y}$.

These conditions are reasonable requirements for an operation that is supposed to differentiate $\boldsymbol{Y}$ in the direction $\boldsymbol{X}$. Note that (iii) is analogous to the product rule for differentiation. We will return more in detail to the important concept of covariant derivative in section B.6. But for the moment we will introduce the *Christoffel symbols* of a connection (this will be needed for introduce the *Riemann connection* on a Riemann manifolds in section B.5, and for defining the covariant derivatives of higher order tensor in section B.6):

Definition B.3.9. *The **Christoffel symbols** Γ^{C}_{AB} of a connection ∇ on $\mathcal{B}$ are defined on a coordinate system $\{X^A\}$ by the relations:*

$$\nabla_{\boldsymbol{E}_A} \boldsymbol{E}_B = \Gamma^{C}_{AB} \boldsymbol{E}_C$$

The form of the above derivative follows from B.3.8, obviously, the Γ^{C}_{AB} are function of the point X. If we consider two different coordinate systems $\{X^A\}, \{\bar{X}^A\}$ on $\mathcal{B}$ it can be proven that the Christoffel symbols for the two vector bases $\{\boldsymbol{E}^A = (\partial/\partial X^A)\}$ and $\{\bar{\boldsymbol{E}}^A = (\partial/\partial \bar{X}^A)\}$, are related by:

$$\bar{\Gamma}^{A}_{BC} = \frac{\partial \bar{X}^A}{\partial X^D} \left(\Gamma^{D}_{EF} \frac{\partial X^E}{\partial \bar{X}^B} \frac{\partial X^F}{\partial \bar{X}^C} + \frac{\partial^2 X^D}{\partial \bar{X}^B \partial \bar{X}^C} \right)$$

We denote the Christoffel symbols of $\mathcal{B}$ by Γ^{C}_{AB} and those of $\mathcal{S}$ by γ^{c}_{ab}.

In the section B.6 an intuitive example is developed that will justify this definition. For the moment we retain this formal definition for what follows.

B.4 Tensor Analysis

The current notion used here is the same of Marsden and Hughes: $\mathcal{B}$ and $\mathcal{S}$ are manifolds (the first one represents the initial shape of the body and the second one the ambient space in which the body moves, thus a body motion will be a uniparametric group of diffeomorphisms $\phi_t : \mathcal{B} \to \mathcal{S}$, see definition 2.3.2 for details). Points in $\mathcal{B}$ will be denoted by X and those in $\mathcal{S}$ by x. The tangent spaces are written $T_X\mathcal{B}$ and $T_x\mathcal{S}$. Coordinate systems are denoted by $\{X^A\}$ and $\{x^a\}$ for $\mathcal{B}$ and $\mathcal{S}$, respectively, with the bases $\boldsymbol{E}_A = \partial/\partial X^A$ and $\boldsymbol{e}_a = \partial/\partial x^a$ (note that the expressions $\partial/\partial x$ can be interpreted as a vector because the act in the linear space of germs of functions on the manifold), the dual bases (bases of the dual space of the tangent space) are denoted by $\boldsymbol{E}^A = dX^A$ and $\boldsymbol{e}^a = dx^a$. Notice that

$$\langle \boldsymbol{E}^J, \boldsymbol{E}_I \rangle = \left\langle dX^J, \frac{\partial}{\partial X^J} \right\rangle = \delta_I^I$$

In all cases the summation convention on repeated indexes is enforced.

Definition B.4.1. *A **tensor** of type $\binom{p}{q}$ at $X \in \mathcal{B}$ is a multi-linear mapping:*

$$\mathbf{T} : \underbrace{T_X^*\mathcal{B} \times \cdots \times T_X^*\mathcal{B}}_{p \text{ copies}} \times \underbrace{T_X\mathcal{B} \times \cdots \times T_X\mathcal{B}}_{q \text{ copies}} \to \mathbb{R}$$

The components *of* $\mathbf{T}$ *are defined by:*

$$T^{A_1 A_2 \ldots A_p}{}_{B_1 B_2 \ldots B_q} = T^{A_1 A_2 \ldots A_p}_{B_1 B_2 \ldots B_q} = \mathbf{T}(\boldsymbol{E}^{A_1}, \ldots, \boldsymbol{E}^{A_p}, \boldsymbol{E}_{B_1}, \ldots, \boldsymbol{E}_{B_q})$$

*A **tensor field** of type $\binom{p}{q}$ is an assignment $X \mapsto \mathbf{T}(X)$ of a tensor to each point of the manifold $\mathcal{B}$. The set of all tensor fields of the same type for a fiber bundle (indeed, a vector bundle) called $T_q^p\mathcal{B}$ (for a definition of fiber bundle see section B.8)*

The upper indexes in definition B.4.1 are called *contravariant* indexes, and the lower ones *covariant* indexes (when no possible confusion arises we will write the first ones just on top of the other ones, note the two possible styles in the components). A tensor field is said to be of *class $\mathscr{C}^r$* if all its components are $\mathscr{C}^r$ functions of $\{X^A\}$ in any coordinate system. We repeat here common denominations for particular types of tensors:

- A tensor of type $\binom{0}{0}$ can be regarded as a **scalar function**.
- A tensor of type $\binom{1}{0}$ can be regarded as a **vector**.
- A tensor of type $\binom{0}{1}$ can be regarded as a **covector** or **1-form**.
- A tensor of type $\binom{1}{1}$ can be regarded as a **linear application** of the tangent bundle.
- A tensor of type $\binom{0}{2}$ can be regarded as an application of the tangent bundle into the cotangent bundle.
- A tensor of type $\binom{2}{0}$ can be regarded as an application of the cotangent bundle into the tangent bundle.

One interesting thing about tensors are that they are mathematical objects on its own (they are not just sets of components). For this reason the one and the same tensor can be expressed in different systems of coordinates. Physically, a particular set of components representing a tensor can be interpreted as relative components to a frame of reference. Obviously, this is related to the discussion about the mathematical consequences of assumption of the *objectivity of physical word* as was stated at the beginning of section B.1. The we can explicitly state the rules relating the components measured by different observers, interpreting such relations as a change of coordinates:

Proposition B.4.1. *Let* $\{X^A\}$ *and* $\{\bar{X}^A\}$ *be two coordinates sets on* $\mathcal{B}$ *and* $\mathbf{T}$ *a tensor field of type* $\binom{p}{q}$. *Then the components of* $\mathbf{T}$ *in these two systems are related by*

$$\bar{T}^{A_1...A_p}_{B_1...B_q} = \frac{\partial \bar{X}^{A_1}}{\partial X^{C_1}} \cdots \frac{\partial \bar{X}^{A_p}}{\partial X^{C_p}} \bar{T}^{C_1...C_p}_{D_1...D_q} \frac{\partial X^{D_1}}{\partial \bar{X}^{B_1}} \cdots \frac{\partial X^{D_p}}{\partial \bar{X}^{B_p}}$$

The proof follows straightforwardly form the definition of components, multilinearity, and the formula relating the bases $\bar{E}_A = (\partial \bar{X}^A / \partial X^B) E_B$.

The notion of pull-back and push-forward, were introduced in definition B.3.6 for vectors of tangent bundle and covectors (1-forms) of the cotangent bundle. The notion can be extended for a general type of tensor field as follows:

Definition B.4.2. *Let* $\phi : \mathcal{B} \to \mathcal{S}$ *be regular mapping. If* $\mathbf{T}$ *is a tensor of type* $\binom{p}{q}$ *on* $\mathcal{B}$, *its* ***push-forward*** $\phi_* \mathbf{T}$ *is a tensor of type* $\binom{p}{q}$ *on* $\mathcal{S}$ *defined by:*

$$\phi_* \mathbf{T}(\boldsymbol{\alpha}_1, \ldots, \boldsymbol{\alpha}_p, \boldsymbol{v}_1, \ldots, \boldsymbol{v}_q) = \mathbf{T}(\phi^* \boldsymbol{\alpha}_1, \ldots, \phi^* \boldsymbol{\alpha}_p, \phi^* \boldsymbol{v}_1, \ldots, \phi^* \boldsymbol{v}_q)$$

*where the pull-backs and push-forward of the $\boldsymbol{\alpha}$s and $\boldsymbol{v}$s is given in definition
B.3.6: that is, $\phi * (\boldsymbol{\alpha}) \cdot \boldsymbol{u} = \boldsymbol{\alpha}(T\phi \cdot \boldsymbol{u})$ and $\phi * (\boldsymbol{v}) = T\phi^{-1} \cdot \boldsymbol{v}$*
*The **pull-back** of a tensor of $\mathbf{t} \in T_q^p \phi(\mathcal{B}) \subset T_q^p \mathcal{S}$ is given by*

$$\phi^* \mathbf{t} = (\phi^{-1})_* (\mathbf{t})$$

In components we have:

$$(\phi_* \mathbf{T})_{b_1 \ldots b_q}^{a_1 \ldots a_p} = F_{A_1}^{a_1} \cdots F_{A_p}^{a_p} T_{B_1 \ldots B_q}^{A_1 \ldots A_p} \bar{F}_{b_1}^{B_1} \cdots \bar{F}_{b_q}^{B_q}$$

where $\bar{F}_a^A := (F^{-1})_a^A$. Similarly:

$$(\phi^* \mathbf{T})_{B_1 \ldots B_q}^{A_1 \ldots A_p} = \bar{F}_{a_1}^{A_1} \cdots \bar{F}_{a_p}^{A_p} T_{b_1 \ldots b_q}^{a_1 \ldots a_p} F_{B_1}^{b_1} \cdots F_{B_q}^{b_q}$$

Let's define two common operations the *product tensor* and the *exterior product*:

Definition B.4.3. *Given a tensor S of type $\binom{p}{q}$ and a tensor T of type $\binom{r}{s}$
the **product tensor** $\mathsf{S} \otimes \mathsf{T}$ is a tensor of type $\binom{p+r}{q+s}$ defined by:*

$$(\mathsf{S} \otimes \mathsf{T})(\boldsymbol{\alpha}^1, \ldots, \boldsymbol{\alpha}^p, \boldsymbol{W}_1, \ldots, \boldsymbol{W}_n, \boldsymbol{\beta}^1, \ldots, \boldsymbol{\beta}^r, \boldsymbol{Y}_1, \ldots, \boldsymbol{Y}_s) = \ldots$$
$$\cdots = \mathsf{S}(\boldsymbol{\alpha}^1, \ldots, \boldsymbol{\alpha}^p, \boldsymbol{W}_1, \ldots, \boldsymbol{W}_n) \cdot \mathsf{T}(\boldsymbol{\beta}^1, \ldots, \boldsymbol{\beta}^r, \boldsymbol{Y}_1, \ldots, \boldsymbol{Y}_s)$$

In components:

$$(\mathsf{S} \otimes \mathsf{T})^{A_1 \ldots A_p}{}_{B_1 \ldots B_q}{}^{C_1 \ldots C_r}{}_{D_1 \ldots D_s} = \ldots$$
$$\cdots = \mathsf{S}^{A_1 \ldots A_p}{}_{B_1 \ldots B_q} \mathsf{T}^{C_1 \ldots C_r}{}_{D_1 \ldots D_s}$$

*The exterior product of an m-form $\boldsymbol{\eta}$ and an n-form $\boldsymbol{\omega}$ (skew-symmetric
tensor of type $\binom{0}{n}$) is an $(m+n)$–form given by:*

$$\boldsymbol{\eta} \wedge \boldsymbol{\omega} = \mathrm{skew}(\boldsymbol{\eta} \otimes \boldsymbol{\omega}) = [\boldsymbol{\eta} \otimes \boldsymbol{\omega}]$$

Next we discuss two-point tensors used in elasticity and early discussed for example in Ericksen (1960) [29]. These objects play an important rôle in continuum mechanics; a prime example is the deformation tensor $F^a{}_A$:

Definition B.4.4. *A **two-point tensor** T of type $\binom{pl}{qm}$ at $X \in \mathcal{B}$ over a
mapping $\phi : \mathcal{B} \to \mathcal{S}$ is a multilinear mapping*

$$\mathsf{T} : (T_X^* \mathcal{B})^p \times (T_X \mathcal{B})^q \times (T_X^* \mathcal{S})^l \times (T_X \mathcal{S})^m \to \mathbb{R}$$

where $x = \phi(X)$. The components of T are defined by:

$$\mathsf{T}^{A_1 \ldots A_p}{}_{B_1 \ldots B_q}{}^{a_1 \ldots a_l}{}_{b_1 \ldots b_m} = \ldots$$
$$\ldots = \mathsf{T}(\boldsymbol{E}^{A_1}, \ldots, \boldsymbol{E}^{A_p}, \boldsymbol{E}_{B_1}, \ldots, \boldsymbol{E}_{B_q}, \boldsymbol{e}^{a_1}, \ldots, \boldsymbol{e}^{a_n}, \boldsymbol{e}_{b_1}, \ldots, \boldsymbol{e}_{b_m})$$

B.5   Riemann manifolds

A very important tensorial object for defining metric concepts (lengths, areas, volumes, angle between curves, curvature, covariant derivatives, etc.) is the *metric tensor*. In Euclidean space the usual inner product provides an example of a metric tensor (when using Cartesian coordinates the metric tensor is precisely the quadratic form given by $g_{\text{Euc}}(\boldsymbol{U}, \boldsymbol{V}) = \delta_{ab} U^a V^b = U^a V^b = \boldsymbol{U} \cdot \boldsymbol{V}$. When using non Cartesian coordinates for vectors or tensor we need to choose the correct components of the metric tensor for computations (see section B.6). Finally when working in n-dimensional spaces that are not part of $\mathbb{R}^n$ (for example, curved surfaces) we need to use a non-Euclidean metric tensor. In continuum mechanics using general curvilinear coordinates the metric tensor is an extremely important object, but it is even more important in other physical theories. For example in General Relativity theory the basic object to define the geometry of the curved four-dimensional space-time is precisely a metric tensor, and the equations of Einstein relate the presence of matter concentrations to the curvature defined by the metric tensor (for weak gravitational fields the metric tensor is the Euclidean tensor modified by a small term depending on the gravitational potential). In elasticity some important tensor such as the right Cauchy tensor and the left Cauchy tensor are respectively the pull-back and the push-forward of the metric tensor of the initial and the final geometry. We proceed to define the important notion of metric tensor and Riemann manifold:

> **Definition B.5.1.** *A **metric tensor** or **Riemannian metric** on a manifold $\mathcal{M}$ is a $\mathscr{C}^\infty$ covariant 2-tensor $\mathbf{g}$, i.e. a tensor of type $\binom{0}{2}$, such that for all $X \in \mathcal{M}$:*
> *(i) $\mathbf{g}_X [:= \mathbf{g}(X)]$ is symmetric; that is for $\boldsymbol{W}_1, \boldsymbol{W}_2 \in T\mathcal{M}$, $\boldsymbol{g}_X(\boldsymbol{W}_1, \boldsymbol{W}_2) = \mathbf{g}_X(\boldsymbol{W}_2, \boldsymbol{W}_1)$*
> *(ii) $\mathbf{g}_X$ is positive-definite: $\mathbf{g}_X(\boldsymbol{W}, \boldsymbol{W}) > 0$ for $\boldsymbol{0} \neq \boldsymbol{W} \in T_X\mathcal{M}$, in other words $\mathbf{g}_X$ defines an inner product on $T_X\mathcal{M}$. If there is no danger of con-*

fusion, it is common to write

$$\mathbf{g}_X(\boldsymbol{W}_1, \boldsymbol{W}_2) = \langle \boldsymbol{W}_1, \boldsymbol{W}_2 \rangle_X = g_{ab}(X) W_1^a W_2^b$$

*A **Riemannian manifold** $(\mathcal{M}, \mathbf{g})$ is an $n-$dimensional differentiable manifold $\mathcal{M}$ where a Riemannian metric $\mathbf{g}$ has been defined.*

The condition (ii) allows to define an application $L_{\mathbf{g}} : \mathcal{M} \to \mathscr{L}(T_x\mathcal{M}, T_x^*\mathcal{M})$ given by $\boldsymbol{W}_1 \mapsto \boldsymbol{\alpha}$ where $\boldsymbol{\alpha}(\boldsymbol{W}_2) = \mathbf{g}_X(\boldsymbol{W}_2, \boldsymbol{W}_1)$, that is: $\boldsymbol{\alpha}(\cdot) = \mathbf{g}_X(\cdot, \boldsymbol{W}_1)$. Since $\mathbf{g}$ is positive-definite this mapping $L_{\mathbf{g}}$ is invertible. It can be proven that the inverse is associated with a second-order tensor of type $\binom{2}{0}$ denoted $\bar{\mathbf{g}} = \mathbf{g}^{\sharp} = g^{ab}\boldsymbol{e}_a \otimes \boldsymbol{e}_b$. The components g^{ab} are the components of inverse matrix of the matrix with components g_{ab}:

$$(L_{\mathbf{g}}(X)(g^{ab}\boldsymbol{E}_a))(\boldsymbol{E}_b) = g^{ab}\mathbf{g}(\boldsymbol{E}_a, \boldsymbol{E}_b) = g^{ab}g_{bc} = \delta_c^a = \boldsymbol{E}^a(\boldsymbol{E}_b)$$

Thus, $L_{\mathbf{g}}(X)(g^{ab}\boldsymbol{E}_b) = \boldsymbol{E}^a$, so we call $\bar{\mathbf{g}}$ the "inverse metric tensor".

In elasticity it is important to distinguish between the metric tensor $\mathbf{G}$ of the initial geometry $\mathcal{M}$ and the metric tensor $\mathbf{g}$ of the space $\mathcal{S}$ where the motion of the body and the deformation process take place.

An important notion used frequently in computation is that in a Riemann manifold there is a natural isomorphism between tensorial fields of type (p, q) and (p', q') for $p + q = p' + q'$. The computation of this isomorphism requires the use of components of the metric tensor (g_{ab}) and the "inverse" of metric tensor (g^{ab}), for example, if we have a tensor

$$\mathbf{T} = T^i{}_{jk} \frac{\partial}{\partial x^i} \otimes dx^j \otimes dx^k \xrightarrow[\substack{3th\ index}]{raising} \uparrow_3(\mathbf{T}) = T^i{}_{j\alpha}g^{k\alpha}\frac{\partial}{\partial x^i} \otimes dx^j \otimes \frac{\partial}{\partial x^k}$$

This can be represented in terms of the operation of contraction as: $\mathsf{C}_3^5[\mathbf{T} \otimes \bar{\mathbf{g}}]$, where $\bar{\mathbf{g}}$ represents the "inverse" metric tensor and the operation $\mathsf{C}_i^k[\cdot]$ the sum contraction between the kth index and the ith index (this latter operation is only defined if k is an upper index and i a lower index). Then for a physical magnitudes defined for a rth-order tensor the are always 2^r associated representations (for each of the k indexes there are two possible positions "up" and "down", then $2 \cdot \ldots k$ times $\cdot 2$). The change between two of these equivalent representations is called "operation of lowering/raising indexes", and is formalized in the next

definition:

> **Definition B.5.2.** *Given a tensor field of type (p, q):*
> (i) *if $q > 0$, the operation of **raising** the kth index is the mapping $\uparrow_k \colon T_q^p \mathcal{M} \to T_{q-1}^{p+1} \mathcal{M}$ given by*
>
> $$\uparrow_k \mathbf{T} = \mathsf{C}_k^{p+q+2}[\mathbf{T} \otimes \bar{\mathbf{g}}]$$
>
> *(notice the above operation is defined only for some ks in $\{1, \dots, q\}$).*
> (ii) *Similarly, if $p > 0$, the operation of **lowering** the kth index is the mapping $\downarrow_k \colon T_q^p \mathcal{M} \to T_{q+1}^{p-1} \mathcal{M}$ given by*
>
> $$\downarrow_k \mathbf{T} = \mathsf{C}_{p+q+2}^k[\mathbf{T} \otimes \mathbf{g}]$$
>
> *If both mappings are defined for a given tensor, then they are inverse operations $\downarrow_k \circ \uparrow_k = \uparrow_k \circ \downarrow_k = \mathrm{Id}$*
> (iii) *The isomorphism $^\flat \colon T_q^p \mathcal{M} \to T_{p+q}^0 \mathcal{M}$ is the result of p consecutive operations of lowering. For any rth-order tensor $\mathbf{T}$, the tensor $\mathbf{T}^\flat$ is called the **full covariant associated tensor** of $\mathbf{T}$.*
> (iv) *The isomorphism $^\sharp \colon T_q^p \mathcal{M} \to T_0^{p+q} \mathcal{M}$ is the result of q consecutive operations of raising. For any rth-order tensor $\mathbf{T}$, the tensor $\mathbf{T}^\sharp$ is called the **full contravariant associated tensor** of $\mathbf{T}$.*

A connection is a mathematical procedure that makes precise the idea of transporting vectors or tensors along a curve (or family of curves) in a "parallel" and consistent manner. To specify a connection on a manifold is equivalent to specify a covariant derivation on it. A covariant derivative is a derivation for tensors, such that the covariant derivative of a tensor is also a tensor (and, therefore, this derivative has the right tensorial transformation properties). As it is explained in section B.6.1 the ordinary directional derivatives do not constitute in general a covariant derivative. A connection is normally represented by a set of functions Γ_{AB}^C called the *Christoffel symbols* related to the covariant derivative $\nabla(\cdot)$ by means of:

$$\nabla_{\mathbf{E}_A} \mathbf{E}_B = \Gamma_{AB}^C \mathbf{E}_C \tag{B.2}$$

In a Riemann manifold, it is possible to define many different connections, but there is a special connection that exists for every Riemann manifold that is *torsion free* and has nice properties, this is called the *Riemann connection* or the *Levi-Civita connection*. A fundamental theorem of Riemannian geometry states that there is a unique connection which satisfies these properties. We define some

previous concepts and then we state the theorem proving the uniqueness of the
Riemann connection.

Definition B.5.3. *A connection is called **torsion free** if*

$$\nabla_{\boldsymbol{W}}\boldsymbol{Y} - \nabla_{\boldsymbol{Y}}\boldsymbol{W} = [\boldsymbol{W}, \boldsymbol{Y}]$$

*for all the vectors $\boldsymbol{W}$ and $\boldsymbol{Y}$ and being $[\cdot, \cdot]$ the commutator of two fields.
In general the **torsion tensor** is defined as*

$$\mathrm{Tor}(\boldsymbol{Y}, \boldsymbol{W}) = \nabla_{\boldsymbol{W}}\boldsymbol{Y} - \nabla_{\boldsymbol{Y}}\boldsymbol{W} - [\boldsymbol{W}, \boldsymbol{Y}]$$

*and is a tensor of type $\binom{1}{2}$. Thus a connection is torsion free when the
torsion tensor is zero.*

It can be easily proved that a connection is torsion free if and only if the Christoffel
symbols are symmetric, *i.e.* $\Gamma^A_{BC} = \Gamma^A_{CB}$. The key result that allows to define a
Riemann connection on a Riemann manifold is the *Fundamental Theorem of
Riemann Geometry*, that we state now and is based on the early pioneering work
of Levi-Civita:

Theorem B.5.1. *Let $(\mathcal{M}, \mathbf{g})$ a Riemann manifold. Then there is a unique
connection on $\mathcal{M}$ that is torsion free and for which parallel translation pre-
serves inner products.*

It can be proven that the unique Riemann connection is characterized by Christof-
fel symbols with the form:

$$\Gamma^a_{bc} = \frac{1}{2}g^{ad}\left(\frac{\partial g_{dc}}{\partial x^b} + \frac{\partial g_{bd}}{\partial x^c} - \frac{\partial g_{bc}}{\partial x^d}\right) \tag{B.3}$$

The proof is simple: it proceeds to compute directly the restrictions in the enun-
ciate of the theorem and concludes that these conditions uniquely determines
Christoffel symbols of the form B.3 [72].

Every connection on a manifold defines a curvature tensor on the manifold.
For an immersed surface on $\mathbb{R}^n$ (with the Riemann connection associated with
the induced metric tensor) this curvature tensor allow to compute in every point

the sectional curvatures of the surface. Thus the curvature tensor is related to the intuitive notion of curvature and radius of curvature. For a general abstract manifold we define the *Riemann curvature tensor* as:

Definition B.5.4. *The **Riemann curvature tensor** of a Riemann manifold $(\mathcal{M}, \mathbf{g})$ is a tensor R of type $\binom{1}{3}$ defined from the Riemann connection as follows:*

$$\mathsf{R} : T_x^* \mathcal{M} \times T_x \mathcal{M} \times T_x \mathcal{M} \times T_x \mathcal{M} \to \mathbb{R}$$

where:

$$
\begin{aligned}
\mathsf{R}(\boldsymbol{\beta}, \boldsymbol{W}_1, \boldsymbol{W}_2, \boldsymbol{W}_3) &= \boldsymbol{\beta}(\nabla_{\boldsymbol{W}_1} \nabla_{\boldsymbol{W}_2} \boldsymbol{W}_3 - \nabla_{\boldsymbol{W}_2} \nabla_{\boldsymbol{W}_1} \boldsymbol{W}_3 - \nabla_{[\boldsymbol{W}_1, \boldsymbol{W}_2]} \boldsymbol{W}_3) \\
&= \boldsymbol{\beta}([\nabla_{\boldsymbol{W}_1}, \nabla_{\boldsymbol{W}_2}] \boldsymbol{W}_3 - \nabla_{[\boldsymbol{W}_1, \boldsymbol{W}_2]} \boldsymbol{W}_3)
\end{aligned}
$$

where $\boldsymbol{\beta} \in T_x^* \mathcal{M}$ and $\boldsymbol{W}_i \in T_x \mathcal{M}$ Explicitly in components the Riemann curvature tensor is given by:

$$
\boxed{R^a{}_{bcd} = \frac{\partial \Gamma^a_{bd}}{\partial x^c} - \frac{\partial \Gamma^a_{cb}}{\partial x^d} + \Gamma^a_{ce} \Gamma^e_{db} - \Gamma^a_{de} \Gamma^e_{cb}}
$$

*The contraction $R_{bd} = R^a{}_{bad}$ is called the **Ricci curvature** and its trace $R = R^a_a = g^{ab} R_{ab}$ is called the **scalar curvature**.*

The term curvature is justified because the parallel transport around a closed curve in a Riemann manifold with non-vanishing curvature depends on the curve. In addition, one can show the following fundamental property for the second derivatives of a vector $W^a_{|b|c} - W^a_{|c|b} = R^a{}_{bcd} W^d$, this contrasts with the case of directional derivatives in $\mathbb{R}^n$ which commute for any smooth vector field.

B.6 Covariant derivative

B.6.1 An intuitive example

When general curvilinear coordinates are used some concepts need to be checked. For example, in an Euclidean space $\mathbb{R}^n$ the tangent space at every point is an n-dimensional vector space over $\mathbb{R}$, thus, it can be identified again with the space $\mathbb{R}^n$ (then the space and the tangent space are "coincident"). This is not the general case for a manifold or curved space (say, for example, a curved surface), the tangent space at different points is not the same (although all the tangent spaces are isomorphic, they are not the same). It is not immediate how to obtain a derivative of a vector field defined on a curved manifold. In we consider coordinate lines on a curved surface, then at each point one can select as a basis the tangent vectors to these lines. But this procedure implies that the basis vectors at different points do not belong to the same space (see for example figure B.2). The same problem appears when non Cartesian coordinates are employed in an Euclidean space (so the problem is more generalized than we can think appearing even in Euclidean spaces). For example consider a classical particle moving in a straight line with constant velocity, we have:
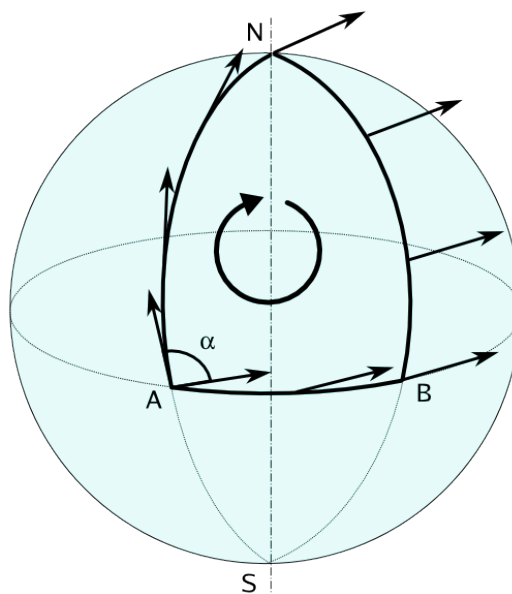
Figure B.2. The tangent vector to coordinate lines belong to different tangent spaces, consider the coordinate line AN then the tangent vector in A belong to a two-dimensional plane, but the tangent vector in N belong to another plane, thus working with two dimensional vector fields on the surface it is not immediate how to relate vectorial or tensorial magnitudes defined at different points.

$$\begin{cases} x(t) = d\cos\theta_0 - vt\sin\theta_0 \\ y(t) = d\sin\theta_0 + vt\cos\theta_0 \end{cases} \Rightarrow \qquad y(t) = \frac{d - x\cos(\theta_0)}{\sin\theta_0}$$

A straightforward computation shows that the above equations correspond to

a motion with constant velocity v:

$$\begin{cases} v^x = \dfrac{dx}{dt} = -v\sin\theta_0 \\[2mm] v^y = \dfrac{dy}{dt} = +v\cos\theta_0 \end{cases}, \qquad \begin{cases} a^x = \dfrac{dv^x}{dt} = \dfrac{\partial v^x}{\partial x}\dot{x} + \dfrac{\partial v^x}{\partial y}\dot{y} = 0 \\[2mm] a^y = \dfrac{dv^y}{dt} = 0 \end{cases}$$

Being zero the accelerations, we have checked the velocity is constant. The same straightforward calculation could be done in polar coordinates. It is obvious from the above equations that the particle moves along a straight line which does not pass through the origin, the trajectory in polar coordinates is given by:

$$\begin{cases} \rho(t) = \sqrt{d^2 + v^2 t^2} \\[2mm] \theta(t) = \theta_0 + \arctan\left(\dfrac{vt}{d}\right) \end{cases} \Rightarrow \qquad \begin{array}{c} \rho(t) = \dfrac{d}{\cos(\theta(t) - \theta_0)}, \\[2mm] \text{with}(\theta_0 - \pi/2 < \theta < \theta_0 + \pi/2) \end{array}$$

Computing the velocities we obtain the right expression:

$$v^\rho = \dot{\rho} = v\sin(\theta - \theta_0), \qquad v^\theta = \dot{\theta} = \frac{v}{\rho}\cos(\theta - \theta_0)$$

Using the metric tensor in polar coordinates we can compute the modulus of velocity as $v^2 = g_{\alpha\beta}v^\alpha v^\beta = v^\rho v^\rho + \rho^2 v^\theta v^\theta = v^2\left[\sin^2(\theta - \theta_0) + \rho^2\left(\cos(\theta - \theta_0)/\rho^2\right)\right]$

But a problem arises when acceleration is computed in the same way we did for Cartesian coordinates, because:

$$\begin{cases} a^\rho \neq \dfrac{dv^\rho}{dt} = \dfrac{\partial v^\rho}{\partial \rho}\dot{\rho} + \dfrac{\partial v^\rho}{\partial \theta}\dot{\theta} \\[2mm] a^\theta \neq \dfrac{dv^\theta}{dt} = \dfrac{\partial v^\theta}{\partial \rho}\dot{\rho} + \dfrac{\partial v^\theta}{\partial \theta}\dot{\theta} \end{cases}$$

The problem, in fact, is that the basis formed by the radial vector and the polar azimuthal vector $\{e_\rho, e_\theta\}$ does not have the same orientation at each point. It is clear that for a right derivation of the acceleration we need to take into account the change in the basis vectors:

$$\boldsymbol{a} = \frac{d\boldsymbol{v}}{dt} = \frac{d}{dt}\left(v^\rho \boldsymbol{e}_\rho + v^\theta \boldsymbol{e}_\theta\right) = \left(\dot{v}^\rho \boldsymbol{e}_\rho + \dot{v}^\theta \boldsymbol{e}_\theta\right) + \left(v^\rho \dot{\boldsymbol{e}}_\rho + v^\theta \dot{\boldsymbol{e}}_\theta\right)$$

Note that for Cartesian coordinates only the first term of the last second member appears. But for polar or general coordinates, we need to add the second term in order to take into account the variation the basis vectors. This is the motivation for the covariant derivative $\bar{\partial}/\bar{\partial}x^a$ to define the new terms properly. By chain rule we will have for a vector in the basis a derivative of the form:

$$\dot{\boldsymbol{e}}_a = \frac{\bar{\partial}\boldsymbol{e}_a}{\bar{\partial}\rho}\frac{\bar{\partial}\rho}{\bar{\partial}t} + \frac{\bar{\partial}\boldsymbol{e}_a}{\bar{\partial}\theta}\frac{\bar{\partial}\theta}{\bar{\partial}t}$$

For scalar functions we define $\bar{\partial}f/\bar{\partial}t := \partial f/\partial t$, and for the vectors of the basis, being its derivative another vector we can rewrite it in terms of the basis:

$$\nabla_b \boldsymbol{e}_a = \frac{\bar{\partial}\boldsymbol{e}_a}{\bar{\partial}x^b} = \gamma^c_{ab}\boldsymbol{e}_c \tag{B.4}$$

where γ^c_{ab} are the *Christoffel symbols* of the definition B.3.9. Thus the main conclusion of this section is that when using general curvilinear coordinates we need to define the covariant derivative denoted ∇_a different from the ordinary derivatives ∂_a in order to take into account the variation in basis vectors. The same is true for general manifold calculus, when only curvilinear coordinates are possible.

As an illustration of that, we will return to the example of the particle moving with constant velocity along a straight line, then the acceleration correctly computed is:

$$a^\rho = \frac{Dv^\rho}{Dt} = \dot{\rho}\left(\frac{\partial v^\rho}{\partial \rho} + \gamma^\rho_{\rho\rho}v^\rho + \gamma^\rho_{\rho\theta}v^\theta\right) + \dot{\theta}\left(\frac{\partial v^\rho}{\partial \theta} + \gamma^\rho_{\theta\rho}v^\rho + \gamma^\rho_{\theta\theta}v^\theta\right) =$$

$$= \dot{\rho}(0 + 0 + 0) + \dot{\theta}\left(v\cos(\theta - \theta_0) + 0 - \rho\frac{v}{\rho}\cos(\theta - \theta_0)\right) = 0$$

$$a^\theta = \frac{Dv^\theta}{Dt} = \dot{\rho}\left(\frac{\partial v^\theta}{\partial \rho} + \gamma^\theta_{\rho\rho}v^\rho + \gamma^\theta_{\rho\theta}v^\theta\right) + \dot{\theta}\left(\frac{\partial v^\theta}{\partial \theta} + \gamma^\theta_{\theta\rho}v^\rho + \gamma^\theta_{\theta\theta}v^\theta\right) =$$

$$\dot{\rho}\left(-\frac{v\cos(\theta - \theta_0)}{\rho^2} + 0 + \frac{1}{\rho}\frac{v\cos(\theta - \theta_0)}{\rho}\right) + \dot{\theta}\left(-\frac{v\sin(\theta - \theta_0)}{\rho} + \frac{1}{\rho}v\sin(\theta - \theta_0) + 0\right) = 0$$

Now the computation is right and both components of acceleration are effectively zero.

B.6.2 The general case

We have shown in the previous section that the computation of derivatives of vectors in general coordinates can not be calculated just by deriving components. The same is true for a general tensor. When using general curvilinear coordinates, we need to use covariant derivatives in order to achieve the right results. The computation of the covariant derivatives requires the use of Christoffel symbols (introduced in B.3.9, in an abstract context). In order to introduce them in a motivated way we will return to the context of definition B.2.1, the covariant derivative of frame vectors $e_a = (\partial z^j/\partial x^a)\hat{i}_j$ can be defined as:

$$\frac{\partial e_a}{\partial x^b} = \frac{\partial^2 z^j}{\partial x^a \partial x^b}\hat{i}_j = \frac{\partial^2 z^j}{\partial x^a \partial x^b}\frac{\partial x^x}{\partial z^j}e_c$$

This last object arises frequently in manifold calculus, it is clearly recognizable as the Christoffel symbols associated to the spatial coordiantes, the we offer a second definition of Christoffel symbols here:

Definition B.6.1. *The **Christoffel symbols** of the coordinate system $\{x^a\}$ on $\mathbb{R}^3$ are defined by*

$$\gamma^c_{ab} = \frac{\partial^2 z^i}{\partial x^a \partial x^b}\frac{\partial x^c}{\partial z^i}$$

which are regarded as functions of x^d. The Christoffel symbols of a material coordinate system $\{X^A\}$ are denoted Γ^A_{BC}

Note that the γ's are symmetric in the sense that $\gamma^c_{ab} = \gamma^c_{ba}$ For a general Riemann manifold a more general there is a more general definition. The Christoffel symbols allow to define "parallel transport" and "covariant derivatives" on a Riemann manifold, these notions generalize the concept of parallel lines and invariant derivatives to curved spaces/manifolds.

Then using the Christoffel symbols we can demonstrate the following general result for the material acceleration (see definition 2.3.3) in general coordinates:

Proposition B.6.1. *Let $\phi(X,t)$ be a $\mathscr{C}^2$ motion of a body $\mathcal{B}$ and V $\mathcal{A}$ the material velocity and acceleration. Then the components A^a of $\boldsymbol{A}$ in the basis $\boldsymbol{e}_a$ of a coordinate system $\{x^a\}$ are given by:*

$$A^a = \frac{\partial V^a}{\partial t} + \gamma^a_{bc} V^b V^c$$

Moreover A^a transforms as a vector; that is $\bar{A}^b = (\partial \bar{x}^b)/(\partial x^a) A^a$

▶*Proof*

$$\begin{aligned}
\boldsymbol{A} \quad &= \frac{\partial \boldsymbol{V}}{\partial t} = \frac{\partial V^i_E}{\partial t}\hat{\boldsymbol{i}}_i = \frac{\partial}{\partial t}\left(\frac{\partial z^i_E}{\partial x^c}V^c\right)\hat{\boldsymbol{i}}_i \\
&= \frac{\partial^2 z^i_E}{\partial x^b \partial x^c}\frac{\partial x^b}{\partial t}V^c\hat{\boldsymbol{i}}_i + \frac{\partial z^i_E}{\partial x^a}\frac{\partial V^a}{\partial t}\hat{\boldsymbol{i}}_i \quad = \frac{\partial^2 z^i_E}{\partial x^b \partial x^c}V^b V^c\frac{\partial x^a}{\partial z^i_E}\boldsymbol{e}_a + \frac{\partial V^a}{\partial t}\boldsymbol{e}_a
\end{aligned}$$

Comparison with $\boldsymbol{A} = A^a\boldsymbol{e}_a$ yields to the first part of proposition.

For the second part, define a coordinate change $\bar{\boldsymbol{e}}_a = (\partial \bar{x}^b)/(\partial x^a) A^e_b$ and comparing $\mathcal{A} = A^a\boldsymbol{e}_a = \bar{A}^b\bar{\boldsymbol{e}}_b$. ■

Now we proceed to the general definition of covariant derivative for vectors:

Definition B.6.2. *Let $\boldsymbol{v}$ and $\boldsymbol{w}$ be two vector fields on $\mathbb{R}^3$, that is, maps of open sets of $\mathbb{R}^3$ to $\mathbb{R}^3$. Assume that $\boldsymbol{v}$ is $\mathscr{C}^1$. Thus $D\boldsymbol{v}$ is a linear map of $\mathbb{R}^3$ to $\mathbb{R}^3$, so $D\boldsymbol{v}(x) \cdot \boldsymbol{w}(x)$ is a vector field on $\mathbb{R}^3$. It is called the **covariant derivative** of $\boldsymbol{v}$ along $\boldsymbol{w}$ and is denoted $\nabla_{\boldsymbol{w}}\boldsymbol{v}$ or $\boldsymbol{w} \cdot \nabla\boldsymbol{v}$*

This particular definition is given by Marsden and Hughes (1983) [72]. A more general definition can be given without the need to assume that the body

is immersed in $\mathbb{R}^3$, but the definition needs to be a little more abstract. We will state the following proposition without a proof (the proof is similar to that of B.6.1):

Proposition B.6.2. *In a coordinate system system $\{x^a\}$,*

$$\left(\nabla_{\boldsymbol{w}}\boldsymbol{v}\right)^a = \frac{\partial v^a}{\partial x^b} + \gamma^a_{bc}w^b v^c$$

and $(\nabla_{\boldsymbol{w}}\boldsymbol{v})^a$ transforms as a vector.

For the components of covariant derivatives, the following abbreviated notation is commonly used: $V^a_{|b}, T^{ab}_{c|d}$ denote the covariant derivatives $\nabla_b V^a, \nabla_d T^{ab}_c$, thus a notable saving of space is obtained without any ambiguity. Where for a general tensor of type $\binom{p}{q}$ the covariant derivatives are defined in components as:

$$
\begin{aligned}
(\nabla \mathsf{T})^{a_1...a_p}_{b_1...b_q k} &= \nabla_k \mathsf{T}^{a_1...a_p}_{b_1...b_q} = T^{a_1...a_p}_{b_1...b_q|K} \\
&= \frac{\partial}{\partial x^k} T^{a_1...a_p}{}_{b_1...b_q} + T^{la_2...a_p}_{b_1...b_q}\gamma^{a_1}_{lk} + T^{a_1 l...a_p}_{b_1...b_q}\gamma^{a_2}_{lk} + \text{(all upper indexes)} - ... \\
&\quad \cdots - T^{a_1...a_p}_{lb_2...b_q}\gamma^l_{b_1 k} - T^{a_1...a_p}_{lb_2...b_q}\gamma^l_{b_2 k} - \text{(all lower indexes)}
\end{aligned}
$$

$$\text{(B.5)}$$

It can be proven that for the Riemann connection one have $\nabla \mathbf{g} = 0$, and thus ∇ preserves inner products.

More in general for a two-point tensor of type $\binom{pm}{qn}$ using coordinates $\{X^A\}, \{x^a\}$, and the associated Christoffel symbols $\gamma^a_{bc}, \Gamma^A_{BC}$ the covariant derivative is extended by means of:

$$
\begin{aligned}
T^{A_1...A_p a_1...a_m}_{B_1...B_q b_1...b_n |K} &= \frac{\partial}{\partial X^K} T^{A_1...A_p a_1...a_m}_{B_1...B_q b_1...b_n} + ... \\
&\cdots + T^{L...A_p a_1...a_m}_{B_1...B_q b_1...b_n}\Gamma^{A_1}_{LK} + \text{(all upper capital indexes)} - ... \\
&\cdots - T^{A_1...A_p a_1...a_m}_{L...B_q b_1...b_n}\Gamma^L_{B_1 K} + \text{(all lower capital indexes)} + ... \\
&\cdots + T^{A_1...A_p l...a_m}_{B_1...B_q b_1...b_n}\gamma^{a_1}_{kl} F^l_K - \text{(all upper lowercase indexes)} - ... \\
&\cdots - T^{A_1...A_p a_1...a_m}_{B_1...B_q l...b_n}\Gamma^k_{b_1 l} F^l_K + \text{(all lower lowercase indexes)}
\end{aligned}
$$

$$\text{(B.6)}$$

B.6.3 Gradient, divergence and material derivative

The covariant derivate allow to generalize the concepts of vector calculus on $\mathbb{R}^n$
to a Riemann manifold. For example given a scalar function $f : \mathcal{M} \to \mathbb{R}$ defined
on a Riemann manifold we define the **gradient** as the vector field on $\mathcal{M}$ defined
by:

$$\nabla f = g^{ab} \frac{\partial f}{\partial x^b} \boldsymbol{e}_a, \quad \text{or} \quad (\nabla f)^a = g^{ab} \frac{\partial f}{\partial x^b} \tag{B.7}$$

The divergence of tensor field F of type $\binom{p}{q}$ is a tensor div F of type $\binom{p-1}{q}$ obtained
by contracting the last contravariant and covariant indexes in $\nabla\mathsf{F}$:

$$\boxed{(\text{div } \mathsf{F})^{a_1 \ldots a_p}_{b_1 \ldots b_q} = \mathsf{F}^{a_1 \ldots a_{p-1}c}_{b_1 \ldots b_q | c}} \tag{B.8}$$

For applications in elasticity we distinguish between "DIV" and "div" for tensor
in the material or spatial configurations of a deformed body. When the tensor
field is in fact a vector field is the above formula reduces to:

$$(\text{div } \boldsymbol{W}) = W^a_{|a} = \frac{1}{\sqrt{\det g}} \frac{\partial}{\partial x^a} (W^a \sqrt{\det g}) \tag{B.9}$$

The **material derivative** associated with a motion ϕ_t of a vector field $\boldsymbol{W} \in T\mathcal{B}$
along a material trajectory $\xi(t) = \phi_t(X) = \phi(X,t) \in \mathcal{S}$ denoted by $D\boldsymbol{W}/Dt$ or $\dot{\boldsymbol{W}}$
is defined as:

$$\dot{\boldsymbol{W}} = \frac{D\boldsymbol{W}}{Dt} = \nabla_{\dot{\xi}} \boldsymbol{W}, \quad \left(\frac{D\boldsymbol{W}}{Dt}\right)^A = \frac{d}{dt}(W^A(\xi(t))) + \Gamma^A_{BC} W^B(\xi(t)) \dot{\xi}^C \tag{B.10}$$

For short, $D\boldsymbol{W}/Dt = \partial\boldsymbol{W}/\partial t + \nabla_{\dot{\xi}} \boldsymbol{W}$. This definition can be generalized to tensors
of any type. With the previous definition it is easy to see the relation between
the spatial acceleration and the spatial velocity:

$$\boldsymbol{a} = \frac{\partial \boldsymbol{a}}{\partial t} + \nabla_{\boldsymbol{v}} \boldsymbol{v} = \dot{\boldsymbol{v}} \tag{B.11}$$

B.7 Deformation measures

In section B.3 the differential of a configuration (see definition B.3.4) was ex-
amined. The tangent map generalizes the concept of "Jacobian matrix" of the

calculus in $\mathbb{R}^n$. In elasticity theory the term "deformation gradient" is used for the tangent map of manifold calculus (we consider this a misleading name because it has nothing to do with a real gradient, but we keep this denomination). This section is devoted to the properties of such mapping and the additional deformation measures constructible from it. Elasticity theory makes an extensive use of all the notions explained in this section. We begin with a formal definition of the deformation gradient:

Definition B.7.1. *Let* $\phi : \mathcal{B} \to \mathcal{S}$ *be a* $\mathscr{C}^1$ *configuration of* $\mathcal{B}$ *(*$\mathcal{B}, \mathcal{S}$ *are general manifolds here). The tangent map of* ϕ *is denoted* **F** *and is called the* ***deformation gradient*** *of* ϕ*; thus* **F** $= T\phi$*. For* $X \in \mathcal{B}$*, we let* $\mathbf{F}_X$ *of* $\mathbf{F}(X)$ *denote the restriction of* **F** *to* $T_X\mathcal{B}$*. Thus* $\mathbf{F}(X) : T_X\mathcal{B} \to T_{\phi(X)}\mathcal{S}$ *is a linear mapping for each* $X \in \mathcal{B}$

The following proposition works out the coordinate description of $\mathbb{F}$:

Proposition B.7.1. *Let* $\{X^A\}$ *and* $\{x^a\}$ *denote coordinate systems of* $\mathcal{B}$ *and* $\mathcal{S}$*, respectively. Then the matrix of* $\mathbf{F}(X)$ *with respect to the coordinate bases* $\boldsymbol{E}_A(X) = \partial/\partial X^A$ *and* $\boldsymbol{e}_a(X) = \partial/\partial x^a$ *[where* $x = \phi(X)$ *is given by*

$$ F^a{}_A = \frac{\partial \phi^a(X)}{\partial X^A} $$

For a motion $\phi_t(X)$ the we write $\mathbf{F}(X, t) = T\phi_t(X)$ and frequently is written simply as **F**, which is an important example of a *two-point tensor*. These objects were discussed in B.4. Notice that the coordinate expression for $F^a{}_A$ does not involve any covariant derivatives. This is because ϕ us bit a vector, but rather is a poing mapping of $\mathcal{B}$ to $\mathcal{S}$. We will assume in this section $\mathcal{S} = \mathbb{R}^n$ and $\mathcal{S} \subset \mathbb{R}^n$ is a simple body (these assumptions are not essential, the details for general Riemann manifolds can be generalized without difficulties). Let $\langle, \rangle_x$ denote the standard inner product $\mathcal{S}$ for vectors based at $x \in \mathcal{S}$ and similarly let $\langle, \rangle_X$ be the standard inner product in $\mathcal{B}$ at $X \in \mathcal{B}$. For a vector $\boldsymbol{v} \in T_x\mathcal{S}$ we let $\|\boldsymbol{v}\|_x = \langle \boldsymbol{v}, \boldsymbol{v} \rangle_x^{1/2}$ be the length of $\boldsymbol{v}$. Similarly the length of $\boldsymbol{W} \in T_x\mathcal{B}$ is denoted $\|\boldsymbol{W}\|_X$ (when there is no danger of confusion, the subscripts may be dropped.) Let $\mathbf{A} : T_X\mathcal{B} \to T_x\mathcal{S}$ be

a linear transformation. Then the *transpose*, or *adjoint* of $\mathbf{A}$, denoted $\mathbf{A}^T$, is the linear transformation

$$\mathbf{A}^T : T_x\mathcal{S} \to T_X\mathcal{B} \qquad \text{such that} \quad \langle \mathbf{A}\boldsymbol{W}, \boldsymbol{v}\rangle_x = \langle \boldsymbol{W}, \mathbf{A}^T\boldsymbol{v}\rangle_X$$

For all $\boldsymbol{W} \in T_X\mathcal{B}$ and $\boldsymbol{v}$. If $\mathbf{B} : T_x\mathcal{S} \to T_X\mathcal{B}$ is a linear transformation, it is called *symmetric* if $\mathbf{B} = \mathbf{B}^T$. In a coordinate system $\{x^a\}$ on $\mathcal{S}$, let the metric tensor g_{ab} be defined by $g_{ab}(x) = \langle \boldsymbol{e}_a, \boldsymbol{e}_b\rangle_x$ and similarly define $G_{AB}(X)$ on $\mathcal{B}$ by $G_{AB}(X) = \langle \boldsymbol{E}_A, \boldsymbol{E}_B\rangle_X$. We let g^{ab} and G^{AB} denote the inverse matrices of g_{ab} and G_{AB}; these exist since g_{ab} and G_{AB} are non-singular. In Euclidean space, $\boldsymbol{e}_a = (\partial z^i/\partial x^a)\hat{\boldsymbol{i}}_i$, so we have the expression

$$g_{ab} = \frac{\partial z^i}{\partial x^a}\frac{\partial z^j}{\partial x^b}\delta_{ij}$$

Similarly

$$G_{AB} = \frac{\partial Z^I}{\partial X^A}\frac{\partial Z^J}{\partial X^B}\delta_{IJ}$$

Proposition B.7.2. (i) *For $\boldsymbol{v}, \boldsymbol{w} \in T_x\mathcal{S}$ and for a coordinate system $\{x^a\}$. We have*

$$\langle \boldsymbol{v}, \boldsymbol{w}\rangle_x = g_{ab}v^a v^b$$

(ii) *If $\{x^a\}$ and $\{X^A\}$ are coordinate system of $\mathcal{S}$ and $\mathcal{B}$, respectively, and $\phi : \mathcal{B} \to \mathcal{S}$ is a $\mathscr{C}^1$ configuration of $\mathcal{B}$, the matrix of $\mathbf{F}^T$ is given by*

$$(\mathbf{F}^T(x))^A{}_a = g_{ab}(x)F^b{}_B(X)G^{AB}(X)$$

where $x = \phi(X)$.

▶*Proof* (i) This follows form the definition of g_{ab} and the expression $\boldsymbol{v} = v^a\boldsymbol{e}_a$ and $\boldsymbol{w} = w^b\boldsymbol{e}_b$:

$$\langle \boldsymbol{v}, \boldsymbol{w}\rangle_x = \langle v^a\boldsymbol{e}_a, w^b\boldsymbol{e}_b\rangle = v^a w^b\langle \boldsymbol{e}_a, \boldsymbol{e}_b\rangle = v^a w^b g_{ab}$$

(ii) By definitions,

$$\langle \mathbf{F}^T\boldsymbol{w}, \boldsymbol{W}\rangle_X = \langle \mathbf{F}\boldsymbol{W}, \boldsymbol{w}\rangle_x; \quad \text{that is,} \quad (\mathbf{F}^T(x))^B{}_b w^b W^A G_{AB} = F^a{}_A W^A w^b g_{ab}$$

for all $\boldsymbol{W} \in T_x\mathcal{B}$ and $\boldsymbol{w} \in T_x\mathcal{S}$, where $\mathbf{F}^T$ and $\mathbf{F}$ have their arguments suppressed. Since $\boldsymbol{W}$ and $\boldsymbol{w}$ are arbitrary, $(\mathbf{F}^T)^B{}_b G_{AB} = F^a{}_A g_{ab}$. Multiplying by G^{AC} and

using $G_{AB}G^{AC} = \delta^C{}_B$ gives the result. In order for the map $\mathbf{F}^T : T(\phi(\mathcal{B}) \to T\mathcal{B}$ to well defined, ϕ must be regular. ∎

Then we can pass to the definition of strain measures, that involves the tangent derivative and, therefore, the deformation gradient:

Definition B.7.2. *The **right Cauchy-Green tensor**, also called the **Green deformation tensor**, $\mathbf{C}$ is defined by:*

$$\boxed{\mathbf{C}(X) : T_X\mathcal{B} \to T_X\mathcal{B}, \qquad \mathbf{C}(X) = \mathbf{F}^T(X)\mathbf{F}(X)}$$

*Or, for short, $\mathbf{C} = \mathbf{F}^T\mathbf{F}$. If $\mathbf{C}$ is invertible, we let $\mathbf{B} = \mathbf{C}^{-1}$, called the **Piola deformation tensor**.*

If $\{x^a\}$ and $\{X^A\}$ are coordinate systems on $\mathcal{S}$ and $\mathcal{B}$, respectively, then:

$$C^A{}_B = \left(\mathbf{F}^T\right)^A_a F^a_B = g_{ab}G^{AC}\frac{\partial\phi^b}{\partial X^C}\frac{\partial\phi^a}{\partial X^B} \tag{B.12}$$

It can be proved that $\mathbf{C}$ is symmetric and positive-semidefinite; that is, $\langle \mathbf{C}\boldsymbol{W}, \boldsymbol{W}\rangle_X \geq 0$, and if $\mathbf{F}_X$ is one-to-one, then $\mathbf{C}$ is invertible and positive-definite; that is, $\langle \mathbf{C}\boldsymbol{W}, \boldsymbol{W}\rangle_X > 0$ if $\boldsymbol{W} \neq \mathbf{0}$. Note that $\mathbf{F}$ is one-to-one if ϕ is regular.

The symmetry of $\mathbf{C}$ means that $C_{AB} = C_{BA}$, where $C_{AB} = G_{AC}C^C{}_B$. We call C_{AB} the *associated components* of $\mathbf{C}$. The notion of associated components and the was clarified in definition B.5.2. The same definition allowed us to construct the tensor $\mathbf{C}^\flat$ from the defined $\mathbf{C}$ and the metric. From the definition of the pull-back and the right Cauchy-Green tensor, we observe that $\mathbf{C}^\flat = \phi^*\mathbf{g}$, that is, the full lowered right Cauchy-Green tensor is the pull back to $\mathcal{B}$ of the metric tensor $\mathbf{g}$ of the space $\mathcal{S}$. In a similar way, we can push the metric $\mathbf{G}$ on $\mathcal{B}$ forward to $\mathcal{S}$. This leads to a new metric tensor $\mathbf{b} = \mathbf{c}^{-1}$ with $\mathbf{c}^\flat = \phi_*\mathbf{G}$. The explicit definition follows:

Definition B.7.3. *Let ϕ be a regular $\mathscr{C}^1$ configuration of $\mathcal{B}$ in $\mathcal{S}$. Then the **Finger deformation tensor**, also called the **left Cauchy-Green tensor**, is defined on $\phi(\mathcal{B})$ by*

$$\mathbf{b}(x) : T_x\phi(\mathcal{B}) \subset \mathcal{S} \to T_x\mathcal{S}, \qquad \mathbf{b}(x) = \mathbf{F}(X)\mathbf{F}^T(X)$$

Or, for short, $\mathbf{b} = \mathbf{F}\mathbf{F}^T$. *Also we define* $\mathbf{c} = \mathbf{b}^{-1}$. *In coordinates we have:*

$$b^a{}_b = g_{ac}G^{AB}\frac{\partial\phi^a}{\partial X^A}\frac{\partial\phi^c}{\partial X^B}$$

In addition we have that $\mathbf{b}$ is positive-definite. Finally we introduce the strain measures:

Definition B.7.4. (i) *The* **material** [or **Lagrangian**] **strain tensor**
$\mathbf{E} : T\mathcal{B} \to T\mathcal{B}$ *is defined by* $\mathbf{E} = (\mathbf{C} - \mathbf{I})/2$. *The associated full lowered* $\mathbf{E}^\flat =$
$(\mathbf{C}^\flat - \mathbf{G})/2$. *In components* $E^A{}_B = (C^A{}_B - \delta^A_B)/2$ *and* $E_{AB} = (C_{AB} - G_{AB})/2$.
Thus $\mathbf{E} = \mathbf{0}$ *is equivalent to* $\mathbf{C} = \mathbf{I}$.
(ii) *The* **spatial** [or **Eulerian**] **strain tensor** $\mathbf{e} : T\mathcal{S} \to T\mathcal{S}$ *is defined by*
$\mathbf{e} = (\mathbf{I} - \mathbf{c})/2$. *The associated full lowered* $\mathbf{e}^\flat = (\mathbf{g} - \mathbf{c})/2$. *In components*
$e^a{}_b = (\delta^a_b - c^a{}_b)/2$ *and* $e_{ab} = (g_{ab} - c_{ab})/2$. *Thus* $\mathbf{e} = \mathbf{0}$ *is equivalent to* $\mathbf{c} = \mathbf{I}$.

It is interesting to resume the relations among the deformation tensors, metric tensors and strain tensors:

$$
\boxed{
\begin{aligned}
\mathbf{C}^\flat &= \phi^*(\mathbf{g}), & \mathbf{c}^\flat &= \phi_*(\mathbf{G}), \\
\mathbf{B}^\sharp &= \phi^*(\mathbf{g}^\sharp), & \mathbf{b}^\sharp &= \phi_*(\mathbf{G}^\sharp), \\
\mathbf{E}^\flat &= \phi^*(\mathbf{e}^\flat), & \mathbf{e}^\flat &= \phi_*(\mathbf{E}^\flat).
\end{aligned}
}
\tag{B.13}
$$

Explicitly in coordinates we have:

$$
\begin{aligned}
C_{AB} &= g_{ab}F^a{}_A F^b{}_B, & c_{ab} &= G_{AB}(F^{-1})^A{}_a(F^{-1})^B{}_b, \\
B^{AB} &= g^{ab}(F^{-1})^A{}_a(F^{-1})^B{}_b, & b^{ab} &= G^{AB}F^a{}_A F^b{}_B, \\
E^{AB} &= e_{ab}F^a{}_A F^b{}_B, & e_{ab} &= E_{AB}(F^{-1})^A{}_a(F^{-1})^B{}_b.
\end{aligned}
\tag{B.14}
$$

The following conditions are equivalent:

$$
\begin{aligned}
\mathbf{C} = \mathbf{I}, & \quad \mathbf{C}^\flat = \mathbf{G}, & \mathbf{c} = \mathbf{I}, & \quad \mathbf{c}^\flat = \mathbf{g}, \\
\mathbf{B} = \mathbf{I}, & \quad \mathbf{B}^\sharp = \mathbf{G}^\sharp, & \mathbf{b} = \mathbf{I}, & \quad \mathbf{b}^\sharp = \mathbf{g}^\sharp, \\
\mathbf{E} = \mathbf{0}, & \quad \mathbf{E}^\flat = \mathbf{0}, & \mathbf{e} = \mathbf{0}, & \quad \mathbf{e}^\flat = \mathbf{0}.
\end{aligned}
\tag{B.15}
$$

B.8 Fiber bundles

Some of the geometrical properties of a manifold $\mathcal{M}$ can be most easily examined by constructing a manifold called a fiber bundle, which is locally a direct product of $\mathcal{M}$ and a suitable space. In this section we shall give the definition of a fiber bundle and shall consider four examples that will be used later: the *tangent bundle* $T\mathcal{M}$, the *the tensor bundle* $T_s^r\mathcal{M}$, the *bundle of linear frames* or bases $\mathrm{Lin}(\mathcal{M})$, and the *bundle of orthonormal frames* $\mathrm{Orth}(\mathcal{M})$.

A $\mathscr{C}^k$ *bundle* over a $\mathscr{C}^s(s \geq k)$ manifold $\mathcal{M}$ is a $\mathscr{C}^k$ is a triple $(\mathcal{E}, \mathcal{M}, \pi)$ where $\mathcal{E}$ is a manifold and π is a $\mathscr{C}^k$ surjective map $\pi : \mathcal{E} \to \mathcal{M}$. The manifold $\mathcal{E}$ is called the total subspace, $\mathcal{M}$ is called the base space and π the projection. Where no confusion can arise, we will denote the bundle simply by $\mathcal{E}$. In general, the inverse image $\pi^{-1}(p)$ of point $p \in \mathcal{M}$ need not be homeomorphic to $\pi^{-1}(q)$ for another $q \in \mathcal{M}$. The simplest example of a bundle is a *product bundle* $(\mathcal{M} \times \mathcal{A}, \mathcal{M}, \pi)$ where $\mathcal{A}$ is some manifold and the projection π is defined by $\pi(p, v) = p$ for all $p \in \mathcal{M}, v \in \mathcal{A}$. For example if one

Figure B.3. A cylindrical hairbrush showing the intuition behind the term "fiber bundle". This hairbrush is like a *fiber bundle* in which the base space is a cylinder and the fibers bristles are line segments. The mapping $\pi : \mathcal{E} \to C^2$ would take a point on any bristle and map it to the point on the cylinder where the bristle attaches.

chooses $\mathcal{M}$ as the circle S^1 and $\mathcal{A}$ as the real line $\mathbb{R}$, one constructs the cylinder C^2 as a product bundle over S^1 (see B.4).

Definition B.8.1. *A bundle which is locally a product bundle is called the fiber bundle. Thus a bundle is a **fiber bundle** with fiber $\mathcal{F}$ if there exist a neighborhood $\mathcal{U}$ of each point of $\mathcal{M}$ such that $\pi^{-1}(\mathcal{U})$ is isomorphic with $\mathcal{U} \times \mathcal{F}$, in the sense that for each point $p \in \mathcal{U}$ there is a diffeomorphism ϕ_p of $\pi^{-1}p$ onto $\mathcal{F}$ such that the map $\psi : \pi^{-1}(\mathcal{U}) \to \mathcal{U} \times \mathcal{F}$ defined by $\phi(u) = (\pi(u), \phi_{\pi(u)}$ is a diffeomorphism.*

If $\mathcal{M}$ is required to be paracompact, for each point p, we can choose a locally finite covering of $\mathcal{M}$ by local charts $(\mathcal{U}_\alpha, \phi_{\alpha,p}$. If $\mathcal{U}_\alpha$ and $\mathcal{U}_\beta$ are two members of such covering, the map

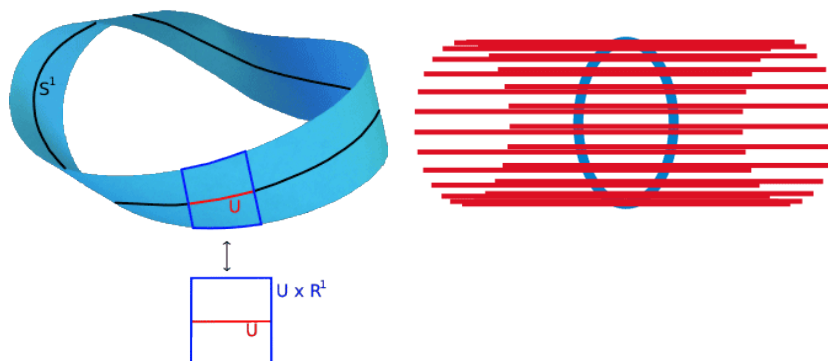$$(\phi_{\alpha,p}) \circ (\phi_{\beta,p}^{-1})$$

Figure B.4. The Möbius strip is a line bundle over the 1-sphere S^1. Locally around
every point in S^1, it looks like $U \times \mathbb{R}$ (where U is an open arc including the point)
(*Right*), but the total bundle is different from the product bundle $S^1 \times \mathbb{R}$ which is a
cylinder instead (*Left*).

is a diffeomorphism of $\mathcal{F}$ onto itself for each $p \in (\mathcal{U}_\alpha \cap \mathcal{U}_\beta)$. The inverse images
$\pi^{-1}(p)$ of points $p \in \mathcal{M}$ are therefore necessarily all diffeomorphic to $\mathcal{F}$ (and so
to each other). For example, the finite Möbius strip is a fiber bundle over S^1
with fiber $(0,1) \subset \mathbb{R}$ (see B.4), we need two open sets $\mathcal{U}_1, \mathcal{U}_2$ to give a covering by
sets of the form $\mathcal{U}_i \times (0,1)$. This example shows that if a manifold is locally the
direct product of two other manifolds, it is nevertheless not, in general, a product
manifold; and for this reason the concept of a fiber bundle is so useful.

- The **tangent bundle** $T\mathcal{M}$ is the fiber bundle over a $\mathscr{C}^k$ manifold $\mathcal{M}$ ob-
tained by giving the set $\mathcal{E} = \bigsqcup_{p \in \mathcal{M}} T_p\mathcal{M}$ its natural manifold structure and
its natural projection into $\mathcal{M}$. Thus the projection π maps each point of
$T_p\mathcal{M}$ into p. The manifold structure in $\mathcal{E}$ is defined by local coordinates
$\{z^A\}$ in the following way. Let $\{x^i\}$ be local coordinates in an open set
$\mathcal{U} \subset \mathcal{M}$. Then any vector $\boldsymbol{V} \in T_p\mathcal{U}$ can be expressed as $\boldsymbol{V} = V^i \partial/\partial x^i|_p$. The
coordinates $\{z^A\}$ are defined in $\pi^{-1}(\mathcal{U})$ by $\{z^A\} = \{x^i, V^a\}$. On choosing a
covering of $\mathcal{M}$ by coordinate neighborhoods $\mathcal{U}_\alpha$, the corresponding charts
define a $\mathscr{C}^{k-1}$ atlas on $\mathcal{E}$ which turn it into $\mathscr{C}^{k-1}$ manifold (of dimension
$2n$, where n is the dimension of $\mathcal{M}$). The fiber $\pi^{-1}(p)$ is $T_p\mathcal{M}$ and so is a
vector space of dimension n. This space structure is preserved by the map
$\phi_{p,\alpha} : T_p\mathcal{M} \to \mathbb{R}^n$, which is given by $\phi_{p,\alpha}(u) = V^a(u)$, *i.e.* $\phi_{p,\alpha}$ maps a vector
at p into its components with respect to the coordinates $\{x^a_\alpha\}$. If $\{x^a_\beta\}$ are
another set of local coordinates then the map $(\phi_{\alpha,p}) \circ (\phi^{-1}_{\beta,p})$ is a linear map
of $\mathbb{R}^n$ onto itself. Thus it is an element of the general linear group $\mathbf{GL}(n, \mathbb{R})$

(see section A.3).

- The **tensor bundle** $T_s^r \mathcal{M}$ is the bundle of tensor of type (r, s) over $\mathcal{M}$ is defined in a very similar way. One refers to the set $\mathcal{E} = \bigsqcup_{p \in \mathcal{M}} T_s^r(p)$ (here, $T_s^r(p)$ which is the set of tensor over the tangent space at p); it defines the projection π as a mapping at each point in $T_s^r(p)$ into p, and, for any coordinate neighborhood $\mathcal{U} \subset \mathcal{M}$, assigns local coordinates $\{z^A\}$ to $\pi{-}1(\mathcal{U})$ by $\{z^A\} = \{x^i, T_{c...d}^{a...b}\}$ where $\{x^i\}$ are the coordinates of the point p and $\{T_{c...d}^{a...b}\}$ are the coordinate components of $\mathbf{T}$ (that is, $\mathbf{T} = T_{c...d}^{a...b} \partial/\partial x^a \ldots \partial/\partial x^b dx^c \ldots dx^d|_p$). This turns $\mathcal{E}$ into $\mathscr{C}^{k-1}$ manifold of dimension $n + n^{r+s}$; any point u of $T_s^r \mathcal{M}$ corresponds to a unique tensor $\mathbf{T}$ of type (r, s) at $\pi(u)$.

- The **bundle of linear frames** (or bases) $\mathrm{Lin}(\mathcal{M})$ is a $\mathscr{C}^{k-1}$ fiber bundle defined as follows: the total space $\mathcal{E}$ consists of all bases at all points of $\mathcal{M}$, that is all sets of non-zero linearly independent n-tuples of vectors $\{\boldsymbol{E}_a\}, \boldsymbol{E}_a \in T_p \mathcal{M}$, for each $p \in \mathcal{M}$. The projection π is the natural one which maps a basis at a point p ti the point p. If $\{x^i\}$ are local coordinates in an open set $\mathcal{U} \subset \mathcal{M}$, then

$$\{z^A\} = \{x^a, E_1^j, E_2^k, \ldots, E_n^m\}$$

are local coordinates in $\pi{-}1(\mathcal{U})$, where E_a^j is the jth components of the vector $\boldsymbol{E}_a$ with respect to the coordinate bases $\partial/\partial x^i$. The general linear group $\mathbf{GL}(n, \mathbb{R})$ acts on $\mathrm{Lin}(\mathcal{M})$ in the following way: if $\{\boldsymbol{E}_a\}$ is a basis at $p \in \mathcal{M}$, then $A \in \mathbf{GL}(n, \mathbb{R}$ maps $u = \{p, \boldsymbol{E}_a\}$ to

$$A(u) = \{p, A_a^b \boldsymbol{E}_b\}$$

- The **bundle of orthonormal frames** $\mathrm{Orth}(\mathcal{M})$ is a sub-bundle of $\mathrm{Lin}(\mathcal{M})$; if there is metric g on $\mathcal{M}$, one can define $\mathrm{Orth}(\mathcal{M})$ as the bundle of orthonormal bases (with respect to g) at all points of $(\mathcal{M})$. This consists of the non-singular real matrices A_a^b such that:

$$A_a^b A_b^c = \delta_a^c$$

It maps $(p, \boldsymbol{E}_a) \in \mathrm{Orth}(\mathcal{M})$ to $(p, A_a^b \boldsymbol{E}_b) \in \mathrm{Orth}(\mathcal{M})$.

The linear bundle can serve as the configuration space for a micromorphic

solid, and the orthonormal bundle as the configuration space for a micropolar
solid. The next step in order to do this is to define a *cross-section* of a bundle:

Definition B.8.2. *A $\mathscr{C}^k$ **cross-section** of a bundle which is a $\mathscr{C}^r$ map Φ :
$\mathcal{M} \to \mathcal{E}$ such that $\pi \circ \Phi$ is the identity map on $\mathcal{M}$; thus a cross-section is a $\mathscr{C}^r$
assignment to each point p of $\mathcal{M}$ of an element $\Phi(p)$ of the fiber $\pi^{-1}(p)$.*

(a) *A cross-section of the tangent bundle $T\mathcal{M}$ is a **vector field** on $\mathcal{M}$.*

(b) *A cross-section of the tensor bundle $T_s^r\mathcal{M}$ is a **tensor field** of type (r, s) on
$\mathcal{M}$.*

(c) *A cross-section of $\mathrm{Lin}(\mathcal{M})$ is a set of n non-zero vectors fields $\{\boldsymbol{E}_a\}$ which
are linearly independent at each point.*

(d) *And a cross-section of $\mathrm{Orth}(\mathcal{M})$ is a set of orthonormal vector fields on $\mathcal{M}$
(sometimes this latter assignment is called an **observer**.*

As curious geometrical/topological facts we can recall that since the zero vec-
tors and tensors define cross-sections in $T\mathcal{M}$ and $T_s^r\mathcal{M}$, these fiber bundles will
always admit cross-sections. If $\mathcal{M}$ is orientable and non-compact, or is compact
with a vanishing Euler number, there will exist nowhere-zero vector fields, and
hence cross-sections of $T\mathcal{M}$ which are nowhere-zero. The bundles $\mathrm{Lin}(\mathcal{M})$ and
$\mathrm{Orth}(\mathcal{M})$ may or may not admit cross-sections, for example $\mathrm{Lin}(S^2)$ (linear bun-
dle of the surface of a sphere) does not, but $\mathrm{Lin}(\mathbb{R}^n)$ does. If $\mathrm{Lin}(\mathcal{M})$ admits
a cross-section, $\mathcal{M}$ is said to be *parallelizable*. Some physical requirements need
those properties, for example R. P. Geroch has shown (1968) that a non-compact
four-dimensional Lorentz manifold $\mathcal{M}$ (*i.e.* a space-time) admits a spinor struc-
ture if and only if it is parellelizable (and spinor fields seems completely necessary
for describing fermionic matter).

Bibliography

[1] ABRAHAM, R., MARSDEN, J. E., RAȚIU, T. S., AND CUSHMAN, R. *Foundations of mechanics.* Benjamin/Cummings Publishing Company Reading, Massachusetts, 1985.

[2] ARNDORFER, R., STEF, J., DODDS, W., LINEHAN, J., AND HOGAN, W. Improved infusion system for intraluminal esophageal manometry. *Gastroenterology 73*, 1 (1977), 23.

[3] ASSIDI, M., DOS REIS, F., AND GANGHOFFER, J.-F. Equivalent mechanical properties of biological membranes from lattice homogenization. *Journal of the Mechanical Behavior of Biomedical Materials 4*, 8 (2011), 1833–1845.

[4] AVEZ, A. *Calcul différentiel.* Masson, 1983.

[5] BABUŠKA, I. *Modeling, mesh generation, and adaptive numerical methods for partial differential equations*, vol. 75. Springer, 1995.

[6] BALL, J. M. Constitutive inequalities and existence theorems in nonlinear elastostatics. In *Nonlinear Analysis and Mechanics: Heriot-Watt Symposium* (1977), vol. 1, pp. 187–241.

[7] BOEHLER, J. Lois de comportement anisotrope des milieux continus. *Journal de Mécanique 17*, 2 (1978), 153–190.

[8] BOEHLER, J.-P. A simple derivation of representations for non-polynomial constitutive equations in some cases of anisotropy. *ZAMM-Journal of Applied Mathematics and Mechanics/Zeitschrift für Angewandte Mathematik und Mechanik 59*, 4 (1979), 157–167.

[9] BORDAS, J. M., LLACH, J., AND MATA, A. Utilidad de la enteroscopia de simple y de doble balón. *Gastroenterología y hepatología 32*, 6 (2009), 424–430.

[10] CAO, Y., JIANG, Y., LI, B., AND FENG, X. Biomechanical modeling of surface wrinkling of soft tissues with growth-dependent mechanical properties. *Acta Mechanica Solida Sinica 25*, 5 (2012), 483–492.

[11] CARTAN, H., AND CARTAN, H. P. *Differential calculus*, vol. 1. Hermann, 1971.

[12] CAUCHY, A.-L. De la pression ou tension dans un corps solide. *Exercises de Mathématiques 2* (1827), 42–56.

[13] CAUCHY, A. L. *Mémoire sur les sytèmes isotropes de points materiels.* Institut National de France, 1850.

[14] CHEN, Y., LEE, J. D., AND ESKANDARIAN, A. Atomistic viewpoint of the applicability of microcontinuum theories. *International journal of solids and structures 41*, 8 (2004), 2085–2097.

[15] CHRISTENSEN, W. N., AND STERNBERG, S. S. Adenocarcinoma of the upper esophagus arising in ectopic gastric mucosa: two case reports and review of the literature. *The American journal of surgical pathology 11*, 5 (1987), 397–402.

[16] CIARLET, P. *Three-Dimensional Elasticity.* No. v. 1 in Studies in mathematics and its applications. Elsevier Science, 1988.

[17] CIARLET, P. G., AND GEYMONAT, G. Sur les lois de comportement en élasticité non-linéaire compressible. *CR Acad. Sci. Paris Sér. II 295* (1982), 423–426.

[18] COLEMAN, B. D., AND NOLL, W. The thermodynamics of elastic materials with heat conduction and viscosity. *Archive for Rational Mechanics and Analysis 13*, 1 (1963), 167–178.

[19] COSSERAT, E., COSSERAT, F., BROCATO, M., AND CHATZIS, K. *Théorie des corps déformables.* A. Hermann Paris, 1909.

[20] COWIN, S., AND DOTY, S. *Tissue mechanics. 2007.* Springer, New York, 2007.

[21] DEMIRBAG, S., TIRYAKI, T., ATABEK, C., SURER, I., OZTURK, H., AND CETINKURSUN, S. Conservative approach to the mediastinitis in childhood secondary to esophageal perforation. *Clinical pediatrics 44*, 2 (2005), 131–134.

[22] DENG, S., TOMIOKA, J., DEBES, J., AND FUNG, Y. New experiments on shear modulus of elasticity of arteries. *American Journal of Physiology-Heart and Circulatory Physiology 266*, 1 (1994), H1–H10.

[23] DOBLARÉ, M., AND GARCÍA, J. Application of an anisotropic bone-remodelling model based on a damage-repair theory to the analysis of the proximal femur before and after total hip replacement. *Journal of Biomechanics 34*, 9 (2001), 1157.

[24] DOMMELEN, V. J., BREKELMANS, W., AND BAAIJENS, F. Micromechanics of particle-modified semi-crystalline materials.

[25] DOS REIS, F. Homogenization automatique de milieux discrets périodiques. applications aux mousses polymères et aux milieux auxétiques.

[26] DOS REIS, F., AND GANGHOFFER, J. Equivalent mechanical properties of auxetic lattices from discrete homogenization. *Computational Materials Science 51*, 1 (2012), 314–321.

[27] EJIMA, F. H., DANTAS, R. O., SIMOES, M. V., NETO, J. A. M., AND MENEGHELLI, U. G. Intraesophageal balloon distension test in chagas' disease patients with noncardiac chest pain. *Digestive diseases and sciences 43*, 11 (1998), 2567–2571.

[28] ERICKSEN, J. Deformations possible in every compressible, isotropic, perfectly elastic material. *J. Math. Phys 34*, 2 (1955).

[29] ERICKSEN, J. Tensor fields. *Encyclopedia of Physics 3* (1960), 1.

[30] ERINGEN, A. C. Theory of thermo-microstretch elastic solids. *International Journal of Engineering Science 28*, 12 (1990), 1291–1301.

[31] ERINGEN, A. C. *Microcontinuum field theories: foundations and solids*, vol. 487. Springer New York, 1999.

[32] ERINGEN, A. C., AND SUHUBI, E. Nonlinear theory of simple micro-elastic solids—i. *International Journal of Engineering Science 2*, 2 (1964), 189–203.

[33] FAN, Y., GREGERSEN, H., AND KASSAB, G. S. A two-layered mechanical model of the rat esophagus. experiment and theory. *Biomedical engineering online 3*, 1 (2004), 40.

[34] FELIPPA, C. A. Principios variacionales parametrizados para elasticidad micropolar. *Revista Internacional de Métodos Numéricos para Cálculo y Diseño en Ingeniería 8*, 3, 267–281.

[35] FISHER, R., AND TIPPETT, L. Limiting forms of the frequency distribution of the largest and smallest member of a sample. *Proc. Cambridge Phil. Soc. 24* (1928), 180–190.

[36] FLORY, P.-J. Statistical thermodynamics of semi-flexible chain molecules. *Proceedings of the Royal Society of London. Series A. Mathematical and Physical Sciences 234*, 1196 (1956), 60–73.

[37] FOREST, S., AND SIEVERT, R. Nonlinear microstrain theories. *International Journal of Solids and Structures 43*, 24 (2006), 7224–7245.

[38] GARCÍA-HERRERA, C. Comportamiento mecánico de la aorta ascendente: Caracterización experimental y simulación numérica.

[39] GARCÍA-HERRERA, C. M., CELENTANO, D. J., AND CRUCHAGA, M. A. Bending and pressurisation test of the human aortic arch: experiments, modelling and simulation of a patient-specific case. *Computer Methods in Biomechanics and Biomedical Engineering*, ahead-of-print (2011), 1–10.

[40] GIRARD, A. Calcul automatique en optique geometrique. *Rev. Opt. 37* (1958), 225–241.

[41] GNEDENKO, B. Sur la distribution limit du terme maximum dune serie aleatoir. *Ann. Math*, 44 (1943).

[42] GODA, I., ASSIDI, M., BELOUETTAR, S., AND GANGHOFFER, J. A micropolar constitutive model of cancellous bone from discrete homogenization. *Journal of the mechanical behavior of biomedical materials* (2012).

[43] Golub, G. H., and Van Loan, C. F. *Matrix computations*, vol. 3. JHU Press, 2012.

[44] Götzen, N., Cross, A. R., Ifju, P. G., and Rapoff, A. J. Understanding stress concentration about a nutrient foramen. *Journal of biomechanics 36*, 10 (2003), 1511–1521.

[45] Gregersen, H., Lee, T., Chien, S., Skalak, R., Fung, Y., et al. Strain distribution in the layered wall of the esophagus. *Journal of biomechanical engineering 121*, 5 (1999), 442.

[46] Gregersen, H., Liao, D., and Fung, Y. C. Determination of homeostatic elastic moduli in two layers of the esophagus. *Journal of biomechanical engineering 130*, 1 (2008), 011005–011005.

[47] Grekova, E. F., and Maugin, G. A. Modelling of complex elastic crystals by means of multi-spin micromorphic media. *International journal of engineering science 43*, 5 (2005), 494–519.

[48] Gumbel, E. J. *Statistics of extremes*. DoverPublications. com, 1958.

[49] Hahn, T., and of Crystallography, I. U. *International tables for crystallography: Brief teaching edition of volume A, Space-group symmetry*, vol. 1. Kluwer Academic Pub, 1996.

[50] Hawking, S. W., and Ellis, G. *The large structure of space-time*. Cambridge Monographs on Mathematical Physics, 1973.

[51] Holzapfel, G. *Nonlinear Solid Mechanics: A Continuum Approach for Engineering*. John Wiley & Sons, 2000.

[52] Holzapfel, G. A., Gasser, T. C., and Ogden, R. W. A new constitutive framework for arterial wall mechanics and a comparative study of material models. *Journal of elasticity and the physical science of solids 61*, 1-3 (2000), 1–48.

[53] Holzapfel, G. A., and Weizsäcker, H. W. Biomechanical behavior of the arterial wall and its numerical characterization. *Computers in biology and medicine 28*, 4 (1998), 377–392.

[54] Hudesman, D., Korman, A., Lipp, M., Yancovitz, S., and Bednarek, K. Acute herpetic esophagitis in an immunocompetent woman. In *American Journal of Gastroenterology* (2009), vol. 104, Nature Publishing Group 75 Varick st, 9th flr, New York, NY 10013-1917 USA, pp. S194–S194.

[55] Jackson, A. R., Travascio, F., and Gu, W. Y. Effect of mechanical loading on electrical conductivity in human intervertebral disc. *Journal of biomechanical engineering 131*, 5 (2009), 054505.

[56] James, H. M., and Guth, E. Theory of the elastic properties of rubber. *The Journal of Chemical Physics 11* (1943), 455.

[57] Juhl, C. O., Vinter-Jensen, L., Djurhuus, J., Gregersen, H., and Dajani, E. Z. Biomechanical properties of the oesophagus damaged by endoscopic sclerotherapy: An impedance planimetric study in minipigs. *Scandinavian journal of gastroenterology 29*, 10 (1994), 867–873.

[58] Kaufman, J. A., and Oelschlager, B. K. Treatment of achalasia. *Current treatment options in gastroenterology 8*, 1 (2005), 59–69.

[59] Kroon, M., and Holzapfel, G. A. A new constitutive model for multi-layered collagenous tissues. *Journal of biomechanics 41*, 12 (2008), 2766–2771.

[60] Kuhn, W., and Grun, F. Relationships between elastic constants and stretching double refraction of highly elastic substances. *Kolloid-Z 101* (1942), 294.

[61] Kuhn, W., and Grün, F. Statistical behavior of the single chain molecule and its relation to the statistical behavior of assemblies consisting of many chain molecules. *Journal of Polymer Science 1*, 3 (1946), 183–199.

[62] Lampton, M. Damping–undamping strategies for the Levenberg–Marquardt nonlinear least-squares method. *Computers in Physics 11* (1997), 110.

[63] Levenberg, K. A method for the solution of certain non-linear problems in least squares. *Quarterly of Applied Mathematics 2* (1944), 164–168.

[64] LIMBERT, G., AND TAYLOR, M. On the constitutive modeling of biological soft connective tissues: A general theoretical framework and explicit forms of the tensors of elasticity for strongly anisotropic continuum fiber-reinforced composites at finite strain. *International journal of solids and structures 39*, 8 (2002), 2343–2358.

[65] LIU, I.-S. On representations of anisotropic invariants. *Int J. Engng. Sci. 10* (1982), 1099–1109.

[66] LOKHIN, V., AND SEDOV, L. Nonlinear tensor functions of several tensor arguments. *Journal of Applied Mathematics and Mechanics 27*, 3 (1963), 597–629.

[67] LOURAKIS, M. I. A brief description of the Levenberg-Marquardt algorithm implemented by Levmar. *Institute of Computer Science, Foundation for Research and Technology 11* (2005).

[68] LU, J. A covariant constitutive theory for anisotropic hyperelastic solids with initial strains. *Mathematics and Mechanics of Solids 17*, 2 (2012), 104–119.

[69] LU, X., AND GREGERSEN, H. Regional distribution of axial strain and circumferential residual strain in the layered rabbit oesophagus. *Journal of Biomechanics 34*, 2 (2001), 225–233.

[70] LUKEŠ, V., AND ROHAN, E. Microstructure based two-scale modelling of soft tissues. *Mathematics and Computers in Simulation 80*, 6 (2010), 1289–1301.

[71] MARQUARDT, D. W. An algorithm for least-squares estimation of nonlinear parameters. *Journal of the Society for Industrial & Applied Mathematics 11*, 2 (1963), 431–441.

[72] MARSDEN, J., AND HUGHES, T. *Mathematical Foundations of Elasticity.* Dover books on mathematics. Dover Publ., 1983.

[73] MARSHALL, R., ANGGIANSAH, A., ANGGIANSAH, C., OWEN, W., AND OWEN, W. Esophageal body length, lower esophageal sphincter length, position and pressure in health and disease. *Diseases of the Esophagus 12*, 4 (1999), 297–302.

[74] Mindlin, R. Micro-structure in linear elasticity. *Archive for Rational Mechanics and Analysis 16*, 1 (1964), 51–78.

[75] Mittal, R. Sphincter mechanisms at the esophago-gastric junction. In *Principles of Deglutition*. Springer, 2013, pp. 319–341.

[76] Mittal, R. K. The sphincter mechanism at the lower end of the esophagus: an overview. *Dysphagia 8*, 4 (1993), 347–350.

[77] Moré, J. J. The Levenberg-Marquardt algorithm: implementation and theory. In *Numerical analysis*. Springer, 1978, pp. 105–116.

[78] Morrison, D. D. Methods for nonlinear least squares problems and convergence proofs, jpl seminar proceedings. *Space Technology Laboratory Inc* (1960).

[79] Mühlhaus, H., and Vardoulakis, I. The thickness of shear bands in granular materials. *Geotechnique 37*, 3 (1987), 271–283.

[80] Natali, A. N., Carniel, E. L., and Gregersen, H. Biomechanical behaviour of oesophageal tissues: material and structural configuration, experimental data and constitutive analysis. *Medical engineering & physics 31*, 9 (2009), 1056–1062.

[81] Noll, W. Representations of certain isotropic tensor functions.

[82] Ogden, R. Large deformation isotropic elasticity-on the correlation of theory and experiment for incompressible rubberlike solids. *Proceedings of the Royal Society of London. A. Mathematical and Physical Sciences 326*, 1567 (1972), 565–584.

[83] Ogden, R., Saccomandi, G., and Sgura, I. Fitting hyperelastic models to experimental data. *Computational Mechanics 34*, 6 (2004), 484–502.

[84] Ottani, V., Raspanti, M., and Ruggeri, A. Collagen structure and functional implications. *Micron 32*, 3 (2001), 251–260.

[85] Patel, R. S., and Rao, S. S. Biomechanical and sensory parameters of the human esophagus at four levels. *American Journal of Physiology-Gastrointestinal and Liver Physiology 275*, 2 (1998), G187–G191.

[86] Pathria, R. Statistical mechanics, 1996.

[87] PIPKIN, A., AND WINEMAN, A. Material symmetry restrictions on non-polynomial constitutive equations. *Archive for Rational Mechanics and Analysis 12*, 1 (1963), 420–426.

[88] PIPKIN, A. C., AND RIVLIN, R. The formulation of constitutive equations in continuum physics. i. *Archive for Rational Mechanics and Analysis 4*, 1 (1959), 129–144.

[89] RANGANATHAN, A. The Levenberg-Marquardt algorithm. *Tutorial on LM Algorithm* (2004).

[90] REINER, M. Elasticity beyond the elastic limit. *Amer J Math 70* (1948), 433–446.

[91] RIVLIN, RS, E. J. Stress-deformation relations for isotropic materials. *J Rat Mech Anal 4* (1955), 323–425.

[92] RIVLIN, R. S., AND SAUNDERS, D. Large elastic deformations of isotropic materials. vii. experiments on the deformation of rubber. *Philosophical Transactions of the Royal Society of London. Series A, Mathematical and Physical Sciences 243*, 865 (1951), 251–288.

[93] RODRIGUEZ, E. K., HOGER, A., AND MCCULLOCH, A. D. Stress-dependent finite growth in soft elastic tissues. *Journal of biomechanics 27*, 4 (1994), 455–467.

[94] ROHAN, E., CIMRMAN, R., AND LUKEŠ, V. Numerical modelling and homogenized constitutive law of large deforming fluid saturated heterogeneous solids. *Computers & structures 84*, 17 (2006), 1095–1114.

[95] ROSENBERG, J., AND CIMRMAN, R. Microcontinuum approach in biomechanical modeling. *Mathematics and Computers in Simulation 61*, 3 (2003), 249–260.

[96] SCHWARTZ, L. Cours d'analyse, tome 1. *Hermann, Paris* (1967).

[97] SMITH, G. On isotropic functions of symmetric tensors, skew-symmetric tensors and vectors. *International Journal of Engineering Science 9*, 10 (1971), 899–916.

[98] Sánchez-Molina, D., Velazquez-Ameijide, J., Arregui-Dalmases, C., Crandall, J., and Untaroiu, C. Minimization of analytical injury metrics for head impact injuries. *Traffic injury prevention 13*, 3 (2012), 278–285.

[99] Sánchez-Molina, D., Velázquez-Ameijide, J., Arregui-Dalmases, C., Rodríguez, D., Quintana, V., Shafieian, M., and Crandall, J. A micro-continuum model for mechanical properties of esophageal tissue: experimental data and constitutive analysis (in press). *Annals of Biomedical Engineering 42?*, ? (2013), XXX–XXX.

[100] Spencer, A. J. M., et al. *Continuum theory of the mechanics of fibre-reinforced composites*, vol. 282. Springer New York, 1984.

[101] Steeb, H., and Diebels, S. A thermodynamic-consistent model describing growth and remodeling phenomena. *Computational materials science 28*, 3 (2003), 597–607.

[102] Tarantola, A. *Elements for physics*. Springer, 2006.

[103] Tong, J., Wong, K., and Lupton, C. Determination of interfacial fracture toughness of bone–cement interface using sandwich brazilian disks. *Engineering fracture mechanics 74*, 12 (2007), 1904–1916.

[104] Treolar, L. G. 1958. the physics of rubber elasticity.

[105] Truesdell, C., and Toupin, R. *The classical field theories*. Springer, 1960.

[106] Vainshtein, B. K. Modern crystallography. vol. 1. fundamentals of crystals. symmetry, and methods of structural crystallography. *Acta Cryst 51* (1995), 234–235.

[107] Vaishnav, R. N., and Vossoughi, J. Estimation of residual strains in aortic segments. *Biomedical engineering II, recent developments 2* (1983), 330–333.

[108] Vaishnav, R. N., and Vossoughi, J. Residual stress and strain in aortic segments. *Journal of biomechanics 20*, 3 (1987), 235–239.

[109] WANG, C.-C. A new representation theorem for isotropic functions: An answer to professor gf smith's criticism of my papers on representations for isotropic functions. *Archive for Rational Mechanics and Analysis 36*, 3 (1970), 166–197.

[110] WANG, C.-C. Corrigendum to my recent papers on "representations for isotropic functions". *Archive for Rational Mechanics and Analysis 43*, 5 (1971), 392–395.

[111] WINEMAN, A. S., AND PIPKIN, A. Material symmetry restrictions on constitutive equations. *Archive for Rational Mechanics and Analysis 17*, 3 (1964), 184–214.

[112] WYNNE, C. Lens designing by electronic digital computer: I. *Proceedings of the Physical Society 73*, 5 (1959), 777.

[113] YANG, J., AND LAKES, R. S. Experimental study of micropolar and couple stress elasticity in compact bone in bending. *Journal of biomechanics 15*, 2 (1982), 91–98.

[114] YANG, J., ZHAO, J., LIAO, D., AND GREGERSEN, H. Biomechanical properties of the layered oesophagus and its remodelling in experimental type-1 diabetes. *Journal of biomechanics 39*, 5 (2006), 894–904.

[115] YANG, W., FUNG, T., CHIAN, K., CHONG, C., ET AL. 3d mechanical properties of the layered esophagus: experiment and constitutive model. *Journal of biomechanical engineering 128*, 6 (2006), 899.

[116] ZEMANSKY, M. W., AND DITTMAN, R. H. *Heat and thermodynamics: an intermediate textbook*. McGraw-Hill, 1997.

[117] ZHENG, Q.-S. On the representations for isotropic vector-valued, symmetric tensor-valued and skew-symmetric tensor-valued functions. *International journal of engineering science 31*, 7 (1993), 1013–1024.

[118] ZHENG, Q.-S. Theory of representations for tensor functions—a unified invariant approach to constitutive equations. *Applied Mechanics Reviews 47*, 11 (1994), 545–587.

[119] ZHENG, Q.-S., AND BOEHLER, J. The description, classification, and reality of material and physical symmetries. *Acta Mechanica 102*, 1-4 (1994), 73–89.